87 Wissenschaftliche Berichte des Instituts für Meteorologie und Klimaforschung des Karlsruher Instituts für Technologie

JAN LUCAS WANDEL

Representation of warm conveyor belts in sub-seasonal forecast models and the link to Atlantic-European weather regimes

KIT Scientific Publishing

Jan Lucas Wandel

Representation of warm conveyor belts in sub-seasonal forecast models and the link to Atlantic-European weather regimes

Wissenschaftliche Berichte des Instituts für Meteorologie und Klimaforschung des Karlsruher Instituts für Technologie (KIT)
Band 87

Herausgeber: Prof. Dr. C. Hoose
Prof. Dr. P. Knippertz
Prof. Dr. J. G. Pinto

Institut für Meteorologie und Klimaforschung
am Karlsruher Institut für Technologie (KIT)
Kaiserstr. 12, 76128 Karlsruhe

Eine Übersicht aller bisher in dieser Schriftenreihe erschienenen Bände finden Sie am Ende des Buches.

Representation of warm conveyor belts in sub-seasonal forecast models and the link to Atlantic-European weather regimes

by
Jan Lucas Wandel

KIT Scientific Publishing

Karlsruher Institut für Technologie
Institut für Meteorologie und Klimaforschung

Representation of warm conveyor belts in sub-seasonal forecast models and the link to Atlantic-European weather regimes

Zur Erlangung des akademischen Grades eines Doktors der Naturwissenschaften von der KIT-Fakultät für Physik des Karlsruher Instituts für Technologie (KIT) genehmigte Dissertation

von Jan Lucas Wandel, M.Sc.

Tag der mündlichen Prüfung: 24. Juni 2022
Referent: Jun.-Prof. Dr. Christian Grams
Korreferent: Prof. Dr. Peter Knippertz

Impressum

KIT Scientific Publishing

Karlsruher Institut für Technologie (KIT)
KIT Scientific Publishing
Straße am Forum 2
D-76131 Karlsruhe

KIT Scientific Publishing is a registered trademark
of Karlsruhe Institute of Technology.
Reprint using the book cover is not allowed.

www.ksp.kit.edu

This document – excluding parts marked otherwise, the cover, pictures and graphs – is licensed under a Creative Commons Attribution-Share Alike 4.0 International License (CC BY-SA 4.0): https://creativecommons.org/licenses/by-sa/4.0/deed.en

The cover page is licensed under a Creative Commons Attribution-No Derivatives 4.0 International License (CC BY-ND 4.0): https://creativecommons.org/licenses/by-nd/4.0/deed.en

Print on Demand 2023 – Gedruckt auf FSC-zertifiziertem Papier

ISSN 0179-5619
ISBN 978-3-7315-1249-3
DOI 10.5445/KSP/1000151831

Abstract

Warm conveyor belts (WCBs) are important components of the large-scale flow in the midlatitudes since they transport air from the lower troposphere into the tropopause region and contribute to upper-level ridge building and the formation of blocking anticyclones. These anticyclones make up an important fraction of the variability of the large-scale atmospheric circulation in midlatitudes which is characterised by transient extratropical Rossby waves and stationary patterns. Recent studies indicate that the WCB constitutes an important source and magnifier of forecast uncertainty and errors in numerical weather prediction (NWP) models and might be co-responsible for relatively low forecast skill for certain upper-tropospheric large flow regimes. These flow regimes (also called weather regimes) are of particular importance on sub-seasonal time scales (several weeks to a month in the future) due to their implications for surface weather extremes and socio-economic impacts.

Despite the importance of the WCB for the large-scale circulation, a systematic evaluation of the representation of WCBs in NWP models and their link to large-scale flow regimes has yet to be determined. Therefore, this study systematically investigates the representation of WCBs in large reforecast data sets of different NWP models from the Subseasonal-to-Seasonal (S2S) database and evaluates the role of WCBs for the onset and life cycle of Atlantic-European weather regimes in the reforecasts.

The first part of the study investigates the representation of WCBs in the European Centre for Medium-Range Weather Forecasts (ECMWF) sub-seasonal reforecasts in the period January 1997 to December 2017. The representation of the WCB is verified in terms of systematic occurrence frequency biases, forecast reliability, and forecast skill. Systematic WCB frequency biases emerge already

at early lead times of around 3 days with an underestimation for the WCB outflow over the North Atlantic and eastern North Pacific of around 20% relative to climatology. Biases in the inflow and ascent stage of the WCB can be partly explained by biases in meridional moisture flux in the lower and mid troposphere. Skillful WCB forecasts are on average possible up to a lead time of 8–10 days with more skill over the North Pacific compared to the North Atlantic region. The results corroborate that the current limited forecast skill for the large-scale extratropical circulation on sub-seasonal time scales beyond 10 days might be tied to the representation of WCBs and associated upscale error growth.

The second part of the study evaluates the role of WCBs for the onset and life cycle of atmospheric blocking over the European region (EuBL) in the extended winter priod of the ECMWF's IFS reforecasts (1997–2017). The prediction and correct representation of EuBL is still a major challenge for numerical weather prediction (NWP) and climate models while the regime itself is strongly influenced by WCB activity over the central and eastern Atlantic. The analysis of the WCB activity prior the the onset of the regime shows a strong underestimation of WCB activity over the eastern Atlantic. It reveals that the reforecasts establish large-scale flow anomalies via WCB outflow differently than observed with a more amplified large-scale flow and high WCB activity upstream of the incipient block. Furthermore, the results point to upstream precursors from the eastern North Pacific which can impact the predictive skill of the EuBL regime. The findings show that forecast biases in WCB activity might be partly responsible for the relatively poor skill of blocking forecasts and highlight the potential for further improvement of sub-seasonal prediction by improving the representation of WCBs in NWP models.

In the third part of the study, the role of the WCB is then further evaluated for other large-scale flow regimes, in particular other blocked weather regimes. Besides the importance for EuBL onsets, WCB activity also plays an important role for the prediction of Scandinavian and Greenland blocking regimes (ScBL and GL) in the reforecasts while the role for the Atlantic Ridge (AR) seems to be smaller. For ScBL, there is high WCB outflow activity over the northern part of the incipient block (Barents Sea) which is not resolved well in the reforecasts.

For GL, the reforecasts have difficulties in capturing the WCB outflow frequencies over both the Atlantic and North America. Furthermore, the role of the WCB is evaluated for blocked regimes over Europe in boreal summer which have high correlations with summer heat waves over the continent. WCB activity is enhanced during episodes with low predictive skill of EuBL and ScBL indicating that the WCB also plays a role for the prediction of regimes in summer. All in all, the findings underline that an improved prediction of WCBs would likely yield in improvements of forecast skill on sub-seasonal time scales.

Lastly, the representation of WCBs and the link to weather regimes is evaluated in different NWP models from the S2S database. The analysis shows that similar WCB biases emerge already at early forecast lead times in all S2S models. This finding shows that all NWP models have difficulties in correctly capturing WCB activity which might have strong implication for the forecast of the large-scale flow. The biases are generally weaker in the ECMWF reforecast and the reforecasts of the National Centers for Environmental Prediction (NCEP). The forecast skill horizon for the Northern Hemisphere varies between the S2S models and is highest in the ECMWF's reforecasts and the reforecasts of Environmental and Climate Change Canada (ECCC) (around 8 days). A comparison of the link between WCB activity and blocking over the European region in the four NWP models with highest WCB forecast skill shows that all models establish EuBL via strong WCB activity over the Atlantic. Despite similar pathways into EuBL small differences in terms of WCB activity and Z500 patterns occur between the four S2S models.

The results in this study help to better understand the representation of WCBs in NWP models and the role for the prediction of large-scale flow regimes. They emphasize the importance of accurate forecast of synoptic-scale processes (like latent heat in WCBs) for sub-seasonal prediction on time scales beyond two weeks. Furthermore, they indicate that the WCB plays an important role for the forecast of blocking anticyclones and that the low forecast skill of blocking over Europe is very likely tied to misrepresented WCBs in the NWP models.

Zusammenfassung

Warm Conveyor Belts (WCBs) sind wichtige Komponenten der großräumigen Strömung in den mittleren Breiten, da sie Luft aus der unteren Troposphäre in die Tropopausenregion transportieren und zur Bildung von Höhenrücken und blockierender Wetterlagen beitragen. Diese blockierenden Wetterlagen machen einen wichtigen Teil der Variabilität der großräumigen atmosphärischen Zirkulation in mittleren Breiten aus, die durch westwärts propagierende außertropische Rossby-Wellen und stationäre Muster gekennzeichnet ist. Die Ergebnisse von kürzlich veröffentlichten Studien weisen darauf hin, dass der WCB eine wichtiger Ort für Vorhersageunsicherheiten und Fehler in numerischen Wettervorhersagemodellen (NWP) darstellt und möglicherweise mitverantwortlich für die relativ geringe Vorhersagegüte von bestimmten großräumigen Wetterlagen ist. Diese großräumigen Wetterlagen (oder Wetterregime) sind auf subsaisonalen Zeitskalen (mehrere Wochen bis zu einem Monat in der Zukunft) aufgrund ihrer sozio-ökonomische Auswirkungen und Verbindung zu Wetterextremen von enormer Bedeutung.

Trotz der großen Bedeutung der WCBs für die großräumige Zirkulation fehlt bisher eine systematische Auswertung der Vorhersagbarkeit von WCBs in NWP-Modellen und ihrer Verbindung zu großräumigen Wetterregimen. Daher untersucht diese Studie die Repräsentation von WCBs in großen Datensätzen von Wettervorhersagen aus der Subseasonal-to-Seasonal (S2S)-Datenbank und evaluiert die Rolle von WCBs für den Lebenszyklus von Wetterregimen in der Atlantic-Europa Region in den Vorhersagen.

Der erste Teil der Studie untersucht die Vorhersagbarkeit von WCBs in dem sub-seasonalen Wettervorhersagemodells des Europäischen Zentrums für mittelfristige Wettervorhersage (EZMW) im Zeitraum Januar 1997 bis Dezember 2017.

Die Vorhersage der WCB wird hinsichtlich der systematischen Auftretenshäufigkeit verifiziert und die Vorhersagegüte des WCBs im Modell evaluiert. Systematische Fehler in der WCB-Frequenz im Modell entstehen bereits zu frühen Vorhersagezeitpunkten von etwa 3 Tagen mit einer Unterschätzung der WCB-Aktivität von etwa 20% relativ zur Klimatologie in der oberen Troposphäre über dem Nordatlantik und dem östlichen Nordpazifik. Abweichungen in der WCB Frequenz in der unteren und mittleren Tropospähre können teilweise durch Abweichungen im meridionalen Feuchtigkeitsfluss erklärt werden. Die Vorhersage des Auftretesn eines WCBs an einem festen Ort ist bis ca. 8–10 Tage im Voraus möglich, was auch der typischen Vorhersagbarkeit des Auftretens eines Tiefdruckgebiets entspricht. Die Vorhersagegüte von WCBs ist dabei besser über dem Nordpazifik im Vergleich zur Nordatlantik. Die Ergebnisse deuten darauf, dass die derzeit begrenzte Vorhersagbarkeit für die großräumige außertropische Zirkulation auf subsaisonalen Zeitskalen von über 10 Tagen in der Zukunft mit der Auflösung von Prozessen im WCBs verbunden sein könnte.

Der zweite Teil der Studie bewertet die Rolle der WCBs für den Lebenszyklus blockierender Hochdruckwetterlagen über Europa (EuBL) in der verlängerten Winterperiode der sub-saisonalen Wettervorhersagen des EZMW (1997–2017). Im Vergleich zu anderen Wetterlagen ist die Vorhersage von EuBL immer noch eine große Herausforderung für die NWP und Klimamodelle. Die Analyse der WCB-Aktivität vor Beginn des Regimes zeigt eine starke Unterschätzung der WCB-Aktivität über dem Ostatlantik. Darüber hinaus zeigen die Ergebnisse, dass die WCB-Aktivtät in den Vorhersagen anders zum Aufbauen der blockierende Wetterlage beiträgt und dass diese durch eine höhere Geopotentialanomalie und starker WCB-Aktivität an der Vorderseite des Blocks gekennzeichnet ist. Darüber hinaus weisen die Ergebnisse auf den Einfluss der Zirkulation über dem östlichen Nordpazifik auf die Vorhersagegüte des EuBL-Regimes hin. Die Ergebnisse zeigen, dass eine ungenaue Vorhersage der WCB-Aktivität teilweise für die relativ schlechte Vorhersagbarkeit von blockierenden Wetterlagen über Europe verantwortlich sein könnten, und verdeutlichen das Potenzial für eine weitere Verbesserung der subsaisonalen Vorhersage durch eine verbesserte Darstellung von WCBs in NWP-Modellen.

Im dritten Teil der Studie wird die Rolle des WCBs dann weiter für andere großräumige Wetterregime bewertet, insbesondere für andere blockierende Hochdruckwetterlagen. Neben der Bedeutung für EuBL spielt die WCB-Aktivität auch eine wichtige Rolle für die Vorhersage blockierender Hochdruckgebiete über Skandinavien und Grönland (ScBL und GL), während die Rolle für blockierende Wetterlagen über dem Atlantik (AR) geringer ist. Bei ScBL gibt es eine hohe WCB-Aktivität über dem nördlichen Teil des Blocks (Barentssee), die in den Vorhersagen nicht gut aufgelöst wird. Bei GL haben die Vorhersagen Schwierigkeiten, die WCB-Aktivität über dem Atlantik und über Nordamerika zu erfassen. Darüber hinaus wird die Rolle des WCB für blockierende Wetterlagen über Europa im borealen Sommer bewertet, die häufig zu sommerlichen Hitzewellen über dem Kontinent führen. Die WCB-Aktivität ist während Episoden mit geringer Vorhersagegüte von EuBL und ScBL verstärkt, was darauf hinweist, dass der WCB auch eine Rolle für die Vorhersage von blockierenden Hochdruckwetterlagen über Europa im Sommer spielt. Alles in allem unterstreichen die Ergebnisse, dass eine verbesserte Vorhersage von WCBs wahrscheinlich zu Verbesserungen der Vorhersagegüte auf subsaisonalen Zeitskalen führen würde.

Abschließend wird die Darstellung von WCBs und die Verbindung zu Wetterregimen in verschiedenen NPW-Modellen aus der S2S-Datenbank evaluiert. Die Analyse zeigt, dass ähnliche Fehler in der WCB-Aktivität bereits zu frühen Vorhersagezeitpunkten in allen S2S-Modellen auftreten. Die Fehler sind in den Vorhersagen des EZMW und des National Centers for Environmental Prediction (NCEP) schwächer als in den anderen Modellen. Der Vorhersagehorizont für WCBs für die Nordhalbkugel variiert zwischen den S2S-Modellen und ist in den Vorhersagen des EZMW und von Environmental and Climate Change Canada (ECCC) am Höchsten (ca. 8 Tage). Ein Vergleich zwischen den Modellen bezüglich des Zusammenhangs zwischen WCB-Aktivität und blockierender Hochdruckwetterlagen über Europa zeigt, dass in allen Modellen der WCB eine wichtige Rolle spielt und dass die Modellen den Block in ähnlicher Weise aufbauen. Trotz dieser Ähnlichkeiten gibt es Unterschiede in den Modellen bezogen auf die WCB Aktivität und die großräumige Zirkulation.

Die Ergebnisse dieser Studie tragen dazu bei, WCBs in NWP-Modellen und deren Rolle für die Vorhersage großräumiger Strömungsregime besser zu verstehen. Die Eregbnisse betonen die Bedeutung einer genauen Vorhersage von kleinräumigen Prozessen in außertrpischen Tiefdruckgebieten (wie das Freiwerden von latenter Wärme in WCBs) für die subsaisonale Vorhersage auf Zeitskalen von über zwei Wochen in der Zukunft. Darüber hinaus weisen die Ergebnisse darauf hin, dass der WCB eine wichtige Rolle für die Vorhersage blockierender Hochdruckwetterlagen spielt und dass deren geringe Vorhersagegüte über Europa sehr wahrscheinlich mit falsch dargestellten WCBs in den NWP-Modellen zusammenhängt.

Preface

The PhD candidate confirms that the research presented in this thesis contains significant scientific contributions by himself. It is important to note that Chapter 5 of this thesis is based on the following publication:

Wandel, J., Quinting, J. F., Grams, C. M. (2021). Toward a systematic evaluation of warm conveyor belts in numerical weather prediction and climate models. Part II: Verification of operational reforecasts. Journal of the Atmospheric Sciences, 78(12), 3965-3982.

However, the results in the publication were calculated with a previous version of the statistical models to study WCBs (Quinting and Grams, 2021b). All results in the thesis are based on the new version of the statistical WCB models (Quinting and Grams, 2021a).

Contents

Abstract i

Zusammenfassung v

Preface ix

1 Introduction 1

2 Theoretical background 5
2.1 Warm conveyor belts (WCBs) 5
2.2 Atlantic-European weather regimes 12
2.3 Predictability on sub-seasonal time scales 18

3 Research questions 29

4 Data and Methods 33
4.1 Model and reanalysis data 33
4.1.1 Subseasonal-to-Seasonal (S2S) database 33
4.1.2 ERA-Interim reanalysis 37
4.2 Statistical model to study WCBs in NWP models 38
4.3 Year-round Atlantic-European weather regimes 40
4.4 Verification methods 45
4.4.1 WCB representation 46
4.4.2 Link between WCBs and weather regimes 48

5 Verification of warm conveyor belts 53
5.1 Model bias 53
5.2 Forecast reliability 57
5.3 Forecast skill 59

5.4 Link between WCB bias and bias of predictor variables 63
5.5 WCB biases on sub-seasonal time scales and their link to MJO . . 67
5.6 WCB forecast skill on sub-seasonal time scales and its link to the MJO 73
5.7 Seasonal variation of WCB bias and skill 77
5.8 Conclusions 82

6 Impact of WCBs on atmospheric blocking over Europe 85
6.1 Representation of EuBL onsets in reforecasts 85
6.2 EuBL onset evolution in ERA-interim and reforecasts 89
6.3 Influence of WCBs on EuBL forecast skill 94
6.3.1 The role of WCBs for EuBL onsets 95
6.3.2 Remote influences 98
6.3.3 Local influences 103
6.3.4 Sources of forecast error 108
6.4 Conclusions 113

7 The role of WCBs for Atlantic-European weather regimes . . 117
7.1 Predictability of weather regimes onsets 118
7.2 WCB activity around regime onsets 120
7.2.1 Scandinavian Blocking 120
7.2.2 Greenland Blocking 127
7.2.3 Atlantic Ridge 137
7.2.4 Zonal Regime 143
7.3 Link between WCB activity and blocked regimes over Europe in summer 148
7.4 Conclusions 153

8 Comparison of sub-seasonal forecast models 157
8.1 WCB bias and skill 157
8.2 European blocking onset evolution 165

9 Conclusions and Outlook 175

A Appendix for Chapter 5 183

B Appendix for Chapter 6 191

C Appendix for Chapter 7 . . . . . **197**

Bibliography **203**

Acknowledgments **219**

1 Introduction

The forecast of meteorological phenomena, such as heat waves, cold spells, or extended periods of rain is of high importance for society, political decision makers and stakeholders. Due to the chaotic nature of the atmosphere, accurate weather predictions of day to day weather are limited to around two weeks into the future (Lorenz, 1963). However, the increase in computational power, better data assimilation and the shift from deterministic to probabilistic weather forecasts has shifted the limits of predictability for the weather scales even beyond the two week range (Buizza and Leutbecher, 2015). Due to these advances in weather forecasting, there has been a growing interest from various groups in accurate weather prediction on time scales between two weeks and three months. This sub-seasonal to seasonal (S2S) time scale is important to successful organization and preparation in a variety of sectors, including public health, water management, disaster preparedness, energy, and agriculture. Weather prediction on these time scales have been regarded challenging because it has to combine both the initial value problem of the weather scale and the predictability provided by slower climate modes (i.e. ocean, land, and ice surfaces).

Variability of the large-scale atmospheric circulation in the midlatitudes is characterised by transient extratropical Rossby waves and stationary patterns, such as blocking anticyclones. On sub-seasonal time scales, the extratropical variability can be depicted by large-scale flow regimes, so called weather regimes (Michelangeli et al., 1995). These weather regimes are quasi-stationary, persistent, and recurrent flow patterns which can be associated with distinct meteorological conditions in terms of temperature, wind and precipitation. The prediction of regime occurrence and regime transitions on sub-seasonal time scales has been deemed a current goal of weather prediction centers.

Windows of forecast opportunity (enhanced predictability) on sub-seasonal time scales are provided by slower climate models like the stratospheric polar vortex (SPV) or tropical weather phenomena like the Madden-Julian Oscillation (MJO). These phenomena are predictable on time scales of several weeks to a month and modulate occurrence frequencies of weather regimes through complex wave propagation and interaction with the large-scale circulation in mid-latitudes. However, recent studies show that weather regimes are also modulated by smaller-scale processes on the synoptic scale. These processes have a shorter predictability limit and might reduce the overall predictability of weather regimes. In particular, diabatic processes in extratropical cyclones have been shown to play an important role for the onset and the life cycle of certain weather regimes. These diabatic processes are related to latent heat release in the so-called warm conveyor belt (WCB). The WCB is an ascending air stream in the warm sector of an extratropical cyclone and its "diabatic outflow" modulates the upper-level jet, resulting in the amplification of an upper-level ridge and eventually a block. Therefore, the WCB plays an important role especially for blocked weather regimes where around 50% of the air masses are heated before arriving in the block (Pfahl et al., 2015). In current NWP models, latent heating in warm conveyor belts is a sub-grid scale process which needs to be parameterised. Therefore, it can generate or amplify forecast error and project it to the large-scale flow via its diabatic outflow. Due to its strong influence on blocked weather regimes, it potentially dilutes forecast skill for these regimes on sub-seasonal time scales.

This study, for the first time, evaluates the overall representation of WCBs and their role for the prediction of weather regimes over the Atlantic-European region in sub-seasonal forecast models. The study is structured as follow: Chapter 2 introduces WCBs and Atlantic-European weather regimes and describes drivers of sub-seasonal predictability. In Chapter 3, the S2S database and reanalysis data are described, as well different methods to quantify the representation and role of WCBs. Chapter 4 introduces the different research questions and objectives of this study. Chapter 5–8 then investigate the WCB and Atlantic-European weather regimes in different S2S models: Chapter 5 investigates the representation of WCBs in terms of forecast bias, reliability and skill and evaluates the link to the

large-scale extratropical circulation. Chapter 6 investigates the role of WCBs for atmospheric blocking over the European region. Many studies point to challenges in both model representation and forecast skill of this regime. In Chapter 7, the analysis is extended to other weather regimes in the Atlantic-European region. The overall forecast skill for regime onsets is evaluated, as well as the role of WCBs for regimes with high and low forecast skill. Chapter 8 then compares WCB biases and skill across S2S models and evaluates the role of model configuration. Lastly, it compares the link between WCB activity and the European Blocking regimes for the models. The study ends with concluding remarks and an outlook to future work.

2 Theoretical background

2.1 Warm conveyor belts (WCBs)

Warm conveyor belts (WCBs) are cloudy regions of strong, diabatically enhanced ascent ahead of the cold front of extratropical cyclones (Browning et al., 1973, Carlson, 1980, Harrold, 1973). WCBs contribute a major fraction of precipitation in the midlatitudes (Pfahl et al., 2014), and can cause heavy precipitation (Agel et al., 2019, Catto et al., 2015, Flaounas et al., 2016, Pfahl et al., 2014) and flooding (Grams et al., 2014). They were first described by Green et al. (1966) who identify a southerly air stream that ascended along the leading edge of an upper level trough where it produced an elongated cloud band. They conclude that trade winds appear to rise over a front into a jet stream in the upper troposphere. Similar findings were made by Browning et al. (1973) using isentropic analysis of radiosonde data. They find a very reasonable ascent magnitude for the slantwise ascent of the air masses (around 10 cm/s) which is modified by small-scale convection with updraft velocities of 1 m/s. Furthermore, they highlight that the generation of the precipitation mainly occurs within a narrow band of warm air which was named the "conveyor belt". The air masses in the conveyor belt region flow ahead of the cold front before ascending above the warm front (Fig. 2.1). Here, they mix with air masses from the upper troposphere to produce a lapse of near constant potential temperature.

The WCB air stream is typically identified as coherent bundle of Lagrangian air parcel trajectories which ascend 600 hPa in 48 h (Madonna et al., 2014). This trajectory based definition was first established in the late 1990s (Wernli and Davies, 1997, Wernli, 1997). In Wernli (1997), this definition is used to identify two different WCB branches in a coherent ensemble of trajectories for a case study in

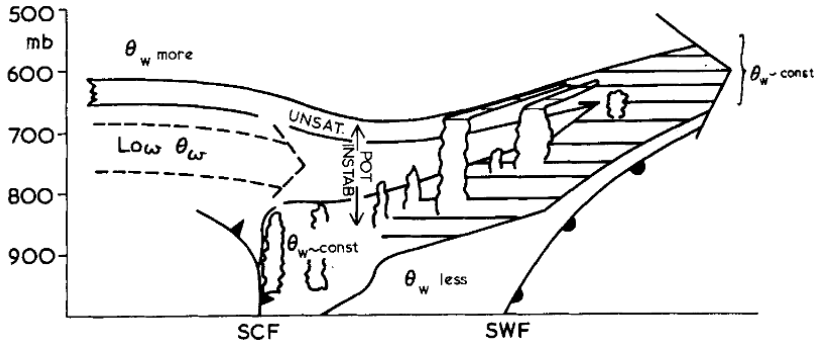


Figure 2.1: Schematic representative of the flows in the region of the cold front after Harrold (1973). Hatching denotes layer cloud and convective overturning is depicted by the small cumuli form shapes. Two initially separate flows, with lower θ_w (wet bulb potential temperature) between, mix to produce a lapse of near constant θ_w above the warm frontal zone.

November 1992 (Fig.2.2a). The results underline the previous theory of two different WCB branches by Browning (1997): one turning cyclonically towards to centre of the cyclone and one turning anticyclonically into the downstream ridge. In general, the outflow height is higher in the anticyclonic branch compared to the cyclonic branch. As shown in Fig. 2.2a, the most coherent phase of the WCB occurs after the start of the trajectories and before the end and corresponds to the period with strongest ascent.

The evolution of a WCB can be described in three distinct stages: WCB inflow, WCB ascent, and WCB outflow. During the inflow stage, WCB air is located in the planetary boundary layer of an extratropical cyclone's warm sector (blue colours in Fig. 2.2b). Though at this stage the air mass can be considered as passive tracer, an inaccurate representation of its moisture content may affect important characteristics of the WCB such as its diabatic heating rate and thus ascent and outflow height (Schäfler and Harnisch, 2015). During WCB ascent air rises ahead of the cold front and across the warm front (Fig. 2.1) in a region of quasi-geostrophic forcing for ascent (Binder et al., 2016) which results in precipitation below the WCB air stream. The strong latent heat release due to condensation further contributes to upward motion through cross-isentropic ascent (black dots in Fig. 2.2b). On average, this latent heat release amounts

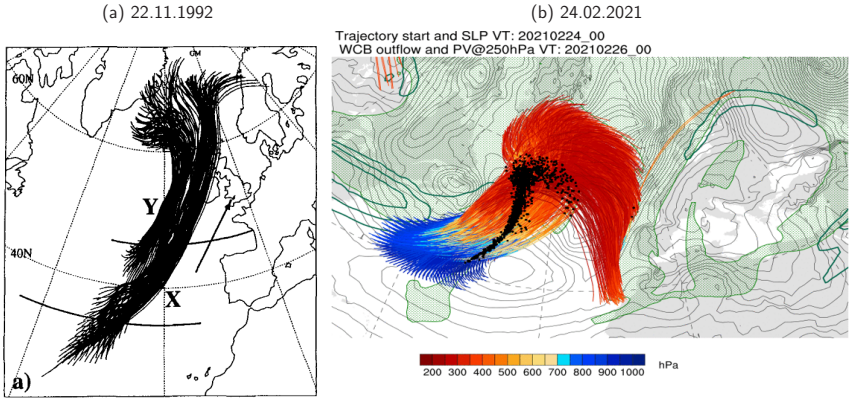


Figure 2.2: a) Coherent ensemble of trajectories on November 22 nd, 1992 identified with the selection criteria of ascent of at least 620 hPa after Wernli (1997). b) Trajectories ascending at least 500 hPa within two days on February 24 th, 2021. Black contours indicate mean sea level pressure at the start of the trajectory and shaded green areas show isentropic potential vorticity (>2PVU) at the outflow stage two days later. Black dots show region were latent heating occurs which leads to cross-isentropic ascent.

to 20 K within 48 h (Madonna et al., 2014). WCB outflow occurs in the upper troposphere around 400–200 hPa where cirrus clouds can form due to relatively high moisture content of the air stream (Green et al., 1966).

In the following, the potential vorticity (PV) - potential temperature (θ) framework (Hoskins et al., 1985) is used in order to describe the two major effects of the latent heat release on the further evolution of the WCB and its impact on midlatitude dynamics: the formation of cyclonic PV anomalies in the lower troposphere and the transport of low PV air to the upper troposphere. PV provides a unique framework to study dynamical processes in the atmosphere because it combines multiple meteorological variables (wind, temperature and pressure) in one scalar quantity:

$$PV = \frac{1}{\rho}\eta \cdot \nabla\theta, \tag{2.1}$$

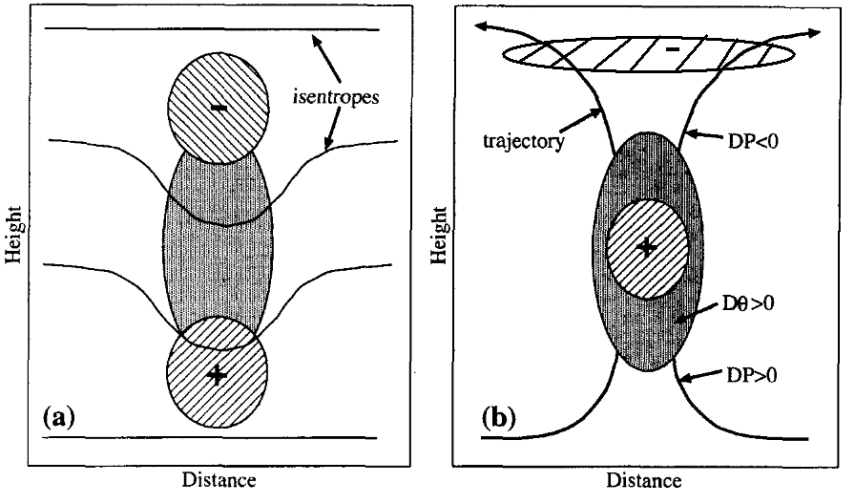


Figure 2.3: Schematic representations of diabatically produced positive and negative PV anomalies in the case of (a) impulsive diabatic heating and (b) steady diabatic heating after Wernli and Davies (1997). The region with diabatic heating is indicated by shading, and the diabatically produced PV anomalies by hatching with a plus or minus sign. The solid lines in (a) are isentropes and the curved arrows in (b) are ascending trajectories. Dθ and DP indicate material derivatives of potential temperature and PV, respectively.

with ρ being the density of the air mass and θ the potential temperature. The absolute vorticity (η) is defined as the sum of the relative vorticity ($\nabla \times \vec{v}$) and the planetary vorticity (2Ω) with $\vec{v}$ being defined as the three-dimensional wind vector. PV is conserved in an adiabatic and frictionless flow and commonly expressed in PV units (PVU): 1 PVU = $10^{-6} m^2 s^{-1} K kg^{-1}$. On the other hand, PV is modified by diabatic heating and frictional processes which typically occur in the atmospheric boundary layer.

$$\frac{D(PV)}{DT} = \frac{1}{\rho}\eta \cdot \nabla\dot{\theta} + \frac{1}{\rho}\nabla\theta \cdot (\nabla \times F), \tag{2.2}$$

where $\dot{\theta}$ stands for diabatic heating rate and F describes the frictional force. In the free atmosphere, the frictional force is generally small and the vertical gradient of diabatic heating on synoptic scales is higher compared to the horizontal contribution. Therefore Eq. 2.2 can be approximated by:

$$\frac{D(PV)}{DT} \approx \frac{1}{\rho}(\zeta + f)\frac{d\dot{\theta}}{dt}, \tag{2.3}$$

with the vertical vorticity ζ and the Coriolis parameter $f = 2\Omega \cdot sin(\phi)$. Diabatically produced positive and negative PV anomalies can develop in two different ways (Fig. 2.3). In the case of impulsive diabatic heating, PV anomalies are generated above and below the region of maximum heating. On the other hand, steady heating over a longer period of time leads to the vertical advection of the generated PV anomalies. Positive anomalies are advected into the region with maximum diabatic heating and contribute to the formation of the extratropical cyclone's PV tower (Rossa et al., 2000) and thus to its overall intensity (Binder et al., 2016, Davis et al., 1993). On the other and, low-PV air is transported into the upper-troposphere where the diabatically driven outflow of the flow amplifies the upper-level Rossby wave pattern and enhances or even triggers upper-tropospheric ridge building (Grams and Archambault, 2016).

In their study, Grams and Archambault (2016) investigate diabatic outflow from three different weather systems: a predecessor rain event, a tropical cyclone undergoing extratropical transition, and a warm conveyor belt. They highlight that the weather systems differ in terms of their associated outflow height and generated PV anomalies with the tropical cyclone having the highest outflow height and the WCB generating the strongest negative PV anomalies. Other case studies point to the importance of diabatically generated PV anomalies in establishing an upper level flow which favours downstream development of elongated PV streamers (Massacand et al., 2001). These PV streamers can lead to heavy precipitation events and flooding (Grams et al., 2014, Lenggenhager et al., 2019). When the diabatically generated low-PV air interacts with the upper-level flow, its is further advected polewards where it results in a marked anticyclonic PV anomaly in a region of climatologically high PV (Madonna et al., 2014). This

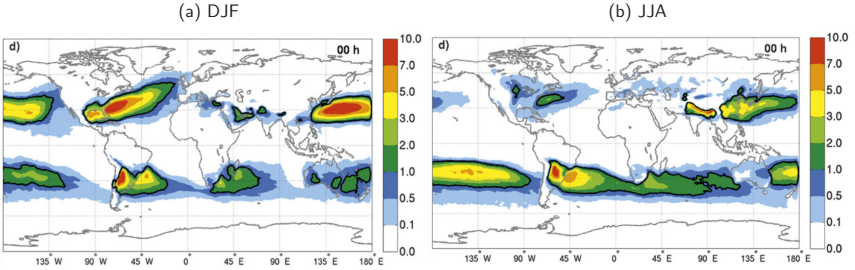


Figure 2.4: Climatological frequency of WCB trajectories in a) DJF and b) JJA at the start of the 2-day ascent after Madonna et al. (2014). Colors represent the relative frequency (in percent) of WCB trajectories at each grid point. The black contour in all panels represents a WCB frequency of 1%.

anticyclonic PV anomaly can become stationary and persistent, and might contribute to a blocking anticyclone (Pfahl et al., 2015).

In their study, Pfahl et al. (2015) for the first time, quantify the overall contribution of air masses that are diabatically heated before arriving in the blocked anticyclone in a large 21-year climatology. They show that 60–70% of the air masses are heated by at least 2 K in the seven days prior to the blocking onset (30–45% in the last three days). The analysis underlines that latent heating in clouds is of first-order importance for the formation and maintenance of blocking in addition to quasi-horizontal advection of low-PV air in the upper troposphere. These findings are further underlined by Steinfeld and Pfahl (2019) who show that the latent heating is most important during the onset of the block and in more intense and larger blocks. They also highlight a considerable variability of the contribution of latent heat release between the individual blocking events and different regions. The variability is especially large between oceans and continents with highest contribution over the North Pacific and North Atlantic region.

In these storm track regions over the North Pacific and North Atlantic region, the overall climatological WCB occurrence is highest throughout the Northern Hemisphere (Fig. 2.4). WCBs also occur in the storm track region over the Southern Hemisphere and generally vary in frequency between the summer and the winter season. Over the Northern Hemisphere, the highest WCB inflow frequencies in DJF can be found east of the USA and over the western Pacific

southeast of Japan (Fig. 2.4a). Frequencies are generally lower over the eastern North Pacific and over the eastern part of the North Atlantic. In summer, WCB activity in the Northern Hemisphere is highest over eastern Asia and the western North Pacific and lower over the North Atlantic region (Fig. 2.4b).

Due to the major dynamical impacts of diabatic processes in general and in particular in WCBs, errors that occur in NWP models in any of the three WCB stages may affect the representation of the large-scale midlatitude flow. Indeed, recent studies show growing evidence that errors in the representation of WCBs may lead to errors in the downstream Rossby wave pattern. Lamberson et al. (2016) investigate a strong cyclone which effected western Europe in December 2011. They show that forecast errors in the warm sector of an upstream cyclone over the eastern North Pacific propagated downstream and lead to an overestimation of the overall cyclone strength over the North Atlantic. For one of the most severe forecast busts for Europe in the European Centre for Medium-Range Weather Forecasts (ECMWF) Integrated Forecasting System (IFS) in recent years, Grams et al. (2018) highlight the role of WCBs for the onset of a blocking anticyclone over Europe. They find that a misrepresentation of the WCB in the ensemble forecasting system amplified the initial condition error and triggered a nonlinear feedback mechanism that communicated the forecast error far downstream and lead to the missed onset of the block. Other studies also point to the generation of errors in potential temperature and PV in the WCBs which can lead to downstream errors in Rossby waves (Berman and Torn, 2019, Martínez-Alvarado et al., 2016). Moreover, Rodwell et al. (2018) show that episodes with strong latent heat release in mesoscale convective systems over the USA lead to an insufficient representation of the jet stream downstream over the Atlantic. In summary, these case studies show that a more accurate representation of WCBs and PV anomalies may reduce forecast uncertainty in the downstream wave guide.

On the medium range, the representation of WCBs in NWP models was first evaluated by Madonna et al. (2015) for three winter periods (December, January, and February - DJF) in the operational high resolution deterministic forecast of the

ECMWF Integrated Forecasting System (IFS) model. They use a novel feature-based verification technique that was originally developed to verify precipitation forecasts (Wernli et al., 2008) and find evidence that periods with low forecast skill in terms of geopotential height can be connected to a misrepresentation of the WCB outflow in the forecast model. Furthermore, Madonna et al. (2015) find an improvement in WCB forecast skill from the winter season of 2002/2003 to 2010/2011 which they assign to the overall improvement in model forecast skill over this decade (Magnusson and Källén, 2013). Still, a systematic investigation of the representation and forecast skill of WCBs has not been addressed yet. This is due to the high computational costs in calculating 3D trajectories and availability of model data at high horizontal ($\mathcal{O}(\sim 1^\circ)$), vertical ($\mathcal{O}(\sim 10\,\mathrm{hPa})$), and temporal resolution ($\mathcal{O}(\sim 3-6\,\mathrm{hrs})$) which is usually not archived. Novel approaches are therefore needed in order to systematically investigate the representation of WCBs in NWP models.

2.2 Atlantic-European weather regimes

Weather regimes are quasi-stationary, persistent, and recurrent large-scale flow patterns in the midlatitudes (Michelangeli et al., 1995, Vautard, 1990). They are based on the idea that the large-scale atmospheric circulation can in practice be represented by a finite number of possible atmospheric states which describe the long-lived, large-scale circulation pattern perturbed by individual highs and lows. These patterns present themselves quite frequently and are in contrast to day to day weather which evolves continuously with time.

The weather regimes were first introduced on the basis of atmospheric blocking which hinders the westerly flow and eastward propagation of synoptic eddies and is characterised by persistent, large-scale anticyclonic circulation anomalies (Berggren et al., 1949, Rex, 1950). In his study of 112 blocking events over the Atlantic and Pacific, Rex (1950) finds a relatively long persistence of 12 to 16 days of the blocks. Furthermore, the analysis of the characteristics of different summer and winter blocking events over Europe identify only small variations in the blocks (Rex, 1951). The persistence and small variations of the blocks

gave him assurance to introduce a weather regime for the first time which was associated with blocking over the European region (Rex, 1951).

In the following, barotropic or quasi-geostrophic models were used to develop corresponding theories. Charney and DeVore (1979) use a barotropic model with topography and identify two stable equilibrium states of very different character which may be produced by the same forcing. This concept was expanded by Legras and Ghil (1985) who use more degrees of freedom and identify multiplicity of weather regimes, some with a more zonal flow and others with blocking. Other studies developed theories for the formation and maintenance of blocking by planetary waves or orographic forcing (Hoskins and Karoly, 1981).

A statistical-dynamical approach was introduced by Vautard and Legras (1988) to quantify weather regimes incorporating the feedback of transient eddies which themselves depend non-linearly on the large-scale flow. They identify several regimes corresponding to zonal and blocking situations and show that the block is maintained against dissipation by small scale fluxes. These findings are in line with previous studies which had pointed to the importance of transient eddies and synoptic-scale processes for the formation and maintenance of atmospheric blocking (Shutts, 1983) since certain aspects of the blocking life cycle (i.e. the fluctuation of size and intensity) could not be explained by previous theories (Dole, 1986).

Vautard (1990) then applies the algorithm used in the previous study (Vautard and Legras, 1988) to a large data set containing 37 winter periods. He identifies weather regimes based on nine nonlinear statistical equations giving the balance of the large-scale average tendency. With this approach, four weather regimes are found (Fig. 2.5): one with a more zonal flow (ZO) (Fig. 2.5a), one with a block over Greenland (GL) (Fig. 2.5b), one characterised by the blocking over the European region (BL) (Fig. 2.5c), and lastly one regime with a block over the eastern Atlantic (AR) (Fig. 2.5d).

Furthermore, he shows that the onset of the regime is rather sudden and identifies preferred regime transitions. Blocking over Europe is more likely established

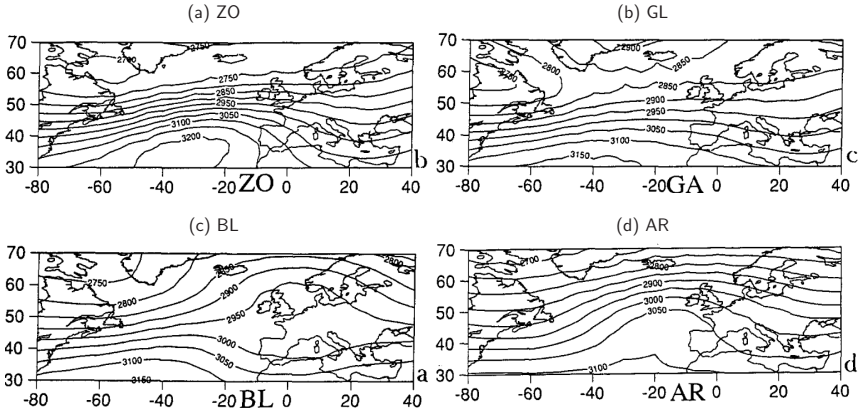


Figure 2.5: Contours of the 700 mb anomalies (in m) associated with the four quasi-stationary patterns a) ZO, b) GL, c) BL, d) AR after Vautard (1990).

from a zonal regime and the European blocking typically precedes blocking over Greenland. The identification of four weather regimes is underlined by Michelangeli et al. (1995) who compare the calculation of regimes with nonlinear statistical equations and cluster analysis. Both calculations give the same number of regimes but differ in the regime patterns. Other clustering approaches calculate the regimes as clusters in a multi-dimensional principal component phase space (Corti et al., 1999).

These studies in the 1980s and 1990s show that there are many possible definitions of weather regimes. This is due to several degrees of freedom in terms of the selected region, number of regimes, persistence, as well as seasonality. Still, common characteristics emerge between the regime definitions: the large spatial extent of the regimes affecting continent size and their persistence of typically longer than 10 days. Most studies come up with four regimes in the Atlantic-European sector: Michelangeli et al. (1995) calculate that the ZO regime occurs at 32% and GL at 21% of the times. Furthermore, the Atlantic Ridge and Blocking over Europe make up 22 and 25% of the times, respectively. The definition of four regimes seems to be optimal regimes which are only defined in a specific

season.

Weather regimes modulate surface weather strongly and are connected to weather extremes on a regional scale (Buehler et al., 2011, Ferranti et al., 2015, Pfahl and Wernli, 2012, Spensberger et al., 2020). Recent studies show connections between episodes with anomalously cold temperatures in winter (cold spells) and weather regime life cycles. Buehler et al. (2011) point to the strong connection between cold spells and extremes in blocking frequency. They highlight that the number of cold spell days increases with the duration of the blocking event. Other studies describe that cold air outbreaks over the Atlantic ocean basin can occur during Atlantic Ridge and Greenland Blocking regimes, as well as different cyclonic regimes (Papritz and Grams, 2018).

On the other hand, the persistence of a weather regime in summer can trigger heat waves with temperatures exceeding 30 degrees Celcius for an extended period of time. Pfahl and Wernli (2012) show that more than 80% of the warm temperature extremes over the Northern Hemisphere can be associated with atmospheric blocking. These findings are underlined by Schaller et al. (2018) who find a significant correlation between summer heatwave magnitude and the number of days influenced by atmospheric blocking in northern Europe and western Russia. Lastly, Spensberger et al. (2020) show that heat waves over Scandinavia and central Europe can occur simultaneously in a blocked regime over Scandinavia which is characterised by strong positive geopotential height anomalies over Scandinavia and negative anomalies over the eastern Atlantic.

Other studies show the role of weather regimes in modulating surface precipitation in the Atlantic-European region or thunderstorm episodes in summer (Mohr et al., 2019). Yiou and Nogaj (2004) show that the positive phase of the North Atlantic Oscillation (NAO+) which is similar to the ZO regime is most important for precipitation extremes over northern Europe. On the other hand, the negative phase of the NAO (NAO-) which is similar to the GL regime can lead to high precipitation over southern Europe. The European blocking regime can cause heavy precipitation predominantly over eastern Greenland and the Mediterranean region.

Piaget et al. (2015) and Lenggenhager et al. (2019) evaluate the role of large-scale flow regimes for flooding events over the Alps in October 2000 and 2011. The findings show that there is an interaction between weather regimes and long range moisture transport from the tropics (Piaget et al., 2015). Furthermore, flooding events can be linked to PV streamer upstream or downstream of blocked regimes over Europe and the North Atlantic (Lenggenhager et al., 2019). They further highlight the important contribution of diabatically heated air masses from the region of heavy precipitation for the maintenance of the block. As described in the previous Section, these air masses are a first-order process for the onset and maintenance of blocking anticyclone. These studies underline the modulation of smaller scale processes (like heave precipitation or moisture transport) by large-scale flow regimes but also show that the large-scale regimes themselves are modulated by processes on the smaller synoptic scales. The study at hand aims to link the two scales and increase knowledge about the modulation of the flow regimes by the synoptic scale.

The occurrence frequency of weather regime in the Atlantic-European region is for instance modulated by organized deep moist convection associated with the Madden-Julian oscillation (MJO) (Cassou, 2008, Lee et al., 2019) and fluctuations of the stratospheric polar vortex (Beerli and Grams, 2019, Charlton-Perez et al., 2018). The MJO consists of large-scale coupled patterns in atmospheric circulation and deep convection and is the dominant component of the intraseasonal (30–90 days) variability in the tropical atmosphere (Madden and Julian, 1971, 1972, Zhang, 2005). It affects the midlatitudes through the propagation of Rossby waves which can lead to wave breaking in the North Pacific and changes in the circulation over the North Atlantic (Cassou, 2008, Lin et al., 2009).

Cassou (2008) shows that the positive phase of the NAO occurs predominantly after active MJO phases 2–5 (Fig. 2.6) which results from a mid-latitude low frequency train initiated by the MJO over the western-central Pacific. On the other hand, MJO phases 6–8 leads the enhanced occurrence frequencies of the negative phase of the NAO. These teleconnections are further modulated by other tropical heat anomalies like the El Nino Southern Oscillation (Lee et al., 2019).

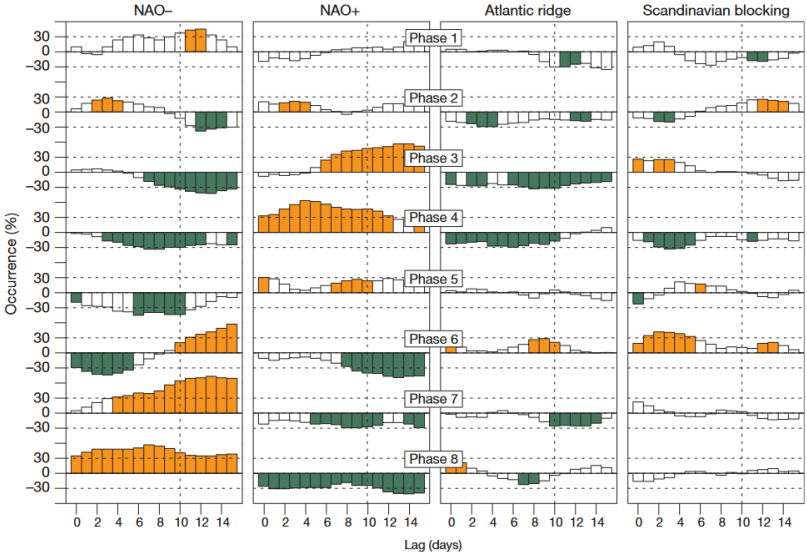


Figure 2.6: Lagged relationships between the eight phases of the MJO and the four North Atlantic weather regimes after Cassou (2008).

During El Nino years, the teleconnection into the positive phase of the NAO is strongly enhanced due to the enhanced Rossby wave activity. On the other hand, the teleconnection is suppressed during La Nina years. The teleconnection into the negative phase of the NAO is enhanced during La Nina years and surpressed during El Nino years.

Other studies point to the modulation of blocking in the midlatitudes after active MJO phases (Henderson et al., 2016). Blocking frequencies over the eastern North Pacific and over the North Atlantic are smaller after MJO phase 3 while MJO phase 7 enhances blocking frequencies over the eastern Pacific and the Atlantic.

The extreme states of the stratospheric polar vortex modulate weather regime frequencies over the North Atlantic through stratosphere/troposphere interaction

(Baldwin and Dunkerton, 2001). The negative phase of the NAO is most sensitive to the polar vortex where 33% of the days follow weak vortex conditions and only 5% of days follow strong vortex conditions (Charlton-Perez et al., 2018). For events with strong polar vortex states, the NAO positive regime becomes more likely while it is suppressed following weak vortex states. The modulation by the stratosphere is weaker for other Atlantic-European weather regimes that project less into the NAO (Beerli and Grams, 2019). In their study, Beerli and Grams (2019) use a novel approach of seven year-round weather regimes (Grams et al., 2017) and identify two different pathways for high wind events over Europe which usually occur during NAO+ regimes. However, they also occur during the Atlantic trough regime which is associated with strong cyclone activity over the eastern Atlantic and unaffected by anomalous stratospheric polar vortex states. Therefore, it provides a pathway to Central European high wind events during weak stratospheric polar vortex states where the NAO- regime response is typically associated with low wind cold temperatures.

Their study shows the advantages of using a novel approach of seven Atlantic-European weather regimes which are based on a strict persistence criteria and which can occur all year round instead of only in a specific season. In the study at hand, the seven year-round weather regime definition is therefore used to evaluate the link of WCBs and weather regimes. The calculation of the regimes and their definition is further introduced in Chapter 4.3.

2.3 Predictability on sub-seasonal time scales

At the beginning of the 20 th century, Abbe (1901) and Bjerknes (1904) corroborated that a prediction of a subsequent state of the atmosphere develops from a preceding one according to physical law. An accurate prediction of the future state then depends on both a sufficient knowledge about the state of the atmosphere at initial time and a sufficient knowledge about the physical laws according to which one state of the atmosphere develops from another (Bjerknes, 1904).

The change in space and time of different variables in the atmosphere (i.e. wind, temperatures, pressure, and density) depends on a variety of different equations (Navier-Stokes equation, mass continuity equation, first law of thermodynamics, and ideal gas law). The Navier-Stokes equation combines the rate of change of the three-dimensional wind vector and the forces which impact an air parcel in the atmosphere:

$$\frac{d\vec{v}}{dt} = -\frac{1}{\rho}\nabla p - g \cdot \vec{k} - 2(\vec{\Omega} \times \vec{v}) + \vec{F}, \tag{2.4}$$

with the three-dimensional wind vector $\vec{v}$, the density ρ, the pressure force p, and the gravitational force g. Ω describes the rotation of the earth and $\vec{F}$ includes all frictional forces. The rate of change of the wind field is then determined by the pressure gradient force, the gravitational force, the Coriolis force and frictional forces. The mass continuity equation combines local changes and the advection of density:

$$\frac{\partial \rho}{\partial t} = -\nabla(\rho \cdot \vec{v}), \tag{2.5}$$

and the first law of thermodynamics describes the internal energy of an air mass which increases according to the heat supplied and diminishes according to the work done by the system:

$$dU = dQ - dW, \tag{2.6}$$

with the internal energy of a system U, sensible heat Q and the work done due to expansion and contraction W. Lastly, the ideal gas law which expresses the relationship of the pressure a gas exerts to the volume it occupies and its temperature. It is described as:

$$p = \rho RT, \tag{2.7}$$

with the gas constant R. These equations need to be solved to predict the state of the atmosphere for a given time in the future.

However, analytical solutions of the equations are not possible at this point in time which requires numerical solutions. This problem creates a distinction between scales that are resolved and those that are unresolved. Unresolved scales are for instance processes on scales below the grid space of a numerical weather prediction model (like latent heat release in WCBs). These processes need to be parameterised since they are unresolved in terms of reaction with the resolved scales. Uncertainties in the interaction of resolved and unresolved scales can create forecast errors in numerical weather prediction models and can limit the overall predictive skill of the model.

The predictive skill of the NWP models are further limited by the behaviour of the atmosphere which lacks complete periodicity in its evolution (Lorenz, 1963). This is i.e. expressed in two slightly different initial states which evolve based on the same laws of physic but in time develop into two entirely different states. The slightly different initial state can emerge from a lack of observations in a regions, errors in measurements or simply the inability to cover the entirety of the state of the atmosphere. Therefore, there is a lack of knowledge which of the multitude of considerable different states will evolve at a given time in the future.

Charney (1966) summarises the different modeling studies at that time and find that the forecast error doubles within 5 days after the initialisation. Smagorinsky (1969) for the first time develops a more refined model which includes moist processes and other features not represented in earlier models. In his model, the smallest errors double within three days. This doubling time of the errors equals a limit of predictability of around 2 weeks given the initial condition error at that time.

The reduction of errors at the initial state of the forecast does not automatically yield longer predictability (Lorenz, 1969). This is due to faster error growth on smaller spatial scales which leads to a similar predictability limit of i.e. two states that differ considerably at forecast initialisation and two states which are

very similar at initialisation time. Lorenz (1969) further corroborates different predictability limits for different spatial scales with a limit of around one hour for the cumulus scale (convective scale), a few days for the synoptic scale, and a few weeks for the largest scales. For this larger scale, Lorenz (1982) corroborates that forecasts for weather patterns nearly two weeks in the future seem possible.

In the following two decades, there has been a considerable improvement in the accuracy of NWP models which lead to realistic prediction of certain weather patterns three weeks in advance (Simmons and Hollingsworth, 2002). This improvement can be attributed to new observation techniques (satellites and ground observations), global efforts in data assimilation to decrease the errors at forecast initialisation and a growing knowledge about physical processes and their representation in the models.

Another major contribution to exploit the limits of predictability has been made by the introduction of ensemble forecasts at operational weather centers like the European Center for Medium-Range Weather Forecast (ECMWF) and the National Center for Environmental Prediction (NCEP) in the early years of the 1990s (Buizza and Palmer, 1995, Palmer, 1993, Toth and Kalnay, 1993). They use a variety of different forecasts instead of only one single forecast to estimate different probabilistic states of the atmosphere at a given time in the feature. These ensemble forecasts account for uncertainties in the initial conditions and uncertainties in the NWP model which arises from parameterisation of unresolved processes. The generation of ensembles provides a more complete estimate of the future state since they include a range of different possible scenarios of the state of the atmosphere or a likelihood of occurrence of an event of interest (Buizza et al., 2008, Palmer et al., 2007). The probabilistic forecasts can carry useful information even close to the limits of predictability.

The improvements in NWP models and the shift to ensemble forecasting systems lead to the start of monthly weather forecasts in the early 2000s (Vitart, 2004). The ECMWF's forecasting system was able to produce skillful weekly forecast for forecast day 12–18 suggesting that forecasts at these time scales might be

useful. Vitart (2004) shows that at the time range beyond 20 days, forecasts over Europe are particularly difficult while some useful skill can be found over North America and Asia.

Over the years, significant improvements have been made for monthly weather forecasts. The skill in the prediction of the Madden-Julian oscillation has increased by about 10 days over the course of 10 years yielding in predictive skill of the tropical phenomena up to forecast day 27 (Vitart, 2014). Since the MJO modulates the large-scale circulation in the midlatitudes (see Section 2.2), this also resulted in a significant increase of the forecast skill in the extratropics. The skill of the North Atlantic Oscillation (NAO) has increased from 9 days at the beginning of the operational monthly forecast to around 13 days in 2012. Vitart (2014) further notes that most of the improvements in the forecast skill can be attributed to changes in model physics which were primarily introduced to improve the model climate and medium-range forecasts. However, monthly forecasts also benefited from these changes while the horizontal and vertical resolution of the model only played a minor role.

The progresses in the monthly numerical weather forecasts has resulted in a growing interests from various socio-economic groups in accurate weather predictions on time scales that have long been seen as the predictability desert of weather forecasts (Fig. 2.7). Recent studies especially point to the usefulness of sub-seasonal forecasts for the energy sector (Beerli and Grams, 2019, Bloomfield et al., 2021, Grams et al., 2017), for the provision of early warnings for heat wave and cold spells (Ferranti et al., 2018, Kautz* et al., 2020), and for the agriculture sector (Gibson et al., 2020, Zamora et al., 2021). However, the generation of sufficient forecast skill on sub-seasonal time scales is still a major challenges for numerical weather prediction models.

Sub-seasonal time scales occur between the medium-range time scales of around 2 weeks and the seasonal time scales of several months. In the medium-range, the initial conditions of the atmosphere provide predictability (Fig. 2.7) which decreases relatively fast due to the chaotic nature of the system (Lorenz, 1963).

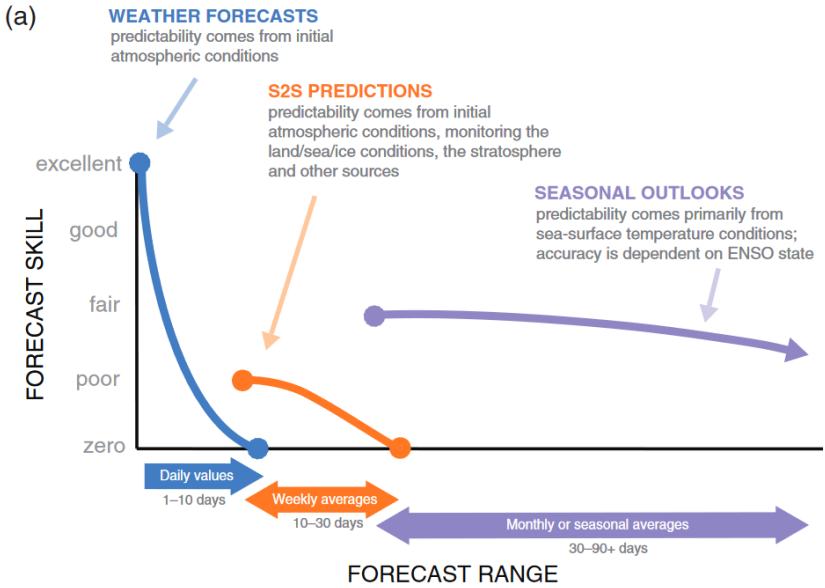


Figure 2.7: Qualitative estimate of forecast skill based on forecast range from short-range weather forecasts to long-range seasonal predictions, including potential sources of predictability after White et al. (2017). Relative skill is based on differing forecast averaging periods.

On seasonal time scales, slower climate modes (i.e. ocean, land surface, sea ice) provide predictability for the atmosphere through complex interactions on different spatial and temporal scales (Fig. 2.7). Sub-seasonal time scales depend on both the initial conditions of the medium-range forecasts and information about boundary conditions of drivers of seasonal predictability.

The important drivers of sub-seasonal predictability in the Northern Hemisphere are summarised in Fig. 2.8. As introduced in the previous Section, the MJO, ENSO and the stratospheric polar vortex modulate weather regimes and are important drivers of sub-seasonal predictability (see f.e. Lee et al. (2019)). They interact with the large-scale extratropical circulation which is governed by large-scale Rossby waves. The Rossby wave activity in the midlatitudes determines the

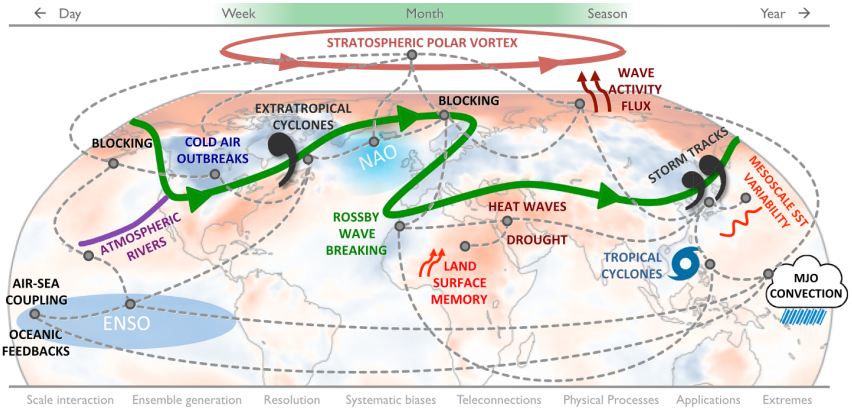


Figure 2.8: Overview of processes on different spatial and temporal scales that are important drivers of predictability on sub-seasonal time scales after Lang et al. (2020).

location of extratropical cyclones and can lead to atmospheric blocking resulting in heat waves or cold air outbreaks.

The breaking of Rossby waves can further enhances the blocked regimes or lead to transitions into other large-scale flow patterns. Processes over the land and ocean further influence the location of the jet stream and the Rossby wave pattern providing predictability on sub-seasonal time scales (Dirmeyer et al., 2019, Subramanian et al., 2019). As introduced in Section 2.1, processes on the synoptic scales (like WCBs in extratropical cyclones) can further influence the Rossby wave propagation and breaking and influence predictability and forecast skill on sub-seasonal time scales. Thus, the combination of different processes which interact on different spatial and temporal scales remains a major challenge for sub-seasonal weather prediction.

However, with growing forecast skill for the MJO and NAO on sub-seasonal time scales (Vitart, 2014), there also have been substantial efforts to improve sub-seasonal forecast skill for region with generally lower forecast skill (e.g. Europe). The improvement of the overall sub-seasonal forecast skill over region like Europe is likely tied to an improvement in the prediction of Atlantic-European

weather regimes. A recent study by Bloomfield et al. (2021) shows that the predictive skill for energy variables is enhanced using pattern based conditioning on time scales beyond 12 days compared to grid point based. Furthermore, Mastrantonas et al. (2022) use weather regimes to predict extreme precipitation over the Mediterranean region and find that the connection between regimes and precipitation extends the forecast skill for the extreme event by around three days. They conclude that it is beneficial to use predicted patterns instead of predicted precipitation. These recent findings indicate that improving the prediction of Atlantic-European weather regimes would likely also yield an increase in the overall predictive skill for surface variables and extreme events in the European region.

As introduced in Section 2.2., weather regimes in the Atlantic-European region are modulated by slower climate modes (i.e. MJO, stratospheric polar vortex (SPV)) and influenced by synoptic scale processes (i.e. latent heat release in WCBs). Thus, in principle, the MJO and SPV provide predictability for weather regimes on sub-seasonal time scales where synoptic-scale processes are more challenging for the NWP model to capture. However, recent studies show that an incorrect representation of the synoptic-scale processes in the NWP model might dilute the provided predictability by the MJO and SPV which would cause a systematic reduction in the predictive skill of regimes (Grams et al., 2018, Maddison et al., 2019).

For an earlier version of the statistical WCB models, Wandel et al. (2021) find a systematic link between the forecast skill for the large-scale circulation over the North Atlantic and periods with high and low WCB activity (Fig. 2.9). For the analysis, they calculate the Anomaly correlation coefficient (ACC) for the upper-level large-scale flow in 200 hPa in the ECMWF's IFS reforecasts (DJF; 1997–2017) during times with high WCB outflow frequencies (upper 33%) compared to times with low WCB activity (lower 33%). They find a significant different forecast skill horizon of slightly more than 1 day which indicates that there might be a systematic link between high WCB activity and low forecast skill, and that a better representation of WCBs in the forecast model could lead

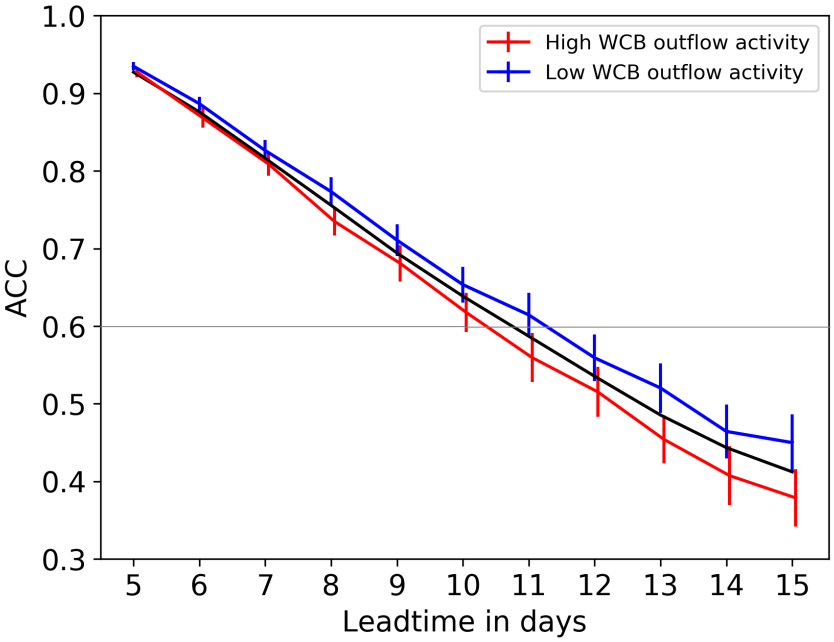


Figure 2.9: ACC of 200-hPa geopotential height over the North Atlantic region (20–90°N, 80°W–20°E) for DJF in the period January 1997 to December 2017 from Wandel et al. (2021). Black line shows area-averaged ACC for all 920 forecasts. Red (blue) lines indicate forecast skill during periods with highest 25% (lowest 25 %) WCB outflow activity in this region (230 forecasts, respectively). The red (blue) bars highlight the 95 th confidence interval when applying a bootstrapping and generating 1000 subsamples.

to an increase in forecast skill for the large-scale extratropical circulation.

Büeler et al. (2021) calculate the overall forecast skill of the seven year-around Atlantic-European introduced by Grams et al. (2017) in the sub-seasonal reforecasts of the European Center for Medium-Range Weather Forecasts (ECMWF) Integrated Forecasting System (IFS) (1997–2017). The average skill of the regimes is around 15–20 days with generally higher forecast skill in winter compared to summer (around 5 days longer) (Büeler et al., 2021). The forecast skill

of all regimes is relatively high after MJO phases 4 and 7 which indicates that the NWP model can capture some aspects of the enhanced predictability of the atmosphere provided by the slower climate mode. However, the forecast skill is reduced after MJO phase 2. Recalling that the teleconnections after MJO phase 2/3 typically lead to NAO+ patterns, these findings indicate that the model might have difficulties in establishing the midlatitude circulation leading to NAO+ patterns.

Büeler et al. (2021) further show that the reforecasts have enhanced skill after strong SPV states and reduced skill after weak states. For the individual weather regimes, the forecast skill varies strongly with highest year-round skill for GL and ZO. This enhanced skill is mostly driven by their strong persistence in winter. Blocking over Europe (EuBL) has the lowest overall forecast skill in all seasons which is 3–5 days lower compared to the other regimes.

The representation of atmospheric blocking over Europe has been investigated in numerous studies in the last two decades. Matsueda and Palmer (2018) use the four seasonal weather regimes and identify the forecast skill in the winter season. They find the lowest overall forecast skill for Blocking over Europe initialised from Atlantic Ridge. Furthermore, low forecast skill can also be found for the same regime when initialised from NAO+. The findings are in line with Büeler et al. (2021) and show that the NWP models still have problems in predicting blocking over Europe. These difficulties can partly be linked to its lower intrinsic predictability (Faranda et al., 2016, Hochman et al., 2021), but might also arise from physical processes (like LHR in WCBs) that are still challenging for the model to capture. The NWP model especially struggles in predicting the rapid onset of EuBL (Ferranti et al., 2015, Rodwell et al., 2013) which could point to an important role of synotpic-scale processes in significantly contributing to low forecast skill since they are in particular important for the onset of blocking (Steinfeld and Pfahl, 2019). On top of the relatively low forecast skill of EuBL, many studies further find an underestimation of blocking frequency (negative bias) over the European region (d'Andrea et al., 1998, Masato et al., 2014). This bias increases with longer lead time (Jia et al., 2014, Quinting and

Vitart, 2019) and can be reduced with higher horizontal and vertical resolution (Anstey et al., 2013, Dawson et al., 2012). However, the improvement due to increased resolution partly results from compensating effects of errors at upper and lower levels (Davini et al., 2017).

In conclusion, major progress in weather forecasting has led to a growing interest in forecasts on sub-seasonal time scales between two weeks and several months. Forecasts on these time scales depend on well-resolved initial states of the atmosphere, as well as an accurate prediction of slower climate modes. However, the predictability on sub-seasonal time scales provided by slower climate modes might be diluted by synoptic-scale processes (like latent heat release in WCBs) which are typically more challenging for the model to capture. The relatively low forecast skill of sub-seasonal forecast models over Europe together with the low skill and misrepresented frequency of EuBL might point to an important role of synoptic-scale processes in diluting the provided predictability. The study at hand evaluates the role of the WCB for the low forecast skill and its overall representation in sub-seasonal forecast models.

3 Research questions

In this study, the representation of WCBs in NWP models and their link to Atlantic-European weather regimes is evaluated to understand the role WCBs for weather prediction on sub-seasonal time scales. Therefore, different research questions are introduced which are then investigated in detail in Chapter 5–8 of this study.

In chapter 5, the WCBs are evaluated in ECMWF's IFS sub-seasonal reforecasts (1997–2017) and the following research questions are addressed:

- How well are warm conveyor belts represented in Numerical Weather Prediction models?
  - Are there systematic biases for the inflow, ascent, and outflow stage of the WCB and is there a link to meteorological variables which are closely related to processes in the WCB?
  - Until which lead time can WCBs be skillfully predicted and how reliable are the forecasts?
  - Is there a systematic relationship between errors in the forecast of WCBs and errors in the large-scale flow?

These questions are motivated by (1) the impact of WCBs on the large-sale extratropical circulation, especially on the amplification of upper-level ridges which can become persistent blocking anticyclones, (2) the forecast errors which can be generated or amplified in the WCB and which can lead to downstream forecast errors and missed onsets or transitions of weather regimes, and (3) the lack of

systematic analyses of WCB representation in data sets including a large number of reforecasts from multiple decades.

For the analysis, a novel approach from Quinting and Grams (2021a) is used to calculate WCB inflow, ascent, and outflow masks based on a set of convolutional neural networks and WCB predictor variables. This approach allows the systematic verification of WCB representation in a data set where the trajectory definition (Wernli and Davies, 1997) can not be applied due to lack of model level data. Thus, for the first time, this study is able to evaluate the overall representation of WCBs in NWP model.

In Chapter 6, the representation of WCBs in the NWP model is investigated around the onset of blocking over the European region (EuBL) and the following research questions are addressed:

- Is there a link between the prediction of atmospheric blocking over Europe and warm conveyor belt activity?
  - How well can the reforecasts represent the characteristics of EuBL in terms of geopotential height in 500 hPa (Z500) and WCB activity?
  - Are there structural differences between reforecasts and reanalysis in the evolution of Z500 and WCB activity prior to EuBL onsets?
  - Does the predictive skill for EuBL depend on WCB activity?

These questions are motivated by the (1) importance of latent heat release in WCBs for the onset and maintenance of blocked anticyclones (Pfahl et al., 2015, Steinfeld and Pfahl, 2019), (2) the overall low skill of EuBL in medium-range and sub-seasonal forecast models (Büeler et al., 2021, Matsueda and Palmer, 2018), (3) and case studies pointing to the role of synoptic scale processes for missed EuBL onsets (Grams et al., 2018, Maddison et al., 2019). The analyses evaluate the importance of diabatic processes in WCBs for the predictive skill of EuBL and show how the NWP model establishes EuBL onset via WCB activity.

In Chapter 7, the overall predictability and forecast skill for the onset of Atlantic-European weather regimes across different forecast lead times in the medium-range and on sub-seasonal time scales is evaluated. Furthermore, the role of WCBs for the onset of the regimes (predominantly blocked regimes) is assessed and the following research questions are addressed.

- Do WCBs influence predictability and forecast skill of Atlantic-European weather regimes?
  - How well can the NWP model predict the onset of weather regimes?
  - What is the role of WCBs for the regime onsets and does it need to be resolved well in the model to capture the onset?
  - Do WCBs play a role in the forecast of blocked regimes over Europe in boreal summer which are typically associated with heat waves?

These questions are motivated by the the importance of weather regime for sub-seasonal prediction on time-scale where the prediction of flow patterns is more useful for surface weather and extremes compared to predicted variables (Bloomfield et al., 2021, Mastrantonas et al., 2022). Differences in terms of forecast skill of the regime onsets are evaluated and compared to the overall forecast skill found in Büeler et al. (2021). Furthermore, the role of the WCB for the different regimes is evaluated since diabatic processes in WCBs are in particular important for blocked anticyclones (Pfahl et al., 2015, Steinfeld and Pfahl, 2019).

Chapter 8 then compares the representation of WCBs and the link between WCBs and Atlantic-European weather regimes in different sub-seasonal numerical weather prediction models and the following research questions are addressed:

- Does WCB representation and the link to Atlantic-European weather regimes depend on the configuration of the NWP model?
  - Do similar WCB biases emerge in different NWP models and do the models have a different forecast skill horizon for WCBs?

- Does the role of WCB activity for EuBL onsets vary between the models?

These questions are motivated by the different forecast skill for the large-scale extratropical circulation in sub-seasonal forecast model (Son et al., 2020). This Chapter evaluates how well the WCB is represented in the models and if they have a different representation of WCB activity around EuBL onsets.

4 Data and Methods

This Chapter gives an overview over the data which are used in this study and the methods which are applied to evaluate the representation of WCBs and the link to Atlantic-European weather regimes. The different NWP models to study WCBs and weather regimes are introduced in Section 4.1. together with an introduction of the reanalysis data set which is regarded as the observational truth to evaluate WCB representation. In Section 4.2., the statistical model to study WCBs is introduced together with the predictor variables for the inflow, ascent, and outflow stage of the WCB. Section 4.3. introduces the seven year-round Atlantic-European weather regimes and Section 4.4. gives an overview over the verification methods to quantify WCB representation and the different approaches to link WCB activity and Atlantic-European weather regimes.

4.1 Model and reanalysis data

This Section gives an overview of the NWP models and reanalysis data set used in this study. The forecast data set contains reforecasts from different NWP models from the Subseasonal-to-Seasonal (S2S) database (Vitart et al., 2017). These data sets are compared to the ECMWF's Interim reanalyis (ERA-Interim) (Dee et al., 2011) which serves as a reference for the observational truth.

4.1.1 Subseasonal-to-Seasonal (S2S) database

A systematic investigation of the representation of WCBs in state-of-the-art NWP models requires a consistent data set that covers several years. Therefore, in this study, NWP models from the S2S Prediction Project database (Vitart et al., 2017)

Table 4.1: Characteristics of sub-seasonal weather forecast models from the S2S database in terms of horizontal resolution (longitude and latitude) and model levels (number after L represents the amount of vertical levels), as well as reforecast periods, ensemble members, initialisation times, ocean coupling, and sample size in boreal winter (DJF). *different model cycles are used for the ECMWF model to increase sample size

	resolution	period	members	frequency	Ocean	DJF
BOM	2°x2°,L17	1981–2013	31	6/month	Yes	594
CMA	1°x1°,L40	1994–2013	4	daily	Yes	1800
CNRM	0.7°x0.7°,L91	1993–2014	15	4/month	Yes	352
ECCC	0.45°x0.45°,L40	1995–2014	4	weekly	No	320
ECMWF	0.25°x0.25°(0-10d) 0.5°x0.5°(10-46d),L91	1997–2017	11	2/weekly*	Yes	920
HMCR	1.1°x1.4°,L28	1985–2010	10	weekly	No	289
JMA	0.5°x0.5°,L60	1981–2011	5	3/month	No	279
NCEP	1°x1°,L64	1999–2010	4	daily	Yes	1080
UKMO	0.5°x0.8°,L85	1993–2015	7	4/month	Yes	368

are used with a main focus on the ECMWF's IFS reforecasts. The S2S database was established in 2015 based on the growing interest and potential for improved forecast skill on sub-seasonal time scales. It is the extension of the "THORPEX Interactive Grand Global Ensemble" (TIGGE) database for forecasts up to 15 days which was originally set up for the "The Observing System Research and Predictability Experiment" (THORPEX) (Shapiro and Thorpe, 2004).

The S2S database contains reforecast data from eleven different operational weather centers (Vitart et al., 2017): the Australian Bureau of Meteorology (BoM), the China Meteorological Administration (CMA), the European Centre for Medium-Range Weather Forecasts (ECMWF), Environment and Climate Change Canada (ECCC), the Institute of Atmospheric Sciences and Climate of the National Research Council (CNR-ISAC), the Hydrometeorological Centre of Russia (HMCR), the Japan Meteorological Agency (JMA), the Korea Meteorological Administration (KMA), Météo-France/Centre National de Recherche Meteorologiques (CNRM), the National Centers for Environmental Prediction

(NCEP), and the Met Office (UKMO). In this study, data from the KMA and the CNR-ISAC model are not used due to the lack of specific predictor variables for the calculation of WCBs.

The nine S2S models used in this differ quite significantly in terms of horizontal resolution, ensemble size, amount of initialisation times, and reforecast period (Tab. 4.1). The horizontal resolution is highest in the ECMWF and JMA model (around 30 km) and lowest in the BOM model (several hundred kilometers). The ensemble size varies between 4 (CMA, ECCC, NCEP) and 33 (BOM) ensemble members and reflects the different initialisation strategies of the centers. The NWP models with less ensemble members are typically initialised more frequently while the models with a larger ensemble size are initialised less often.

The reforecast period covers between 12 (NCEP) and 33 (BOM) years and the amount of forecasts initialised in the boreal winter season (DJF) varies between 279 initial times for the JMA model and 1800 for the CMA model. Some models use coupling to the ocean (BOM, CMA, CNRM, ECMWF, NCEP, UKMO) while other are set up without the coupling (ECCC, HMCR, JMA). The large differences in the set up of the NWP models in the S2S database reflects the lack of consensus for best practice of sub-seasonal forecasts (Vitart et al., 2017). Moreover, some centers use their seasonal or climate forecasting system and apply it to the sub-seasonal time scales while other centers use their weather forecasting system and extend it to the sub-seasonal time scale.

In this study, the main focus is on the ECMWF's IFS reforecasts which has the overall highest horizontal resolution, especially in the first ten days of the forecast (Tab. 4.1). The model is run based on the weather forecasting system for the first ten days of the forecast and then extended to the sub-seasonal time scale with a slightly lower resolution. The similar set up compared to the weather forecasting system for the first ten days allows a systematic analysis of the WCBs also at early lead times and the large data set of the reforecasts yields robust results in terms of WCB representation. However, it is important to note that the operational forecasting system of the ECMWF likely has higher WCB skill than the S2S reforecast data set. This is due to the higher horizontal and vertical grid

spacing, more ensemble members, and a newer data assimilation system (Vitart, 2014).

Over the Atlantic-European region, the ECMWF's IFS reforecasts have the highest skill in predicting the NAO compared to the other S2S models. On lead time beyond the medium-range, the model also has the highest overall skill of the S2S models in predicting the MJO (Vitart, 2017) which is an important driver of sub-seasonal predictability for the Atlantic-European region on sub-seasonal time scales (see section 2.3). Therefore, the use of the ECMWF model for the in depth analysis of the WCB representation and the link to weather regimes seems justified (Feng et al., 2021).

The ECMWF's IFS reforecasts are initialized twice a week from ERA-Interim reanalyses with 11 ensemble members (1 unperturbed and 10 perturbed forecasts) for a lead time of 46 days. As done in previous studies (Büeler et al., 2020, DeFlorio et al., 2018, Schiraldi and Roundy, 2017), different model versions (CY43R1, CY43R3, CY43R5) are used to increase the overall sample size. It is important to note that these model versions come with the same resolution for ocean and atmosphere and have the same number of model levels.

The data of the S2S models is retrieved on a regular $1.5^\circ \times 1.5^\circ$latitude–longitude grid from the S2S database and remapped to $1^\circ \times 1^\circ$grid spacing since the statistical models to study WCBs (Section 4.2) were developed for the latter grid spacing (Quinting and Grams, 2021a). The following variables are used from the S2S models: temperature T, geopotential height ϕ, specific humidity q, horizontal wind components u,v (instantaneous at 00 UTC) on pressure levels (1000, 925, 850, 700, 500, 300, and 200 hPa). These variables are employed to derive quantities identified in Quinting and Grams (2021b) as predictor variables to identify footprints of WCB inflow, WCB ascent, and WCB outflow without the necessity of running trajectories.

4.1.2 ERA-Interim reanalysis

In this study, the ECMWF Interim reanalysis data (Dee et al., 2011) is used as the observational truth to estimate the overall representation of WCB forecasts and the link to Atlantic-European weather regimes. In general, reanalyses are large data set which provide a multivariate, spatially complete, and coherent record of the global atmospheric circulation (Dee et al., 2011). They are especially useful for atmospheric research since they can be produced with a single version of a data assimilation system compared to archived weather analyses from operational forecasting systems which are affected by changes in methods (Dee et al., 2011).

ERA-Interim is a global atmospheric reanalysis data set produced by the European Centre for Medium-Range Weather Forecasts (ECMWF) and covers the period from 1 January 1979 onward. The reanalysis includes major progress in terms of the representation of the hydrological cycle, the quality of the stratospheric circulation, and the consistency in time of reanalysed geophysical fields.

ERA-Interim has recently been replaced by a new global reanalysis (ERA5) (Hersbach et al., 2020) which has a higher temporal and spatial resolution, better data assimilation and updated model physics. However, the ECMWF's IFS reforecasts used in this study are initialised from ERA-Interim reanalysis. Therefore, the ERA-interim reanalysis is used as the observational truth to be consistent with the initial conditions of the reforecasts. It is important to note that reforecasts initialised with ERA5 have higher forecast skill (around 1 day) compared to reforecasts initialised from ERA-Interim (Hersbach et al., 2020). For consistency with the reforecast data, the same variables as for the S2S reforecasts are used in ERA-Interim and data is retrieved on a $1.5^\circ \times 1.5^\circ$grid, and remapped to $1^\circ \times 1^\circ$. Since the time steps in the S2S reforecasts are based on 24-h time intervals at 00 UTC, ERA-Interim data is also only used at 00 UTC.

To evaluate the representation of WCB activity and the link to Atlantic-European weather regimes, the S2S reforecasts are directly compared to the observational truth from ERA-Interim for the respective research period of each NWP model. Therefore, ERA-Interim is regarded as the "perfect ensemble member" for each

reforecast of a given model (i.e. the WCB activity at a given lead time of an individual forecast is directly compared to the WCB activity in ERA-interim on this day). This approach then only uses the times in a reforecast period that also coincide with initialisation times of the reforecasts. Due to the large data size of the reforecasts, the results are generally very robust and differences in terms of observed WCB activity between different reforecast periods are small.

In this study, ERA-Interim is labeled the observational truth and used for comparison to the reforecasts. While this approach is a very good approximation for the main processes investigated in this study, ERA-Interim likely still has errors in representing processes like observed precipitation. Therefore, an additional data set is used which includes daily precipitation fields of the Integrated Multi-satellitE Retrievals for GPM (IMERG) observations (Huffman et al., 2020). GPM IMERG is a satellite based observation data set that is especially useful over the ocean where radar data is not available. However, it is only available south of around 60°N and from 2000 onward.

4.2 Statistical model to study WCBs in NWP models

The stages of WCB inflow, ascent, and outflow are identified using a novel framework of convolutional neural networks (CNNs) introduced by Quinting and Grams (2021a). This framework is designed to evaluate WCBs in large data sets at low spatio-temporal resolution for which the original trajectory-based WCB definition (Wernli, 1997) is not applicable. The CNN models now facilitate for the first time a systematic study of WCBs in a large data set. The models take meteorological parameters as predictors, which are characteristic of each WCB stage, and predict two-dimensional WCB footprints. The CNN models successfully reproduce the climatological distribution of WCBs found with the trajectory-based approach (Madonna et al., 2014) and skillfully identify WCBs at instantaneous time steps.

The predictor variables for the inflow, ascent, and outflow stage of the WCB are first identified in a previous version of the statistical WCB metric using multiple logistic regression models (Quinting and Grams, 2021b). The predictor variables for the inflow model are thickness advection at 700 hPa, meridional moisture flux at 850 hPa, moisture flux convergence at 1000 hPa, and moist potential vorticity at 500 hPa (see Table 1 in Quinting and Grams (2021b)). The predictor variables for the inflow stage of the WCB reflect recent studies (Berman and Torn, 2019, Dacre et al., 2019) which especially suggest a link between strong moisture transport and WCBs.

The ascent model is based on relative vorticity at 850 hPa and relative humidity at 700 hPa as the two most important predictors. The relative humidity reflects the condensation which occurs as saturation is reached in the ascent phase of the WCB. On the other hand, the WCB ascent redistributes vorticity above and below the region with maximum heating (see Chapter 2.1.) which leads to an increase in the cyclonic vorticity in the lower troposphere together with a strengthening of the cyclone intensity. The WCB ascent model is further based on thickness advection at 300 hPa and the meridional moisture flux at 500 hPa. Thickness advection can lead to upstream motions due to the quasi-gesostrophic forcing which is in line with the general concepts of the ascent stage of the WCB. It is especially important as a predictor for WCB ascent in regions north of 60°N (Quinting and Grams, 2021b).

Finally, the outflow model uses relative humidity at 300 hPa, the irrotational wind speed at 300 hPa, static stability at 500 hPa, and relative vorticity at 300 hPa. The relative humidity as a predictor reflect the broad cirrus shield which is typically found in the vicinity of the WCB outflow region (Carlson, 1980). The impact of the WCB outflow on the large-scale extratropical circulation (and jet stream) is typically quantified using the irrotational wind speed in upper-levels (Grams and Archambault, 2016).

In this study, a novel framework of convolutional neural networks (CNNs) (Fukushima and Miyake, 1982) is used the to identify the stages of WCB inflow, ascent, and outflow (Quinting and Grams, 2021a). In general, CNNs have

become widely popular in recent years in atmospheric sciences and the framework has been applied to many different meteorological structures (i.e. fronts, cyclones, atmospheric rivers). They are specifically designed to learn from data on spatial grids by using information from nearby grid points. This study uses CNN models developed by Quinting and Grams (2021a) which architecture is based on the semantic-segmentation model UNet.

The CNNs yield the conditional probability $\hat{P}$ of WCB inflow, ascent, and outflow at each grid point which can be transformed into a deterministic dichotomous prediction by applying a local, grid point-based decision threshold. If the conditional probability exceeds the threshold, the respective grid point is considered to feature a WCB inflow, ascent, or outflow and the mask is set to 1, below the threshold the mask is set to 0. For the ensemble forecasts, the dichotomous WCB inflow, ascent, and outflow masks are calculated for each ensemble member. Averaging over the 0/1 mask for all members yields an ensemble probability P of WCB inflow, ascent, and outflow occurrence.

4.3 Year-round Atlantic-European weather regimes

Most regime studies use the set of four weather regimes (Ferranti et al., 2015, Michel and Rivière, 2011) introduced by Vautard (1990) and Michelangeli et al. (1995). However, these regimes can only be used in a specific season since the amplitude of the large-scale flow anomalies are very different in summer and winter which typically yields very different regime patterns. In order to account for this seasonality, Grams et al. (2017) normalise the regime pattern and for the first time, define a novel approach of seven year-round weather regimes.

The seven weather regimes are deviations from the climatological mean conditions and can be divided into two groups of more cyclonic and more anticyclonic regimes. They reflect the definitions with four regimes but also allow variants of the NAO positive regime and different blocked regimes to distinguish blocking over Europe and Scandinavia.

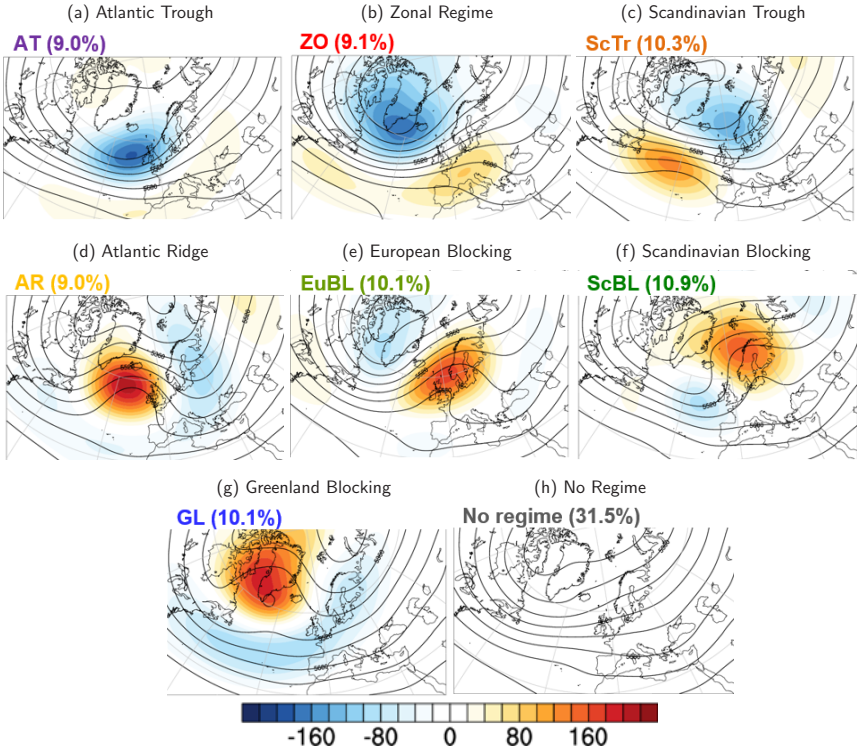


Figure 4.1: Cluster mean 500-hPa geopotential height anomalies (shading) and corresponding absolute fields (contours) of the seven year-round Atlantic–European weather regimes and the "No Regime" after Grams et al. (2017).

The cyclonic regimes are the Atlantic trough (AT), Zonal regime (ZO), and Scandinavian trough (ScTr) since their dominant signature is a negative Z500 anomaly (Fig. 4.1). The AT has negative Z500 east of Iceland and occurs at 9% of the days (Fig. 4.1a). The occurrence frequency varies between the seasons with highest frequencies of 10–15% in winter and lower frequencies in summer (3.5%) (Fig. 4.2). The ZO has negative Z500 anomalies over Greenland and Iceland and positive anomalies over Europe (Fig. 4.1b) which resemble the positive phase of the NAO. As the AT, it occurs more frequent in winter (13.8%) and less frequent

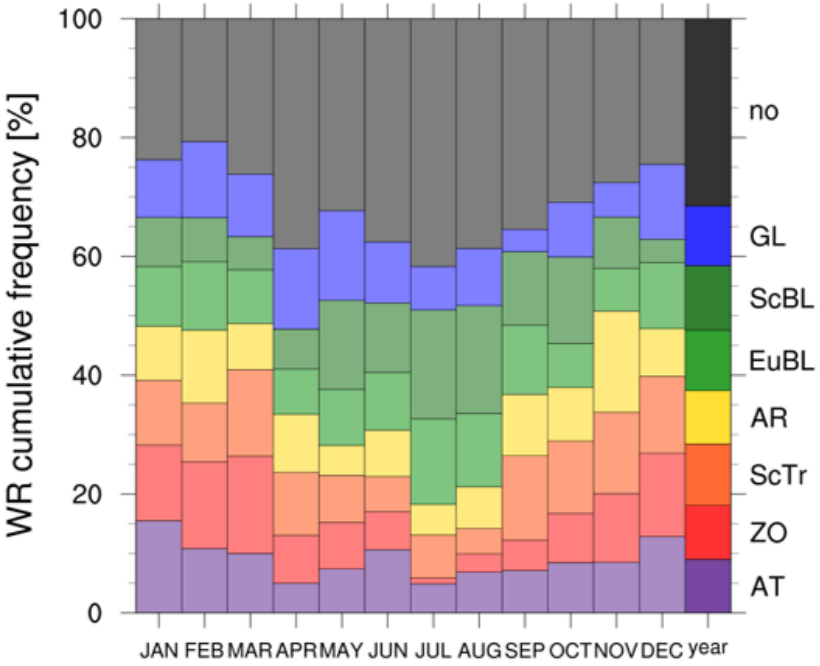


Figure 4.2: Monthly variation of occurrence frequency of the seven year-round weather regimes and the No-Regime after Grams et al. (2017).

in summer (Fig. 4.2). The Scandinavian trough is characterised by a strong negative anomalies over northern and eastern Europe and positive anomalies over the central Atlantic (Fig. 4.1c). It accounts for 10.3% of the days and occurs more often in winter (11.3%) than in other seasons (Fig. 4.2).

On the other hand, the blocked weather regimes are called Atlantic Ridge (AR), European Blocking (EuBL), Scandinavian Blocking (ScBL), and Greenland Blocking (GL) since the dominant signature is a strong positive anomaly. During AR, a blocking anticyclone can be found over the central Atlantic south of

Iceland and a trough with a northwesterly to westerly flow emerges over Europe (Fig. 4.1d). AR occurs at 9% of the days with similar frequencies in all seasons (Fig. 4.2). The EuBL is characterised by a strong block over the European region with positive Z500 anomalies over Great Britain and Scandinavia (Fig. 4.1e). EuBL is the dominant blocked regime over Europe in winter (10.9%) and account at 10.1% of all days (Fig. 4.2).

The ScBL regime has a northward shifted Z500 anomaly pattern compared to EuBL (Fig. 4.1f). The strongest positive anomalies emerge over northern Scandinavia and the Norwegian Sea while negative anomalies accompanied by an upper-level trough emerge over the eastern Atlantic. ScBL occurs less often in winter (6.5%) compared to EuBL, but is the dominant regime in boreal summer (16.0%) (Fig. 4.2). Lastly, GL features a strong positive Z500 anomaly over Greenland and negative anomalies stretching from the eastern Atlantic into Northern Europe (Fig. 4.1g). It resembles the NAO- regime of the definition with four regimes and accounts for 10.1% of all days. As the NAO+ regime (ZO), it occurs more often in winter (11.7%) compared to summer (9.1%).

The definition of the seven year-round weather regimes in Grams et al. (2017) is based on a cluster analysis of the leading empirical orthogonal functions (EOF) as in Michelangeli et al. (1995). Prior to the clustering, six-hourly 500-hPa geopotential height (Z500) anomalies are calculated compared to the corresponding running mean calendar date climatologies (Büeler et al., 2021, Grams et al., 2017). The anomalies are then low pass filtered to remove synoptic scale variability and seasonally normalised. In this study, two definitions are used, one with a 5-day low pass filter (Chapter 6 and 7) and one with a 10-day low pass filter (Chapter 8).

A k-means clustering is then applied to the Z500 anomalies in the phase space spanned by the seven leading EOFs which explain around 70% of the variance. The clustering yields an optimal number of seven cluster means which represent the seven weather regimes. To determine active regime life cycles, instantaneous Z500 fields are projected on the seven weather regimes following Michel and

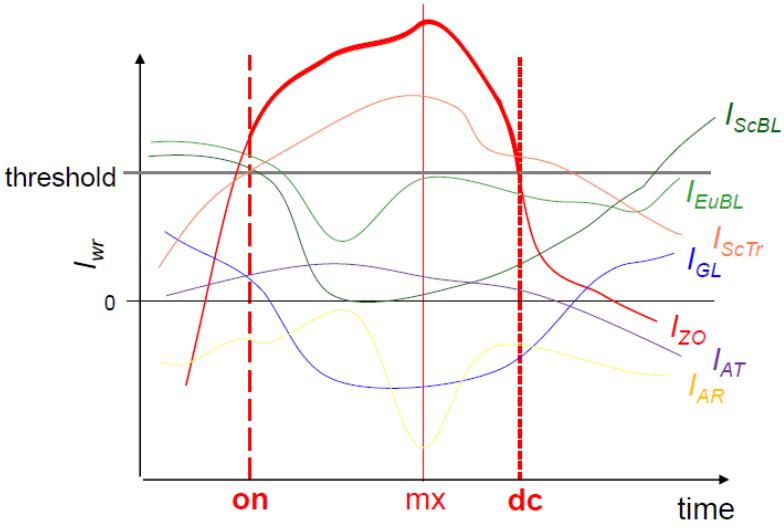


Figure 4.3: Schematic illustration of the weather regime index I_{WR} for a regime life cycle of the Zonal regime after Grams et al. (2017). The onset of the regime occurs on the day, the I_{WR} surpasses a certain threshold and the regime decays on the day the I_{WR} falls below the threshold. The I_{WR} of the other regimes shows no active life cycle.

Rivière (2011). They use a scalar measure P_{WR} which calculates the correlation of the instantaneous anomaly field $\Phi(\lambda,\phi)$ (within the EOF domain) with the cluster mean anomaly field $\phi_{WR}(\lambda,\phi)$ at each grid point with latitude λ and longitude ϕ:

$$P_{WR} = \frac{1}{\sum_{(\lambda,\phi)} cos(\phi)} \sum_{\lambda,\phi} \Phi(\lambda,\phi)\,\Phi_{WR}(\lambda,\phi)\,cos(\phi). \tag{4.1}$$

A regime index I_{WR} (for each regime) is then based on anomalies of the projection P_{WR} with respect to the climatological mean projection $P_{\bar{WR}}$ normalised by the standard deviation:

$$I_{WR} = \frac{P_{WR} - P_{\bar{WR}}}{\frac{1}{N}\sum_{n=1}^{N}[P_{WR} - P_{\bar{WR}}]^2}. \tag{4.2}$$

The calculation of the I_{WR} can be done for each individual regime at a given time step in an analysis or forecast data set (Fig. 4.3). An active regime is defined from the time step when the I_{WR} surpasses a certain threshold criteria (onset) until the day when it falls below it (decay) with the maximum stage being defined as the highest overall I_{WR} of the life cycle. In this study, two different thresholds are used in Chapter 6 and 7 (0.9) and in Chapter 8 (1.0).

The year-round weather regime definition from Grams et al. (2017) has further life cycle criteria: (1) the I_{WR} has to be above the threshold for at least five days to ensure sufficient persistence of the regime and (2) during the life cycle, the regime has to have the overall highest I_{WR} of all regimes at least once. The persistence criteria separates the seven year-round regimes from other regime definitions which do not introduce a persistence criteria and allow quick jumps between regime attributions (Ferranti et al., 2015, Matsueda and Palmer, 2018).

The second criteria excludes for instances life cycle of regimes like the ScTr in the example Fig. 4.3 which has an I_{WR} above the threshold during the time of the active ZO but does not reach the highest I_{WR} at least once in its life cycle. The strict persistence and maximum projection criteria yield sufficiently strong and meaningful life cycles with a clear onset, maximum and decay stage. The definition further enables in depth life cycle analyse and allows the link to physical processes like latent heat release in WCBs.

4.4 Verification methods

This Section describes the different statistical tools which are used in this study to quantify the representation of WCBs in sub-seasonal prediction models and to evaluate the link between WCBs and Atlantic-European weather regimes.

4.4.1 WCB representation

First, verification scores are introduced which quantify the overall representation and forecast skill of WCBs in the reforecasts. At each grid point and for all lead times, the mean error *ME* (bias) compares the ensemble forecast probabilities *P* to the observational truth from ERA-Interim:

$$ME = \frac{1}{N}\sum_{n=1}^{N}(P_n - o_n), \tag{4.3}$$

where $0 \leq P_n \leq 1$ is the ensemble probability of WCB inflow, ascent or outflow at a specific grid point and forecast lead time and o_n the dichotomous observational value from ERA-Interim. N stands for the number of forecasts that are used to calculate the mean error. Since the ECMWF's reforecast are initialised from ERA-interim, systematic biases do not emerge at the forecast initialisation time. However, for the other S2S models, biases occur already at forecast day 0. Therefore, biases at lead time beyond day 0 are reduced by the systematic bias at initialisation time.

A common score to verify ensemble probabilities is the Brier Score (*BS*) which is the mean squared error for a probabilistic forecast (Wilks, 2011). Due to the relatively low number of ensemble members in the S2S data set, the Fair Brier Score (*FBS*; Ferro, 2014) is used which provides an unbiased estimate which one would get for an infinite ensemble of exchangeable members (Ferro et al., 2008):

$$FBS = \frac{1}{N}\sum_{n=1}^{N}\left[\left(\frac{i_n}{m} - o_n\right)^2 - \frac{i_n\,(m-i_n)}{m^2\,(m-1)}\right], \tag{4.4}$$

where i is the number of ensemble members that identify a WCB inflow, ascent, or outflow for a given lead time and m is the total number of ensemble members (with $P_n = \frac{i_n}{m}$). The first term compares the ensemble probability P_n to the observations o_n and the second term generally reduces the Brier Score

for small ensembles. Additionally, a reference Brier Score is calculated using the seasonal climatology $\overline{o_n}$ of a given reforecast period as a predictor variable ($BS_{CLIM} = \frac{1}{N}\sum_{n=1}^{N}(\overline{o_n} - o_n)^2$). The Fair Brier Skill Score $FBSS$ then compares the FBS of the ensemble forecasts to the BS_{CLIM} of the climatological reference forecast:

$$FBSS = 1 - \frac{FBS}{BS_{CLIM}}. \tag{4.5}$$

The forecast model performs better than the reference forecast for a Fair Brier Skill Score larger than 0 with higher values indicating a better model forecast.

In contrast to short- and medium-range weather prediction, for which the forecast of a specific event on a given day M is of interest, on sub-seasonal time scales, a skillful forecast of the mean value of a variable over a certain period of multiple days is of interest (White et al., 2017). Therefore, weekly mean WCB frequencies are evaluated by computing the Fair Brier Score (FBS_M) for a 7-day WCB frequency forecast with

$$FBS_7 = \frac{1}{N}\sum_{n=1}^{N}\left[\left(\frac{1}{7}\sum_{k=1}^{7}\frac{i_n}{m} - \frac{1}{7}\sum_{k=1}^{7}o_n\right)^2 - \frac{1}{7}\sum_{k=1}^{7}\left(\frac{i_n\,(m-i_n)}{m^2\,(m-1)}\right)\right], \tag{4.6}$$

where the 7-day mean of ensemble probability P_n ($= \frac{i_n}{m}$) is compared to the 7-day mean of the observations o_n. As in equation 4.4, the second term accounts for the small ensemble size. It is simply an average of the Ferro (2014) correction term over all 7 days. Seasonal climatologies $\overline{o_n}$ are used again as a predictor for the reference forecast. The Fair Brier Skill Score is then obtained in predicting M-day mean WCB frequencies. The model skill is evaluated individually for each forecast lead time (day 0–6, day 1–7, ...). The forecast for days 0–6 typically correspond to a week 1 forecast in other studies.

To assess whether the biases and skill scores are systematic and robust among the forecasts, a bootstrap approach is used that generates 1000 subsets of X randomly chosen forecast initial times with replacement from the X total forecast initial dates in a specific season. The mean values of biases and skill scores are then calculated for each of the 1000 subsets at each grid point. This yields a distribution of the mean biases and skill scores. This approach follows a recent study by Papritz (2020) and defines the biases/scores to be robust on the first level, if their absolute values are greater than the interquartile range of the sample distribution. Robustness on the second level is defined, if the absolute value of the bias/score is greater than the difference between the 90 th and 10 th percentiles.

For the area-averaged skill scores, the same sampling approach is used but now distributions of area-averaged Fair Brier Skill Scores are generated for each lead time. The difference between the 90 th and 10 th percentile is then defined as the variability of the area-averaged Fair Brier Skill Score. Forecasts in two regions have a significantly different skill if the variability bars for the two regions do not overlap (i.e., the 10 th percentile for the first region exhibits a higher skill value than the 90 th percentiles for the other region).

4.4.2 Link between WCBs and weather regimes

Now, the different methods are introduced which are used in this study to link WCB activity and Atlantic-European weather regimes. Two main approaches are used to disentangle the role of the WCB for the prediction of weather regimes: (1) the predictive skill of the weather regimes across different time scales is linked to WCB activity, and (2) the climatology of WCB activity around regime onsets is evaluated in the reforecasts in comparison to ERA-Interim.

The first approach evaluates how well the reforecasts can predict a regime and the associated WCB activity at different forecast lead times of a given forecast. In order to evaluate observed regime onsets across different lead times, the regime onsets in ERA-Interim are matched with the initialisation times of the S2S reforecasts. Therefore, ERA-Interim is treated as the perfect ensemble member and regime onsets are defined in forecast week 1 (between day 2–7), week 2

(day 8–14), and week 3 (day 15–21). This weekly forecast window is commonly used in sub-seasonal prediction studies (Lee et al., 2020, Manrique-Suñén et al., 2020).

The characteristics of the observed regime onsets and their representation in the ensemble mean of the reforecasts are then evaluated by calculating weekly composites of geopotential height in 500 hPa (Z500) and WCB activity. This approach shows the predictive skill of WCB and Z500 patterns in the reforecasts across lead times and further allows the evaluation of the patterns in the week before and after the regime onset.

In this study, the focus is on regime onsets in forecast week 2 (between day 8–14) since onsets of large-scale flow regimes on these time scales are of particular interest from a sub-seasonal prediction perspective. Due to the average life cycle length of around 10 days Büeler et al. (2021), onsets in week 2 lead to active regime life cycles into week 3 and sometimes even week 4. Furthermore, onsets in week 2 are also interesting from a synoptic-scale perspective since processes on these time scales have a shorter predictability limit compared to processes which occur on larger continent scale sizes (Buizza and Leutbecher, 2015). It is important to note that the analysis of WCBs and regime onsets in forecast week 1 and 3 yield generally similar results in terms of the role of WCBs for the onset of the regimes.

There are between 68 and 144 observed regime onsets in forecast week 2 in the extended winter period from 1997–2017 (Tab. 4.2). The amount of observed onsets varies between the regimes and is generally in line with the regime frequencies in a given season (Fig. 4.2). For instance, the relatively low number of onsets for ScBL reflects the low occurrence frequency of the regime in the winter season (around 7%).

It is important to note that due to the previously introduced stratification which uses ERA-Interim as the "perfect ensemble member", the 68 to 144 regime onsets include the same regime onset in ERA-interim multiple times. The stratification allows for double counting which yields around 3.5 times the amount of actually

Table 4.2: Amount of onsets of Atlantic-European weather regimes in the extended winter season (1997–2017) during initialisation times of the ECMWF's IFS reforecasts. ERA-Interim is treated as the "perfect ensemble member" and only regime onsets in forecast week 2 (between day 8–14) are considered. The columns show observed onsets in ERA-Interim, all regime onsets in the reforecasts, as well as onsets in the categories Hits, False Alarms and Misses. The ECMWF's IFS reforecasts have 11 ensemble members which are considered individually to calculate the reforecast climatology. Therefore the values in brackets indicate the amount of onsets per member for the reforecasts and show the amount of members with a hit/miss of an observed onset.

	Observed (individual events)	Reforecasts (per member)	False Alarms	Hits (per observed onset)	Misses (per observed onset)
ZO	140 (40)	1598 (145)	1314	284 (2.0)	1258 (9.0)
ScBL	68 (19)	1046 (95)	970	76 (1.1)	673 (9.9)
GL	106 (30)	1391 (126)	1194	197 (1.9)	969 (9.1)
AT	118 (34)	1396 (127)	1243	153 (1.3)	1145 (9.7)
EuBL	137 (38)	1254 (114)	1099	155 (1.1)	1352 (9.9)
ScTr	144 (41)	1632 (148)	1422	210 (1.5)	1374 (9.5)
AR	144 (40)	1310 (119)	1086	224 (1.6)	1360 (9.4)

observed onsets. The number of actually observed onsets is between 19 and 41 for the different regimes in the extended winter season of the ECMWF's IFS reforecast period (Tab. 4.2). Overall, the number of observed onsets still indicates a general robustness of the large data set of events for the analyses in this study.

In this study, the sample of all observed regime onsets (between 68 and 144) is further split into subsets which have a good predictive skill of the regime in the reforecasts and subsets with a bad predictive skill. For this stratification, the best and worst 33% of the events are selected and weekly composites of Z500 and WCB activity are calculated. The two categories are set up based on the average Fair Brier Skill Score (FBSS) for the first five days of the regime life cycle after Büeler et al. (2021). The stratification allows a direct comparison of regime onset events which are well predicted and events with a low forecast skill together with the evaluation of the role of the WCB for the predictive skill of the regimes. Since one observed onset is covered by multiple forecasts (3.5 times for the ECMWF's reforecasts), both subsets could theoretically contain the same event which is well predicted by one forecast and badly predicted by another.

The second approach to link WCBs and weather regimes evaluates if structural differences in the evolution of large-scale flow patterns and WCB activity emerge around regime onsets in the reforecasts compared to regime onsets in ERA-Interim. This stratification splits up the ensemble members of the reforecasts into different categories and investigates regime onsets in the reforecasts independently from ERA-Interim. Three categories of ensemble members are defined: False Alarms cover all ensemble members with an onset of a given regime which occurs without an observed regime in ERA-Interim. Hits include all ensemble members which have a regime onset together with an observed onset. The combination of the Hits and False Alarms category reflect the reforecast climatology. Lastly, a third category is defined (Misses) which includes all ensemble members which miss an observed regime onset in ERA-Interim.

For the ECMWF's IFS reforecasts, the reforecast climatology includes a total amount of around 1100–1600 regime onsets using all 11 ensemble members in the extended winter season of the reforecast period (1997–2017) (Tab. 4.2). This yields a total number of 95–148 onsets per ensemble member. The amount of events per member show that the reforecasts have more onsets for the ScBL regime compared to the observation (95 compared to 68). This indicates that the model might establish ScBL onsets too frequently. On the other hand, the reforecasts have a lower number of EuBL onsets compared to the observations (114 compared to 137) which might point to a potential under-representation of EuBL onsets in the reforecasts. These findings are important to keep in mind for the evaluation of the role of the WCB for the forecast skill of EuBL and ScBL onsets in the following Chapters.

As previously introduced, the reforecast climatology combines regime onsets from the False Alarms and Hits category. Recalling that False Alarms occur without an observed onset in ERA-Interim, the relatively high number in the False Alarms category (Tab. 4.2) shows that the overall climatology is strongly dominated by these events. On the other hand, the Hits category makes up around 10% of all events in the reforecasts climatology. The values in brackets indicate that the reforecasts have more Hits per observed regime onset for ZO and GL and less Hits per observed event for ScBL and EuBL onsets. On the other hand, the

Misses are higher for EuBL and ScBL compared to GL and ZO. As for the overall representation of regime onsets, this statistics gives a first hint that the NWP model might have difficulties in correctly capturing EuBL and ScBL onsets.

These different categories are then primarily evaluated in terms of WCB activity and large-scale flow evolution and the findings are compared to ERA-Interim. For the analysis, lagged composites centered on the onset are used for all events of a given regime. This approach allows a direct comparison of Z500 evolution and WCB activity in the days before and after a regime onset. Anomalies of WCBs and Z500 are calculated based on 90-day running mean climatology for each respective onset events. Since the extended winter period includes onsets from November to March, this approach yields a robust analysis independent of seasonal variations in WCB activity and Z500 fields. To evaluate significant differences between the two data sets, a Student t-test is used which accounts for the different sample sizes and directly compares the calculated anomalies.

5 Verification of warm conveyor belts

This Chapter provides a systematic investigation of WCBs in the ECMWF's sub-seasonal weather prediction model in the winter season from 1997–2017. WCBs are cloudy regions of strong, diabatically enhanced ascent and contribute a major fraction to precipitation in the midlatitudes (Pfahl et al., 2014). They are a major source and amplifier of forecast error and can influence the upper-level large-scale circulation through their diabatically enhanced outflow. The analysis, for the first time, quantifies the overall representation of WCBs in a large data set of 20 years of reforecasts. This Chapter provides an overview over systematic WCB biases, as well as the reliability and the overall skill horizon of WCB forecasts. It further evaluates links to biases in WCB predictor variables and seasonal variations of WCB representation. Lastly, the role of the WCB for the upper-level circulation is evaluated on sub-seasonal time scales with a link to the MJO.

5.1 Model bias

First, the overall representation of WCBs is evaluated by investigating WCB frequency biases over the Northern Hemisphere at lead times of 3, 7, and 15 days. In the following all WCB stages - WCB inflow, ascent, and outflow will be discussed with a focus on the North Atlantic and North Pacific.

For all WCB stages, frequency biases emerge already at forecast day 3 and remain at a similar level or increase towards later lead times (Fig. 5.1). The absolute frequency biases for all three WCB stages reach values of up to 5% corresponding to a bias of 30 to 100% relative to the climatological frequency (5–15% in regions of strongest biases).

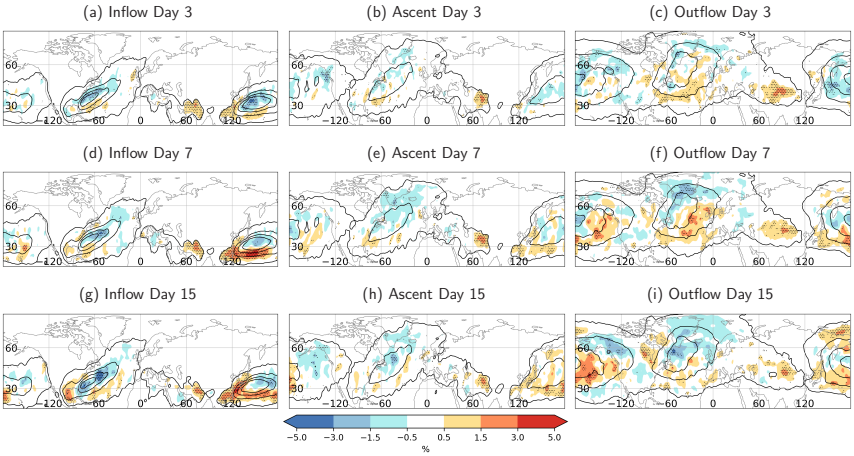


Figure 5.1: Frequency bias of WCB (a,d,g) inflow, (b,e,h) ascent, (c,f,i) outflow for DJF 1997–2017 (shading) at different forecast lead times: (a-c) day 3, (d-f) day 7 and (g-i) day 15. Robustness on the second level is indicated by the point stippling. The black contours indicate a frequency of 1, 5, 10, 15 % in the respective layer.

In almost all regions that experience a bias of more than 1%, the findings are robust on the first level. Therefore, only robustness on the second level (indicated by the point stippling) is shown. As explained in Chapter 3, the robustness is calculated based on a bootstrap approach which generates 1000 subsets of the total amount of initial times (here 920). The WCB biases are then considered robust on the first level if their absolute values are larger than the interquartile range of the sample distribution and robust on the second level if the values are larger than the difference between the 90 th and 10 th percentile. In the following, the focus is on the storm track regions over the North Atlantic and North Pacific where the climatological WCB frequency is highest (Madonna et al., 2014).

For the reforecast period 1997–2017, the observed WCB frequencies are highest in the inflow region over the southwestern North Atlantic and over the western North Pacific (around 15%) (Fig. 5.1a). WCB ascent frequencies are generally lower (around 5%) (Fig. 5.1b) which is probably due to generally smaller WCB

ascent objects (Quinting and Grams, 2021a). WCB outflow frequencies are highest over the central North Atlantic (around 10%) and the central North Pacific (around 15%) (Fig. 5.1c).

Starting with the North Atlantic, the model underestimates WCB inflow on day 3 in most regions (Fig. 5.1a). In particular over the western and central North Atlantic (30–45°N, 80–30°W) the forecast model underestimates the inflow frequency by 1–3%. Recalling that the climatological WCB inflow frequency in this region range from 10–15%, these absolute biases correspond to a relative frequency bias ranging from 20–30%. Positive biases of around 1% occur south and southeast of the climatological frequency maximum (25–35°N, 70–50°W).

For WCB ascent, a structurally similar dipole of negative and positive biases is found over the North Atlantic (Fig. 5.1b). The negative biases of around 1% correspond to a relative underestimation of around 20% and extend over a large area along the North American East Coast towards Greenland and Iceland.

WCB outflow is underestimated by around 1% over the North Atlantic between Greenland and the Norwegian Sea on day 3 (Fig. 5.1c). This absolute underestimation corresponds to a relative bias of 10–20%. On the other hand, positive biases occur more over the southern part the North Atlantic to the southeast of the climatological maximum (30–60°N, 60°W–0°).

At lead times of 7 and 15 days, the WCB inflow and ascent frequency biases over the North Atlantic remain structurally similar with negative (positive) biases in and to the north (south) of the regions with climatologically highest WCB activity (Figs. 5.1d,e,g,h). The magnitude of the biases increases only slightly in most regions except for the main inflow region and the Gulf of Mexico where biases exceed 3% at 15 days lead time (Fig. 5.1g). For WCB outflow, the negative bias over the North Atlantic increases to around 3% at 7 and 15 days lead time (Fig. 5.1f,i).

For the North Pacific region, an area with positive WCB inflow frequency biases of 1% spans from the South China Sea to Japan and further east towards the climatological frequency maximum (20–30°N, 120–150°E) on day 3 of the

forecasts (Fig. 5.1a). Pronounced negative biases of up to 3% are prevalent in and north of the region with the climatological frequency maximum (30–40°N, 140–170°E). Recalling that the climatological WCB inflow frequency ranges from 5–15%, these absolute biases correspond to a relative frequency bias ranging from 20–50%.

For WCB ascent, a negative bias of 1–3% occurs in the region of the climatological frequency maximum between 120°E–180°E and over the eastern North Pacific (Fig. 5.1b). As for the WCB inflow, the absolute WCB ascent biases correspond to a relative frequency bias of 20–50%.

For the WCB outflow, negative biases of 1–3% occur over the western North Pacific, over Alaska and portions of western Canada (Fig. 5.1c). The absolute biases correspond to a relative underestimation of 10–30%.

At later lead times, the magnitude of the positive WCB inflow biases over the North Pacific increase. With an overestimation of 3–5%, the inflow bias is most pronounced over the South China Sea (Fig. 5.1d,g). Recalling that the climatological WCB inflow frequencies range from 5–15%, this corresponds to a relative overestimation of up to 100%. For WCB ascent, the negative biases over the western North Pacific weaken with forecast lead time and significant positive biases occur on forecast day 15 (Fig. 5.1e,h). In line with the changes of the WCB ascent bias, there is a shift to a positive outflow bias over the western North Pacific on day 15 and an overall increase of the negative bias over Alaska and western Canada (absolute values around 1–3%; Figs. 5.1f,i). This negative bias corresponds to a relative underestimation of 30–60%.

In conclusion, significant WCB frequency biases occur already at early lead times (forecast day 3) which increase to forecast day 7, and saturate afterwards. There is a tendency towards a general overestimation of 1–3% over the southern part and an underestimation of 1–5% over the northern part of the North Atlantic for all WCB stages. Over the North Pacific, a relatively large overestimation (2–4%) of the WCB inflow occurs in some regions of the western part of the ocean basin

and both positive and negative biases of similar magnitude can be found over the central and eastern part of the ocean basin for WCB outflow.

Previous studies have shown that an inaccurate representation of WCBs in NWP models can lead to errors in the downstream Rossby wave pattern (e.g., Baumgart et al., 2018, Berman and Torn, 2019, Grams et al., 2018, Lamberson et al., 2016, Maddison et al., 2019, Martínez-Alvarado et al., 2016, Rodwell et al., 2018). The systematic WCB biases in the climatologically most active regions as well as north of these regions may have an impact on the downstream flow evolution and thus contribute to error in the downstream Rossby wave pattern. The results corroborate that the underestimation of the WCB outflow in the northern part of the North Atlantic and over western North America could lead to an underestimation of upper-level ridges in these regions. On the other hand, the overestimation over the western and central Pacific for lead times 7 and 15 days point to a reversed impact of WCB activity on the circulation in this region. The impact of WCBs on the upper-level flow is further analysed in Section 5.5.

5.2 Forecast reliability

In this Section, the agreement between ensemble probabilities and the observed frequencies of WCB occurrence is assessed via reliability diagrams at each grid point in the Northern Hemisphere. Since there are 11 ensemble members in the reforecast data set, 12 regular bins (x-axis) are created for the probabilities predicted by the ensemble. Bin 0 contains those forecasts when zero members predicted the occurrence of a WCB at the respective grid point and at a specific lead time, bin 1 contains those forecasts when one member predicted the occurrence of a WCB, and so on. Accordingly, each bin corresponds to a predicted probability (e.g., 0% for bin 0 and 64% for bin 7).

For each grid point and each forecast lead time, the forecasts in each bin are then compared against the actual observed frequency (y-axis). In a final step, the reliability curves and the number of forecasts falling into each bin are averaged

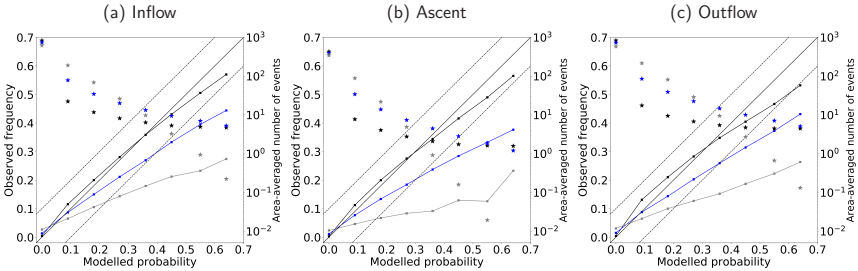


Figure 5.2: Reliability diagrams for a) inflow, b) ascent, and c) outflow at forecast days 3 (black), 7 (blue) and 15 (grey) (DJF; 1997–2017). Modelled probabilities (x-axis) and observed frequencies (left y-axis) are shown together with the average number of forecasts per bin and grid point (asterisks, right logarithmic y-axis). Due to the small sample size for the last four bins, only modelled probabilities up to 64% are shown (bins 0–7). Furthermore, the perfect WCB forecast and a 10% interval about the perfect WCB forecast are indicated by the solid and dashed diagonals, respectively.

(area-weighted) over all Northern Hemisphere grid points and evaluated for forecast days 3, 7, and 15 (Fig. 5.2). Due to the relatively small number of forecasts in bins 8–11 for these lead times (1–5% of all forecasts), only results for bins 0–7 are shown.

Around 80% of the total number of forecasts fall into bin 0, i.e., none of the ensemble members predicts WCB inflow, ascent or outflow (Fig. 5.2). Still in 1–3% of these forecasts, a WCB is observed in the reanalysis. This underconfidence of the model in a large number of forecasts and at many grid points contributes to the overall negative biases found in Section 5.1. The model is also underconfident for bins 1–2 at forecast day 3 while it is mostly overconfident for bins 4–7. This overconfidence is larger for day 7 and 15 compared to day 3. The reliability of the WCB forecast decreases from forecast day 3 to forecast days 7 and 15. The relatively flat curve for forecast day 15 indicates the difficulty of the forecast model in predicting the WCB reliably at this lead time.

5.3 Forecast skill

Now, the overall forecast skill is investigated as the area-average of grid-point based *FBSS* over the Northern Hemisphere, the North Atlantic, and the North Pacific. The forecast skill horizon is subjectively defined as the forecast lead time at which the *FBSS* falls below 0.08 since it only decreases very slowly afterwards.

For all three regions, the skill horizon for WCB inflow is reached after 8 to 9 days forecast lead time with generally higher skill over the North Pacific than over the North Atlantic (Fig.5.3b). For lead times between day 6 and 8, the forecast skill over the North Pacific is higher compared to the North Atlantic. However, the differences are not significant at the 80% confidence interval indicated by overlapping error bars.

The forecast skill for WCB ascent exhibits a similar evolution with forecast lead time (Fig.5.3c). The forecast skill horizon is reached after 7 days for the North Atlantic and 8 days for the North Pacific. For lead times between 6 and 8 days, the forecast skill over the North Pacific is significantly higher than over the North Atlantic.

In particular at early lead times, the forecast skill for WCB outflow is highest on average (Fig.5.3d). However, the overall forecast skill horizon is similar to WCB inflow with 8 days for the North Atlantic and 9 days for the North Pacific. Similar to WCB ascent, the skill is significantly higher over the North Pacific than over the North Atlantic between forecast days 6 and 10.

At forecast day 0, the *FBSS* is around 0.7–0.8 for the three WCB stages. This result indicates that on forecast day 0, the reforecasts are not able to reach a score of 1 which equals a "perfect" forecasts. This is likely due to the ensemble configuration in the ECMWF's IFS reforecasts where the 11 ensemble members are initialised with varying initial conditions at forecast day 0 to account for uncertainties in the observations. Therefore, initialisation differences could lead to slightly different WCB object which results in ensemble probabilities below 1 for the WCB stages. Probabilities below 1 can then lead to an increase of the

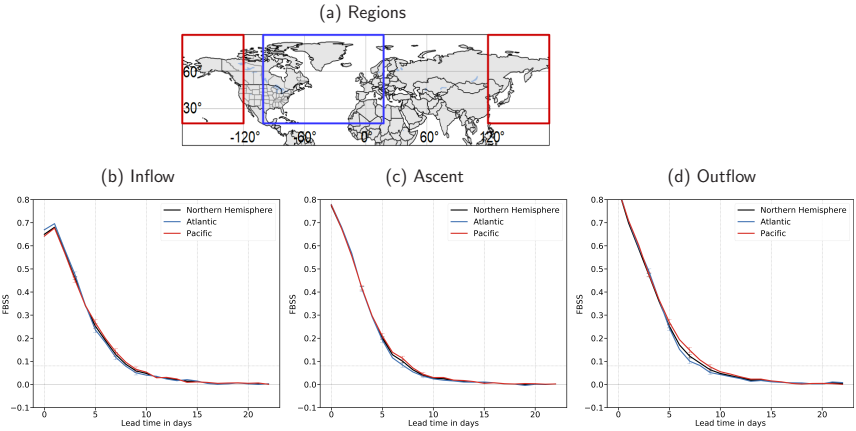


Figure 5.3: Area-averaged Fair Brier Skill Score (*FBSS*) for DJF 1997–2017 at different forecast lead times for the different WCB stages b) inflow, c) ascent, and d) outflow. The regions for the area-averaged *FBSS* are indicated in a). Error bars centered on forecast lead times day 3, 5, 7, and 9 show the difference between the 10 and 90 th percentile of the sampled data (variability of the *FBSS*) and are used to estimate the significant differences between the ocean basins.

Brier Score which reduces the overall Brier Skill Score to values below zero. In the following, the *FBSS* is further evaluated at each grid point individually.

Maps of the *FBSS* on forecast days 3 and 7 reveal that the skill varies not only between the North Atlantic and North Pacific region but also between different sub-areas within these large regions (Fig. 5.4). As for the biases, the focus is on the forecast skill over the North Atlantic and North Pacific.

On forecast day 3, the *FBSS* for WCB inflow locally exceeds the North Atlantic mean *FBSS* of 0.47 (cf. Fig 5.3b) in the region with the highest climatological frequency, towards the southeast of this region (25–35°N, 70–50°W), and in the Gulf of Mexico (around 0.6, respectively) (Fig. 5.4a). In contrast, the skill level is lower over the central and northeastern North Atlantic towards the southwest of Iceland. Here, a relatively low skill around 0.4 can be found.

For WCB ascent, the areas with highest skill are located between 30 to 60°N and 80 to 40°W (Fig. 5.4c). In line with the skill for WCB inflow, lower skill

than the area-average of 0.41 occurs over the eastern North Atlantic and towards Western Europe. Also for WCB outflow highest skill levels, which exceed the North Atlantic mean of 0.48, are found over the western North Atlantic with values between 0.5 and 0.7 on forecast day 3 (Fig. 5.4e). Skill tends to be lower over the eastern North Atlantic, the Norwegian Sea, Scandinavia and the eastern part of Europe.

For forecast day 7, the regions over the North Atlantic with high skill for WCB inflow and ascent are similar to forecast day 3 with relatively high skill over the southwestern part of the climatological frequency maximum (Figs. 5.4b,d). As for forecast day 3, low skill can be found to the northeast of the climatological maximum. For the WCB outflow, relatively high skill occurs north and west of the climatological maximum (40–80°N, 80–20°W) and lower skill southeast of it (Fig. 5.4f).

Over the North Pacific, the region east of Japan (30–40°N, 140–160°E) and the region around 20–30°N over the central part have the highest skill for the WCB inflow on day 3 (around 0.6, Fig. 5.4a). Generally, skill is lower than the area-average of 0.47 over the eastern North Pacific, especially in the region to the north and east of the climatological frequency maximum (40–50°N, 170–130°W). For WCB ascent, forecasts exhibit the highest skill on day 3 between 40 to 60°N and 140 to 180°E (Fig. 5.4c). Similar to the skill for WCB inflow, lower skill (compared to the area-average of 0.41) is found over the southern part of the western North Pacific and in most regions of the eastern North Pacific. The highest skill for WCB outflow (0.5–0.7) is found to the northwest of the climatological maximum (40–80°N, 130–180°E, Fig. 5.4e). In this region, the outflow skill is higher than the area-average of 0.48. It further decreases towards the eastern part of the ocean basin and western North America (0.3–0.5).

On forecast day 7, the the regions with high and low skill for WCB inflow do not vary compared to day 3 (Fig. 5.4b). The large skill difference for WCB ascent between the southern and northern part of the WCB ascent region for forecast day 3, is no longer evident for day 7 (Fig. 5.4d). There is similar skill of around

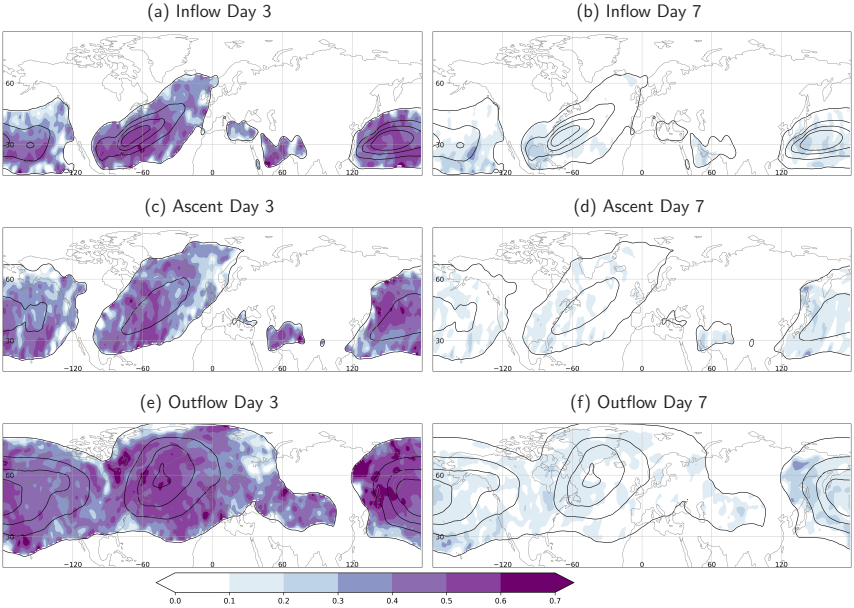


Figure 5.4: Fair Brier Skill Score (*FBSS*) of WCB forecast for (a,b) inflow, (c,d) ascent, (e,f) outflow for DJF 1997–2017 (shading) at different forecast lead times: (a,c,e) day 3, (b,d,f) day 7. The black contours indicate a WCB frequency of 1, 5, 10, 15% in the respective layer.

0.2 over large parts of the western North Pacific. The areas with relatively high (low) skill for WCB outflow are similar to forecast day 3 with higher skill over the western Pacific compared to the eastern part (Fig. 5.4f).

In summary, the reforecasts have a forecast skill horizon of 8–10 days for instantaneous prediction of all three WCB stages. There is significantly higher skill over the North Pacific region compared to the North Atlantic region for most lead times and WCB stages. Moreover, WCB skill is higher over the western part of both ocean basins compared to the eastern part. A possible explanation of the lower skill over the eastern part of the ocean basins could be the relatively higher frequency of secondary cyclones (Priestley et al., 2020, Schemm et al., 2018) which are smaller in scale and potentially harder to predict.

5.4 Link between WCB bias and bias of predictor variables

Next the link between systematic biases in WCB inflow, ascent, or outflow and biases of the predictor variables is evaluated (Fig. 5.1). In order to identify variables that are potentially related to the frequency biases, the correlation between WCB inflow, ascent, and outflow biases and erros in the representation of the predictor variables is first estimated at different lead times using the Pearson correlation coefficient (Tab. 5.1). For this analysis the North Atlantic and North Pacific region (Fig. 5.3a) are used and the correlation of WCB and predictor biases is calculated using all grid points in a given region.

WCB inflow biases correlate relatively well with biases in meridional moisture flux at 850 hPa for both the North Atlantic and North Pacific region and all lead times (between 0.28 and 0.62), as well as biases in moisture flux convergence at 1000 hPa (between 0.16 and 0.38) suggesting that these variables are important drivers of WCB inflow biases.

The WCB ascent bias can be mostly related to biases in meridional moisture flux at 500 hPa for both the North Atlantic and North Pacific and all lead times (correlation between 0.29 and 0.61). Biases in relative vorticity at 850 hPa and relative humidity at 700 hPa show a smaller correlation to the WCB ascent biases (0.02 to 0.16 and 0.07 to 0.33, respectively).

For the WCB outflow biases, the correlation to the biases in the predictor variables varies more between forecast lead times and ocean basins compared to WCB inflow and ascent. For the North Atlantic, the correlation is largest to biases in divergent wind speed at 300 hPa (0.31 to 0.57) and static stability at 500 hPa (0.32 to 0.64). For the North Pacific, the highest correlation occurs to biases in divergent wind speed and relative vorticity at 300 hPa (0.24 to 0.52 and 0.27 to 0.55, respectively). Over the North Pacific, the relative humidity bias has a high correlation for forecast day 15 (0.47) but very low correlation for other lead times.

Table 5.1: Correlation (Pearson correlation coefficient) between WCB inflow, ascent, and outflow frequency bias and biases WCB predictor variables over the North Atlantic and North Pacific region for forecast day 3,7, and 15 in DJF (1997–2017)

	Atlantic			Pacific		
Inflow	Day 3	Day 7	Day 15	Day 3	Day 7	Day 15
Thickness Advection 700 hPa	0.35	0.16	0.31	0.30	0.19	-0.11
Meridional Moisture Flux 850 hPa	0.45	0.41	0.62	0.28	0.35	0.28
Moisture Flux Convergence 1000 hPa	0.25	0.16	0.38	0.32	0.30	0.36
Moist Potential Vorticity 500 hPa	0.37	0.12	0.28	0.30	0.00	-0.11
Ascent						
Relative Vorticity 850 hPa	0.04	0.02	0.13	0.16	0.14	0.05
Relative Humidity 700 hPa	0.27	0.32	0.33	0.07	0.18	0.17
Thickness Advection 300 hPa	-0.27	-0.49	-0.37	-0.05	-0.13	-0.31
Meridional Moisture Flux 500 hPa	0.33	0.61	0.57	0.29	0.38	0.59
Outflow						
Relative Humidity 300 hPa	-0.28	-0.42	-0.07	-0.12	0.12	0.47
Divergent Wind Speed 300 hPa	0.31	0.57	0.39	0.24	0.38	0.52
Static Stability 500 hPa	0.35	0.64	0.32	0.10	0.19	-0.27
Relative Vorticity 300 hPa	0.26	0.10	0.33	0.27	0.28	0.55

In the following, the spatial patterns of the predictor variables with the highest bias correlations on forecast day 7 are investigated in more detail. In the North Atlantic region, the bias in meridional moisture flux at 850 hPa has a pronounced tilted dipole pattern with negative biases in the northern central Atlantic, and positive biases to the south (Fig. 5.5a). In a addition a strong positive bias extends from the Gulf of Mexico into the southeast U.S. Biases for moisture flux convergence at 1000 hPa have both positive and negative signs in the North Atlantic and are mostly confined to subtropical latitudes (Fig. 5.5b). Positive biases occur predominantly around 20–30°N and in the Gulf of Mexico.

Thickness advection is overestimated along the east coast of the USA and over the western part of the North Atlantic (Fig. 5.5c). These positive biases contribute to the negative biases of the WCB inflow due to the reversed sign in the CNN equations. The patterns for the three variables correlate well with the WCB

inflow bias at day 7, especially along 20–30°N and over the Gulf of Mexico (Fig. 5.1d).

Likewise in the western North Pacific a strong positive bias in meridional moisture flux and moisture flux convergence is evident south of Japan (Fig. 5.5a,b). Thickness advection is overestimated over Japan and the western part of the North Pacific likely contributing to the negative inflow bias in this region (Fig. 5.5c).

The biases in meridional moisture flux at 500 hPa show a dipole in the North Atlantic with negative biases over the northern and positive biases over the southern part and over Europe (Fig. 5.5d). Relative humidity biases at 700 hPa are negative in a large region around Greenland, Iceland and further north over the polar sea (Fig. 5.5e). Positive biases emerge west of Europe and over the southern North Atlantic and can be found in similar region compared to positive biases in meridional moisture flux at 500 hPa (Fig. 5.5d). The relative vorticity at 850 hPa is slightly underestimated over the western part of the Atlantic and overestimated over the eastern part (Fig. 5.5f).

In the North Pacific region, both meridional moisture flux and relative humidity are overestimated over the eastern and underestimated over the central and western North Pacific (Fig. 5.5d,e). These biases correlate well with WCB ascent biases (Fig. 5.1e).

The bias in divergent wind speed at 300 hPa has the highest correlation with WCB outflow biases (Tab. 5.1). In the North Atlantic region there is an overall positive bias in divergent wind speed flanked by negative biases at high and low latitudes (Fig. 5.5g) which correlates well with dipole pattern of WCB outflow biases in that region (Fig. 5.1f). Biases in static stability at 500 hPa can be found only over the northern part of the Atlantic (Fig. 5.5h). The biases are widely negative from Newfoundland over Greenland to the Norwegian Sea. Relative vorticity has a lower correlation to WCB outflow biases and is overestimated in particular south of Iceland and west of the UK (Fig. 5.5i).

Divergent wind speed is overestimated over large parts of the eastern North Pacific and some parts of the western North Pacific (Fig. 5.5g). The model underestimates static stability over large parts (Fig. 5.5g) and has both negative and

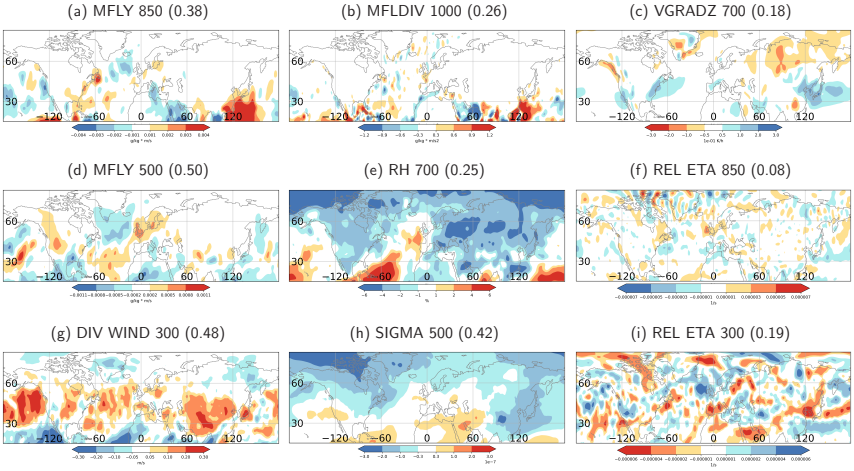


Figure 5.5: Bias at forecast day 7 of predictor variables with highest correlation (brackets) to WCB biases: (a-c) WCB inflow ((a) meridional moisture flux (850 hPa), (b) moisture flux convergence (1000 hPa), (c) thickness advection (700 hPa)), (d-f) WCB ascent ((d) meridional moisture flux (500 hPa), (e) relative humidity (700 hPa), (f) relative vorticity (850 hPa)), and (g-i) WCB outflow ((g) divergent wind speed (300 hPa), (h) static stability (500 hPa), (i) relative vorticity (300 hPa))in DJF 1997–2017

positive biases for relative vorticity (Fig. 5.5h).

All in all, these findings show that biases in meridional moisture flux at 850 and 500 hPa have a high correlation to WCB inflow and ascent biases. The biases in moisture flux, in particular over the North Pacific, correspond to biases in the atmospheric river frequency in ECMWF's S2S forecasts reported by DeFlorio et al. (2019). The results further corroborate that a bias reduction in meridional moisture flux in the lower and mid troposphere would likely result in a reduction of WCB biases. For an earlier version of the statistical models, a bias correction of the input variables for WCB inflow, ascent, and outflow yields a general reduction of the WCB inflow and ascent biases (not shown). This is not the case for the WCB outflow, where the correlation to biases in the predictor variables varies between regions and lead times and where the bias correction even leads to an increase in WCB outflow bias in some regions. This is very likely due to

the strong influence of all predictor variables on the outflow bias and the reversed signals in some regions (Fig. 5.5g,h,i).

5.5 WCB biases on sub-seasonal time scales and their link to MJO

So far the instantaneous and local representation of WCBs have been investigated at a given instantaneous day and specific grid-point. This is admittedly a challenging forecasting task and not suitable for sub-seasonal lead times beyond 15 days. In the following, biases for weekly averaged WCB frequencies are evaluated.

On average in week 1 (defined as days 1–7) negative WCB inflow biases extend in the western and northern part of the North Atlantic inflow region, with some positive biases in the southern part of the region (Fig. 5.6a), consistent with the patterns on days 3 and 7 (Fig. 5.1a,d). The western North Pacific experience a dipole pattern with negative biases to the north and positive biases south of the climatological maximum. In week 2 (defined as days 8–14) the patterns are similar to week 1, but biases increase in magnitude and saturate towards week 3 and 4 (defined as days 15–21, 22–28, respectively): over the Gulf of Mexico, a positive bias emerges in week 2 and over the eastern North Pacific, a dipole of positive biases in the south and negative biases in the north develops in week 2 (Fig. 5.6d,g,j).

The saturation of the bias can be further underlined by evaluating the area-averaged bias for week 1 to 4 for the North Atlantic and North Pacific region (Fig. 5.7). As in previous analyses, the North Atlantic and North Pacific regions are defined as in Fig. 5.3a. WCB inflow biases over the North Atlantic are dominated by negative biases that develop at early lead times and increase until mid week 3 (Fig. 5.7a). Afterwards biases saturate and slightly decrease in week 4. Positive biases dominate in week 1 and 2 over the North Pacific and slightly decrease and saturate in week 3 and 4.

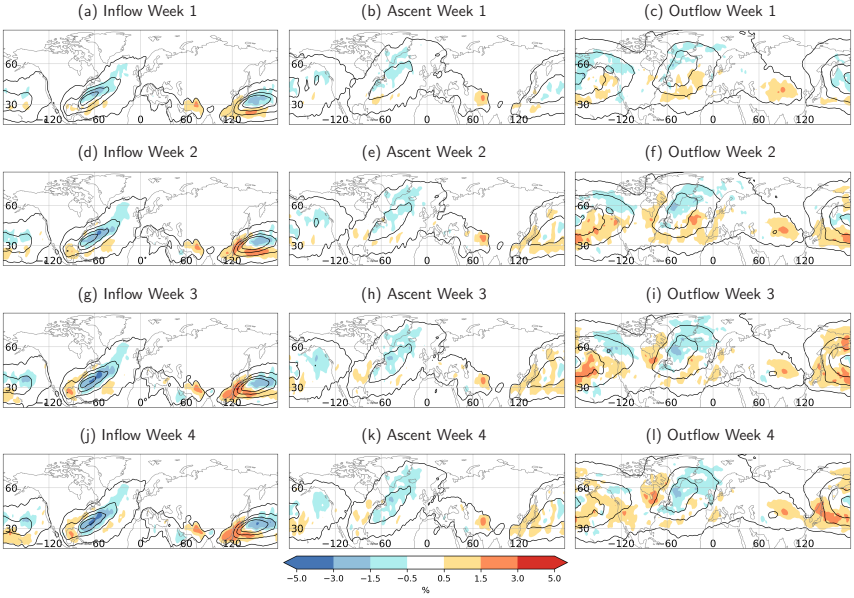


Figure 5.6: Weekly frequency bias of WCB (a,d,g,j) inflow, (b,e,h,k) ascent, (c,f,i,l) outflow for DJF 1997–2017 (shading) for (a-c) week 1, (d-f) week 2, (g-i) week 3, and (j-l) week 4. The black contours indicate a frequency of 1, 5, 10, 15 % in the respective layer.

WCB ascent is underestimated in week 1 north of the climatological maximum and over Greenland (Fig. 5.6b). The regions with negative biases further increase in week 2 and saturate in week 3 and 4 (Fig. 5.6e,h,k and Fig. 5.7b). WCB ascent biases over the North Pacific are also predominantly negative in week 1 (Fig. 5.6b). Negative biases over the eastern part increase in week 2 and saturate in week 3 and 4 (Fig. 5.6e,h,k). However, over the western part of the ocean basin, positive biases develop in week 2 and are dominant also in week 3 and 4. This is reflected in the averaged bias for the North Pacific: at the beginning of week 1 the skill is negative and then shifts to a positive bias in week 2 and saturates in week 3 and 4 (Fig. 5.7b).

The bias for WCB outflow is negative over the northern part and positive over the southern part of the North Atlantic in week 1 (Fig. 5.6c). Both negative and positive bias increase in magnitude in week 2 (Fig. 5.6f). The negative bias then

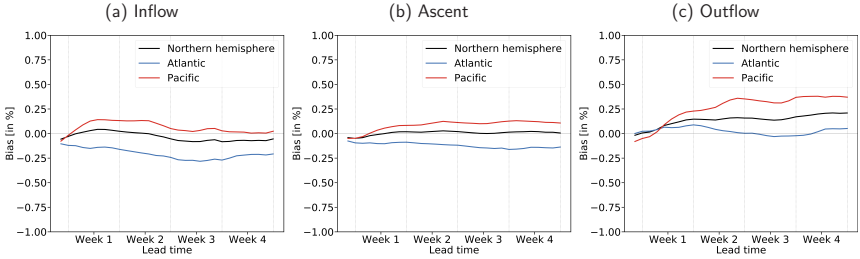


Figure 5.7: Area-averaged frequency bias for DJF 1997–2017 at different forecast lead times for the different WCB stages a) inflow, b) ascent, and c) outflow. The regions for the area-averaged frequency bias are indicated in Fig. 5.3a.

saturates in week 3 and 4 whereas the positive bias decreases (Fig. 5.6i,l). Averaged over the whole region, positive biases dominate in the first two weeks of the forecasts (Fig. 5.7c). Afterwards, negative biases occur predominantly in week 3 due to the decrease of positive biases.

The bias for WCB outflow is negative over the central North Pacific and western North America in week 1 (Fig. 5.6c). Positive biases occur over the southeastern North Pacific. Strong positive biases then develop in week 2 over a wide part of the central and eastern North Pacific (Fig. 5.6f). The outflow is still underestimated along the American west coast. However, these negative biases further decrease in week 3 and 4 (Fig. 5.6i,l). On the other hand, positive biases saturate over most regions over the ocean basin. The average over the North Pacific shows negative biases at early lead times in week 1 (Fig. 5.7c). The shift to strong positive biases occurs midway through week 1. The bias increases in week 2 and saturates in week 3 and 4.

Next the focus is on week 2, the time when most of the WCB outflow frequency biases saturate (Fig. 5.7c). First the link between WCB outflow biases and biases in the upper-tropospheric large-scale flow, as depicted by geopotential height at 300 hPa, is evaluated. Generally the forecasted large-scale extratropical flow in winter is too zonal and the planetary wave pattern is slightly shifted in week

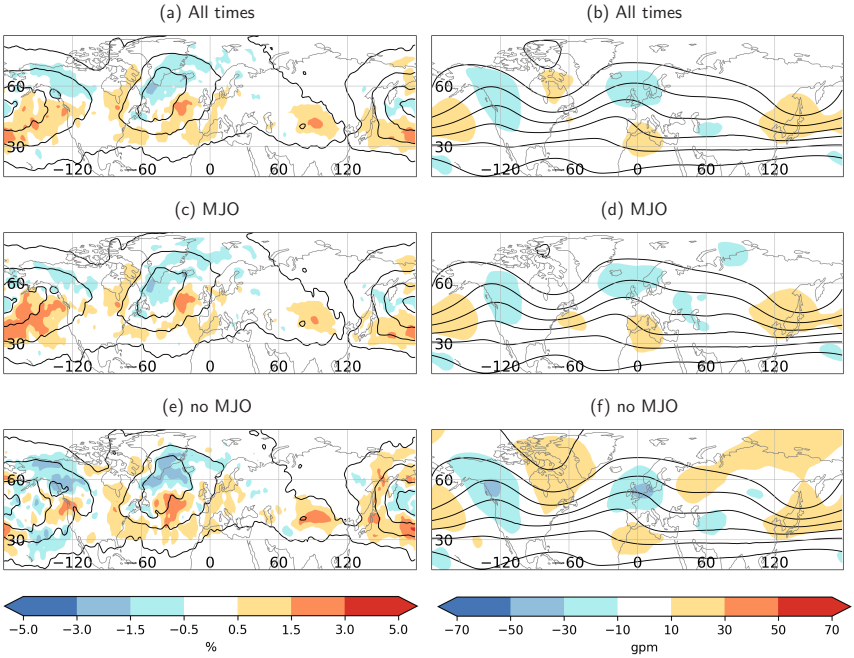


Figure 5.8: Frequency bias of WCB outflow (a,c,e) and bias of geopotential height field at 300 hPa (b,d,f) for day 8–14 (week 2) (DJF 1997–2017) (shading) using different forecast initial times: (a,b) all 920 initial times, (e,f) all 622 initial times with an active MJO at initialization, and (e,f) all 298 initial times with an inactive MJO at initialization. The black contours indicate a frequency of 1, 5, 10, 15 % and a geopotential height of 8400, 8600, 8800, 9000, 9200, 9400, and 9600 gpm in the respective layer.

2 (Fig. 5.8b): over the eastern North Pacific and western North America a pronounced dipole of around 20 gpm bias is evident with the negative pole slightly east of the apex of the stationary ridge. This is followed by a weaker positive anomaly centred on the stationary trough over eastern North America and a negative anomaly in the stationary ridge over Europe.

Consistently, the negative WCB outflow frequency biases occur just east of the too weakly amplified stationary troughs in both basins, and extend into the region of the stationary ridges downstream (Fig. 5.8a). These findings corroborate that the underestimated WCB outflow plays an important role for the underestimation

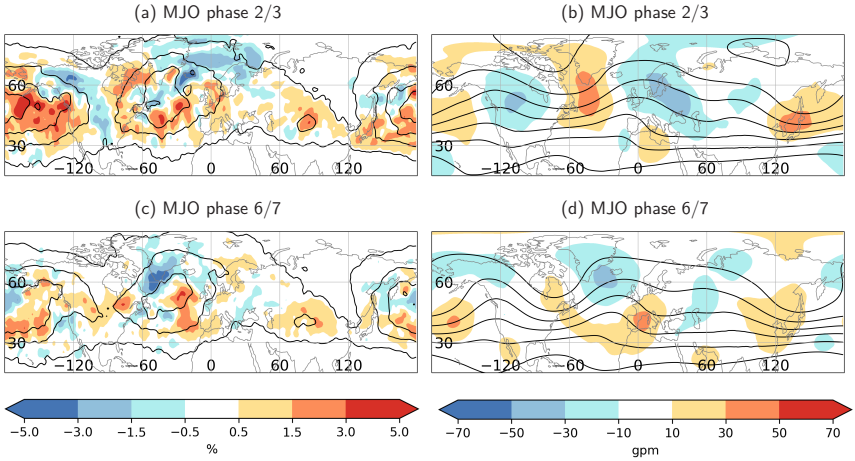


Figure 5.9: Frequency bias of WCB outflow (a,c,e,g) and bias of geopotential height field at 300 hPa (b,d,f,h) for day 8–14 (week 2) (DJF 1997–2017) (shading) using different forecast initial times: (a,b) all 134 initial times with an active MJO in phase 2/3 at initialization, and (c,d) all 219 initial times with an active MJO in phase 6/7 at initialization. The black contours indicate a frequency of 1, 5, 10, 15 % and a geopotential height of 8400, 8600, 8800, 9000, 9200, 9400, and 9600 gpm in the respective layer.

of the ridges. It is noteworthy that the geopotential height biases at 300 hPa also reflect a Rossby wave train spanning from the tropical central North Pacific, via North America into the Middle-East (Fig. 5.8b). This raises the question if the found biases can be related to tropical convection like the MJO. The MJO teleconnection is a main driver of sub-seasonal variability in winter and known to be too weakly represented in models (Vitart, 2017).

Interestingly, both WCB outflow biases and biases in 300 hPa geopotential height are enhanced if the MJO is inactive [1] at initialization time (Fig. 5.8e,f). On the other hand, an active MJO with an amplitude ≥ 1 overall yields a bias reduction (Fig. 5.8c,d). However, investigating biases in week 2 after an active MJO phase

[1] Here, inactive MJO means that the amplitude of the daily real-time multivariate MJO (RMM; Wheeler and Hendon, 2004) index $\sqrt{RMM1^2 + RMM2^2}$ is <1.

2/3 and 6/7 at initialization time reveals cancelling effects in bias patterns as discussed in the following (Fig. 5.9).

MJO phases 2/3 and 6/7 have been shown to be the most effective in establishing teleconnections from the tropics to the North Atlantic through Rossby wave propagation. An active MJO phase 2/3 typically leads to an increased probability of the positive phase of the North Atlantic Oscillation (NAO) one to two weeks later (Cassou, 2008, Lin et al., 2009). The model does not fully capture this teleconnection by underestimating the southward extent of the trough and the northward extent of the ridge over the North Atlantic and Europe (Fig. 5.9b) resulting in a generally too zonal planetary wave pattern. Biases in WCB outflow activity might explain these patterns. Negative WCB outflow biases emerge over the eastern North Atlantic in the region between Greenland and western Europe (Fig. 5.9a). On the other hand, WCB outflow frequencies are overestimated over northeastern North America and the southern tip of Greenland co-located with regions of overestimated geopotential height (Fig. 5.9a,b).

An active MJO phase 6/7 typically leads to a negative phase of the NAO one to two weeks later with ridging over Greenland. The model underestimates the northward extension of the ridge (Fig. 5.9d). This goes along with a strong underestimation of WCB outflow activity in this region (Fig. 5.9c). Interestingly, biases in 300 hPa geopotential height are weaker over the North Pacific and North America (Fig. 5.9d) compared to MJO phases 2/3 (Fig. 5.9b). This suggests the model's ability to establish the teleconnection into North America, but a lack of its continuation into Europe. At the same time WCB outflow biases are also smaller over western North America compared to phases 2/3 (Fig. 5.9b,d).

In summary, there is a remarkable link of negative/positive biases in WCB outflow and negative/positive geopotential height biases which change depending on the MJO state at forecast initialization time. Although the results cannot infer causality, they indicate that a better representation of WCB activity and its modulation by the MJO could reduce systematic errors in the planetary Rossby wave pattern and large-scale midlatitude flow.

5.6 WCB forecast skill on sub-seasonal time scales and its link to the MJO

The forecast skill for weekly averaged WCB frequencies is now further evaluated for the inflow, ascent, and outflow (Fig. 5.10). As described in Chapter 4, the skill at day 0 represents the skill for days 0–6, on day 1 for days 1–7, and so on. The skill horizon is again subjectively defined as the forecast lead time at which the $FBSS$ falls below 0.08.

For weekly WCB inflow forecasts, the skill horizon is reached around forecast day 11–17 (week 2–3) (Fig. 5.10a). It is significantly extended compared to the skill horizon for daily WCB inflow forecasts (8–9 days, Fig. 5.3b). As for daily WCB inflow forecasts, the skill for weekly forecasts is generally higher over the North Pacific compared to the North Atlantic. Significant differences emerge around forecast day 3–9 and prevail until day 5–11. However, before and after these lead times, the skill is similar over both Pacific and Atlantic.

The WCB ascent has a similar skill evolution with generally lower skill for weekly forecasts compared to WCB inflow (Fig. 5.10b). The forecast skill horizon is reached around day 9–15 (forecast week 2). Between day 3–9 and day 9–15, the ascent skill is higher over the Pacific compared to the Atlantic region.

As for daily forecasts, WCB outflow skill is highest on average (Fig. 5.10c). The skill for week 1 forecasts is around 0.48 compared to 0.45 for WCB inflow and 0.4 for WCB ascent. The skill horizon is around day 9–15 for the Atlantic and day 11–17 for the Pacific. The Pacific region exhibits significantly higher skill from around day 1–8 until 10–16.

These findings for weekly WCB forecasts indicate that the model can skillfully predict WCB signals beyond the medium range into forecast week 3 with again more skill for the North Pacific compared to the North Atlantic. This is line with Zheng et al. (2019) who found generally higher skill for extratropical cyclones in S2S forecasts over the North Pacific than over the North Atlantic (e.g., their Fig. 4b, c). A hypothetical explanation for the generally higher WCB skill over the North Pacific might be related to a link between WCB activity and the MJO

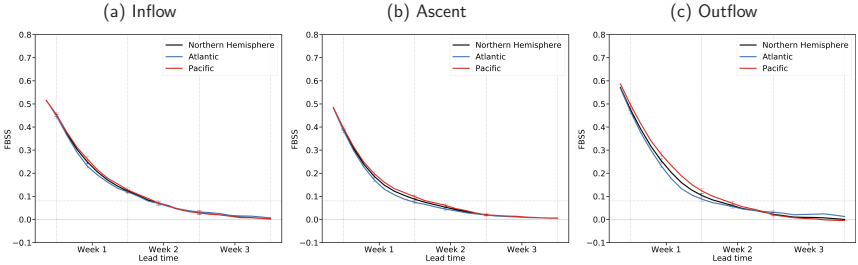


Figure 5.10: Area-averaged Fair Brier Skill Score (*FBSS*) for weekly mean WCB frequencies (in observation and forecast) for DJF 1997–2017 dependent on forecast lead time for a) inflow, b) ascent, c) outflow. For a specific lead time the value consists of the mean over the day and the following six days. I use the same regions as in Fig. 5.3a.

which exhibits significant forecast skill at even longer lead times (Vitart, 2017). This hypothesis will be further evaluated in the following Section.

First, maps of *FBSS* for weekly WCB frequencies in week 1 and 2 are evaluated to identify regions with higher and lower skill for weekly forecasts (Fig. 5.11). The skill patterns in week 1 for WCB inflow reflect patterns for daily inflow forecasts (cf. Fig. 5.4a,b, Fig. 5.11a). High WCB inflow skill over the Atlantic can be found south of the climatological maximum (0.5–0.7) (Fig. 5.11a). The skill is lower further north along 40–50N and over the eastern Atlantic.

For the WCB ascent, the skill for weekly forecasts is more evenly distributed with skill around 0.4–0.6 over most parts of the Atlantic (Fig. 5.11c). For WCB the outflow, the *FBSS* is relatively low over the east of the climatological maximum and over Europe (0.3–0.5) (Fig. 5.11e). In contrary, high skill (0.5–0.6) can be found over the other parts of the Atlantic.

For forecast day 8–14 (week 2), the regions with high skill for WCB inflow and outflow are similar to forecast week 1 (Fig. 5.11b,f). WCB ascent skill exhibits generally low skill at forecast week 2 over the Atlantic (Fig. 5.11d). In a few regions of the Atlantic, sufficient skill prevails also for this lead time.

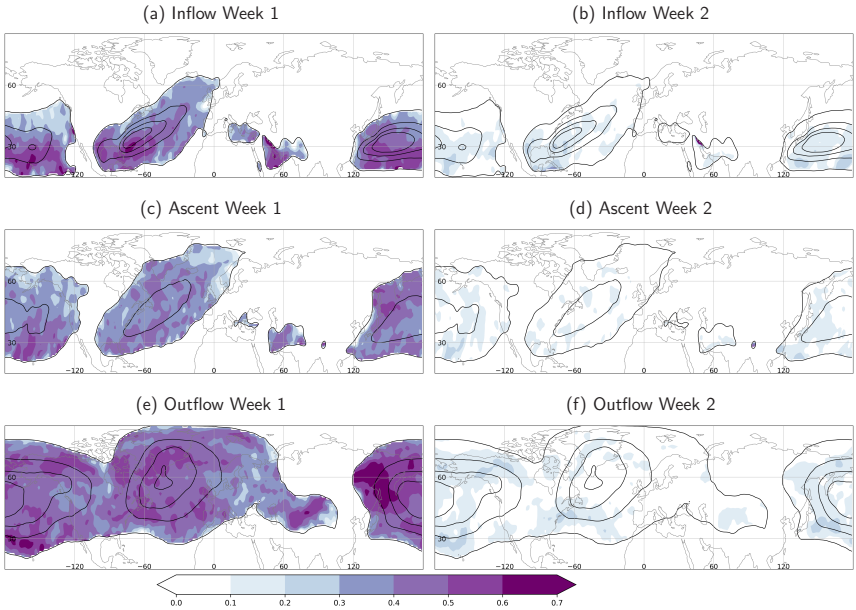


Figure 5.11: Fair Brier Skill Score (*FBSS*) of WCB forecast for (a,b) inflow, (c,d) ascent, (e,f) outflow for DJF 1997–2017 (shading) at different forecast lead times: (a,c,e) week 1, (b,d,f) week 2. The black contours indicate a WCB frequency of 1, 5, 10, 15% in the respective layer.

Over the Pacific, the regions south of the climatological maximum have the highest skill for weekly WCB inflow frequencies in week 1 (Fig. 5.11a). The skill is generally lower over the northern inflow regions. WCB ascent exhibits high skill to the northwest and southeast of the climatological maximum (Fig. 5.11c). These regions with high skill are similar compared to daily ascent forecasts for day 3 and 7 (Fig. 5.4c,d). In line with high WCB ascent skill, the WCB outflow has high skill to the northwest, north and south of the climatological maximum (Fig. 5.11e). The skill is lower in the region with highest outflow frequencies and over the western USA. In forecast week 2, the regions with high skill for WCB inflow, ascent, and outflow are similar to forecast week 1 (Fig. 5.11b,d,f). All WCB stages still have relatively high WCB skill above 0.1 for these lead times indicating the higher predictability of weekly frequencies.

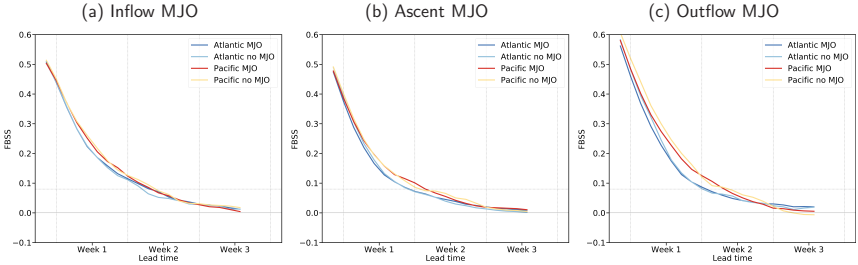


Figure 5.12: Area-averaged Fair Brier Skill Score (*FBSS*) for weekly mean WCB frequencies as in Fig. 5.10 for (a,d) inflow, (b,e) ascent, (c,f) outflow depending on (a-c) active (inactive) MJO and (d-f) different MJO phases at initialisation.

As a final step the link between the generally higher WCB skill over the North Pacific and the MJO is investigated. Therefore, the *FBSS* for the North Pacific and North Atlantic regions is computed during active (inactive) MJO phases at initialization time.

For the North Pacific region, there is similar skill in predicting WCB inflow and ascent for weeks 1 and 2 when there is an active MJO at initialization time compared to the times with an inactive MJO at initial time (Fig. 5.12a,b). For WCB outflow, the skill is somewhat lower for week 1 after active MJO phases (Fig. 5.12c). The skill differences decreases for week 2 where skill levels are similar. The analysis for the Pacific region shows that averaged WCB skill is not enhanced after active MJO phases. This results refutes the hypothesis that the MJO yields enhanced WCB skill over the Pacific region. However, it is important to mention that the WCB skill varies between MJO phases. For example, there is very low skill over the eastern North Pacific after MJO phases 2/3 (see Appendix Fig. A.1). Contrary, WCB skill is enhanced after other MJO phases indicating that the model captures the teleconnection signals from the MJO for these cases better.

For the North Atlantic region, there is generally higher WCB forecast skill for week 1 and 2 when there is an inactive MJO at initial time. This is particularly pronounced for WCB outflow in week 1 (days 4–10). These findings corroborate that the MJO signal is lost before reaching the North Atlantic region.

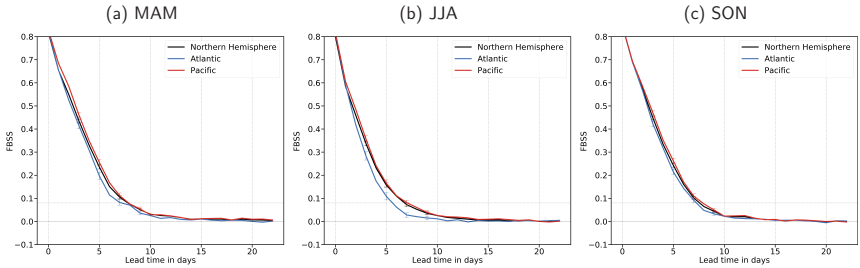


Figure 5.13: Area-averaged Fair Brier Skill Score (*FBSS*) as in Fig. 5.3 for WCB outflow in a) MAM, b) JJA, and c) SON.

5.7 Seasonal variation of WCB bias and skill

So far WCB representation has been analysed for the boreal winter season since WCB frequencies are higher compared to other seasons. In general, WCB frequencies are lowest in summer and vary strongly between seasons and regions (Madonna et al., 2014). Therefore, WCB outflow is now further analysed in terms of bias and skill for the other seasons.

The skill horizon for daily WCB outflow forecasts in MAM is around 8 to 9 days (Fig.5.13a) and thus very similar to the skill horizon in DJF (Fig.5.3c). The forecast skill in the North Pacific is significantly higher between forecast day 3 and 7 compared to the North Atlantic.

In boreal summer, WCB outflow skill is lower compared to MAM and DJF (cf. Fig.5.13a,b, Fig.5.13c). The lower skill emerges around day 2 leading to a forecast skill horizon of 6 to 7 days. These findings are in agreement with other studies which find lower forecast skill for the ECMWF forecasting system in summer (Buizza et al., 1999). As for the other seasons, WCB outflow skill is significantly higher in the Pacific compared to the Atlantic from day 3–9.

Lastly, the forecast skill horizon in SON is around 7 to 8 days (Fig.5.13c). Again, forecast skill is higher in the North Pacific region from day 2 to 9 with significant differences between day 3 and 6.

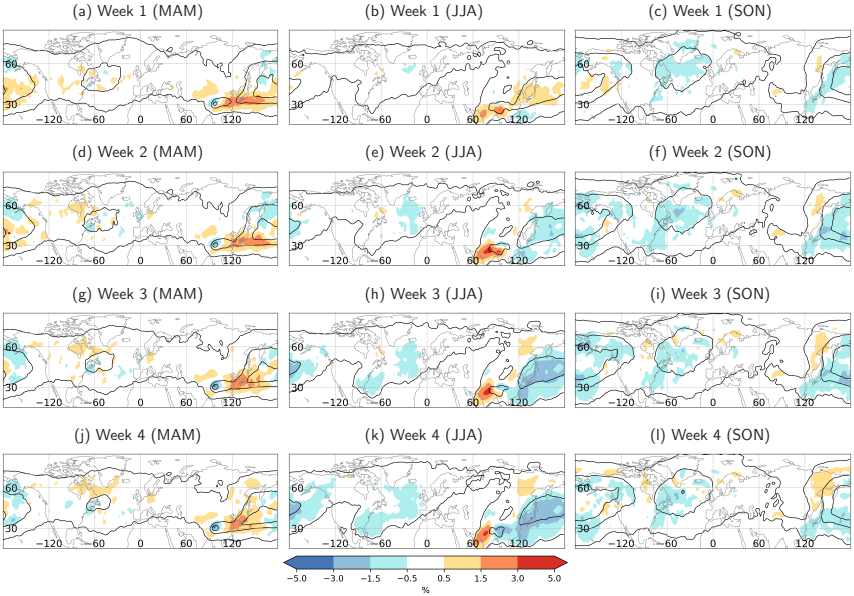


Figure 5.14: Weekly frequency bias of WCB outflow in (a,d,g,j) MAM, (b,e,h,k) JJA, (c,f,i,l) SON 1997–2017 (shading) for (a-c) week 1, (d-f) week 2, (g-i) week 3, and (j-l) week 4. The black contours indicate a frequency of 1, 5, 10, 15 % in the respective layer.

The representation of WCB outflow in other seasons is now further analysed in terms of weekly frequency biases. Over the Atlantic, the frequency maximum in spring occurs over the western part and is around 5% lower compared to the winter season (cf. Fig. 5.6c, Fig. 5.14a). Positive biases emerge in forecast week 1 south and east of the climatological maximum. The model overestimates the frequency by around 1% which corresponds to a relative overestimation of 20–30%.

In forecast week 2, positive biases over eastern Canada cover a larger area compared to week 1 while negative biases evolve along the US East Coast (Fig. 5.14d). As seen in Fig. 5.7c, WCB outflow biases in winter generally saturate around forecast week 2–3. The area-averaged WCB outflow bias in MAM is lower compared to winter and saturates in forecast week 3 (Fig. 5.15a). Biases

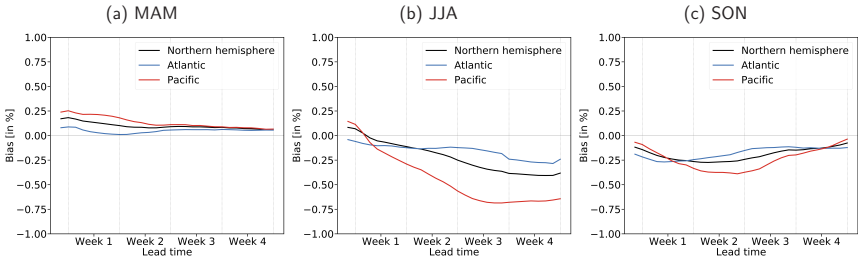


Figure 5.15: Area-averaged frequency bias for WCB outflow at different forecast lead times for a) MAM, b) JJA, and c) SON. The regions for the area-averaged frequency bias are indicated in Fig. 5.3a.

in forecast week 3 and 4 (Fig. 5.14g,j) reflect the dipole pattern found in week 2 (Fig. 5.14d).

Over the western Pacific, the maximum of WCB outflow frequencies is shifted to the west in MAM compared to DJF (cf. Fig. 5.6c, Fig. 5.14a). In the Pacific region, WCB outflow forecasts exhibit strong positive biases already at early lead times in forecast week 1 (Fig. 5.14a). The reforecasts strongly overestimate the outflow frequency over eastern China, southern Japan and the western North Pacific along 30–40°N (Fig. 5.14a). The positive biases range from 1–3% which equals a relative overestimation of 20–60% in this region.

In spring and summer, the Meiyu front causes large amounts of the precipitation over southeastern Asia and the western Pacific (Ninomiya and Shibagaki, 2007). The WCB activity is likely linked to these activity corroborating a potential overestimation of Meiyu frontal rainfall in spring in the model. Further east, there is a dipole structure along the date line with positive biases to the south and negative biases to the north. The positive and negative biases over the North Pacific region saturate already in forecast week 1 (Fig. 5.15a) and remain similar in sign and magnitude for later lead times (Fig. 5.14d,g,j).

In boreal summer, WCB frequencies decrease over southeastern Asia and the western Pacific compared to spring (Fig. 5.14b). These frequencies are likely connected to the Meiyu front as well as the Indian and East Asian Monsoon (Yihui and Chan, 2005). In most regions a WCB frequency overestimation occurs already in forecast week 1 (Fig. 5.14b). In particular, the outflow frequencies are

overestimated by around 1–3% over southeast Asia and the western North Pacific which equals a relative overestimation of 20–60% in these regions.

In forecast week 2, positive biases over southeast Asia increase in magnitude and reach 3–5% (Fig. 5.14e). Contrary, the overestimation of outflow frequencies over the western Pacific in week 1 can not be found in week 2 where negative biases of 1–3% emerge in this region (Fig. 5.14e).

The average bias for the Pacific is strongly dominated by this bias shift over the western Pacific in forecast week 2 (Fig. 5.15b). The average biases are positive in week 1 and negative from week 2 to week 4. The negative bias over the western Pacific further increases in forecast week 3 and saturates afterwards (Fig. 5.14h,k, Fig. 5.15b).

The magnitude of the average bias over the Pacific in summer is higher compared to other seasons. This large WCB bias likely leads to forecast errors in the large-scale circulation over the Pacific.

Over the North Atlantic, WCB outflow frequencies in summer are lowest compared to the three other seasons (Fig. 5.14b). In forecast week 1, the reforecasts underestimate the frequencies south of Iceland by around 1% (Fig. 5.14b). Due to the low climatological frequency this equals a relative underestimation of 20–50%.

In forecast week 2, the area with negative biases of around 1% increases over the eastern Atlantic (Fig. 5.14e). For later lead times, a negative bias also emerges along the US East coast while the negative bias over the eastern Atlantic prevails (Fig. 5.14h,k). The development of negative bias in forecast week 3 and 4 along the US east coast is reflected in the area-averaged bias which shows an overall increase of the negative bias from forecast week 1 to forecast week 4 with a saturation in week 4 (Fig. 5.15b).

Lastly, the WCB frequency biases are now investigated for forecasts initialised between September and November. WCB outflow over the Atlantic is enhanced compared to the summer with a maximum of around 5% over the western part of the ocean basin (Fig. 5.14c). The reforecasts underestimate outflow frequencies

in forecast week 1 (around 1%) which equals a relative underestimation of around 20–30%. In forecast week 2, the magnitude of negative biases increases and an underestimation of 1–3% can be found along the east coast of the USA and southeast of Iceland. (Fig. 5.14f).

In boreal autumn, the frequency of northeastward recurving tropical cyclones (TCs) is highest compared to other seasons (Hart and Evans, 2001). Over the western Atlantic, TCs typically undergo extratropcial transitions (ET) and subsequently propagate eastwards toward Europe (Jones et al., 2003). The negative WCB outflow bias in this region is likely also influenced by the strong diabatic outflow from these TCs. In forecast week 3 and 4, the magnitude of the negative bias decreases again (Fig. 5.14i,l) which results in a decrease of the area-averaged bias for these lead times (Fig. 5.15c).

High TC activity also occurs in the western Pacific in autumn and likely affect WCB biases in this region. In general, the reforecasts both over- and underestimate WCB outflow frequencies over parts of the Pacific region in forecast week 1 (Fig. 5.14c). Positive biases occur over the eastern North Pacific and negative biases can be found over the western and central North Pacific (around 1% respectively). These biases equal a relative over- and underestimation of 10–30%.

The negative biases increase in forecast week 2 (1–3%) (Fig. 5.14f) which is reflected in the increase of area-averaged biases over the entire Pacific region (Fig. 5.15c). In forecast week 3, positive biases over eastern Russia cover a larger area compared to earlier lead times (Fig. 5.14i). This development together with a decrease of the magnitude of negative biases over the eastern Pacific leads to a decrease of the area-averaged negative bias in forecast week 3 and 4 (Fig. 5.15c).

In conclusion, WCB outflow biases also emerge already at early lead times for other seasons. Over the North Atlantic, negative biases occur predominantly in summer and autum while biases are lower in spring. The WCB outflow is strongly overestimated over southeast Asia and the western Pacific for early lead times in spring and summer.

5.8 Conclusions

This Chapter presents a systematic investigation of the representation of warm conveyor belts (WCBs) in terms of frequency bias, forecast reliability, and forecast skill in the ECMWF's IFS sub-seasonal reforecasts (1997–2017). The analysis uses the statistical models for the WCB inflow, ascent, and outflow stage based on convolutional neural networks (CNNs) (Quinting and Grams, 2021a) and WCB predictor variables which are identified in a previous version of the statistical models (Quinting and Grams, 2021b). The CNNs are applied to 20 years (1997–2017) of forecast data in all four seasons yielding a total of around 900–1000 initial times for each respective season.

Significant WCB frequency biases occur already at early lead times (forecast day 3) which increase to forecast day 7, and saturate afterwards. In boreal winter, there is a tendency towards a general overestimation of WCB frequency over the southern part and an underestimation over the northern part of the North Atlantic for all WCB stages. Over the North Pacific, there is a relatively large overestimation of 30–100% of the WCB inflow in some regions of the western part of the ocean basin and a large underestimation of similar magnitude for the WCB outflow over the eastern part of the ocean basin.

In boreal summer and autumn, WCB outflow frequencies are generally underestimated over the North Atlantic and for lead times beyond forecast week 1 also over the North Pacific. In boreal spring, the outflow frequencies are generally overestimated over the North Atlantic region and the western Pacific.

The results for the WCB frequency biases yield the question if WCB biases can be linked to biases in the predictor variables of the logistic regression models. The results in this Chapter show strong correlations between WCB inflow (ascent) biases and biases in meridional moisture flux at 850 hPa (500 hPa). These biases in moisture flux, in particular over the North Pacific, correspond to biases in the atmospheric river frequency in ECMWF's S2S forecasts reported by DeFlorio et al. (2019).

For the WCB outflow, the correlation varies between the different predictor variables and the North Atlantic and North Pacific region. The correction of the biases in the predictor variables of a previous version of the statistical models (Wandel et al., 2021) leads to a reduction in biases for the WCB inflow and ascent, but only in some regions for the WCB outflow. These findings indicate a potential pathway to a reduced WCB inflow and ascent bias by reducing biases in the meridional moisture flux in the lower to mid troposphere.

Finally, the analysis in this Chapter, for the first time, quantifies the overall forecast skill horizon for WCBs in NWP models, facilitated by the availability of the reforecast data set and novel diagnostics. The overall forecast skill horizon is around 8–10 days for instantaneous prediction of all three WCB stages. There is significantly higher skill over the North Pacific region compared to the North Atlantic region for most lead times and WCB stages.

For the North Atlantic and North Pacific, higher WCB forecast skill can be found over the western part of the ocean basins compared to the eastern part. A possible explanation of the lower skill over the eastern part of the ocean basins could be the relatively higher frequency of secondary cyclones (Priestley et al., 2020, Schemm et al., 2018) which are smaller in scale and potentially harder to predict.

Weekly mean WCB frequencies can be skillfully predicted beyond the medium range up to week 3 with again more skill for the North Pacific compared to the North Atlantic. This is line with (Zheng et al., 2019) who found generally higher skill for extratropical cyclones in S2S forecasts over the North Pacific than over the North Atlantic (e.g., their Fig. 4b, c). A hypothetical explanation for the generally higher WCB skill over the North Pacific might be related to a link between WCB activity and the MJO which exhibits significant forecast skill at even longer lead times (Vitart, 2017).

However, the results in this Chapter show that area-averaged WCB skill after active MJO phases over the Pacific is not higher compared to inactive MJO phases. For the North Atlantic, there is even higher skill in predicting WCB ascent and outflow after inactive MJOs which indicates that the MJO signal is lost before

reaching the North Atlantic region.

Since errors in the representation of the WCB can influence the midlatitude large-scale flow, biases for WCB outflow and geopotential height at 300 hPa on sub-seasonal time scales are further investigated. The WCB outflow is underestimated over the eastern North Pacific and western North Atlantic which can be linked to an underestimation of the northward extent of the midlatitude flow at 300 hPa. Furthermore, there is a strong underestimation of the WCB outflow activity and northward extension of the ridge over the eastern North Pacific (western North Atlantic) two weeks after MJO phase 2 and 3 (6 and 7) which has also been shown by Vitart (2017).

Previous studies have shown that an inaccurate representation of WCBs in NWP models can lead to errors in the downstream Rossby wave pattern (e.g., Baumgart et al., 2018, Berman and Torn, 2019, Grams et al., 2018, Lamberson et al., 2016, Maddison et al., 2019, Martínez-Alvarado et al., 2016, Rodwell et al., 2018). The systematic underestimation of WCBs in the climatologically most active regions as well as north of these regions may have an impact on the downstream flow evolution and thus contribute to error in the downstream Rossby wave pattern. Since diabatic processes associated with WCBs can be important in the onset and maintenance of blocking anticyclones (Pfahl et al., 2015, Steinfeld and Pfahl, 2019), the underestimation of WCB activity over the North Atlantic may at least partly explain negative blocking frequency biases over the North Atlantic-European Region (Quinting and Vitart, 2019). This hypothesis is further evaluated in the following Chapter.

6 Impact of WCBs on atmospheric blocking over Europe

In this Chapter the role of WCBs for the onset of atmospheric blocking over the European region (EuBL) is investigated on the basis of ECMWF's IFS reforecasts and reanalysis in the extended winter period from 1997–2017. As discussed in Chapter 2, latent heat release in WCBs is of first order importance for the onset and maintenance of blocking anticyclones (Pfahl et al., 2015). Furthermore, recent studies point to the role of WCBs for severe forecasts busts over the Atlantic-European region (Grams et al., 2018). The misrepresented WCB generates and amplifies forecast errors in the NWP model which leads to a missed onset of a block over the European region. On top of that, the skill of the reforecasts in predicting EuBL is significantly lower compared to other weather regimes (Büeler et al., 2021). Therefore, investigating the role of WCBs for the onset of EuBL is of high interest for medium-range and sub-seasonal weather prediction.

EuBL is the dominant blocking regime over Europe in winter and occurs at around 11% of winter days. The following Sections investigate the representation of WCB activity and geopotential height in 500 hPa (Z500) around EuBL onsets in the reforecasts. They further evaluate the overall role of the WCB by linking WCB activity to EuBL forecasts with high and low forecast skill. Lastly, the role of local influences over the North Atlantic on EuBL skill are identified together with upstream precursors from North America and the North Pacific.

6.1 Representation of EuBL onsets in reforecasts

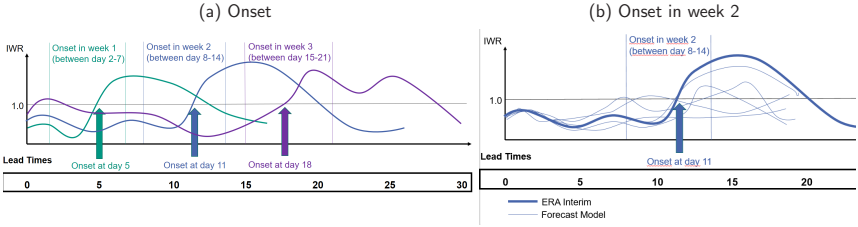


Figure 6.1: Illustration of weather regime life cycles based on the I_{WR} (Michel and Rivière, 2011) with onsets at different forecast lead times in a) ERA-Interim and b) for different ensemble members and a regime onset in forecast week 2.

First, the representation of EuBL in the reforecasts is investigated around observed onsets that occur at different forecast lead times. The analysis evaluates how well the reforecasts can represent characteristics of Z500 and WCB activity. As described in Chapter 4, ERA-Interim is treated as the perfect ensemble member to calculate observed regime onsets in forecast week 1, 2, and 3. The regime onset is defined as the day the I_{WR} surpasses a certain threshold (Fig. 6.1a). In order to fulfill the life cycle criteria, the I_{WR} has to be above this threshold for at least five days and the regime must have the highest overall I_{WR} of all regimes at least once (Grams et al., 2017).

Onsets in forecast week 1 are considered when they occur between forecast day 2 and 7. Due to the persistence of the regime, this leads to active life cycles of the regime in week 2 and sometimes even week 3. Onsets in forecast week 2 occur between day 8 and 14 and lead to life cycles in week 3 and 4 while onsets in week 3 (between day 15 and 21) have life cycles in week 4 and sometimes even week 5. By construction, regime onsets occur on average on day 5 in week 1, day 11 in week 2 and day 18 in week 3. In the extended winter period from 1997 to 2017, a total of 117 observed EuBL onsets occur in forecast week 1, 137 events in week 2, and 140 events in week 3.

First, weekly mean composites of Z500 and WCB outflow around EuBL onsets are calculated in ERA-Interim to evaluate characteristics of the observed patterns and a potential link between Z500 and WCB activity (Fig. 6.2). For all EuBL

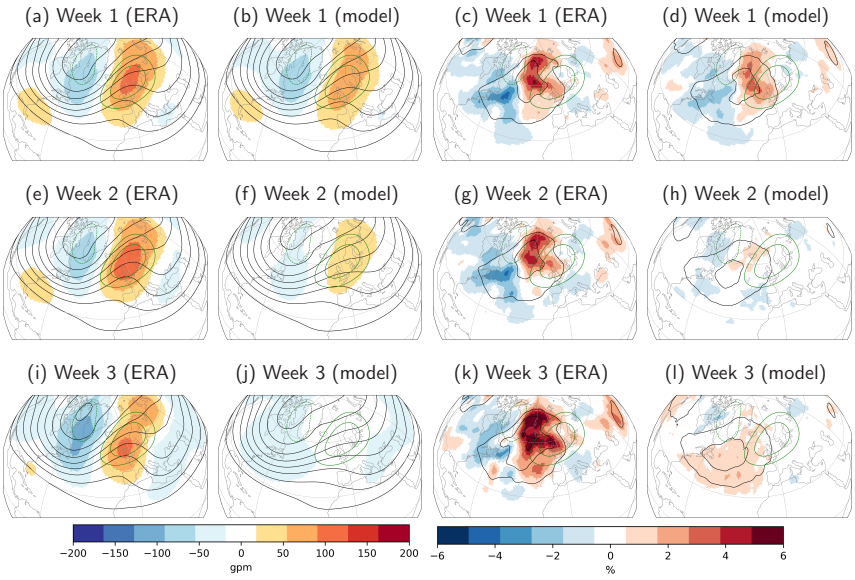


Figure 6.2: Weekly mean 500 hPa geopotential height anomalies (shading) around EuBL onset in (a,b) forecast week 1, (e,f) week 2, and (i,j) week 3 for (a,e,i) ERA-Interim and (b,f,j) ECMWF's IFS reforecasts. Black contours show absolute fields (5100–5800 gpm, every 100 gpm). Weekly mean WCB outflow frequency anomalies (shading) around EuBL onset in (c,d) forecast week 1, (g,h) week 2, and (k,l) week 3 for ERA-Interim (c,g,k) and ECMWF's IFS reforecasts (d,h,l). Black contours show absolute frequencies for ERA-Interim and reforecasts (5, 10, 15%). Green contours indicate geopotential height anomalies (-50,50,100 gpm) for all EuBL cases from 1979–2015.

onsets across lead times, the large-scale flow reflects the developing block over Europe with marked positive Z500 anomalies extending from western Europe to Scandinavia (Fig. 6.2a,e,i). Upstream, negative anomalies indicate a strong trough over the western and central North Atlantic.

The WCB outflow activity is strongly enhanced over Greenland and northwestern Europe around the onset (Fig. 6.2c,g,k), i.e., upstream and in the region of the EuBL Z500 anomaly. Outflow frequencies are reduced over the western North Atlantic with negative anomalies of 2–4%. As for Z500, WCB outflow anomaly patterns are similar for the different lead times. As reported in earlier studies (Grams et al., 2018, Pfahl et al., 2015, Steinfeld and Pfahl, 2019), the characteristics of Z500 and WCB activity around EuBL onsets corroborate that WCBs

play a vital role in the formation of the blocked regime. The small differences between the forecast weeks indicate a general robustness of the sample size.

Next, the representation of the observed Z500 and WCB patterns is evaluated in the reforecasts for the different lead times. The ensemble mean of all members is calculated around the observed regime onsets in week 1, 2, and 3. As illustrated in Fig. 6.1b, the reforecasts capture the observed regime onsets and subsequent life cycles with some ensemble members while other members miss the onset and have smaller I_{WR} values. NWP models can generally predict regimes well in forecast week 1 with decreasing skill for week 2 and 3 (Büeler et al., 2021). Therefore, the ensemble mean typically contains more members that correctly capture the onset in week 1 compared to week 2 and 3.

In week 1, the reforecasts capture the Z500 anomaly patterns over the Atlantic and Europe generally well (Fig. 6.2b). However, the positive anomalies over Europe are underestimated by around 20–30 gpm. Since the ensemble mean of the reforecast is used, the reasons for the underestimation are likely two-fold: first, the composites include ensemble members that miss the EuBL onset and likely have a more zonal wave pattern over Europe. Second, the ensemble members that capture the onset might have different magnitude, location, and timing of the corresponding Z500 anomaly. Still, the negative anomaly patterns over the Atlantic are better captured than anomalies over Europe which indicates that forecast errors primarily emerge in the region of the block over Europe. The relation of these errors to WCB activity is further evaluated after the analysis of EuBL onset forecasts in week 2 and 3.

In week 2, the reforecasts capture the anomaly patterns around EuBL onsets but underestimate their magnitude (in particular positive anomalies; Fig. 6.2f). Furthermore, the model underestimates the positive anomalies along the US East coast. In week 3, the reforecasts strongly underestimate the positive anomalies over Europe and predict a more zonal flow (Fig. 6.2j). It shows the challenges of predicting EuBL onsets at this forecast lead time.

WCB outflow anomaly patterns are generally well represented in forecast week 1 by the reforecasts (Fig. 6.2d). Still, the frequencies are underestimated by around 1–2%. This frequency underestimation points to a potential link to the underestimation of the positive Z500 anomalies in this region. In week 2, the reforecasts then strongly underestimate the enhanced WCB activity over the central and eastern North Atlantic (Fig. 6.2h). The outflow frequency underestimation is similar in forecast week 3 while small positive anomalies emerge over the southern and eastern North Atlantic (Fig. 6.2l).

In summary, the ensemble mean of the reforecasts underestimates the positive Z500 anomalies in the region of the block over Europe for onsets in forecast week 1, 2, and 3. The anomaly patterns are captured and only slightly underestimated in week 1 and not captured in week 3. For all lead times, the underestimation of Z500 coincides with an underestimation of WCB outflow frequencies over the central and eastern Atlantic. The results indicate that there is a potential link between the underestimation of Z500 and WCBs over the Atlantic and Europe in the reforecasts.

6.2 EuBL onset evolution in ERA-interim and reforecasts

The findings for the ensemble mean forecasts indicate that errors in the prediction of the EuBL regime might be related to high WCB activity which is not represented well in the reforecasts. As illustrated in Fig. 6.1b, certain ensemble members can capture the onset of the block while other miss it due to a shorter persistence of the regime or a stronger projection into a different regime.

The ensemble members that do capture an observed life cycle are now further evaluated. These members are defined as Hits and make up one part of the reforecast climatology of EuBL events. The other part is added by the False Alarms and contain all EuBL onsets in the reforecasts that occur without an observed onset at the same time (see Chapter 4.4.2 for further explanation). This reforecast

climatology of EuBL events is now evaluated in terms of the evolution of Z500 and WCB activity prior to the onset of the regime.

The investigation reveals how the reforecast establish Z500 patterns around EuBL onsets in their own climatology. For this analysis, only EuBL onsets in forecast week 2 are considered, since onsets of large-scale flow regimes in week 2 are of particular interest from a sub-seasonal prediction perspective. Due to the persistence of regimes, they strongly influence the circulation in forecast week 3 and sometimes even week 4. Differences of the temporal evolution of WCB frequencies and Z500 patterns in the reforecasts are evaluated compared to observed EuBL onsets.

Around observed EuBL onsets, there is a zonal flow with negative Z500 anomalies (around -70 gpm) on the western flank of the incipient block and positive anomalies over eastern Scandinavia and southwestern Europe six to four days prior to the onset (Fig. 6.3a). Subsequently, the wave pattern amplifies increasing positive anomalies and weakening negative anomalies (Fig. 6.3d). The developing block becomes more evident two to zero days prior to the onset with positive anomalies of 20-90 gpm over western Europe and Scandinavia (Fig. 6.3g). Upstream, an upper-level trough is established with negative anomalies reaching from Greenland to eastern Canada.

In the reforecast climatology of ensemble members with EuBL life cycles, negative Z500 can be found in the region of the incipient block and small positive anomalies occur over the central North Atlantic (Fig. 6.3b). Compared to the observations, the flow pattern is shifted eastwards resulting in significantly higher Z500 (20–40 gpm) on the western flank of the incipient block and lower Z500 over Scandinavia (Fig. 6.3c). Subsequently, the wave pattern amplifies and the developing ridge becomes evident over Iceland (Fig. 6.3e). In this region positive differences prevail while negative differences increase over the eastern Atlantic and western Europe (Fig. 6.3f).

Two to zero days prior to the onset, the upstream trough is evident over eastern Canada and Greenland and the block forms over western Europe (Fig. 6.3h). The

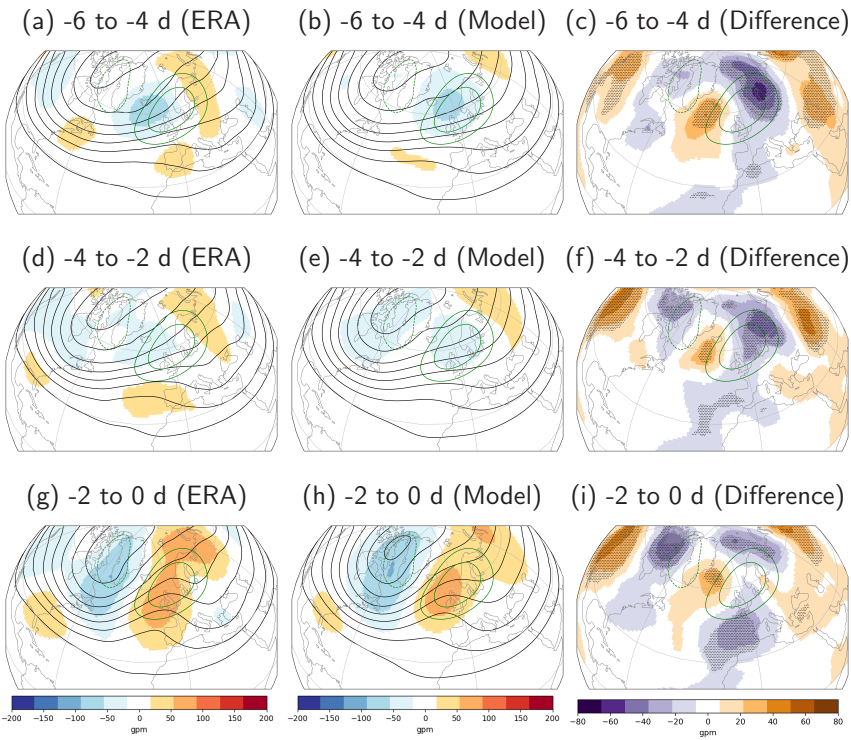


Figure 6.3: Z500 anomalies (shading) six to four days (a-c), four to two days (d-f), and two to zero days prior (g-i) to EuBL onset in (a,d,g) ERA-Interim and (b,e,h) reforecasts (NDJFM; 1997–2017). Contours indicate absolute fields (5100–5800 gpm every 100 gpm; NDJFM 1997–2017). (c,f,i) show differences (shading) with significance indicated by point stippling (t-test; 98 th confidence interval). Green contours as in Fig. 6.2

.

incipient block is shifted northwestwards compared to the observations which results in significantly higher Z500 around Iceland (Fig. 6.3i). Furthermore, the reforecasts have significantly lower positive Z500 anomalies over southwestern Europe and northern Scandinavia.

The analysis of the temporal evolution of Z500 prior to EuBL onsets reveals that the observed block is established from a zonal flow with negative anomalies over Iceland together with a merging and amplification of a pre-existing ridge over

eastern Scandinavia. The reforecasts underestimate Z500 anomalies until two to zero days before the onset. Only from then on similar Z500 anomalies emerge in the region of the incipient block. Structural differences arise predominantly over southwestern Europe and upstream of the incipient block resulting in weaker and northwestward shifted Z500 anomalies in the reforecasts. The temporal evolution of Z500 prior to the onset indicates that the ensemble members that capture EuBL life cycles in the reforecasts establish the block differently than observed. Now, the WCB activity and its potential role in establishing Z500 anomalies is evaluated.

Observed WCB outflow is anomalously high prior to EuBL onset underlining the importance of diabatic processes for the EuBL onset (Fig. 6.4a,d,g). Six to four days prior to the onset, two main areas of high WCB outflow activity can be found (1) over eastern Canada (frequency of 10–15%, anomalies of 7–10%) and (2) over the eastern North Atlantic (Fig. 6.4a). WCB activity strongly increases over the central and eastern North Atlantic four to two days prior to the onset (frequencies 5–10%, anomalies 3–8%) (Fig. 6.4d) likely contributing to the amplification of the large-scale flow in this region (Fig. 6.3d). Subsequently, WCB activity shifts northeastwards with anomalous outflow reaching from Greenland to the northern tip of Scotland (Fig. 6.4g).

The ensemble members with EuBL life cycles have WCB outflow frequencies which are similar to climatology six to two days prior to the onset (Fig. 6.4b,e). Positive anomalies of 1–2% only emerge over western Europe (Fig. 6.4b) and southern Greenland (Fig. 6.4e). Thus, differences compared to the observations mainly reflect the observed frequencies. The reforecasts have significantly lower WCB frequencies over eastern Canada six to four days before the onset (Fig. 6.4c) and over western Europe four to two days before the onset (Fig. 6.4e). Recalling the stronger observed flow amplification over southwestern Europe (Fig.6.3f), these results corroborate that there appears to be a link to high WCB activity.

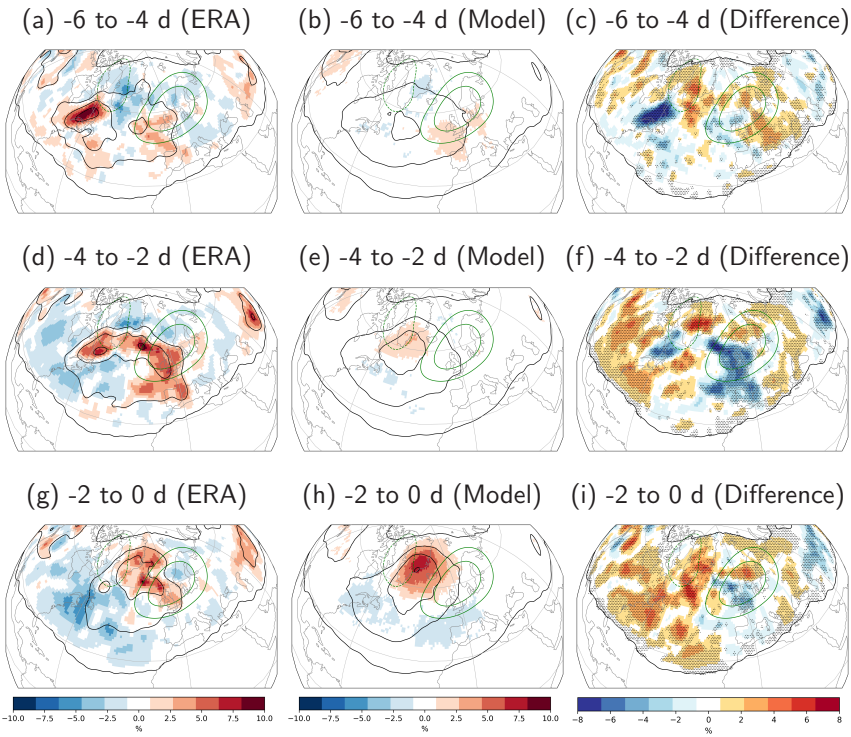


Figure 6.4: WCB outflow frequency anomalies (shading) 6 to 4 days (a–c), 4 to 2 days (d–f), and 2 to 0 days (g–i) prior to EuBL onset in a),d),g) ERA-Interim and b),e),h) reforecasts (NDFJM; 1997–2017). The black contours indicate absolute WCB outflow frequencies (ERA-Interim and reforecasts) of 5, 10, 15 % and a climatological frequency of 0.5 %. (c,f,i) show differences between reforecasts and ERA-Interim (shading) with significant differences (t-test; 98 th confidence interval) indicated by the point stippling. Green contours as in Fig. 6.2

Two to zero days before the onset, substantial positive WCB outflow anomalies (4–8%) emerge over Greenland upstream of the incipient block (Fig. 6.4h). The anomalies in this region are significantly higher than observed (Fig. 6.4i). These findings are in line with the northwestward shift of the incipient block found in Fig. 6.3i and corroborate that the ensemble members with EuBL life cycles develop the block via strong WCB outflow towards Greenland. Contrary, observed outflow frequencies are higher further southeast over western Europe (Fig. 6.4i)

which likely contributes to the higher observed Z500 anomalies in this region (Fig. 6.3i).

To conclude, there is a substantial misrepresentation of WCB outflow prior to the onset of EuBL. The reforecasts first lack enhanced WCB anomalies and then overestimate outflow frequencies over Greenland and the Iceland Sea two to zero days before the onset. On the other hand, WCB outflow is systematically underestimated southeast of Iceland and over western Europe. Thus while the reforecast reflect the enhanced WCB activity in the days prior to the onset, the differences suggest a different pathway into EuBL. This is in line with the northwestward shift of the Z500 anomalies in the reforecasts and the observed Rossby wave pattern.

The results show the importance of WCB activity prior to EuBL and corroborate that WCB activity is needed in the reforecast to establish the block. However, it remains unclear if the overestimated outflow frequencies over Greenland result from challenges of the reforecasts in capturing WCB activity over the eastern Atlantic and western Europe or if errors originate further upstream over North America and the eastern North Pacific and lead to different cyclone and WCB activity downstream over the Atlantic.

6.3 Influence of WCBs on EuBL forecast skill

This Section further evaluates the role of WCBs for the representation of EuBL in the reforecasts. So far, Z500 and WCBs were analysed for the ensemble mean forecast in week 1, 2, and 3 (sec. 6.1) where a general underestimation of the block over Europe together with an underestimation of WCB activity is found. Furthermore, WCB and Z500 pathways were identified for the ensemble members with an EuBL onset in week 2 (sec. 6.2) which shows that these members establish EuBL onsets with strong WCB activity towards Greenland and underestimate outflow frequencies over western Europe. This Section first evaluates the role of WCBs for EuBL for different sub-categories which capture or miss the

EuBL onset. It further investigates remote and local influences over the Pacific and Atlantic on EuBL onsets and elucidates the role of the WCB.

6.3.1 The role of WCBs for EuBL onsets

Now, the analysis of Z500 and WCB activity prior to EuBL onsets is first extended to the ensemble members which miss an observed EuBL onset in forecast week 2. These members are studied to understand the role of the WCB for missed EuBL onsets in the reforecast. The ensemble members that miss the EuBL onset have only small positive WCB outflow anomalies over the North Atlantic two to zero days before the onset (Fig. 6.5d). The outflow frequencies are significantly lower compared to the observed frequencies (Fig. 6.5a) and to members with EuBL onsets (Fig. 6.5b,c). These findings indicate that WCB activity is important in the reforecast to correctly capture the onset of EuBL and that a misrepresented WCB in the model can significantly contribute to missed EuBL onsets.

On the other hand, the ensemble members with an EuBL onset and life cycle (Hits and False Alarms) (Fig. 6.5b,c) reflect the reforecast pathway with high WCB activity towards Greenland found in Fig. 6.4h. As introduced in Chapter 4, the Hits occur at the same time of observed EuBL onsets while False Alarms occur independent of them. Outflow frequencies are generally higher in the Hits compared to False Alarms while both categories overestimate WCB anomalies over Greenland underestimate them over the western part of the incipient block compared to the observations.

The onset of blocking over the European region, amplified by WCBs as discussed above, is typically embedded in Rossby wave propagation and breaking that is originally triggered upstream and also affects forecast skill (Grazzini and Vitart, 2015, Quinting and Vitart, 2019). Therefore, WCB activity is now further evaluated in the upstream region over the North Pacific and North America.

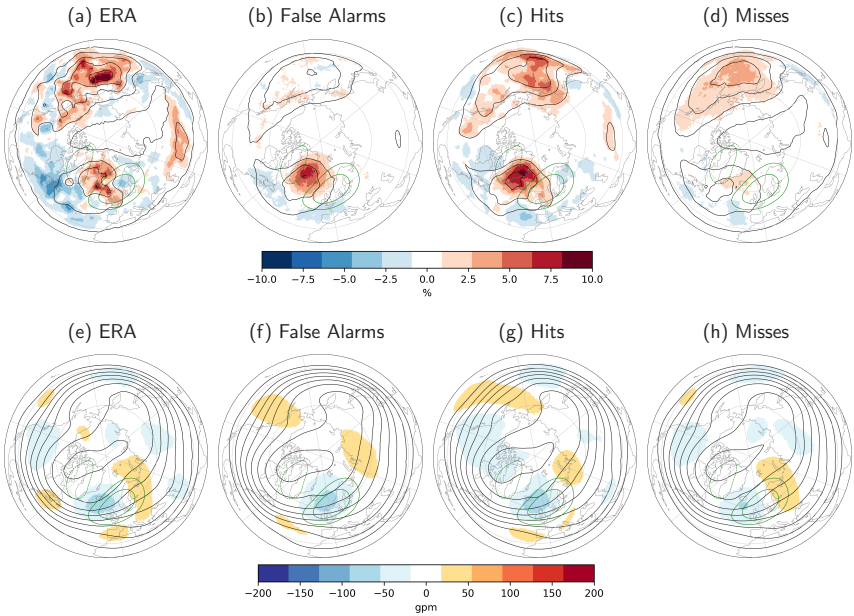


Figure 6.5: (a-d) WCB outflow frequency anomalies (shading) two to zero days before EuBL onsets as in Fig. 6.4 and (e-h) Z500 anomalies six to four days before EuBL onsets (shading) as in Fig. 6.3 for (a,e) ERA-interim and reforecast subcategories: (b,f) False Alarms, (c,g) Hits and (d,h) Misses (NDFJM; 1997–2017). False Alarms, Hits, and Misses show anomalies compared to own climatology. Black and green contours as in Fig. 6.3 and Fig. 6.4.

Observed WCB outflow frequencies are enhanced over large parts of the North Pacific and over western North America (Fig. 6.5a). The False Alarms strongly underestimate the observed WCB activity and have outflow frequencies which are similar to climatology (Fig. 6.5c). The enhanced WCB outflow over the North Pacific is better captured but still mostly underestimated in the Hits and Misses (Fig. 6.5c,d). The Hits underestimate WCB frequencies over Alaska and western Canada and seem to have a different pattern of enhanced outflow frequencies compared to the observations with positive anomalies over the US American west coast and over the northwestern Pacific (Fig. 6.5c). The Misses have generally lower WCB activity compared to the Hits (Fig. 6.5d), but represent observed frequencies over western Canada and Alaska better than both False Alarms and

Hits. These results show that the ensemble members with a EuBL life cycle (False Alarms and Hits) have strongly differing WCB outflow activity in the upstream region two to zero days before the onset.

The large differences in the WCB patterns over western North America likely result from different large-scale flow conditions which modulate the cyclone and WCB activity. Six to four days before the onset, the observed patterns show negative Z500 anomalies over western North America (20–50 gpm) and positive anomalies with similar magnitudes over the eastern Pacific (Fig. 6.5e). Interestingly, the Misses category represents these anomaly pattern generally well (Fig. 6.5h) which is in line with the better represented WCB outflow frequencies in this region (Fig. 6.5d) compared to the Hits and False Alarms (Fig. 6.5b,c). Besides the small differences in Z500 over western North America compared to the observations, the Misses also have a similar large-scale flow over the Atlantic and the region of the incipient block compared to the observations.

These findings indicate that ensemble members which have a similar large-scale flow upstream and in the region of the incipient block six to four days before the EuBL onset are likely not able to correctly capture the block over Europe. Recalling, the strongly underestimated WCB outflow frequencies over the Atlantic (Fig. 6.5d), the missed EuBL onset is very likely influenced by the misrepresentation of WCB activity.

On the other hand, the Hits and False Alarms have different Z500 anomalies upstream over the eastern Pacific and western North America (Fig. 6.5f,g) compared to the observations and the Misses (Fig. 6.5e,h). Strong positive anomalies (20–50 gpm) emerge over the eastern Atlantic and Alaska in the False Alarms which results in an amplification of the climatological ridge in this region (Fig. 6.5f). The Hits have negative anomalies over western North America and positive anomalies over the eastern North Pacific (Fig. 6.5g). These patterns strongly deviate from the observations and likely modulate the differing WCB activity two to zero days before the onset (Fig. 6.5c) compared to the observation (Fig. 6.5a).

The findings for the Hits and False Alarms shows that the ensemble members with EuBL onsets have a different Z500 pattern in the upstream regions and corroborate that the reforecasts might need this pattern to establish the blocking over the European region via downstream Rossby wave propagation resulting in strong WCB activity towards Greenland. On the other hand, the Misses have similar flow conditions compared to the observations which leads to missed EuBL onsets and life cycles.

The results underline the importance of WCB activity for the onset of EuBL and show that the pathway into EuBL in the reforecasts is likely influenced by Rossby wave activity from upstream regions over North America and the eastern North Pacific.

6.3.2 Remote influences

The previous analysis investigates individual ensemble members of the reforecasts and reveals large differences between captured and missed EuBL onsets. As in Section 6.1, EuBL forecasts are now again investigated using the ensemble mean of the reforecasts instead of selecting specific ensemble members. For this analysis, the 137 observed EuBL onsets in forecast week 2 are divided into subsets of initialization times with good and bad skill (best and worst 33% of EuBL skill in week 2, see Chapter 4). By construction, the subset with good EuBL contains relatively more ensemble members from the Hits category compared to the subset with bad EuBL skill. This category is dominated by the Misses category and Hits occur less frequent.

First, all 137 observed EuBL onsets in forecast week 2 and the onsets in the two subsets are evaluated to further understand the role of upstream precursors found in Fig. 6.5 for the EuBL onset. For all EuBL onsets, the Z500 anomalies in the week around the onset (Fig. 6.6a) reflect upstream anomalies six to four days before the onset found in Fig. 6.5e. Negative Z500 anomalies can be found over the western USA and positive anomalies occur over the eastern Pacific.

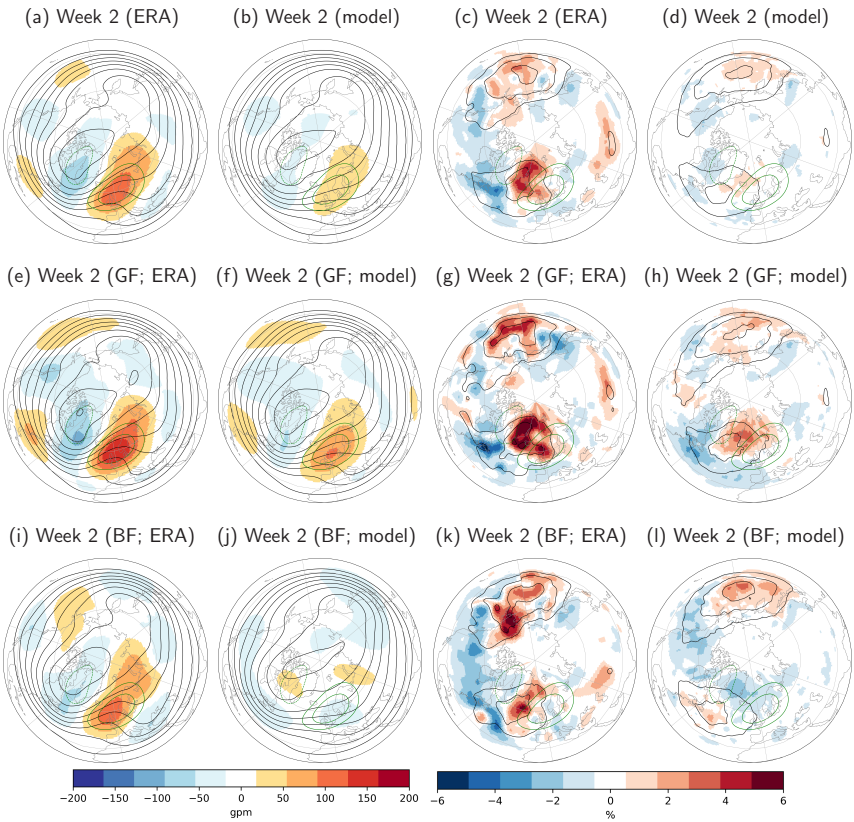


Figure 6.6: As in Fig. 6.2 for (a-d) all EuBL onsets, (e-h) good, and (i-l) bad EuBL skill.

The subsets with good and bad EuBL skill reveal large differences in the upstream flow patterns (Fig. 6.6e,i). The subset with good EuBL skill has similar anomaly patterns compared to all onsets with stronger negative anomalies over the western USA (Fig. 6.6e). On the other hand, the subset with bad EuBL skill has an amplified ridge with positive Z500 anomalies around 50 gpm over Alaska and western Canada (Fig. 6.6i).

The large-scale flow patterns in the two subsets indicate there might be different pathways into EuBL in the observations which originate from the upstream region over the eastern North Pacific and western North America. The pathway in the subset with good EuBL skill resembles a Rossby wave train which originates over the North Pacific and continues into North America and the North Atlantic. On the other hand, the pathway in the subset with bad EuBL skill is characterised by a strong ridge over western North America.

WCB outflow frequencies strongly differ in the region over western North America in the subset with good and bad EuBL skill (Fig. 6.6g,k). The subset with good EuBL skill has only small outflow frequencies while strongly enhanced WCB outflow occurs in the subset with bad EuBL skill. This WCB activity likely contributes to the formation of the ridge over western North America.

In conclusion, the subsets with good and bad EuBL skill reveal that there are likely different observed pathways into EuBL. These pathways seem to emerge from the eastern North Pacific and western North America where different Z500 patterns together with differing WCB activity can be found in the two subsets. Since the subsets were defined based on forecast skill in the reforecasts, these findings show that the reforecasts can likely capture the first pathway generally well and are not able to correctly represent the second one.

In the following, the two upstream pathways into EuBL are further analysed with composites of Z500 and WCB outflow anomalies averaged over forecast week 1 prior to EuBL onset in week 2. The subset with good EuBL skill has similar Z500 anomaly patterns in week 1 compared to week 2 (cf. Fig. 6.6e, Fig. 6.7a). In line with the good EuBL skill, these anomaly patterns resemble the Hits category six to four days before the onset (Fig. 6.5g). The flow is more zonal compared to climatology with positive anomalies over the eastern Atlantic and negative anomalies over western North America. This anomaly patterns indicate a Rossby wave train which emerges already in the week prior to the EuBL onset.

On the other hand, the wave pattern is different in the subset with bad EuBL skill in week 1 (Fig. 6.7e). The large-scale flow is similar to climatology over western

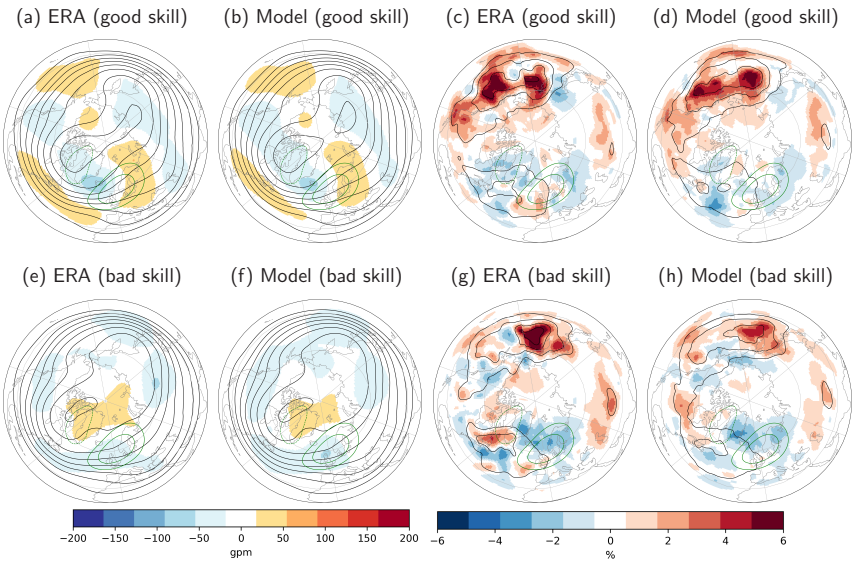


Figure 6.7: As in Fig. 6.6, but for forecast week 1 prior to EuBL onset in week 2.

North America with negative anomalies along the US west coast. Recalling the positive anomalies and strong WCB outflow activity in forecast week 2 over the eastern Pacific (Fig. 6.6i,k), it is evident that ridge building occurs in week 2 around the onset of EuBL and not in the week before.

Over the western North Pacific, strongly enhanced WCB activity can be found in week 1 in this subset with bad EuBL skill (outflow frequencies around 15%) (Fig. 6.7e). In general, WCB activity in the western North Pacific can lead to large-scale flow amplification favouring downstream cyclone activity and WCB activity over the eastern North Pacific (Grams and Archambault, 2016). The high WCB outflow activity and ridge building in week 2 (Fig. 6.6e,g) corroborate that there is a potential link to the WCB activity over the western Pacific in the week prior.

The large-scale circulation over the western Pacific is likely further influenced by tropical phenomena (like the MJO) through the propagation of low frequency

Table 6.1: Madden-Julian Oscillation (MJO) at initial time (in %) before EuBL onset in forecast week 2 (all EuBL onsets (All), subset of onsets with good EuBL skill (good), and subset of onsets with bad EuBL skill (bad)) (NDJFM; 1997–2017)

MJO	All	Good	Bad
Phase 1	4.4	2.5	2.6
Phase 2	8.8	10.0	2.6
Phase 3	11.7	10.0	21.1
Phase 4	11.7	15.0	13.2
Phase 5	10.2	10.0	15.8
Phase 6	2.9	5.0	2.6
Phase 7	6.6	10.0	2.6
Phase 8	5.8	5.0	5.3
No MJO	38.0	32.5	34.2

wave trains into the midlatitudes. In general, these teleconnections provide predictability on sub-seasonal time scales even for the Atlantic-European region (Vitart, 2017). The MJO modulates Atlantic-European weather regimes occurrence frequency (Cassou, 2008) typically leading to an enhanced frequency of EuBL one to two weeks after MJO phase 2/3 (not shown).

The subset of 137 EuBL onsets in forecast week 2 reflects this known frequency modulation generally well (Tab. 6.1). In 62% of the EuBL onsets, an active MJO occurs at forecast initial time. From these 62%, MJO phases 2–5 occur predominantly at 68% of the times. The subset with good and bad EuBL skill have similar distribution of active and inactive MJO events compared to all onsets. There is an active MJO in 67.5% of the cases with good EuBL skill and in 65.8% of the cases with bad EuBL skill. Thus, an active MJO at initial time does not seem to increase the forecast skill for EuBL in week 2. Moreover, active phases 2–5 also occur often in both subsets with even higher percentages for the subset of bad EuBL skill (66.7 and 80% of the active MJO cases in the respective category).

Hence, these findings corroborate that the enhanced EuBL frequencies after active MJO phases 2–5 are not sufficiently captured by the reforecasts.

These misrepresented modulations of EuBL frequencies in the reforecasts might be partly due to forecast errors that are generated or amplified in WCBs over the North Pacific prior to EuBL onset. In the subset with bad EuBL skill, the reforecasts underestimate the WCB activity over the western Pacific in week 1 by 2–5% (Fig. 6.7h) and strongly underestimate WCB outflow frequencies over the eastern Pacific (Fig. 6.6l) together with an underestimation of the ridge over western North America (Fig. 6.6j) in week 2. The forecast errors in the representation of the ridge then likely propagate downstream into the Atlantic region and impact the forecasts of EuBL onsets and life cycles. On the other hand, the reforecasts can represent the Rossby wave train which emerges from the Pacific in the subset with good EuBL skill generally well (Fig. 6.6f, Fig. 6.7b).

6.3.3 Local influences

The previous Section introduced two different upstream pathways into EuBL and indicates that errors in WCB activity over the North Pacific together with errors in the representation of a ridge over western North America might impact the predictive skill of EuBL downstream.

In general, the two observed upstream pathways into EuBL likely modulate the formation of Z500 and WCB anomalies downstream over the Atlantic. In this region, WCB outflow frequencies tend to be more towards Greenland in the subset with good EuBL skill (Fig. 6.6g) and centered further southeast in the subset with bad EuBL skill (Fig. 6.6k). Recalling the WCB pathway in the ensemble members which capture EuBL onsets (Fig. 6.4b,e,h), the WCB activity in the subset with good EuBL skill resembles the pathway into EuBL in the reforecasts with enhanced frequencies over Greenland.

The ensemble mean of the reforecasts can capture the enhanced WCB activity in the North Atlantic region but still underestimates frequency anomalies compared to the observations (Fig. 6.6d). In particular, it does not reproduce the enhanced

outflow frequency anomalies in the centre of the incipient positive Z500 anomaly (green contour). In line with the good forecast skill, the model also only slightly underestimates the positive Z500 anomaly in the region of the incipient block (Fig. 6.6b).

For the subset with bad EuBL skill, the onset of the block is completely missed in the reforecasts which predict a more zonal flow over Europe (Fig. 6.6f). The reforecasts lack enhanced outflow frequencies completely and rather predict reduced WCB activity in the region of the incipient block (Fig. 6.6l).

The results show that different patterns of enhanced WCB outflow frequencies emerge over the Atlantic in the subset with good and bad EuBL skill. The ensemble mean of the reforecasts can capture WCB activity and the block generally well in the subset with good skill and miss the WCB outflow and the block in the subset with bad skill. This is likely influenced by the different observed pathways emerging from upstream regions over western North America which might lead to different Rossby wave propagation over the Atlantic which then modulates WCB activity.

Forecast errors which are generated in the region of the upstream ridge in the subset with bad EuBL skill then propagate downstream and amplify forecast error over the Atlantic which could lead to a missed EuBL onset.

However, forecast errors could also be generated and amplified locally over the North Atlantic and directly impact the onset of EuBL (Grams et al., 2018). This hypothesis is indicated by the different WCB patterns in the subset with good and bad EuBL skill which suggest that there are potentially also different observed pathways into EuBL over the Atlantic: one WCB pathway with enhanced WCB activity towards Greenland and a second pathway with WCB activity predominantly over the eastern Atlantic and enhanced outflow frequencies centered around Iceland.

To further evaluate the hypothesis of two different WCB pathways into EuBL over the Atlantic, the observed WCB frequencies over the North Atlantic are now further evaluated by using lagged composites as in Section 6.2 for the events with

good and bad EuBL skill. The observations in the two subsets are investigated during the four days before and the two days after the EuBL onset.

In the subset with good EuBL skill, positive outflow anomalies emerge over both Greenland and western Europe two to zero days before the onset (Fig. 6.8b). The positive outflow anomalies shift northwards and are centered over northeastern Greenland two to zero days after the onset (Fig. 6.8d). On the other hand, WCB outflow is centered on the eastern Atlantic around Iceland in the subset with bad EuBL skill two to zero days before the onset (Fig. 6.8f). The enhanced outflow remains in a similar region after the onset while frequencies further increase (Fig. 6.8h).

The observed WCB outflow differs strongly between the two subsets of good and bad EuBL skill which indicates that in fact different observed pathways into EuBL might also emerge over the North Atlantic. The first pathway has high WCB activity predominantly towards Greenland (pathway 1) while WCB activity is centered on the eastern Atlantic around Iceland in the second pathway (pathway 2).

The WCB inflow in the subset with good EuBL skill is highest over the central North Atlantic where positive anomalies around 6–10% can be found (Fig. 6.8a,c). In the subset with bad EuBL skill, inflow frequencies are lower four to two days before the onset and positive anomalies can primarily be found over the southeastern North Atlantic (Fig. 6.8e). Subsequently, the relatively high inflow frequencies in this region prevail (Fig. 6.8g) which likely leads to the high WCB outflow frequencies over the eastern Atlantic centered around Iceland. The findings for WCB inflow further underline the two different observed WCB pathways into EuBL over the North Atlantic and corroborate that they originate from different WCB inflow regions.

The previous results suggests that there are both remote and local pathways into EuBL which influence the large-scale flow evolution prior to and around EuBL onsets. At this point, it remains unclear if these local WCB pathways over the Atlantic are strongly modulated by the precursor pathways from upstream or if

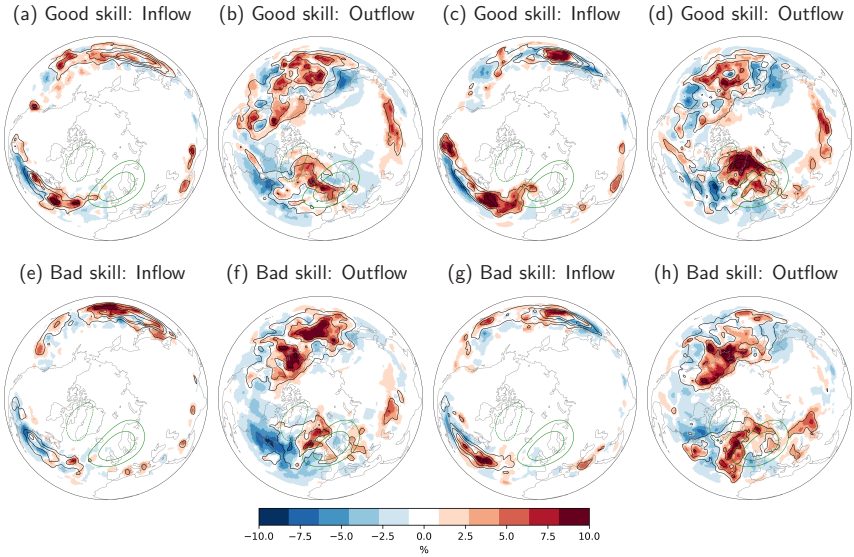


Figure 6.8: WCB inflow frequency anomalies (shading) in ERA-Interim four to two days (a,e) and two to zero days (c,g) before the EuBL onset and WCB outflow anomalies (shading) in ERA-Interim two to zero days before the onset (b,d) and zero to two days after the onset (d,h) in the subsets with (a–d) good and (e–h) bad EuBL skill as in Fig. 6.6. The black contours indicate absolute WCB frequencies of 5, 10, 15, 20 %. Green contours as in Fig. 6.2.

they could also emerge independently of them.

In order to investigate if the WCB pathways over the Atlantic can emerge independent of upstream precursors, the observed EuBL onsets are now further evaluated in terms of WCB activity. The previous investigation reveals that the first WCB pathway into EuBL has high WCB inflow primarily over the central Atlantic (Fig. 6.8a,c) while the second WCB pathway into EuBL has enhanced inflow frequencies also over the southeastern Atlantic (Fig. 6.8e,g). Therefore, a box is defined over the southeastern Atlantic (20–35°N, 30–20°W) and the area-averaged WCB inflow activity is calculated four to two days before the onset for all 137 observed events. The events are then separated in two categories with high and low WCB inflow activity (33 % respectively).

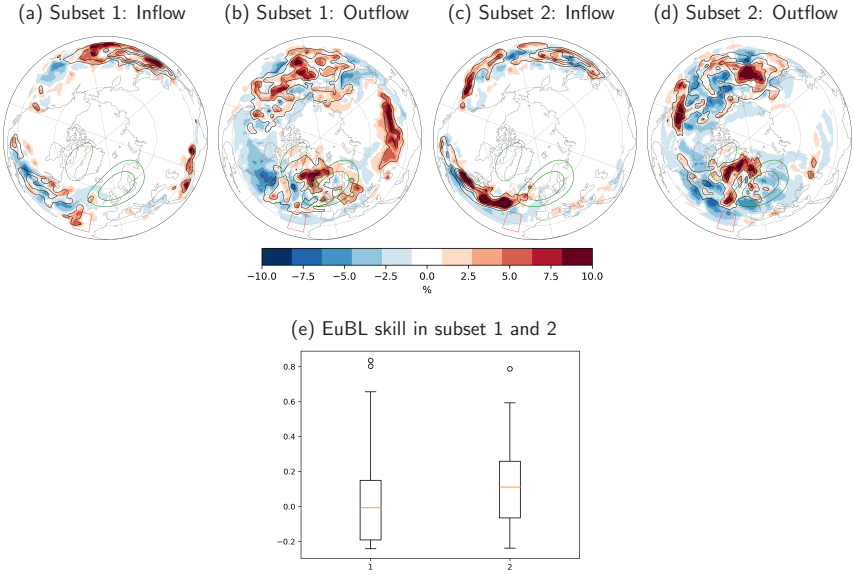


Figure 6.9: WCB inflow frequency anomalies (shading) in ERA-Interim four to two days (a,c) before the EuBL onset and WCB outflow anomalies (shading) in ERA-Interim two to zero days before the onset (b,d) in the subsets with (a,b) high WCB inflow and (c,d) low WCB inflow activity in the red box (20–35°N, 30–20°W) over the southeastern Atlantic four to two days before the onset. The black contours indicate absolute WCB frequencies of 5, 10, 15, 20 %. Green contours as in Fig. 6.2. e) shows the forecast skill of the two subsets in terms of the distribution of *FBSS* for the first five days of the EuBL life cycle after Büeler et al. (2021).

The subset with high WCB inflow is characterised by positive frequency anomalies over the southeastern Atlantic and lower inflow activity over the central Atlantic four to two days before (Fig. 6.9a). On the other hand, the subset with low WCB activity over the southeastern Atlantic has (by construction) lower inflow frequencies in the selected box which are characterised by negative anomalies of 1–2% (Fig. 6.9c). However, this subset has strong positive anomalies over the central Atlantic which lead to high WCB outflow frequencies over eastern Greenland upstream of the incipient block two to zero days before the onset (Fig. 6.9d). This WCB activity resembles the first pathway in the subset with good EuBL skill found in Fig. 6.8a,b. WCB outflow is centered further southeast around Iceland in the subset with high WCB inflow activity over the southeastern Atlantic

(Fig. 6.9b) which is similar to the second pathway in the subset with bad EuBL skill.

In conclusion, the separation of high and low WCB inflow activity over the southeastern Atlantic leads to two data sets with resemble the two different observed pathways identified in the subsets with good and bad EuBL skill (Fig. 6.8). Since the data sets with high and low WCB activity are set up purely based on WCB activity over the southeastern Atlantic, these findings indicate that these local WCB pathways over the Atlantic might emerge independently of upstream precursors.

The subsets with different WCB activity are now further evaluated in terms of their predictive skill for EuBL onsets (Fig. 6.9e). The subset with high WCB inflow activity over the southeastern Atlantic and outflow around Iceland (second WCB pathway) has reduced EuBL forecast skill compared to forecasts with WCB inflow activity over the central Atlantic and outflow towards Greenland (first pathway). Around 50% of the individual events within in the first subset still have skill in predicting EuBL onsets in week 2 compared to 75% in the second. While the distribution of events is shifted towards higher skill in the second subset, events with relatively high skill can also occur in the first subset.

These findings for the predictive skill of EuBL onsets in subsets one and two are in line with the previous investigation in the subsets with good and bad EuBL skill. In general, the skill for EuBL is higher when the WCB activity is characterised by the first WCB pathway and the forecast skill is lower when WCB activity is predominantly characterised by the second WCB pathway. The results underline the importance of the WCB pathways over the Atlantic for the prediction of EuBL in the reforecasts.

6.3.4 Sources of forecast error

As shown in Section 6.2, the ensemble members that capture EuBL onsets underestimate WCB activity over the eastern Atlantic in the region where the second WCB pathway emerges and establish the block over Europe via the first WCB pathway with enhanced outflow frequencies over Greenland. The previous results corroborate that forecast errors generated in the WCBs over the eastern Atlantic

in the second WCB pathway could be responsible for an underestimation of the incipient block and missed EuBL onsets in the reforecasts.

Therefore, potential sources for forecast errors in the WCB activity over the eastern Atlantic are now briefly identified. As introduced in Chapter 2, WCBs contribute a large fraction of precipitation in the midlatitudes (Pfahl et al., 2014). Furthermore, both slantwise and rapid ascent can occur in the WCBs while the latter occurs within embedded convection. The processes in the embedded convection occur typically in the southern region of an extratropical cyclone in the vicinity of its cold front (Oertel et al., 2020). WCBs that originate from these regions generally have more low-level moisture available, which leads to higher heating rates and an increased likelihood of embedded convection compared to WCBs that originate further north. Both WCBs with high heating rates and embedded convection are likely more challenging for the model to capture (Pickl et al., 2022). Therefore, errors in the representation of embedded convection in the first WCB pathway could significantly impact the missed EuBL onsets in the reforecasts.

To evaluate this hypothesis, the observed precipitation before the EuBL onset is now further investigated. Before the onset of EuBL, the observed precipitation is anomalously high over the North Atlantic (see Appendix Fig. B.4a,d,g) which is in line with the enhanced WCB activity (Fig. 6.4g). For all 137 observed EuBL onset, average 24-h precipitation, two to zero days before the onset, is highest over the central Atlantic and west of Iceland (5–7 mm) (Fig. 6.10a).

So far, ERA-Interim was considered the observational truth and used for comparison to the reforecasts. While this approach is a very good approximation for the main processes investigated in this study, ERA-Interim likely still has errors in precipitation compared to observations purely based on satellite or radar data (Nogueira, 2020). Therefore the satellite based precipitation data GPM IMERG is used to evaluate differences to ERA-Interim. GPM IMERG is not available north of around 60–65°N which explains the lack of the precipitation maximum around Iceland (Fig. 6.10b).

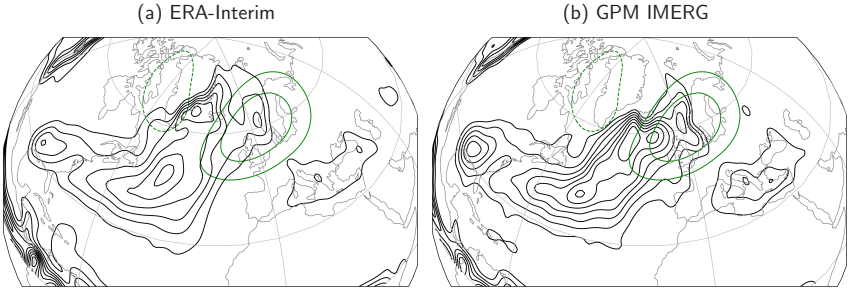


Figure 6.10: Mean 24-h precipitation (contours) two to zero days (g–h) before EuBL onsets in a) ERA-Interim and b) GPM IMERG. The black contours indicate 24-h precipitation of 2–8 mm. Green contours as in Fig. 6.2.

In general, precipitation is higher in GPM IMERG compared to ERA-Interim while the maximum emerges in a similar region over the Atlantic (Fig. 6.10b). Differences in precipitation between the data sets are especially pronounced over the eastern Atlantic.

The comparison between ERA-Interim and GPM IMERG indicates that observed precipitation is likely higher than shown in ERA-interim. This is probably due to the challenges of the models in capturing convective precipitation. The differences are especially pronounced over the eastern Atlantic, a region where the reforecasts have difficulties in correctly capturing WCB activity prior to EuBL onsets (Fig. 6.4f,i). Due to the strong link between precipitation and WCB activity, the results corroborate that WCB underestimation over the eastern Atlantic might even be larger than shown in Fig. 6.4f,i.

In conclusion, these findings point to a potential source of forecast error in the second WCB pathway over the eastern North Atlantic. This pathway is generally not well captured by the model which could be due to challenges in the representation of embedded convection in WCBs. As shown by the GPM IMERG data set, the observed precipitation is likely even higher in this region than indicated in ERA-Interim which would likely also result in a higher impact of diabatically enhanced outflow on the circulation in the upper troposphere.

Table 6.2: Atlantic-European weather regimes (WR) after Grams et al. (2017) in forecast week 1 (in %) before EuBL onset in forecast week 2 (all EuBL onsets (All), subset of onsets with good EuBL skill (good), and subset of onsets with bad EuBL skill (bad) (NDJFM; 1997–2017).

WR	All	Good	Bad
NO	40.6	42.8	32.8
ZO	16.2	20.9	9.4
ScBL	10.5	11.6	8.8
GL	4.1	0.0	11.6
AT	11.7	5.9	20.7
EuBL	3.6	10.6	0.0
ScTr	6.9	4.4	5.3
AR	6.4	3.8	6.6

Errors which are generated in the WCB could then lead to missed onsets of EuBL and significant forecast errors in the model. These results give one potential explanation for the difficulties of the reforecasts in capturing the second WCB pathway into EuBL. However, it is important to note that further investigations are needed to disentangle the different observed WCB pathways over the Atlantic and quantify the complex interactions with upstream precursors from the North Pacific and North America region.

The WCB pathways into EuBL over the Atlantic are likely modulated by the large-scale circulation since the upper-level troughs and ridges typically determine the location of surface cyclones and of WCBs. Therefore, the different observed WCB pathways into EuBL over the Atlantic are now further linked to the Z500 patterns in forecast week 1 prior to EuBL onsets in week 2. These patterns are again investigated in the subsets with good and bad EuBL skill (Fig. 6.7).

In the week prior to the onset, the large-scale circulation is very different in the subset with good EuBL skill compared to the subset with bad EuBL skill (Fig. 6.7a,e). The subset with good skill has negative Z500 anomalies over Iceland (around -100 gpm) and positive anomalies over the Atlantic along 30–40°N

(Fig. 6.7a). Contrary, the subset with bad EuBL skill has positive Z500 anomalies over Greenland and negative anomalies further south (Fig. 6.7e). These anomaly patterns for the two subsets resemble known anomaly patterns for the positive and negative phase of the NAO.

Linking the two subsets to Atlantic-European weather regime, we find a strong modulation of the regime frequency. For the subset with good EuBL skill, the ZO regime is the dominant active regime in forecast week 1 (20,9%) (Tab. 6.2). The ZO regime is strongly connected to the positive phase of the NAO and its anomaly patterns are reflected in Fig. 6.7a. For the subset with bad EuBL skill, we find a different signal with a high frequency of AT (20.7%) and GL (11.6%) and a smaller frequency of ZO (9.4%). Both AT and GL project strongly into the negative phase of the NAO and their anomaly patterns are also reflected in Fig. 6.7e.

Thus, the reforecasts seem to have difficulties establishing EuBL regimes in forecast week 2 from NAO negative patterns. In line with this finding, Büeler et al. (2021) show that the reforecasts struggle to capture regime transitions from AT into EuBL. One possible explanation for these difficulties might be a too strong persistence of NAO negative patterns in the NWP model which can be primarily observed after weak Stratospheric polar vortex events (Kolstad et al., 2020). For the subset with bad EuBL skill, the reforecasts predict the persistence of the NAO negative pattern into forecast week 2 and underestimate the rapid onset of EuBL (Fig. 6.6j).

Furthermore, the second observed WCB pathway over the Atlantic also points to the role of WCB activity in generating forecast errors which could lead to the missed EuBL onsets. In NAO negative regimes, the location of the jet stream is further south compared to climatology (Madonna et al., 2017) along with a southward shift of the surface cyclones. This could lead to WCB inflow regions over the southeastern Atlantic which favours the second WCB pathway into EuBL. This WCB pathway is more challenging for the reforecasts to capture which could be due to the increased likelihood of embedded convection associated with these WCBs. Therefore, errors in the representation of certain EuBL

in the reforcasts could emerge from an overestimated persistence of the NAO patterns together with errors generated in WCBs over the eastern Atlantic.

6.4 Conclusions

Z500 and WCB activity are investigated around the onset of EuBL in ECMWF's IFS sub-seasonal reforecasts and ERA-Interim reanalysis (NDJFM; 1997–2017). EuBL onset is generally not well captured by the reforecasts, which is partly due to its low intrinsic predictability (Faranda et al., 2016, Hochman et al., 2021). These results newly suggests that it is likely also the misrepresentation of WCB activity in the reforecasts that dilutes the skill for EuBL forecasts.

In general, the findings reveal a strong link between the wave amplification around EuBL and high WCB outflow activity over the central and eastern Atlantic. The reforecasts underestimate the incipient block accompanied by an underestimation of the WCB activity.

The analysis of the time evolution leading up to onset shows that the ensemble members which capture EuBL onsets establish large-scale flow anomalies prior to EuBL onset via WCB outflow differently than observed. In the observations, high WCB activity emerges over eastern Canada, as well as the central and eastern Atlantic and shifts northeastwards prior to the onset. The members with an onset have WCB activity predominantly over the central Atlantic with high frequencies upstream of the incipient block. Consequently, the outflow is strongly underestimated over the eastern Atlantic and western Europe and overestimated over Greenland.

Large-scale flow amplification in Z500 is stronger upstream of the incipient block over Iceland in the members with an onset and over southwestern Europe in ERA-Interim. These differences correspond to differences in WCB activity underlining the impact of WCB outflow for wave amplification prior to EuBL.

The analysis of ensemble members which miss a EuBL onsets underlines the important role of the WCB for the EuBL onset in the reforecasts. The Misses

have strongly underestimated WCB outflow frequencies just prior to the onset of EuBL which very likely affects the underestimation of the block.

Interestingly, the Misses also have very similar Z500 patterns over the North Pacific and North Atlantic prior to the onset compared to the observation. The onset of EuBL is therefore likely missed in the reforecasts if ensemble members have a similar preconditioned large-scale flow. The missed EuBL onset is likely due to underestimated WCB activity which underlines the importance of diabatic processes for the onset of EuBL.

Over the North Atlantic region, two different observed WCB pathways into EuBL are identified. One with WCB inflow over the central Atlantic and outflow towards Greenland and another one with inflow over the southeastern Atlantic and outflow centered around Iceland. These pathways potentially have different characteristics in terms of inflow moisture, heating rate and embedded convection.

WCBs with high heating rate and embedded convection are likely more challenging for the NWP models to capture (Oertel et al., 2020, Pickl et al., 2022). Therefore, forecast errors might be generated or amplified in the second WCB pathway which could lead to errors in the representation of EuBL onsets. The findings show that the reforecasts can capture the first WCB pathway well and miss the second WCB pathway completely.

Moreover, the results also suggest that different pathways into EuBL emerge from upstream regions over the eastern Pacific and western North America. The first pathway resembles a Rossby wave train from the central North Pacific into the North Atlantic. The second pathway has a strong ridge over western North America which is established with strong WCB activity.

The reforecasts can capture the first pathway but underestimate the ridge in the second. Forecasts errors which develop in this region could propagate downstream and impact the onset of EuBL. Thus, forecast errors related to strong WCB activity over the Pacific could dilute the Rossby wave signal in the reforecasts and subsequently lead to errors in the downstream flow patterns and missed

EuBL onsets.

The results show the importance of local and remote WCB activity and Z500 patterns for the predictive skill of EuBL forecasts. They point to a crucial role of the WCB in generating and amplifying forecast error which impacts the predictability and forecast skill of EuBL.

7 The role of WCBs for Atlantic-European weather regimes

This Chapter extends the previous analysis for EuBL to other weather regimes over the Atlantic-European region. As shown in Chapter 6, the WCBs seems to play an important role for the onset of EuBL in the reforecasts and likely affects the low predictive skill of EuBL in the NWP models (Büeler et al., 2021, Matsueda and Palmer, 2018).

Besides EuBL, there are three other blocked weather regimes in the Atlantic-European region (ScBL, GL, and AR). Since latent heat release in WCBs is a first order process for blocked anticyclones in general (Pfahl et al., 2015), this Chapter evaluates if the WCB also plays an important role for the predictability of these other three blocked regimes in the reforecasts.

Section 7.1. first investigates the prediction of all seven year-round Atlantic-European weather regimes in the extended winter period (1997–2017) for observed regime onsets in forecast week 1,2, and 3. Section 7.2. then evaluates the role of the WCB for the three other blocked regimes. Furthermore, the ZO regime is evaluated since it has similar large-scale flow anomalies compared to EuBL with a trough over the central Atlantic and a ridge over Europe. However, these anomaly patterns are weaker for ZO and generally well captured by the reforecasts (Büeler et al., 2021). Lastly, Section 7.3. analyses the impact of WCBs for the prediction of blocked regimes over Europe in boreal summer.

7.1 Predictability of weather regimes onsets

The forecast skill of the reforecasts in terms of onsets of Atlantic-European weather regimes is now evaluated. In order to compare the predictive skill on different time scales, the analysis includes regime onsets in forecast week 1, 2, and 3. First, the average percentage of ensemble members that capture the onset is calculated with reference to the day of the observed regime onset.

For regime onsets in forecast week 1, 20–40% of the ensemble members capture an onset on the day it is observed (Fig. 7.1a). Additionally, 20–40% have an onset in the 14 days around it of which most of them occur the day before or after the observed onset (see the 7 days before and after the observed onset in Fig. 7.1a). The model is more often slightly delayed by a day (6–10%) than forecasting the onset too early (3–8%).

Considering the regimes individually, there are strong differences in terms of onset representation. AR is correctly captured by around 39% of the ensemble members on the observed day (Fig. 7.1a). The forecast of ZO, GL, and ScTr is similarly good (around 36%). On the other hand, EuBL and ScBL are only captured by 28 and 25% of the ensemble members in week 1. The findings are in line with Büeler et al. (2021) who find significantly lower forecast skill for EuBL and ScBL regimes already in week 1. Furthermore, the begin of a period with no clear regime characteristics ("No-Regime", grey) is only captured by a small number of around 20% of the ensemble members.

The timing of weather regime onsets in forecast week 2 are more challenging for the model to predict compared to week 1 (Fig. 7.1b). In total, 20–35% of the ensemble members capture the observed onset in the 14 days around it. However, there is only a small difference in the mean percentage of ensemble members that capture the onset on the observed day compared to the days around it. On average, around 3–6% of the members predict it on the observed day while 2–4% capture it one or two days too early or too late. Additionally, around 1–3% of the ensemble members already project into a specific regime 3–7 days before or after the observed onset.

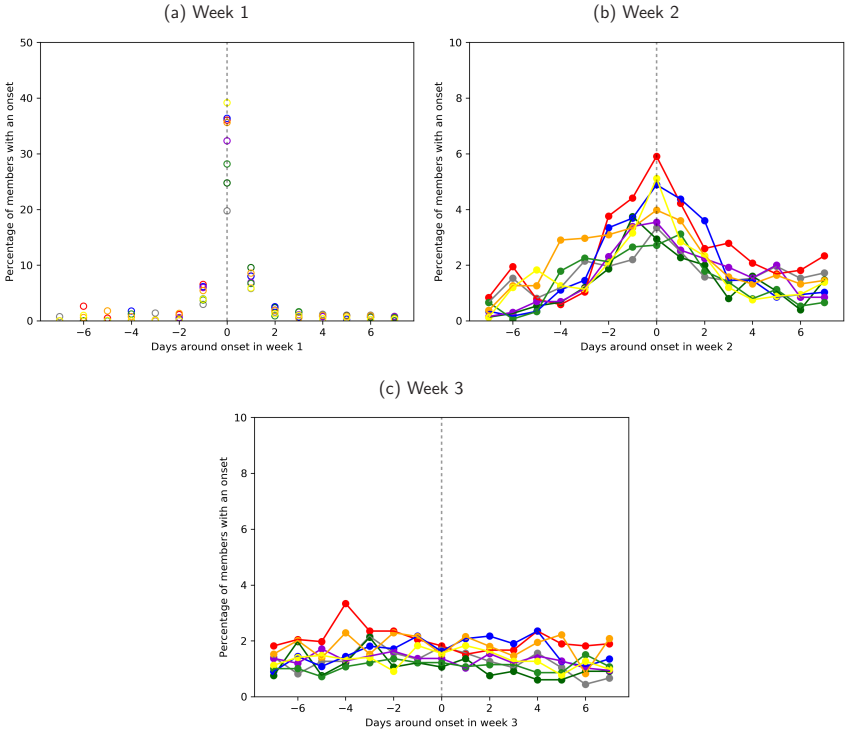


Figure 7.1: Mean percentage of ensemble members with an onset around ERA-Interim onsets in a) week 1, b) week 2, and c) week 3 for Atlantic European weather regimes in ECMWF's IFS reforecasts (NDJFM; 1997–2017).

For the individual regimes, the results are generally similar compared to forecast week 1. Within four days of the observed onset, ZO and GL have the highest percentage of members that capture the onset (around 20 and 19%, respectively). On the other hand, EuBL and ScBL onsets are only captured by around 12% of the members.

In forecast week 3, it becomes increasingly challenging for the model to correctly predict the onset (Fig. 7.1c). The same percentage of ensemble members that capture the onset on the observed day (around 2%) also predict an onset within

14 days around this date. As for week 1 and 2, ZO and GL onsets are captured by more members compared to EuBL and ScBL.

7.2 WCB activity around regime onsets

The previous analysis reveals differences between the seven weather regimes in the percentage of ensemble members which capture an observed regime onset. Out of the four blocked regimes, the reforecasts capture the onset of GL and AR with more ensemble members on average compared to EuBL and ScBL. This Section therefore first evaluates the role of the WCBs for ScBL, GL, and AR in comparison to the findings for EuBL onsets in Chapter 6. Furthermore, the ZO regime is analysed which is captured by a high percentage of ensemble members and has generally similar anomaly patterns compared to EuBL.

7.2.1 Scandinavian Blocking

First, the role of the WCB is investigated for ScBL onsets in the reforecasts. The previous analysis reveals that the observed onsets of ScBL are captured by a relatively low number of ensemble members which is in line with the overall low forecast skill of ScBL (Büeler et al., 2021). The forecast skill is similar to EuBL which is however the dominant blocking regime over Europe in boreal winter and occurs more often than ScBL (11% compared to around 7%, respectively).

For all ScBL onsets in week 2 of the extended winter period 1997–2017 (68 events), strong positive anomalies occur over northern Scandinavia and the Norwegian Sea (Fig. 7.2a). Further south, negative anomalies indicate high frequencies of upper-level troughs over the central and eastern Atlantic and western Europe. Upstream, the wave pattern is more amplified compared to climatology over North America. A ridge with positive anomalies can be found over the western part and a trough with negative anomalies over the eastern part of the continent.

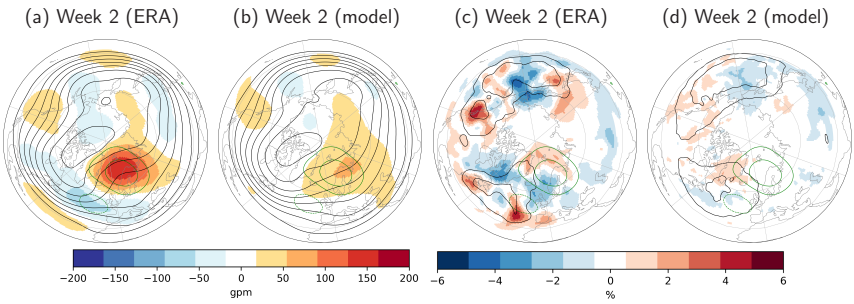


Figure 7.2: Weekly mean 500 hPa geopotential height anomalies (shading) in forecast week 2 (around ScBL onset) for a) ERA-Interim b) and ECMWF's IFS reforecasts. Black contours show absolute fields (5100–5800 gpm, every 100 gpm). Weekly mean WCB outflow frequency anomalies (shading) in forecast week 2 (around ScBL onset) for c) ERA-Interim and d) ECMWF's IFS reforecasts. Black contours show absolute frequencies for ERA-Interim and reforecasts (5, 10, 15%). Green contours indicate geopotential height anomalies (-50,50,100 gpm) for all ScBL cases from 1979–2015.

The WCB outflow frequencies are generally highest over the western and central part of the Atlantic while positive outflow anomalies (1–3%) occur in the crest of the incipient block over the Barents Sea (Fig. 7.2c). Recalling the low WCB activity at these latitudes in winter (Fig. 5.1c), these frequencies are quite remarkable when considering the low tropopause height in this region and the strict ascent criteria of WCBs of at least 600 hPa. Compared to WCB activity around EuBL which occurs predominantly over Greenland and the eastern Atlantic (Fig. 6.2g), the observed outflow frequencies are shifted northwards and occur predominantly over the northern part of the incipient block. These results corroborate that the WCB activity plays an important for ScBL onsets and that the incipient block is established via WCB activity differently than for EuBL.

In the reforecasts, the amplified wave pattern with positive anomalies over Europe is generally well captured (Fig. 7.2b). However, both positive anomalies over Scandinavia and negative anomalies over the Atlantic are underestimated. The reforecasts capture anomaly patterns upstream over the Pacific and North America better than over the European region.

In contrast to ERA-interim, the WCB outflow frequency is highest over the western and central Atlantic with positive anomalies over Greenland (Fig. 7.2d).

These patterns resemble WCB outflow patterns around EuBL onsets in the reforecasts (Fig. 6.2g) and differ markedly from the observed patterns around ScBL (Fig. 7.2c).

The similarities of WCB outflow frequencies during EuBL and ScBL in the reforecasts lead to the hypothesis that the reforecasts might have similar pathways into the two regimes via enhanced WCB outflow over Greenland. On the other hand, the reforecasts miss the enhanced outflow activity during observed ScBL onsets in the northern part of the incipient block over Scandinavia.

The role of the WCB for ScBL and the hypothesis of the similar WCB pathways for EuBL and ScBL in the reforecasts is now further evaluated for the temporal evolution of Z500 and WCB outflow frequencies in ERA-Interim and for the ensemble members with a ScBL onset. Four to two days before the ScBL onset, positive Z500 anomalies emerge over the northern and western part of the incipient block (Fig. 7.3a). These anomalies likely result from both the retrogression of the amplified flow over western Russia and a further amplification of the large-scale flow from upstream regions over the Atlantic.

Two to zero days before the onset, the positive anomalies in the region of the incipient block further increase to values of 100–150 gpm (Fig. 7.3d). As for the previous time interval, the amplification likely results from both the retrogression of the Scandinavian ridge and further flow amplification from upstream. In the upstream region, strong negative Z500 anomalies emerge which are likely associated with upper-level troughs leading to surface cyclones and WCB activity. After the ScBL onset, the block over Scandinavia with positive anomalies of 150–200 gpm is evident together with the strong trough over the eastern Atlantic (negative anomalies around -100 gpm) (Fig. 7.3g).

In the ensemble members with a ScBL onset in the reforecasts, the large-scale flow is similar to climatology in the region of the incipient block four to two days before the onset (Fig. 7.3b) which results in a significant underestimation of the amplified flow compared to ERA-Interim (Fig. 7.3c). This underestimation likely results from both an underestimation of the amplification from upstream regions

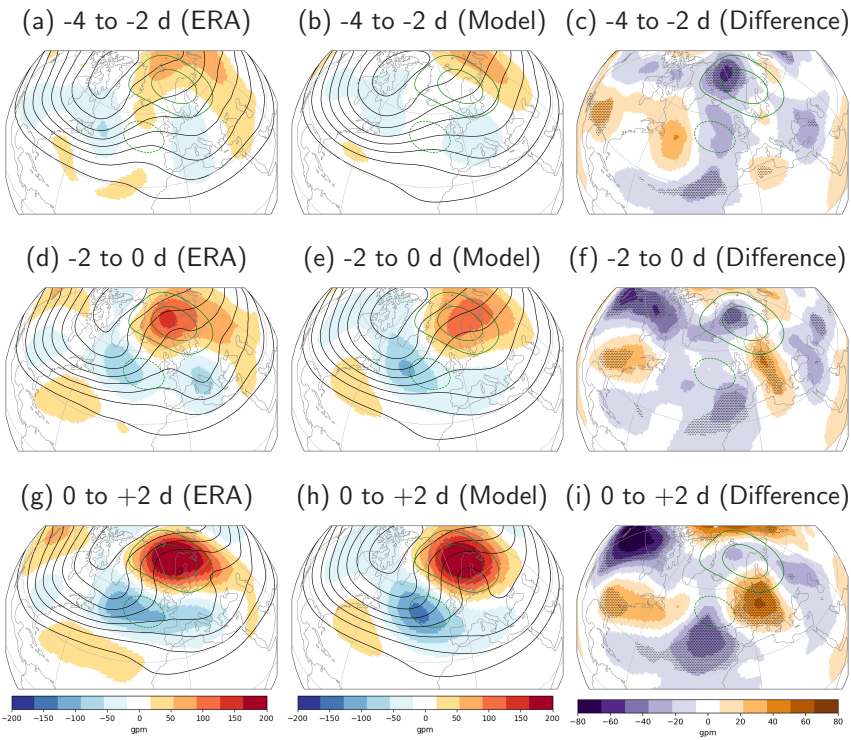


Figure 7.3: 500-hPa geopotential height anomalies (shading) 4 to 2 days prior (a-c), 2 to 0 days prior (d-f), and 0 to 2 days after (g-i) ScBL onset in (a,d,g) ERA-Interim and (b,e,h) reforecasts (NDJFM; 1997–2017). Contours indicate absolute fields (5100–5800 gpm every 100 gpm; NDJFM 1997–2017). (c,f,i) show differences between reforecasts and ERA-interim (shading) with significant differences indicated by the point stippling. Green contours as in Fig. 7.2.

over the Atlantic and the underestimation of the retrogression of positive Z500 anomalies over western Russia (Fig. 7.3b).

Prior to the onset, positive anomalies emerge over Scandinavia and the trough over the central Atlantic intensifies (negative anomalies -50 to -150 gpm) (Fig. 7.3e). Z500 differences over the Norwegian Sea weaken but are still significant (Fig. 7.3f). On the other hand, the trough over the eastern Atlantic is stronger in the reforecasts which likely results in stronger surface cyclones and higher WCB activity towards Greenland. After the onset, the strong block over Scandinavia emerges in

the reforecasts (Fig. 7.3h) and differences to ERA-Interim significantly decrease (Fig. 7.3i).

In summary, the block over Scandinavia develops differently in ERA-Interim and the reforecasts. The large-scale flow is more amplified in the region of the incipient block in ERA-interim prior to the onset. On the other hand, a stronger upper-level trough emerges over the eastern Atlantic in the reforecasts which subsequently yields a stronger flow amplification and leads to the reduction of differences in the region of the block. The stronger flow amplification in the reforecasts is likely influenced by enhanced WCB outflow activity over Greenland which will be further investigated in the following.

The observed WCB outflow frequency anomalies over the Atlantic are mostly negative four to two days before the ScBL indicating that the WCB plays a minor role at this stage of the onset evolution (Fig. 7.4a). The reforecasts have higher WCB outflow frequencies which are very similar to climatology (Fig. 7.4b). The outflow frequencies are strongly overestimated by 1–6% in the reforecasts in a large region over the central Atlantic, Greenland and over the western part of the incipient block (Fig. 7.4c).

Two to zeros days prior to the onset, the observed outflow activity over the eastern part of Greenland strongly increases (frequencies around 10–15%, anomalies 3–6%) (Fig. 7.4d). The strong outflow activity in this region is in line with the upper-level trough further south and indicates that WCB activity contributes to the amplification of the upper-level flow prior to ScBL onsets.

The reforecasts have positive WCB outflow frequencies in a similar region over eastern Greenland (Fig. 7.4e). These frequency anomalies are mostly higher than observed which results in a general overestimation of the outflow frequencies in the reforecasts (Fig. 7.4f). This overestimation of WCB activity over eastern Greenland is in line with the stronger upper-level trough further south and the stronger amplification of the block in the reforecasts (Fig. 7.3e,h).

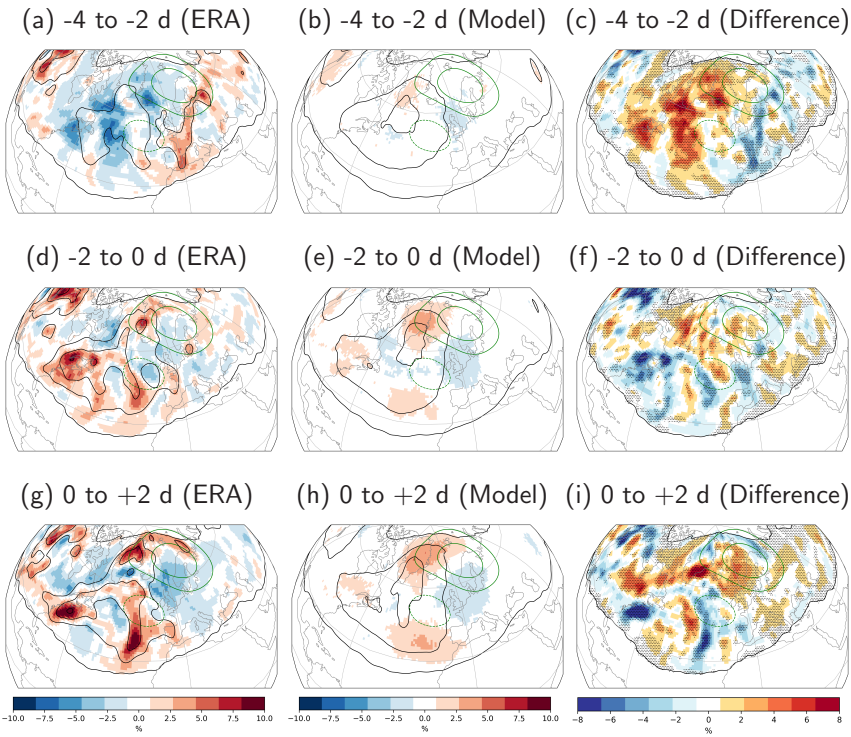


Figure 7.4: WCB outflow frequency anomalies (shading) 4 to 2 days (a–c), 2 to 0 days prior (d–f), and 0 to 2 days after (g–i) ScBL onset in a),d),g) ERA-Interim and b),e),h) reforecasts (NDFJM; 1997–2017). The black contours indicate absolute WCB outflow frequencies (ERA-Interim and reforecasts) of 5, 10, 15 % and a climatological frequency of 0.5 %. (c,f,i) show differences between reforecasts and ERA-interim (shading). Significance between the two data sets (t-test; 98 th confidence interval) is indicated by the point stippling. Green contours as in Fig. 7.2.

After the ScBL onset, a second WCB outflow maximum emerges over the Barents Sea in ERA-interim (Fig. 7.4g). The reforecasts have enhanced WCB outflow activity predominantly over eastern Greenland (Fig. 7.4h) which results in an underestimation of the WCB frequencies over the Barents Sea (Fig. 7.4i).

In summary, the temporal evolution of the Z500 patterns and WCB outflow frequencies around the onset of ScBL underlines the hypothesis that the reforecasts establish the block similarly to EuBL via strong WCB activity over Greenland

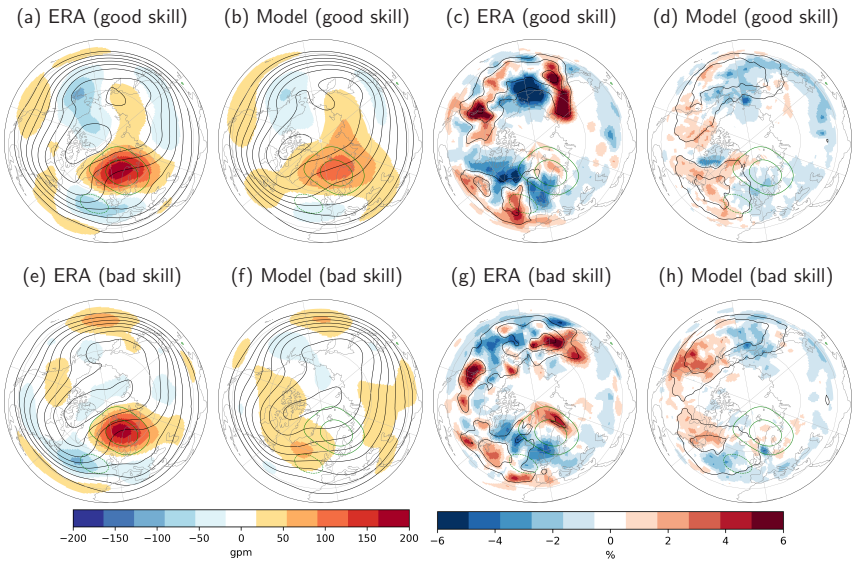


Figure 7.5: As in Fig. 7.2, but for the subset of good (a-d) and bad (e-h) ScBL skill.

and underestimate WCB frequencies over the Barents Sea. The stronger WCB activity over Greenland results from a stronger trough over the eastern Atlantic which is likely associated with high cyclone frequencies over southern Greenland and Iceland. The results indicate that the reforecasts might have difficulties in differentiating between the two regime onsets which might explain the low forecast skill of EuBL and ScBL in boreal winter.

The role of the WCBs for the ScBL is now further evaluated for subsets with good and bad ScBL skill (Fig. 7.5). For the subset with good ScBL, the positive Z500 anomalies are similar compared to all onsets (cf. Fig. 7.2a, Fig. 7.5a). In line with the good forecast skill, the ensemble mean of the reforecasts capture both positive and negative anomaly patterns generally well (Fig. 7.5b). Still, positive Z500 anomalies over Scandinavia are underestimated by the model.

WCB outflow activity is strongest over the western and central Atlantic (Fig. 7.5c) which is similar to all ScBL onsets (Fig. 7.2c). Positive anomalies are also similarly small west and north of the incipient block. The ensemble mean of the reforecasts have the highest WCB outflow activity over the central Atlantic with positive anomalies west of the incipient block but miss outflow in high latitudes in the crest of the incipient block (Fig. 7.5d). The WCB outflow frequencies are higher compared to ERA-interim as in Fig. 7.4 underlining that when the reforecasts capture ScBL onsets, they establish the block via WCB activity over the central Atlantic and Greenland.

For the subset with bad ScBL skill, the Z500 patterns are similar to the other subset (Fig. 7.5a,e). The reforecasts miss the onset entirely and have a more amplified wave pattern with positive anomalies over the central Atlantic (Fig. 7.5f). The WCB outflow activity in this subset might partly explain the challenges of the ensemble mean of the reforecasts in correctly capturing the observed onset. Compared to the subset with good ScBL skill, the observed WCB patterns over the Barents Sea are strongly enhanced in the subset with bad ScBL skill (frequencies around 5%, anomalies 3–5%) (Fig. 7.5c,g). The reforecasts strongly underestimate the WCB activity in this region and have highest frequencies over the western Atlantic (Fig. 7.5h).

In summary, WCB activity seems to play an important role for ScBL onsets in boreal winter. The reforecasts have a similar pathway into ScBL compared to EuBL via strong WCB activity over Greenland but miss the outflow in the high latitude Arctic over the Barents Sea. These difficulties of the reforecasts are reflected in the poor prediction of ScBL onsets. The results suggest that high latitude cyclone activity accompanied by strong WCB outflow over the Barents Sea needs to be resolved in the NWP model to increase the predictive skill for ScBL onset and better distinguish between EuBL and ScBL onsets.

7.2.2 Greenland Blocking

This Section investigates the impact of WCBs on the predictability and forecast skill of blocking over Greenland (GL). GL is generally well predicted by the

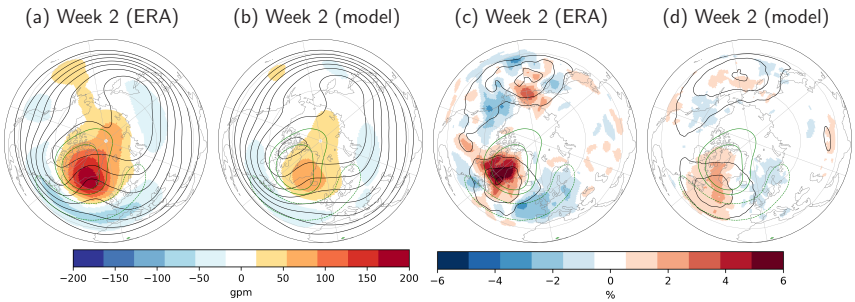


Figure 7.6: Weekly mean 500 hPa geopotential height anomalies (shading) in forecast week 2 (around GL onset) for a) ERA-Interim and b) ECMWF's IFS reforecasts. Black contours show absolute fields (5100–5800 gpm, every 100 gpm). Weekly mean WCB outflow frequency anomalies (shading) in forecast week 2 (around GL onset) for c) ERA-Interim and d) ECMWF's IFS reforecasts. Black contours show absolute frequencies for ERA-Interim and reforecasts (5, 10, 15%). Green contours indicate geopotential height anomalies (-50,50,100 gpm) for all GL cases from 1979–2015.

reforecasts with higher forecast skill compared to other regimes (Büeler et al., 2021). The frequency of the regime is strongly modulated by MJO teleconnections from the tropical Pacific (Cassou, 2008) which could partly explain the enhanced forecast skill. However, the NWP models still do not fully exploit the predictability associated with the MJO over the Northern Atlantic (Vitart, 2017). Therefore, the impact of the WCB is especially investigated for onsets with bad GL skill to understand if the WCB might play a role in diluting predictive skill for these GL events. First, the overall characteristics of GL in terms of Z500 and WCB activity are evaluated around all onsets in ERA-Interim and the ensemble mean of the reforecasts in forecast week 2.

In ERA-interim, the wave pattern in 500 hPa is strongly amplified over Greenland around the onset with anomalies of 150–200 gpm (Fig. 7.6a). Negative anomalies emerge around 40°N from eastern Canada to western Europe and reflect the southward shifted storm track with dense isohypses. WCB outflow activity is high over the western Atlantic in the southwestern part of the incipient block (frequencies between 10–15%) (Fig. 7.6c). This enhanced WCB outflow activity

can be found downstream and northeast of the North American coast where cyclogenesis likely occurs in the southward shifted storm track. On the other hand, WCB activity is low over the eastern Atlantic and Europe, as well as over the eastern Pacific.

The wave pattern over Greenland is captured by the ensemble mean of the reforecasts (Fig. 7.6b), but the magnitude of the positive Z500 anomalies is underestimated by 50–100 gpm (Fig. 7.6b). Furthermore, the reforecasts underestimate negative anomalies further south over the Atlantic and anomaly patterns upstream over the eastern Pacific. The WCB outflow frequencies are highest over the western Atlantic in the ensemble mean of the reforecasts (Fig. 7.6d) with anomalies around 1–3% in similar regions as observed (Fig. 7.6c). However, the reforecasts underestimate the observed frequencies by 3–6%.

In summary, the high WCB activity in the vicinity of the block corroborates that the WCB plays an important role for GL onsets. The highest outflow frequencies can be found over the southwestern part of the incipient block which differs compared to EuBL and ScBL where WCB activity is highest over the western and northern part of the incipient block (Fig. 6.2g, Fig. 7.2c).

The representation of Z500 and WCB activity in the reforecasts is generally similar compared to EuBL onsets (Fig. 6.2e–h) where an underestimation of both Z500 and WCB activity can be found. Still, GL has higher forecast skill compared to EuBL. In order to understand differences between the representation of the regimes, the temporal evolution of Z500 and WCB activity prior to GL onsets is now further evaluated.

Six to four days before the GL onset, Z500 is characterised by an amplified wave pattern with a trough over the western and central Atlantic and a strong ridge with positive anomalies around 100 gpm over Scandinavia (Fig. 7.7a). The positive anomalies subsequently increase and shift westwards towards Iceland (Fig. 7.7d). Two to zero days before the onset, Z500 strongly increases in the eastern half of the incipient block (anomalies 100–150 gpm) (Fig. 7.7g). Additionally, a strong

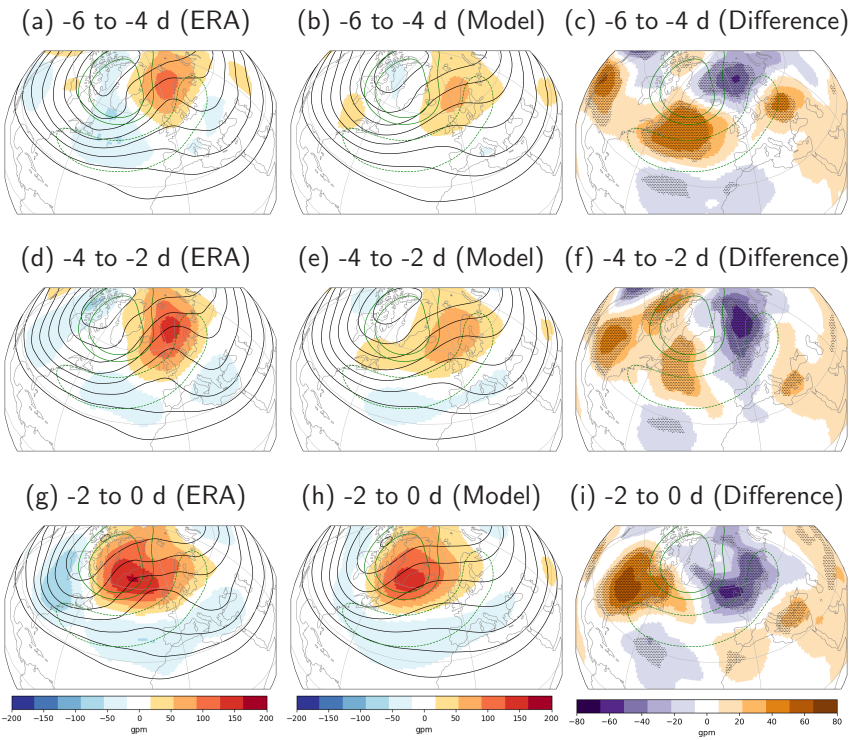


Figure 7.7: 500-hPa geopotential height anomalies (shading; bias corrected in reforecast) 6 to 4 days (a-c), 4 to 2 days (d-f), and 0 to 2 days prior (g-i) to GL onset in (a,d,g) ERA-Interim and (b,e,h) reforecasts (NDJFM; 1997–2017). Contours indicate absolute fields (5100–5800 gpm every 100 gpm; NDJFM 1997–2017). (c,f,i) show differences between reforecasts and ERA-interim (shading) with significant differences indicated by the point stippling. Green contours as in Fig. 7.6.

upper-level trough emerges over the eastern USA which likely leads to increased cyclone activity in this region.

In the reforecasts, the wave pattern is amplified six to four days before the onset with positive anomalies over Scandinavia (Fig. 7.7b). However, the anomaly patterns are significantly weaker resulting in a significant underestimation of the trough over the Atlantic and the ridge over Scandinavia (Fig. 7.7c). In the following, positive Z500 anomalies remain similar over Scandinavia and emerge

in the southern part of the incipient block (Fig. 7.7e). Here, Z500 is overestimated while the underestimation of the ridge over Scandinavia further increases (Fig. 7.7f).

The days prior to the onset are characterised by an increase in Z500 over the southeastern part of the incipient block (Fig. 7.7h). Differences in the region of the block generally weaken due to the strong wave amplification in ERA-Interim (Fig. 7.7i). Upstream, the reforecasts underestimate the emerging trough over eastern North America.

The results reveal that ERA-Interim establishes GL from a more amplified wave pattern over the eastern Atlantic. There seems to be a retrogression of the strong ridge over Scandinavia which increases positive Z500 over the region of the incipient block. At the same time, strong negative Z500 anomalies over eastern North America indicate that emerging surface cyclones could further amplify the wave pattern from the upstream region. The reforecasts have higher Z500 values in the region of the incipient block which decreases prior to the onset due to stronger wave amplification over Greenland in ERA-Interim. To understand the role of the WCB for the temporal evolution of Z500 anomalies, the WCB outflow frequencies are now evaluated in the six days prior to the onset.

WCB outflow is high over the central Atlantic (frequencies 10–15%) in ERA-Interim six to four days before the GL onset (Fig. 7.8a). Recalling the amplified wave pattern in ERA-Interim (Fig. 7.7a), the WCB activity likely contributes significantly to the positive Z500 anomalies over Scandinavia. Subsequently, the outflow frequencies over the central Atlantic further increase (15–20%) together with an increase over wide areas of the Atlantic (Fig. 7.8d). The high WCB activity over the Atlantic might help the retrogressing of the Scandinavian ridge (Fig. 7.7d) while at the same time strong WCB activity also emerges from North America (Fig. 7.8d). On the other hand, WCB outflow activity is still generally low in the region of the incipient block. Two to zero days before the onset, WCB activity from North America and the Atlantic seem to merge and the highest frequencies are now centered over the southern half of the incipient block

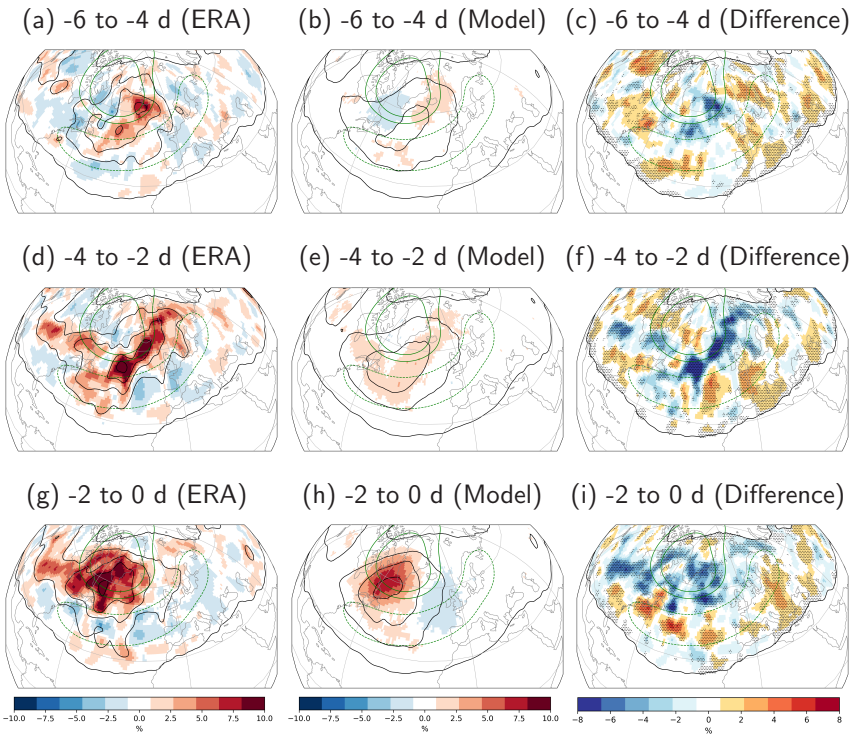


Figure 7.8: WCB outflow frequency anomalies (shading) 6 to 4 days (a–c), 4 to 2 days (d–f), and 2 to 0 days (g–i) prior to GL onset in a),d),g) ERA-Interim and b),e),h) reforecasts (NDFJM; 1997–2017). The black contours indicate absolute WCB outflow frequencies (ERA-Interim and reforecasts) of 5, 10, 15 % and a climatological frequency of 0.5 %. (c,f,i) show differences between reforecasts and ERA-interim (shading). Significance between the two data sets (t-test; 98 th confidence interval) is indicated by the point stippling. Green contours as in Fig. 7.6.

(Fig. 7.8g). In this region outflow frequencies are very high (10–20%) indicating the importance of WCB activity for GL onset.

The reforecasts have outflow frequencies around 10% over the central Atlantic six to four days before the onset (Fig. 7.8b). The outflow maximum occurs in a similar region but is significantly lower compared to ERA-Interim (around 5%) (Fig. 7.8c). The lower outflow frequency is in line with the weaker wave pattern

found in Fig. 7.7b. In the following, the main outflow region shifts slightly westwards in the reforecasts (Fig. 7.8e). The differences are large over the central and eastern Atlantic where the reforecasts have significantly lower outflow frequencies (Fig. 7.8f). Two to zero days before the onset, WCB outflow increases in the reforecasts over the northwestern Atlantic (frequencies 10–15%) (Fig. 7.8h). Despite the similar location of the maximum, frequencies are strongly underestimated over the entire region of the incipient block (Fig. 7.8i).

In summary, the analysis of the temporal evolution of Z500 and WCB activity before the onset of GL show that the block is likely established via (1) the retrogression of a ridge over Scandinavia which is strongly supported by WCB activity and (2) cyclone activity and WCB outflow which emerges just prior to the onset from North America. The ensemble members with a GL onset in the reforecasts have difficulties in capturing the WCB outflow frequencies over both the Atlantic and North America. The underestimated WCB activity likely affects the development of the block which is stronger in ERA-Interim. Therefore, the reforecasts seem to need higher Z500 in the region of the incipient block six to four days before the onset in order to correctly capture the onset of GL.

In the following, the role of the WCB is further evaluated for the ensemble mean of the reforecasts in cases with good and bad GL skill. For the subset with good GL skill, Z500 anomaly patterns are stronger compared to all onsets (cf. Fig. 7.6a, Fig. 7.9a). The reforecasts can represent the circulation better but still underestimate the magnitude of the block (Fig. 7.9b). WCB outflow is similar compared to all onsets with highest frequencies of 10–15% over the southwestern part of the incipient block (Fig. 7.9c). In line with the good representation of the block (Fig. 7.9b), WCB activity is generally well captured. Still the reforecasts underestimate the absolute frequencies by around 2–4% (Fig. 7.9d).

The subset with bad skill has similar Z500 patterns compared to all onsets (cf. Fig. 7.6a, Fig. 7.9e). The reforecasts strongly underestimate the positive anomalies in the region of the block and have an amplified wave pattern further east over the Atlantic (Fig. 7.9f). Recalling the retrogression of the Scandinavian ridge

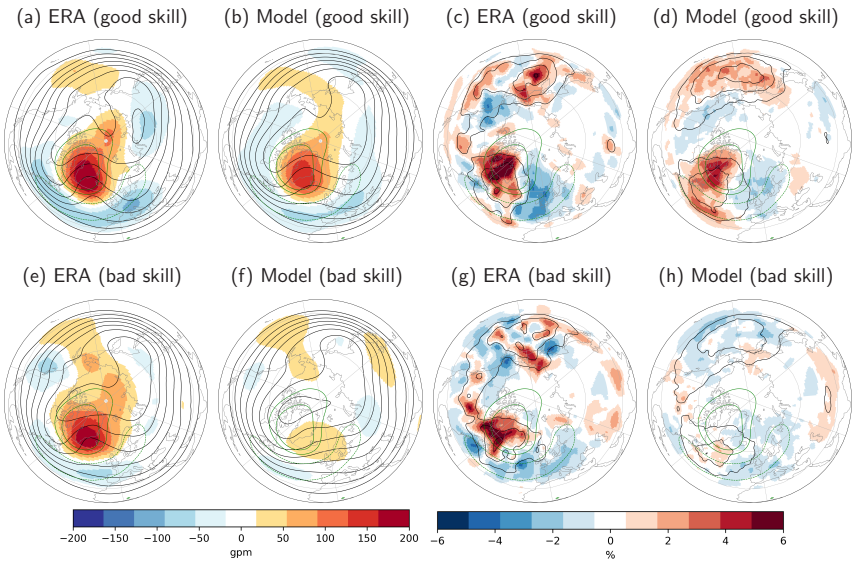


Figure 7.9: As in Fig. 7.6, but for the subset of good (a-d) and bad (e-h) GL skill.

prior to GL onsets (Fig. 7.7a,d,g), these findings might indicate that the ensemble mean of the reforecasts underestimates the retrogression leading to missed GL onsets. The WCB outflow frequency maximum occurs in a similar region compared to all onsets while the area of high WCB outflow frequencies is larger (cf. Fig. 7.6c, Fig. 7.9g). The reforecasts strongly underestimate WCB outflow frequencies around the incipient block (Fig. 7.9h).

As for the onset of EuBL (Fig. 6.6), there is a strong link between WCBs and the forecast skill of GL. WCBs are better represented in the subset with good GL skill and underestimated in the subset with bad GL skill. Still, as seen in Fig. 7.1b, the reforecasts are able to capture GL onsets generally well compared to other regimes. In order to investigate potential drivers of enhanced predictability and forecast skill, the subsets with good and bad GL skill are now further linked to the wave patterns over the Pacific and MJO activity in the tropics.

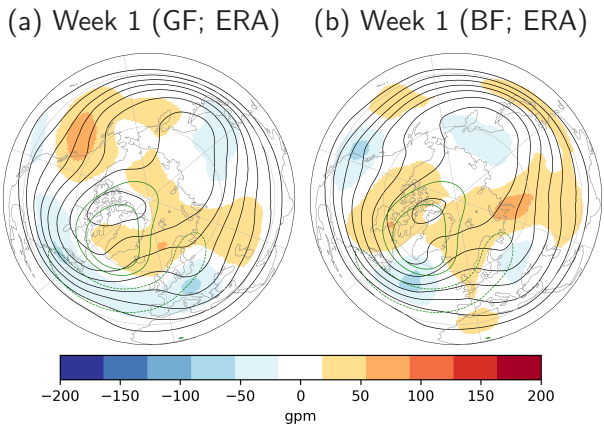


Figure 7.10: As in Fig. 7.9, but for Z500 forecast week 1 in the subset with a) good and b) bad GL skill.

Over the eastern half of the Pacific region, Z500 patterns are similar in the subset with good and bad GL skill (Fig. 7.9a,e). Positive anomalies occur over the central and eastern Pacific and over Alaska while negative anomalies are found along the west coast of the USA. However, in the week prior to the onset, the Z500 anomalies are different in the two subsets (Fig. 7.10). A strong ridge with positive anomalies is evident over the eastern Pacific and western North America in the subset with good GL skill (Fig. 7.10a). These findings show that in this subset the ridge was already established in forecast week 1 and that positive anomalies decrease in week 2 (Fig. 7.9a).

On the other hand, the flow is more zonal in the subset with bad GL skill in week 1 (Fig. 7.10b) and positive anomalies over Alaska develop in forecast week 2 around the GL onset (Fig. 7.9e). WCB activity is enhanced over the Bering Strait (Fig. 7.9g) and likely contributes to the amplification of the ridge over Alaska. These findings suggest that there are different upstream pathways into GL. In the first one, the ridge over western North America is already established in week 1 while the ridge emerges around the GL onset in week 2 in the second one.

The reforecasts strongly underestimate WCB activity over the Bering Strait in week 2 in the subset with bad GL skill together with an underestimation of the

Table 7.1: Madden-Julian Oscillation (MJO) at initial time (in %) before GL onset in forecast week 2 (all GL onsets (all), subset of onsets with good GL skill (good), and subset of onsets with bad GL skill (bad) (NDJFM; 1997–2017).

	All	Good	Bad
Phase 1	6.6	19.4	0.0
Phase 2	2.8	0.0	6.7
Phase 3	2.8	6.5	0.0
Phase 4	6.6	12.9	3.3
Phase 5	12.3	9.7	3.3
Phase 6	12.3	3.3	16.7
Phase 7	10.4	12.9	6.7
Phase 8	13.2	9.7	16.7
No MJO	33.0	25.8	46.7

ridge over Alaska (Fig. 7.9f,h). These findings indicate that forecast errors might be generated in the WCB which then propagate downstream and lead to missed GL onsets in the models.

To further understand the role of the Pacific for GL onsets, the analysis is extended to the impact of the MJO for GL forecast skill. For all GL onsets, an active MJO occurs at 67% of the initial times (Tab. 7.1). This percentage is higher compared to EuBL where 62% of the onsets have an active MJO at initial time (Tab. 6.1). Contrary to EuBL onsets, the percentage of active MJO phases is different in the subsets with good and bad GL skill. The subset with good GL skill has an active MJO at 74.2% of the times while the MJO is active in only 53.3% of the cases in the subset with bad GL skill. These findings corroborate that the MJO plays an important role for the enhanced predictive skill of GL onsets in the ECMWF's reforecasts. For these events with good GL skill, the reforecasts seem to be able to correctly capture teleconnection signals from the MJO leading to good GL forecast skill.

On the other hand, active MJO phases can also lead to bad GL forecast skill. From the 53.3% of the cases with an active MJO in the subset with bad GL skill, 75.2% occur after MJO phases 6–8. In general, these MJO phases enhance the frequency of GL and provide predictability on sub-seasonal time scales (Cassou, 2008). However, these findings highlight that some of the events with potentially increased predictability provided by the MJO are still challenging for the reforecasts to capture.

Recalling the difficulties of the reforecasts in capturing ridge building over the eastern Pacific in the subset with bad GL skill (Fig. 7.9e–h), the WCB might play a vital role in generating or amplifying forecast errors over the eastern Pacific leading to missed GL onsets downstream. The results in this Section suggest that these upstream precursors need to be better resolved in order to fully exploit the predictability associated with the MJO for GL onsets.

7.2.3 Atlantic Ridge

The impact of WCBs on Atlantic-European weather regimes is now further analysed for the Atlantic Ridge (AR) regime. The previous investigation of the three other blocked regimes (EuBL, ScBL, GL) shows that the WCB plays an important for the onset of the regimes and that errors in the representation of WCBs lead to different pathways into a specific regime. Observed onsets of AR in forecast week 1 and 2 are generally well predicted by the reforecasts (Fig. 7.1a,b) with similar skill compared to GL. Therefore, the representation of AR onsets in terms of Z500 and WCB activity are now further analysed.

Around observed AR onsets in forecast week 2, the wave pattern is amplified over the central Atlantic with strong positive Z500 anomalies around 150–200 gpm (Fig. 7.11a). Upstream, the large-scale flow is more zonal compared to climatology with positive anomalies over the central Pacific and eastern North America. The WCB outflow frequencies are highest on the northwestern side of the incipient block (around 15%) (Fig. 7.11c). The frequencies are larger compared to the three other blocked regimes (cf. Fig. 6.2g, Fig. 7.2c, Fig. 7.6c). WCB frequencies

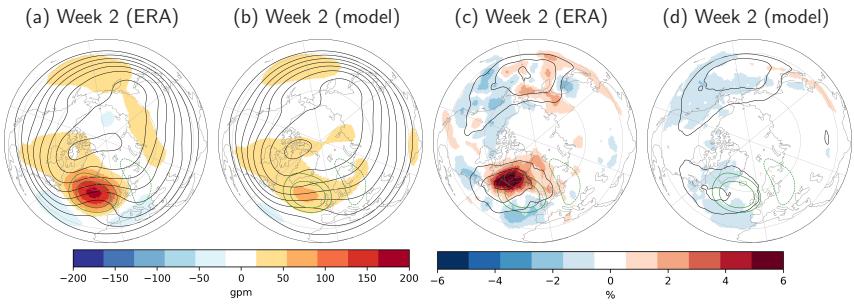


Figure 7.11: Weekly mean 500 hPa geopotential height anomalies (shading) in forecast week 2 (around AR onset) for a) ERA-Interim and b) ECMWF's IFS reforecasts. Black contours show absolute fields (5100–5800 gpm, every 100 gpm). Weekly mean WCB outflow frequency anomalies (shading) in forecast week 2 (around AR onset) for c) ERA-Interim and d) ECMWF's IFS reforecasts. Black contours show absolute frequencies for ERA-Interim and reforecasts (5, 10, 15%). Green contours indicate geopotential height anomalies (-50,50,100 gpm) for all AR cases from 1979–2015.

around AR onsets are low over the eastern Pacific and enhanced over the western part of the ocean basin.

The ensemble mean of the reforecasts generally captures Z500 anomalies around the onset but underestimate the magnitude of the anomalies (Fig. 7.11b). As for the other regimes, Z500 anomalies upstream are generally well predicted. The reforecasts strongly underestimate WCB activity in the region of the incipient block (Fig. 7.11d). In the region of highest observed frequencies (>15%), the reforecasts predict negative anomalies and frequencies around 7%. However, despite the low WCB frequencies, the ensemble mean of the reforecasts seem to be able to capture the amplified wave pattern over the Atlantic. These findings point to a minor role of the WCB for the onset of the AR regime. To understand the role of the WCB for AR onset and the overall high forecast skill, the temporal evolution prior to the onset is now evaluated for Z500 and the WCB activity.

AR ridge emerges from an amplified Rossby-wave pattern which is characterised by positive Z500 anomalies over eastern North America and Europe and negative anomalies in the region of the incipient block over the central Atlantic six to four days before the onset (Fig. 7.12a). In the following, the initial trough over the

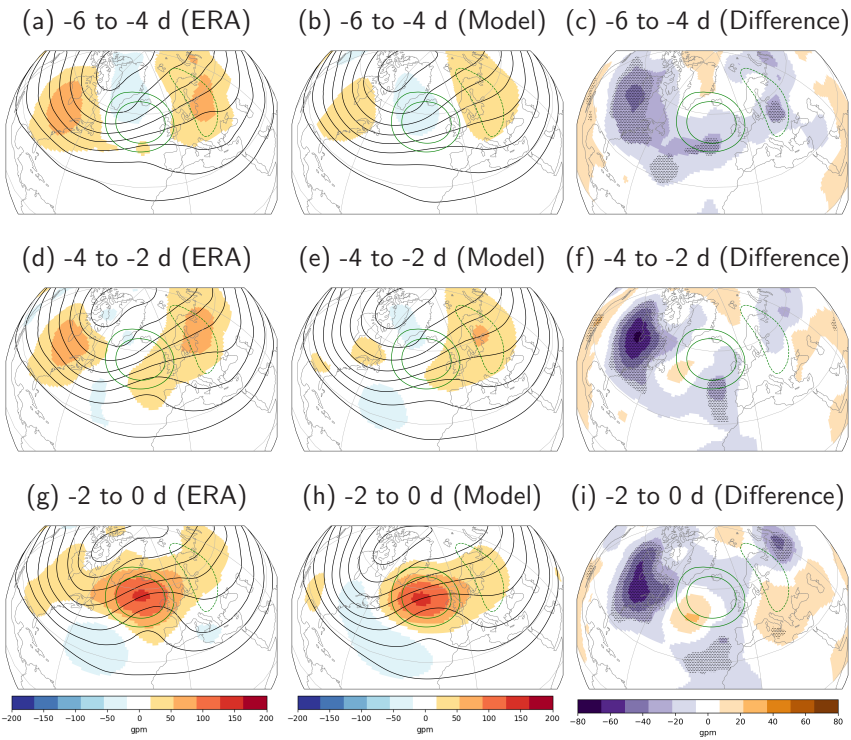


Figure 7.12: 500-hPa geopotential height anomalies (shading) 6 to 4 days (a-c), 4 to 2 days (d-f), and 0 to 2 days prior (g-i) to AR onset in (a,d,g) ERA-Interim and (b,e,h) reforecasts (NDJFM; 1997–2017). Contours indicate absolute fields (5100–5800 gpm every 100 gpm; NDJFM 1997–2017). (c,f,i) show differences between reforecasts and ERA-interim (shading) with significant differences indicated by the point stippling. Green contours as in Fig. 7.11.

central Atlantic develops into a ridge and positive anomalies emerge over the southeastern part of the incipient block (Fig. 7.12d). Two to zero days before the onset, positive anomalies further increase (100–150 gpm) resulting in a strongly amplified wave pattern (Fig. 7.12g).

The ensemble members with a onset of AR in the reforecasts have a similar Rossby wave pattern compared to the observations with positive anomalies over eastern North America and Europe and negative anomalies over the central Atlantic (Fig. 7.12b). Differences are small in the region of the incipient block

while the magnitude of the positive anomalies is weaker resulting in significant differences over eastern North America and Europe (Fig. 7.12c). In the following, the wave pattern strongly amplifies over the central Atlantic and positive Z500 anomalies emerge in the region of the incipient block (Fig. 7.12e,h). Differences in the region of the incipient block are generally weak and not significant (Fig. 7.12f,i) which indicates that the ensemble members with AR onsets have a similar pathway into AR compared to the observations.

The temporal evolution of Z500 prior to AR onsets shows that the regime is established from an amplified Rossby-wave pattern with a trough over the central Atlantic. The initial trough subsequently develops into a ridge leading to the onset of the AR regime. The ensemble members with an AR onset establish the regime similarly and differences in the region of the incipient block are generally small. The representation of the temporal evolution in the reforecasts is in line with the good forecast skill for the onset of AR (Fig. 7.1a,b).

Next, the temporal evolution of the WCB and its role for AR onsets is evaluated. WCB outflow frequencies are around 7% in the region of the incipient block six to four days before the onset (Fig. 7.13a). These frequencies are lower compared to climatology indicating a minor role of the WCB at this time interval. Subsequently, WCB activity increases (around 10%), but positive anomalies only occur in the southern part of the region of the incipient block (Fig. 7.13d). The WCB activity then strongly increase two to zero days before the onset with high outflow frequencies (15%; anomalies 6–8%) over the western part of the block (Fig. 7.13g). The weak WCB activity six to two days before the onset point to a minor role of the WCB in establishing Z500 patterns before the onset. The WCB becomes more important the last days prior to the onset and subsequently during the AR life cycle (not shown). Recalling the high WCB frequencies in Fig. 7.11c, it is important to note that these frequencies occur just prior and predominantly after the AR onset.

The reforecasts have lower WCB frequencies compared to climatology on the western part of the block six to four days before the onset (Fig. 7.13b). Still,

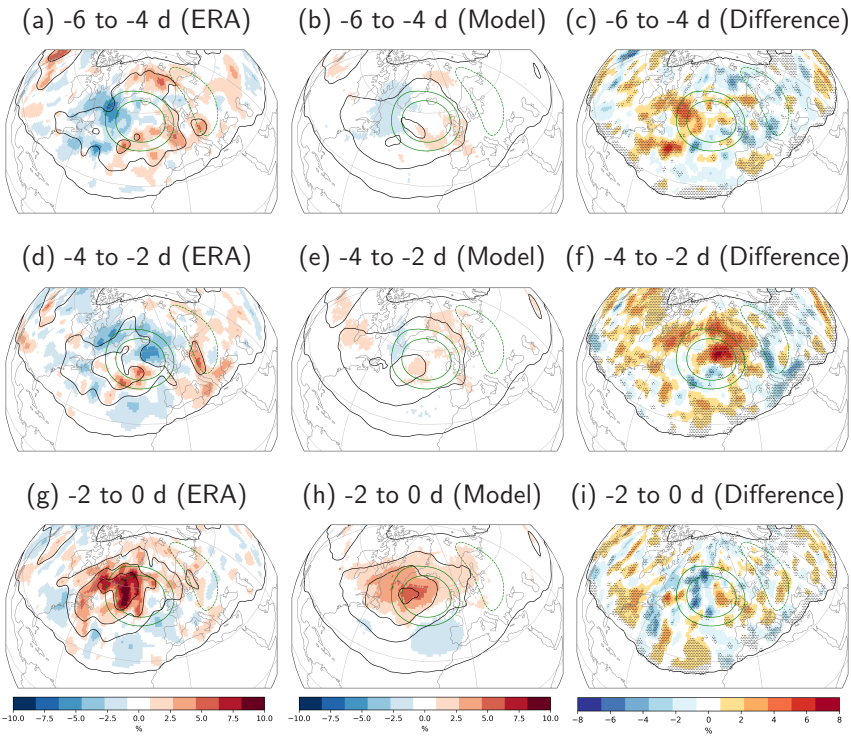


Figure 7.13: WCB outflow frequency anomalies (shading) 6 to 4 days (a–c), 4 to 2 days (d–f), and 2 to 0 days (g–i) prior to AR onset in a),d),g) ERA-Interim and b),e),h) reforecasts (NDFJM; 1997–2017). The black contours and point stippling as in Fig. 7.8. Green contours as in Fig. 7.11.

WCB frequencies are significantly higher than observed in this region (Fig. 7.13c). WCB frequencies slightly increase four to two days before the onset (Fig. 7.13e). Differences weaken over the western part of the block and are highest further east (Fig. 7.13f). The last days prior to the onset are characterised by an increase of WCB outflow frequencies (around 15%) (Fig. 7.13h). The increase is weaker than observed resulting in significant differences (Fig. 7.13i). In summary, the reforecasts capture WCB anomaly patterns prior to AR generally well and only underestimate frequencies in the last days before the onset. These results are in line with the small differences in the evolution of Z500 (Fig. 7.12).

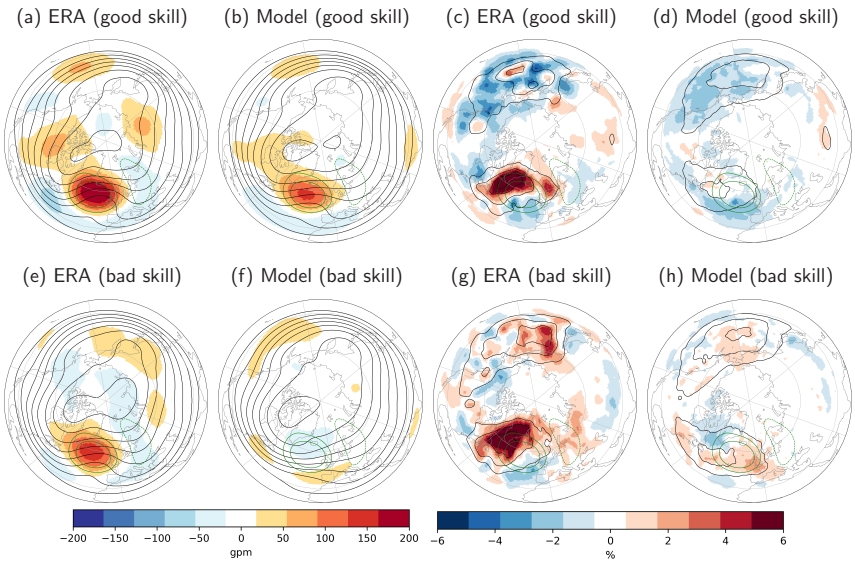


Figure 7.14: As in Fig. 7.11, but for the subset of good (a-d) and bad (e-h) AR skill.

The previous analyses point to a smaller role of the WCB for the onset of AR while the WCB patterns are generally well represented in the reforecasts. This is now further evaluated for the subsets with good and bad AR skill. For the subset with good AR skill, Z500 anomalies are stronger in ERA-Interim compared to all onsets (cf. Fig. 7.11a, Fig. 7.14a). In line with the good forecast skill, the reforecasts capture the anomaly patterns generally well (Fig. 7.14b).

The strongest WCB outflow activity occurs in a similar region as for all onsets while outflow frequencies are further enhanced (15–20%) (cf. Fig. 7.11c, Fig. 7.14c). The reforecasts strongly underestimate the WCB frequencies by 7–10% (Fig. 7.14d). This strong underestimation is different compared to the subset of good regime skill for EuBL, ScBL and GL (Fig. 6.6d, Fig. 7.5d, Fig. 7.9d) where outflow frequencies are better represented compared to all onsets. These findings for AR underline the hypothesis that the WCB plays a minor role for the onset of the regime because the reforecasts can still capture the block despite a relatively low WCB activity.

In the subset with bad AR skill, Z500 anomalies are weaker compared to all onsets (Fig. 7.11a, Fig. 7.14e). The reforecasts miss the onset of the block and project into a more zonal flow with negative anomalies over Iceland and positive anomalies over southwestern Europe (Fig. 7.14f). The WCB outflow frequencies are high (>15%) and in similar region compared to all onsets and the subset with good AR skill (cf. Fig. 7.11c) Fig. 7.14c, Fig. 7.14g). The model strongly underestimates WCB outflow frequencies in the vicinity of the block (Fig. 7.14h). However, WCB frequencies in the reforecasts are generally similar in the subset with bad AR skill compared to the subset with good AR skill (Fig. 7.14d,h).

These findings further underline that the reforecasts can establish Z500 anomaly patterns well around the AR onset with a minor role of the WCB. As seen in the temporal evolution of Z500 and WCB patterns (Fig. 7.12, Fig. 7.13), the reforecasts can generally represent the evolution of these variables well which likely explains part of the overall high forecast skill of the AR onset (Fig. 7.1). The high forecast skill might also result from well represented teleconnections and upstream Rossby-wave precursors.

7.2.4 Zonal Regime

So far the role of WCBs has been analysed for blocked weather regimes. In this Section, it is further evaluated for one of the three cyclonic regimes (ZO). The impact of the WCB activity on these cyclonic regimes is likely lower compared to the blocked regimes since they are mostly dominated by strong negative Z500 anomalies. On the other hand, the ZO regime has similar characteristics in terms of Z500 anomalies compared to EuBL with a trough over the central Atlantic and a ridge over Europe.

The investigation of remote precursors for EuBL onsets in Chapter 6 reveals that the NWP model has difficulties in capturing MJO teleconnections leading to EuBL onsets which might be partly responsible for the overall low forecast skill. Occurrence frequencies of both ZO and EuBL are typically enhanced after MJO phases 2/3 (not shown) while the predictive skill for ZO in the reforecasts

is significantly higher than the skill for EuBL (Büeler et al., 2021). These findings raise the hypothesis that the high skill of the ZO regime mainly results from well captured MJO teleconnections in the NWP model. This hypothesis is now evaluated together with the role of WCBs for ZO onsets.

For all ZO events, strong negative anomalies (100–150 gpm) occur over Greenland and Iceland while positive anomalies (50–100 gpm) can be found over the western Atlantic and over Europe (Fig. 7.15a). These anomaly patterns are similar to the positive phase of the NAO. Over the Pacific, negative anomalies emerge over the Bering Strait and Alaska and positive anomalies can be found further south over the eastern Pacific.

WCB outflow activity is highest over the central Atlantic (around 10%) (Fig. 7.15c) while positive outflow anomalies (3–5%) emerge along 35-50°N over the central and eastern Atlantic. Contrary to the four blocked regimes, this WCB activity likely does not lead to a wave amplification but is merely advected downstream along a strong westerly jet stream. Upstream, WCB activity is reduced over the western Pacific and enhanced over the eastern Pacific. The outflow frequencies over the Pacific are generally lower compared to all EuBL onsets (Fig. 6.6c) which points to a minor role of the WCB in generating or amplifying forecast error before ZO onsets.

In the subsets with good and bad ZO skill, Z500 patterns over the Atlantic are generally similar to all ZO onsets (Fig. 7.15a,e,i) together with similar WCB outflow patters (Fig. 7.15c,g,k). On the other hand, strong differences emerge upstream over the eastern Pacific in the two subsets. The subset with good ZO skill has negative WCB outflow anomalies over large parts of the North Pacific region (Fig. 7.15g) and generally negative Z500 anomalies over the eastern Pacific and Alaska (Fig. 7.15e).

Contrary, the subset with bad ZO skill has strongly enhanced WCB outflow frequencies over western North America (Fig. 7.15k) together with a more amplified ridge which is characterised by positive Z500 anomalies over central Canada (Fig. 7.15i). These different flow patterns together with a strong difference in

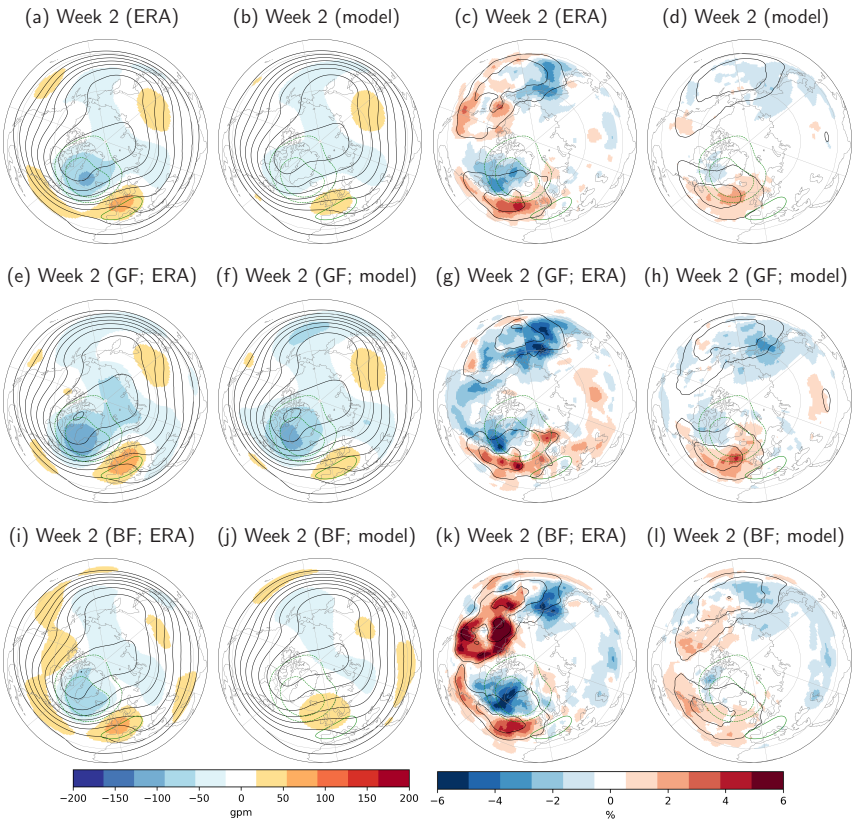


Figure 7.15: As in Fig. 6.6 but for (a-d) all ZO onsets, (e-h) good, and (i-l) bad ZO skill.

WCB activity indicate that certain ZO events might be more challenging to predict than others and that the WCB plays a role in it.

In the week prior to the ZO onset, negative Z500 anomalies emerge over North America for all ZO onsets (Fig. 7.16a). In both subsets, the Z500 anomalies over the Pacific and North America are also predominantly negative (Fig. 7.16e,i). Thus, the ridge over North America in the subset with bad ZO skill in week 2 (Fig. 7.15e) emerges around the ZO onset together with the strong WCB activity in this region (Fig. 7.15g).

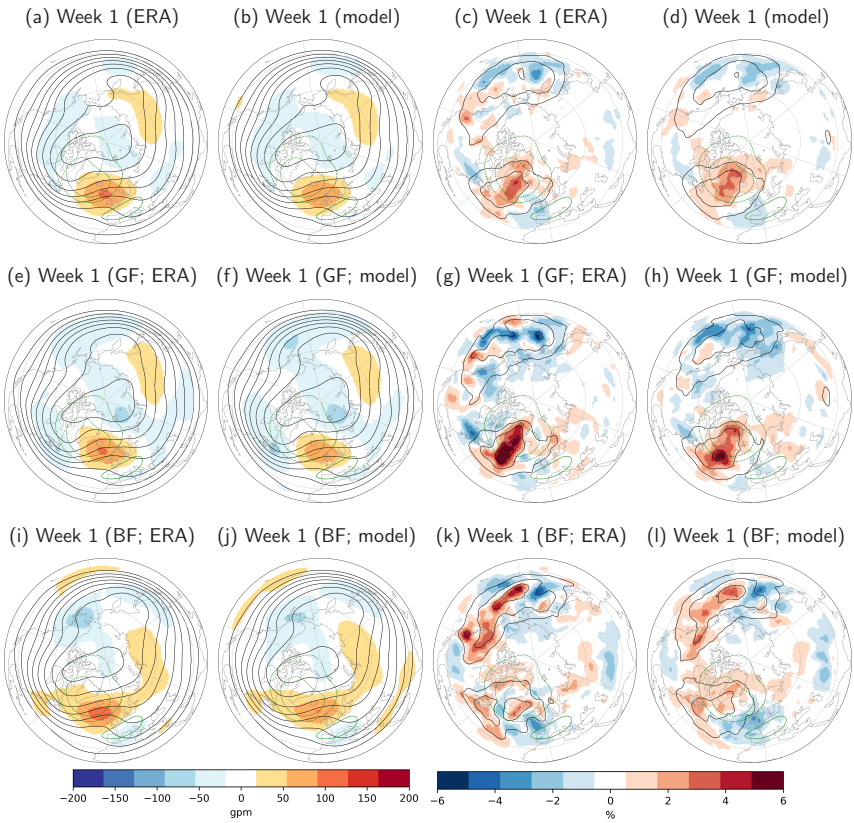


Figure 7.16: As in Fig. 7.15 but for forecast week 1 before ZO onsets in week 2.

Over the North Atlantic, the large-scale flow is strongly amplified with a ridge over the eastern Atlantic and western Atlantic (Fig. 7.16a,e,i). These Z500 anomalies resemble the anomaly patterns of EuBL and AR which can be found as precursor regimes in forecast week 1 before ZO onsets in week 2 (not shown).

The representation of the Z500 and WCB activity in the ensemble mean of the reforecasts is now further evaluated for all ZO onsets and the subsets with good and bad ZO skill. For all ZO onsets in week 2, the ensemble mean of the reforecasts

Table 7.2: As in Tab. 7.1 but for ZO

ZO	All	Good	Bad
Phase 1	7.9	4.8	9.8
Phase 2	10.0	14.3	4.9
Phase 3	7.9	11.9	7.3
Phase 4	6.4	11.9	0.0
Phase 5	7.9	4.8	19.5
Phase 6	10.0	4.8	9.8
Phase 7	10.0	16.6	7.3
Phase 8	7.1	7.1	7.3
No MJO	32.9	23.8	34.2

represent the Z500 patterns over the Atlantic generally well but underestimate the magnitude of the anomalies (especially negative anomalies) (Fig. 7.15b). The WCB outflow is also generally well predicted with a maximum over the central Atlantic (Fig. 7.15d). Frequency anomalies are slightly underestimated in this region but well captured over the eastern Atlantic.

In line with the forecast skill, the flow patterns over the Atlantic in the subset with good ZO skill are well captured (Fig. 7.15f) together well represented WCB outflow frequencies (Fig. 7.15h). On the other hand, in the subset with bad ZO skill, the ensemble mean predicts a general persistence of the ridge pattern over the eastern Atlantic and misses the onset of the ZO regime in week 2 (Fig. 7.15j). Errors in the prediction of the ZO onset likely emerge from upstream regions over the Pacific and western North America. Here, the reforecasts strongly underestimate WCB activity (Fig. 7.15l) and ridge building over Canada (Fig. 7.15j) which likely affects the downstream flow evolution and can lead to missed ZO onsets.

The findings in the subsets with good and bad ZO skill are now further linked to MJO activity in the tropics at forecast initial time. As for GL (Tab. 7.1), there is

a high difference between MJO occurrence in the subset with good and bad ZO skill (Tab. 7.2). In the subset with good ZO skill, the MJO is active at 76.2% of the cases while an active MJO occurs in 65.8% of the events with bad ZO skill. These findings corroborate that the reforecasts can capture teleconnection signals leading to ZO onset generally well which might partly explain the high forecast skill for the regime.

On the other hand, the subset with bad ZO skill is dominated by MJO phase 5 which occurs at 19.5% of the events with bad ZO skill. This is similar to the subset with bad EuBL skill where an active MJO in phase 5 can be found in around 20% of the cases (Tab. 6.1). Recalling the similar flow patterns of the two regimes over Europe, these findings point to difficulties of the reforecasts in correctly capturing the teleconnection patterns leading into EuBL and ZO after MJO phase 5. These difficulties might be partly explained by strong WCB activity over the eastern Pacific and western North America which leads to ridge building in both subsets of bad EuBL and ZO skill (cf. Fig. 6.6i, Fig. 7.15i). An incorrect representation of the timing and location of the ridge might then lead to downstream forecast errors and misrepresented regime onsets.

7.3 Link between WCB activity and blocked regimes over Europe in summer

In this Section, the representation of WCBs is further evaluated in boreal summer around the onset of block regimes over Europe. Recent studies find a significant correlation between blocked regimes over Europe and the occurrence frequency of summer heat waves (Schaller et al., 2018, Spensberger et al., 2020) which underlines the importance of an accurate prediction of the blocks for summer heat extremes.

As shown in Chapter 5, WCB activity is lowest in summer compared to other seasons (Fig. 5.14b,e,h). Therefore, WCBs are expected to have a minor role for the onset and life cycles of the regimes. However, a recent study from Zschenderlein et al. (2020) shows an important contribution of diabatic processes in WCBs and

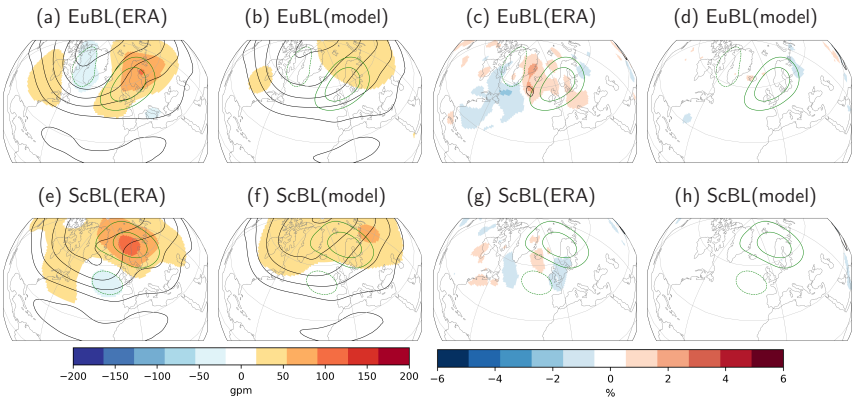


Figure 7.17: Weekly mean 500 hPa geopotential height anomalies (shading) in forecast week 2 around (a,b) EuBL and (e,f) ScBL onsets) for (a,e) ERA-Interim and (b,f) ECMWF's IFS reforecasts in MJJAS (1997–2017). Black contours show absolute fields (5300–5800 gpm, every 100 gpm). Weekly mean WCB outflow frequency anomalies (shading) in forecast week 2 around (c,d) EuBL and (g,h) ScBL onsets for (c,g) ERA-Interim and (d,h) ECMWF's IFS reforecasts. Black contours show absolute frequencies for ERA-Interim and reforecasts (5%). Green contours indicate geopotential height anomalies (-50,50,100 gpm) for all EuBL and ScBL cases from 1979–2015.

other weather systems for the formation of upper-level anticyclones associated with surface heat waves in summer. In total, around 35–50% of the air parcels that arrive in the blocked region are diabatically heated in the seven days prior.

These results point towards an important role of WCBs for summer heat wave events over Europe. Therefore, the prediction of WCBs and Z500 patterns are now investigated around EuBL and ScBL onsets in summer. ScBL is the dominant blocked regime over Europe in summer and accounts for 16.0% of the times. On the other hand, EuBL occurs at 12.2% of the overall dates.

First, the characteristics of Z500 and WCB activity around the onsets are evaluated. For all EuBL onsets, positive Z500 anomalies (50–100 gpm) emerge from the eastern Atlantic to central Scandinavia (Fig. 7.17a). Over Europe, the average geopotential height is very similar over large parts of the continent (around 5650 gpm).

All ScBL onsets in summer are associated with a trough over the eastern Atlantic and a block over western Scandinavia and the Norwegian Sea (Fig. 7.17e). The highest positive Z500 anomalies are stronger compared to EuBL (around 130 gpm) while the large-scale flow is similar over central Europe.

The WCB outflow activity during EuBL onsets is enhanced over the western part of the incipient block (Fig. 7.17c). Outflow frequencies up to 5% (anomalies of 1–3%) indicate a potential role of WCB activity for the onset of EuBL in summer. WCB activity is lower over the western Atlantic and along the US east coast (negative anomalies of 1–3%).

During ScBL onsets, WCB frequencies are lower compared to EuBL onsets (Fig. 7.17g). Weak positive anomalies only emerge over the southwestern part of the incipient block. These findings point to a smaller role of the WCB for ScBL onsets in summer.

For EuBL onsets, the reforecasts capture the amplified wave pattern over northern Europe but underestimate the magnitude of the positive anomalies (Fig. 7.17b). Similarly, the reforecasts also underestimate the positive anomalies over Scandinavia during ScBL onsets (Fig. 7.17f).

The reforecasts predict WCB activity similar to climatology for both EuBL and ScBL onsets (Fig. 7.17d,h). In both cases, positive WCB anomalies are not captured by the reforecasts. The analysis of the Z500 and WCB fields around the onset of EuBL and ScBL in summer show that WCB activity is more important for EuBL onsets compared to ScBL onset. However, outflow frequencies are still relatively small (lower than 5%). Therefore, the impact of WCB activity for EuBL and ScBL onset is now further evaluated in subsets with good and bad forecast skill.

The subset with good EuBL skill has slightly lower Z500 over western Europe compared to all onsets (cf. Fig. 7.17a, Fig. 7.18a). The reforecasts capture the anomaly patterns generally well but underestimate their magnitude (Fig. 7.18b).

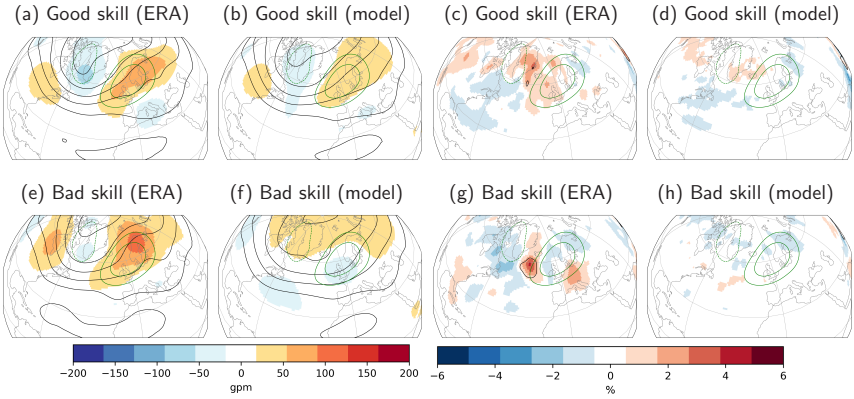


Figure 7.18: As in Fig. 7.17, but for the subset of good (a-d) and bad (e-h) EuBL skill.

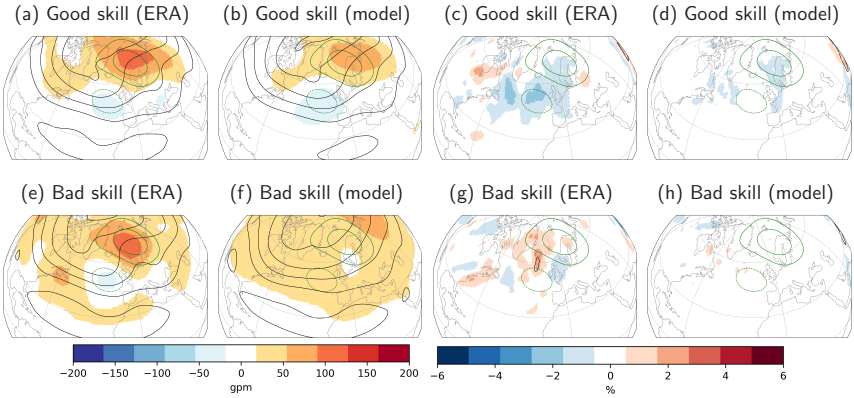


Figure 7.19: As in Fig. 7.17, but for the subset of good (a-d) and bad (e-h) ScBL skill.

WCB activity is generally similar compared to all onsets (cf. Fig. 7.17c, Fig. 7.18c) with positive anomalies over the western part of the incipient block. In line with the good forecast skill, WCB frequencies are better captured in the reforecasts compared to all onsets (cf. Fig. 7.17d, Fig. 7.18d). However, outflow frequencies are still underestimated over western Europe. This underestimation is similar compared to the winter season (Fig. 6.6d) indicating that the reforecasts have

difficulties capturing the WCB activity around EuBL onsets over Europe in all seasons.

The subset with bad EuBL skill has higher Z500 anomalies compared to all onsets (cf. Fig. 7.17a, Fig. 7.18e). The reforecasts do not capture the amplified wave pattern and rather project into a more zonal flow over Europe (Fig. 7.18e).

WCB outflow is enhanced south of Iceland and reduced over Europe compared to all onsets (cf. Fig. 7.17c, Fig. 7.18g). The reforecast strongly underestimate WCB activity in the region of the incipient block by 1–3% (Fig. 7.18h). These findings underline the importance of WCB activity for EuBL onsets in the summer.

For the subset with good ScBL skill, the Z500 patterns are similar to all onsets (cf. Fig. 7.17e, Fig. 7.19a). In line with the good forecast skill, the reforecasts capture the anomaly patterns generally well (Fig. 7.19b). WCB outflow activity is weaker compared to all onsets (cf. Fig. 7.17g, Fig. 7.19c). Negative anomalies emerge over a wide part of the incipient block and to the south of it (Fig. 7.19c). These results show that well predicted ScBL events in summer occur with very low WCB activity. The reforecast can capture these anomaly patterns generally well in line with the captured wave pattern (Fig. 7.19b,d).

The subset with bad ScBL has similar Z500 anomalies compared to all onsets (cf. Fig. 7.17e, Fig. 7.19e). The reforecasts underestimate the amplified wave pattern, in particular the trough over the eastern Atlantic and the magnitude of the block (Fig. 7.19f).

WCB outflow activity is strongly enhanced compared to all onsets (cf. Fig. 7.17g, Fig. 7.19g). Outflow frequencies are around 3–5% over the southwestern part of the incipient block. The enhanced WCB activity in this subset indicates that the WCB plays a role for ScBL events in the summer which are more challenging for the reforecasts to correctly predict. In line with the underestimation of the block (Fig. 7.19f), the reforecasts also underestimate WCB outflow activity in this subset.

In conclusion, the results show that despite the overall lower WCB frequencies in boreal summer, the WCB activity still plays an important role for blocked regimes over the European region. WCB frequencies are especially enhanced around EuBL onsets and generally underestimated by the reforecasts. For ScBL, the role of the WCBs seems smaller due to the overall lower WCB frequency compared to EuBL. However, the events with enhanced WCB activity are especially challenging for the reforecasts to predict.

Recalling the correlation of EuBL and ScBL to surface heat waves in summer (Schaller et al., 2018), these findings point to the importance of correctly capturing WCB activity in summer for the prediction of heat waves. However, this hypothesis needs to be further evaluated specifically for EuBL and ScBL events which occur together with an observed surface heat wave.

7.4 Conclusions

The overall role of WCBs for weather regimes in the Atlantic-European region (in particular blocked regimes) is investigated in the ECMWF's IFS reforecasts (1997–2017). On sub-seasonal time scales, an accurate prediction of weather regimes is desirable due to their strong socio-economic impacts and their modulation of surface weather (Ferranti et al., 2018, Spensberger et al., 2020).

The results show that the reforecasts can predict the onset of GL, AR, and ZO in the extended winter season generally well and has lower skill in predicting EuBL and ScBL onsets. These findings are in line with Büeler et al. (2021) who find comparably low skill for EuBL and ScBL in winter.

As shown in Chapter 6, the WCB likely plays an important role for the onset of EuBL and might be co-responsible for the low forecast skill in the NWP models. The findings in this Chapter also suggest that WCB activity likely plays an important role for the prediction of ScBL and GL onsets in boreal winter while the impact on AR onsets seems to be smaller.

For ScBL onsets, there is high WCB outflow activity over the northern part of the incipient block (Barents Sea) which is not resolved well in the reforecasts. For ScBL onsets with high WCB activity in this region, the reforecasts have difficulties predicting the onset of the regime which suggests that the WCB plays an important role for these events. The NWP model seems to have difficulties resolving high latitude cyclones in the region between Greenland and Iceland which can lead to strong WCB activity over the Barents Sea. On the other hand, the reforecasts establish ScBL very similarly compared to EuBL via strong WCB activity over Greenland. These results indicate that the NWP model has difficulties distinguishing between EuBL and ScBL onsets which might partly explain the overall low forecast skill of the regimes.

For GL onsets, the analysis of the temporal evolution of Z500 and WCB activity before the onset show that the block is likely established via (1) the retrogression of a ridge over Scandinavia which is strongly supported by WCB activity and (2) cyclone activity and WCB outflow which emerges just prior to the onset from North America. The ensemble members with a GL onset in the reforecasts have difficulties in capturing the WCB outflow frequencies over both the Atlantic and North America. Therefore, the reforecasts seem to need higher Z500 in the region of the incipient block six to four days before the onset in order to correctly capture the onset of GL.

The relatively high predictive skill for GL onsets is likely influenced by MJO teleconnections which seem to be generally well by the NWP model leading to good GL forecast skill. On the other hand, after some MJO events, strong WCB activity over the eastern Pacific might play a vital role by developing or amplifying forecast errors leading to missed GL onsets. The results in this Section suggest that these events need to be better resolved in order to fully exploit the predictability associated with the MJO over the Northern Atlantic.

For AR onsets, the reforecasts can establish Z500 anomaly patterns generally well with a minor role of the WCB. These results might partly explain the overall high forecast skill for the onset of the regime. ZO onsets are likely influenced by different upstream pathways over the eastern Pacific and western North America. The NWP models seems to have difficulties in predicting the onset of the

regimes for cases where ridge building occurs over North America together with strong WCB activity. These findings indicate that the WCB might play a role in generating forecast errors leading to missed ZO onsets.

Lastly, the analysis of WCB activity around blocking over Europe in the extended summer season shows a general importance of WCB activity for EuBL and ScBL onsets in summer despite overall lower frequencies. In particular, the results indicate that the reforecasts have difficulties in correctly predicting blocked regimes over Europe which are associated with enhanced WCB activity. Recalling the correlation of EuBL and ScBL to surface heat waves in summer (Schaller et al., 2018), these findings might indicate that WCB representation is important for accurate prediction of summer heat waves.

8 Comparison of sub-seasonal forecast models

This chapter extends the systematic investigation of WCBs and their link to Atlantic-European weather regimes to other sub-seasonal weather prediction models of the S2S database (see explanation of the database in Section 4.1.1). The analysis first quantifies the representation of WCBs in terms of bias and forecast skill in the different S2S models. Additionally, the link between the WCBs and weather regimes is evaluated specifically for the EuBL regime in the S2S models with overall highest WCB forecast skill.

8.1 WCB bias and skill

The S2S models have different reforecast periods, ensemble members, and number of initialisation times (see Tab. 4.1 in Section 4.1.1.). These differences make it challenging to compare the models in terms of bias and forecast skill. On the other hand, the reforecast data sets also cover many different winter seasons (11–23 years) which increases the robustness of the analysis. To evaluate the impact of the different reforecast period, the WCB bias and skill are evaluated for both the respective reforecast period of each model and a common reforecast period of 11 years (1999–2010). Differences between the two approaches are minor (not shown) which highlights the robustness of the large data sets. Therefore, the following results are based on the entire reforecast period of each NWP model.

First, WCB biases and their temporal evolution are evaluated for weekly WCB outflow frequencies in the boreal winter season (DJF). As in Chapter 5, biases

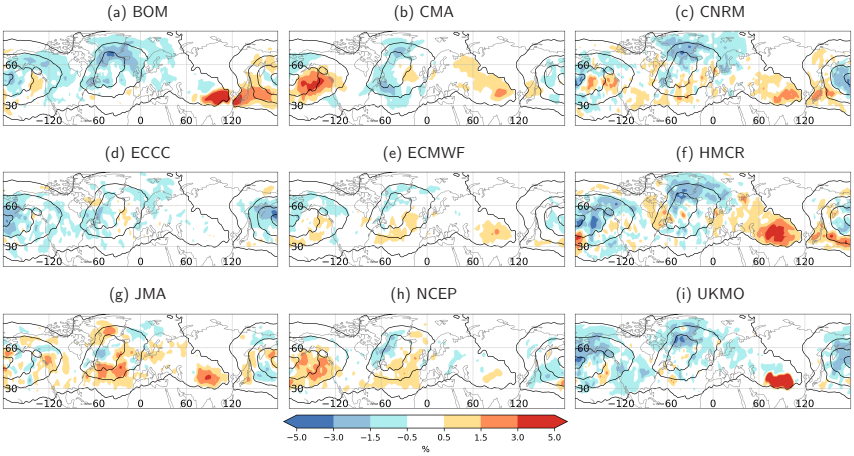


Figure 8.1: Frequency bias of WCB outflow for forecast week 1 (DJF) for a) BOM (1981–2013), b) CMA (1994–2014), c) CNRM (1993–2014), d) ECCC (1995–2014), e) ECMWF (1997–2017), f) HMCR (1995–2009), g) JMA (1981–2012), h) NCEP (1999–2010), i) UKMO (1993–2015). The black contours indicate a frequency of 1, 5, 10, 15 % in in the respective layer.

are calculated compared to ERA-Interim reanalysis data. Since the ECMWF's reforecast are initialised from ERA-interim, systematic biases do not emerge at the forecast initialisation time. However, for the other S2S models, biases occur already at forecast day 0. Therefore, these biases are reduced by the systematic bias at initialisation time.

As shown in Chapter 5.5., the ECMWF's IFS reforecasts underestimate WCB outflow frequencies over the northern part of the Atlantic and overestimate them further south (cf. Fig. 5.6c, Fig. 8.1e). Biases are around 1% for forecast week 1 which equals a relative deviation of around 10–20%.

Compared to the ECMWF model, the other S2S models show higher frequency biases for forecast week 1 with generally similar bias patterns (Fig. 8.1). The only exception is the JMA model which has predominantly positive biases in the North Atlantic region (Fig. 8.1g). The negative bias over the northern part of the Atlantic is especially pronounced in the BOM, CNRM, HMCR, and UKMO model (1–4%) (Fig. 8.1a,c,f,i) and generally weaker in the CMA, ECMWF, NCEP and ECC model (Fig. 8.1b,d,e,h). On the other hand, positive biases over

the southeastern North Atlantic are strongest in the JMA and CNRM model (1–3%) (Fig. 8.1c,g) while weaker positive biases occur in the ECMWF and NCEP model (Fig. 8.1e,h).

Over the Pacific, the WCB outflow is underestimated in the ECMWF model over the main outflow region and western North America and overestimated over the southwestern and southeastern Pacific (around 1% respectively) (Fig. 8.1e). These biases correspond to a relative deviation of 5–20%. As for the Atlantic, biases are generally stronger in the other S2S models while the bias pattern are similar. The negative bias over the central Pacific and western North America is strongest in the BOM, CNRM, ECCC, HMCR, and UKMO model (2–5%) (Fig. 8.1a,c,d,f,i) and weaker in the CMA, ECMWF, JMA, and NCEP model (Fig. 8.1b,e,g,h). Positive biases over the southeastern Pacific emerge predominantly in the CMA, CNRM, and NCEP model (2–5%) (Fig. 8.1b,c,h) while positive biases over the southwestern Pacific are strongest in the BOM, CNRM, and HMCR model (Fig. 8.1a,c,f).

In summary, WCB biases already emerge in forecast week 1 for all S2S models highlighting the difficulties of the NWP models in correctly representing WCB activity at early forecast lead times. The biases are generally weaker for the ECMWF and NCEP model and strongest for the CNRM and HMCR model. The bias patterns have similarities across the different S2S models which corroborates that systematic errors occur independent of the specific model set up.

The temporal evolution of the WCB outflow bias in forecast week 1 to 4 is now further analysed for the different models in the Atlantic and Pacific region (Fig. 8.2). For the ECMWF model biases, both negative and positive biases over the Atlantic increase in week 2 and saturate in week 3 and 4 (Fig. 5.6f,i,l). In week 3, biases reach magnitudes of 1–3% which equals a relative deviation of 20–35% (Fig. 8.3e). The area-average outflow bias remains around zero for forecast week 2 to 4 due to the canceling effects of the positive and negative bias (Fig. 8.2e).

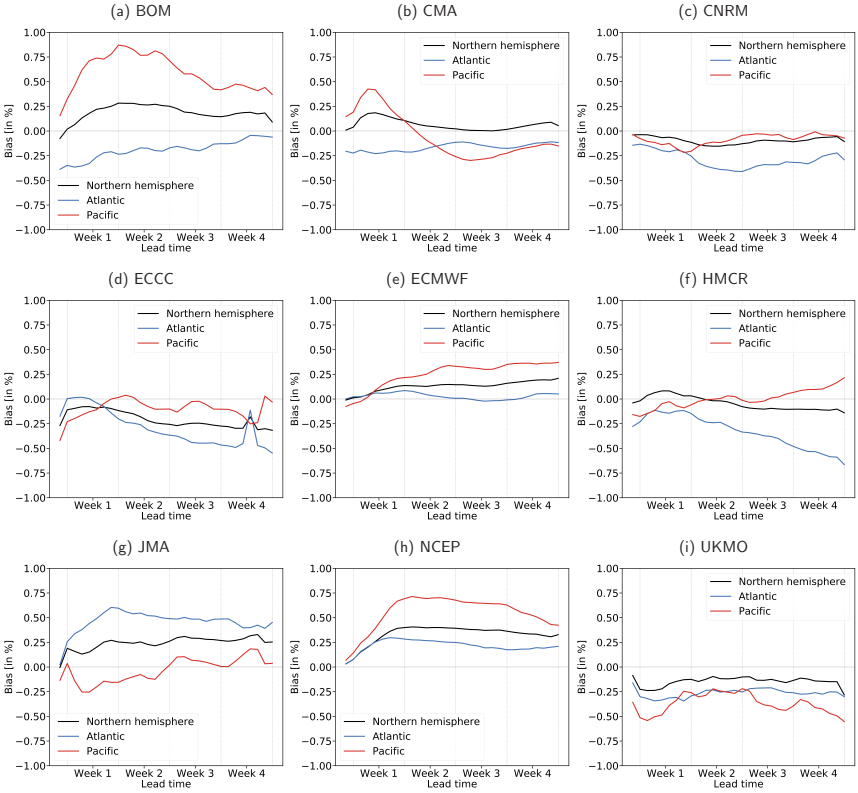


Figure 8.2: Area-averaged frequency bias for DJF 1997–2017 at different forecast lead times for the different S2S models as in Fig. 8.1. The regions for the area-averaged frequency bias are indicated in Fig. 5.3a).

For the different S2S models, there is a large variation in the temporal evolution of the outflow bias over the Atlantic between the models (Fig. 8.2). Some models have an increase in the overall biases while biases in other models remain similar.

For the models with strongest negative biases in week 1 (Fig. 8.1), the biases remain similar for later lead times in the BOM and UKMO model (Fig. 8.2a,i) while outflow frequency biases further increase in the CNRM and HMCR model (Fig. 8.2c,f). In these models a strong underestimation of 4–6% (relative underestimation of 50–100%) can be found over the northwestern Atlantic (Fig. 8.3c,f).

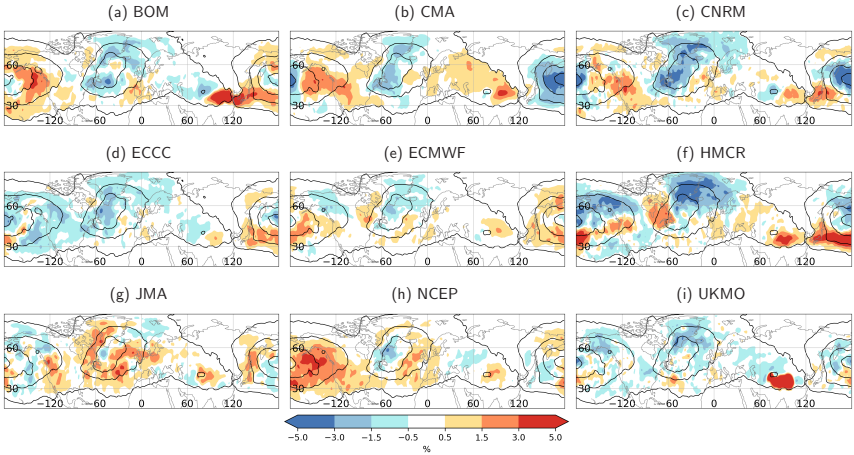


Figure 8.3: As in Fig. 8.1, but for forecast week 3.

An increase of the negative outflow bias also occurs in the ECCC from forecast week 1 to 3 (Fig. 8.2d). While biases are relatively weak in week 1 (Fig. 8.1d), they increase to 2–4% in forecast week 3 (Fig. 8.3d) and saturate afterwards. On the other hand, the JMA and NCEP model show increasing positive bias over the southeastern Atlantic from week 1 to week 3 (Fig. 8.2g,h). The overestimation is around 1–4% for forecast week 3 which equals a relative deviation of 25–75% (Fig. 8.3g,h).

Over the Pacific region, the ECMWF model has a shift to positive outflow biases over the western and central part in forecast week 2 (1–3%) (Fig. 5.6f) which further saturate for later lead times (Fig. 8.2e). Negative biases only occur over western North America and remain at similar magnitudes (Fig. 8.3e).

The bias evolution varies strongly between the S2S models which results in largely different bias patterns for forecast week 3 (Fig. 8.3).

Negative biases over the western Pacific occur predominantly in the CMA, CNRM, NCEP, and UKMO model (Fig. 8.3b,c,h,i) while positive biases can be found especially in the BOM, ECCC, ECMWF, HMCR, and JMA model

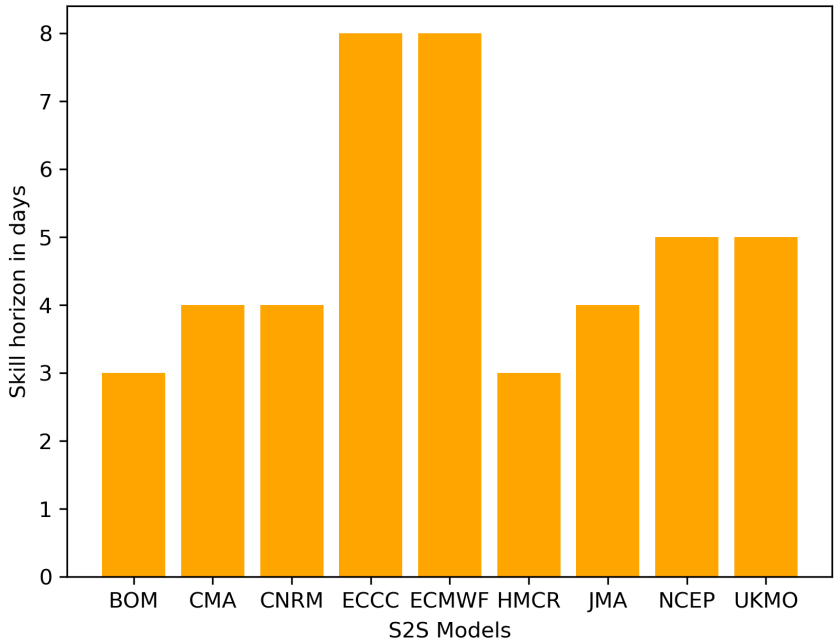


Figure 8.4: Forecast skill horizon (FBSS <= 0.08) of WCB outflow over the Northern Hemisphere in DJF (in days) for different S2S models.

(Fig. 8.3a,d,e,f,g). On the other hand, over the eastern Pacific, the frequency underestimation of WCB outflow is strongest in the ECCC, HMCR, JMA, and UKMO (Fig. 8.3d,f,g,i). Positive biases occur in the BOM, CMA, CNRM, ECMWF, and NCEP model (Fig. 8.3a,b,c,e,g).

These findings highlight the different WCB biases between the models which also vary compared to forecast week 1 (Fig. 8.1).

Next, the WCB forecast skill is investigated for the different S2S models as the area-average of grid-point based *FBSS* over the Northern Hemisphere. As in Fig. 5.3, the forecast skill horizon is defined as the forecast lead time at which the *FBSS* falls below 0.08 since it only decreases very slowly afterwards. In

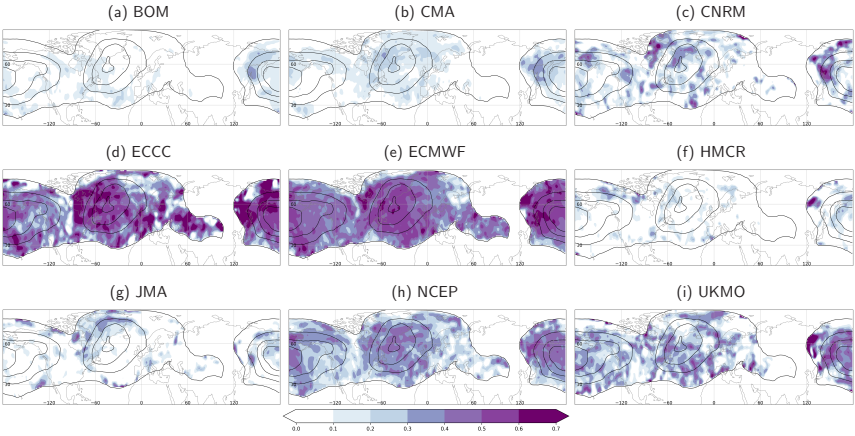


Figure 8.5: Fair Brier Skill Score (*FBSS*) of WCB outflow forecast at day 3 for different S2S models. The black contours indicate a WCB frequency of 1, 5, 10, 15% in the respective layer.

order to compare the results to Fig. 5.3, the forecast skill horizon is evaluated for daily WCB outflow forecasts.

For the ECMWF model, the skill horizon is around 8 days for the entire Northern Hemisphere (cf. Fig. 5.3, Fig.8.4). The ECCC has a similar skill horizon while the other models have substantially less skill for WCB outflow (Fig.8.4). The generally lower forecast skill of most S2S models compared to the ECMWF model goes in line with the overall higher frequency biases found in Fig. 8.1.

Contrary to the high forecast skill in the ECMWF and ECCC model, the skill horizon is lowest in the BOM and HMCR model (Fig.8.4). These findings correspond well with the high frequency biases that occur in these models already in forecast week 1 (Fig. 8.1). The skill horizon is around 4 days in the JMA, CMA and CNRM model and around 5 days for the NCEP and UKMO model.

Maps of the *FBSS* on forecast days 3 reveal that the skill varies not only between the models but also between different sub-areas within these large regions over the North Atlantic and North Pacific (Fig. 8.5). WCB forecast skill for the ECMWF reforecasts is higher over the western part of both North Atlantic and

North Pacific compared to the eastern part (cf. Fig. 5.4e and Fig. 8.5e). Similar findings in terms of regional skill can be made for the ECCC model (Fig. 8.5d) which has a similarly high forecast skill horizon (Fig. 8.4). The skill is even higher compared to the ECMWF model west of the climatological maximum over the Atlantic and Pacific. Relatively low skill can be found over the Norwegian Sea and the eastern Pacific.

The NCEP and UKMO model both have skill until around forecast day 5 (Fig. 8.4). For the NCEP model, a relatively high skill (0.3–0.5) emerges over wide parts of the Atlantic (Fig. 8.5h). Contrary to the ECMWF and ECCC model, differences are lower between the western and eastern part of the ocean basin. Over the Pacific, relatively high skill occurs over the western part and lower skill of the eastern part.

The UKMO model has a similar skill pattern over the Pacific region while the forecast skill is differently distributed over the Atlantic (Fig. 8.5i). Relatively high skill emerges over the southern part of the Atlantic and lower skill around Greenland.

The CMA, CNRM and JMA model all have skill until around forecast day 4 (Fig. 8.4). However, the skill patterns for forecast day 3 vary strongly between the models. The CMA model has a skill of 0.1–0.3 in most areas of the Atlantic with highest skill southeast of Greenland (Fig. 8.5b). The skill over the northwestern part of the ocean basin is higher in the CNRM model and lower further to the southeast (Fig. 8.5c). The JMA has high skill over eastern Canada and Greenland and very low skill over wide parts of the Atlantic (Fig. 8.5g).

Over the Pacific, the forecast skill in the CMA model is highest west of the climatological maximum in the Pacific (0.2–0.4) and lower further east. (Fig. 8.5b). For the CNRM and JMA model, generally similar skill patterns emerge at this lead time (Fig. 8.5c,g).

The BOM and HMCR models have the lowest forecast skill horizon (Fig. 8.4). However, for the BOM model, relatively high skill can be found south of the climatological maximum over the Atlantic which is higher than the skill for CNRM and JMA in this region (cf. Fig. 8.5a, Fig. 8.5c, Fig. 8.5g). Contrary, the skill

is very low northeast of the climatological maximum. The HMCR model has generally low skill at forecast day 3 in most regions of the Atlantic (Fig. 8.5f). Over the Pacific region, both the BOM and HMCR model have relatively high skill west of the climatological maximum in line with most other S2S models (Fig. 8.5a,f).

8.2 European blocking onset evolution

Table 8.1: Number of EuBL onsets in forecast week 2 in NDJFM in ERA-Interim and reforecasts for ECCC (1995–2014), ECMWF (1997–2017), NCEP (1999–2010), and UKMO (1993–2015). Individual events in ERA-Interim in brackets.

	ERA-Interim	reforecasts
ECCC	24 (24)	81
ECMWF	124 (35)	1248
NCEP	140 (20)	475
UKMO	36 (36)	190

In this Section, the representation of WCBs around the onset of EuBL is evaluated for different S2S models. As seen in Chapter 6, WCB activity plays an important role for the onset of EuBL. The ECMWF reforecasts underestimate WCB outflow frequencies over Europe and have a different pathway into EuBL via strong WCB activity on the western flank of the incipient block.

The S2S models with highest WCB outflow forecast skill (ECCC, ECMWF, NCEP, UKMO) (cf. Fig. 8.4) are now selected to evaluate differences in the temporal evolution of Z500 and WCB activity prior to EuBL onset.

Compared to Chapter 6, this Section uses a different threshold definition for the calculation of EuBL life cycles (1.0 instead of 0.9) and 5-day instead of 10-day low-pass filter for the Z500 fields before calculating the regime projection (see Chapter 4.3. for an overview of the computation of the seven weather regimes). This definition is slightly more strict and reduces the amount of EuBL onsets

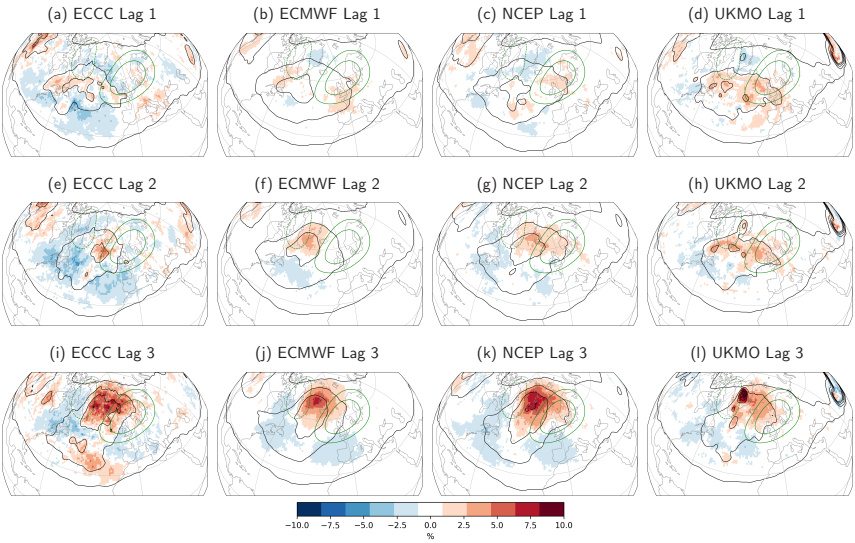


Figure 8.6: WCB outflow frequency anomalies (shading) 6 to 4 days (a–d), 4 to 2 days (e–h), and 2 to 0 days (i–l) prior to EuBL onset in a),e),i) ECCC reforecasts (NDJFM; 1995–2014), b),f),j) ECMWF IFS reforecasts (NDJFM; 1997–2017), c),g),k) NCEP reforecasts (NDJFM; 1999-2010), and d),h),l) UKMO reforecasts (NDJFM; 1993–2015). Reforecasts show anomalies compared to own reforecast climatology. The black contours indicate absolute WCB outflow frequencies (reforecasts) of 5, 10, 15 % and a climatological frequency of 0.5 %. Green contours indicate geopotential height anomalies (-50,50,100 gpm) for all EuBL cases from 1979–2015.

in the ECMWF model in forecast week 2 from 137 to 124 while the amount of events is similar in the reforecasts (1248 compared to 1244).

It is important to note that the different reforecast period and amount of initialisation times, as well as the number of ensemble members in each data set, lead to different amount of EuBL events for the four models (Tab.8.1).

As shown in Fig. 6.4, WCB activity is high prior to the onset of EuBL highlighting the importance for the onset of the regime. Enhanced WCB activity emerges from the western Atlantic and shifts northeastwards prior to the onset. The ECMWF IFS reforecasts capture the activity over the central Atlantic well but underestimate outflow frequencies over Europe (Fig. 6.4).

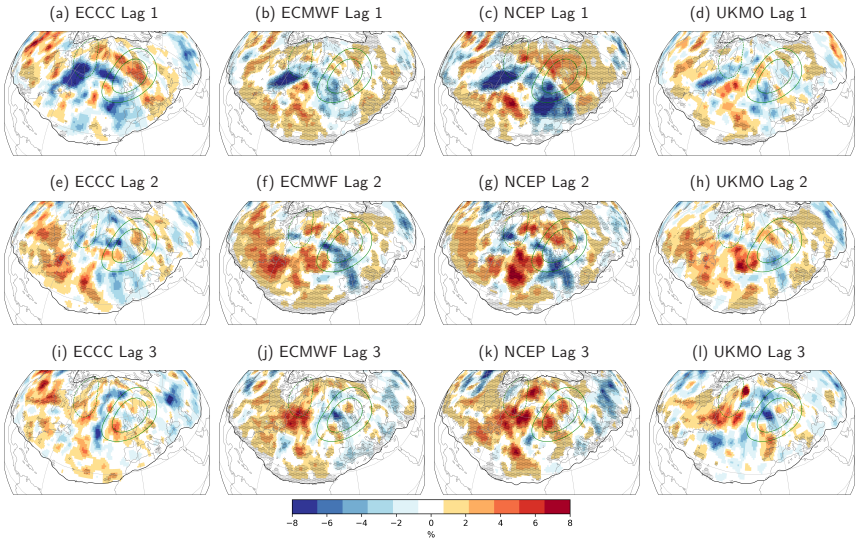


Figure 8.7: WCB outflow frequency differences between reforecasts and ERA-Interim (shading) 6 to 4 days (a–d), 4 to 2 days (e–h), and 2 to 0 days (i–l) prior to EuBL onset in a),e),i) ECCC reforecasts (NDJFM; 1995–2014), b),f),j) ECMWF IFS reforecasts (NDJFM; 1997–2017), c),g),k) NCEP reforecasts (NDJFM; 1999-2010), and d),h),l) UKMO reforecasts (NDJFM; 1993–2015). Significance between the two data sets (t-test; 98 th confidence interval) is indicated by the point stippling. Green contours as in Fig. 8.6.

Compared to Chapter 6, the ECMWF's IFS reforecast have very similar WCB activity using the new life cycle definition which highlights the overall robustness of the results (cf. Fig. 6.4b,e,h, Fig. 8.6b,f,j).

Six to four days prior to the onset, outflow frequencies of around 10% can be found over the western Atlantic (Fig. 8.6b). Compared to ERA-Interim, the ECMWF model underestimates the WCB activity over eastern Canada and upstream of the incipient block over Europe (Fig. 8.7b).

The ECCC model has a similar frequency maximum (around 10%) over the western Atlantic compared to the ECMWF model (Fig. 8.6a). The frequencies are generally lower over the eastern Atlantic, over Iceland and western Europe. Consequently, the ECCC model strongly underestimates outflow frequencies over eastern Canada and around Iceland (6–8%) (Fig. 8.7a). The WCB activity is also

underestimated over western Europe, however, differences in this region are not significant.

The NCEP model has highest WCB outflow activity over the western Atlantic while frequencies are higher further south compared to the ECCC and ECMWF model (Fig. 8.6c). Strong frequency underestimation occurs over both eastern Canada and western Europe (6–8%) while the outflow is overestimated over the central Atlantic around 30–40 W (Fig. 8.7c).

The UKMO has high WCB activity over both the western and eastern Atlantic (up to 10%) (Fig. 8.6d). Outflow frequencies are underestimated in similar regions as for the other models (Fig. 8.7d). However, the underestimation is smaller and not significant in most regions. In summary, the four models have similar WCB activity six to four days prior to the onset which results in a general underestimation of the main WCB outflow frequencies.

Subsequently, the WCB activity shifts northeastwards in the ECMWF model four to two days prior to the onset (Fig. 8.6f). Outflow frequencies around 10% (anomalies 1–3%) occur upstream of the incipient block over the southern part of Greenland. In this region, WCB frequencies are well represented and even overestimated over Greenland and around 50–60°N (Fig. 8.7f). Further east, the ECMWF model strongly underestimates outflow frequencies over western Europe (2–6%).

In the ECCC model, high WCB activity (around 10%) can be found south of Iceland on the western part of the incipient block (Fig. 8.6e). Compared to the ECMWF model, the main activity is shifted southeastwards and lower frequencies can be found over Greenland. The WCB outflow activity over the eastern Atlantic is better represented which results in small and not significant deviations from the observed frequencies (Fig. 8.7e).

The NCEP model has high WCB activity in the region between southern Greenland and Iceland (frequencies 10%, anomalies 1–3%) (Fig. 8.6g). Outflow frequencies in this region are well represented while the WCB activity is overestimated (4–8%) over the central and northern Atlantic and underestimated over western Europe (4–7%) (Fig. 8.7g).

The UKMO model has high outflow frequencies over a wide area over the western to the eastern Atlantic (anomalies around 1–3%) (Fig. 8.6h). Outflow frequencies are generally well represented (Fig. 8.7d) and only significantly overestimated over the southwestern part of the incipient block.

In summary, the ECMWF and NCEP model have similarly strong WCB outflow activity over the central Atlantic towards Greenland four to two days before the onset while the ECCC and UKMO have higher frequencies further east. Consequently, the ECCC and UKMO capture WCB activity over the eastern Atlantic better which results in a smaller underestimations compared to the observed frequencies.

The last days prior to the EuBL onset are characterised by a strong increase in WCB outflow frequencies upstream of the incipient block in the ECMWF model (frequencies 10–13%, anomalies 5–8%) (Fig. 8.6j). The outflow frequencies are generally well represented in this region while frequencies are underestimated further east and overestimated upstream over Greenland (Fig. 8.7j).

The ECCC has similarly high WCB outflow frequencies compared to the ECMWF model upstream of the block (Fig. 8.6i). A second maximum emerges further south over the southeastern Atlantic. WCB frequencies are generally well represented in the ECCC model, significant overestimations of the WCB anomalies only occur over the southwestern part of the incipient block (Fig. 8.7i).

The NCEP model has strong WCB activity on the northwestern flank of the block (frequencies 15%, anomalies 6–8%) (Fig. 8.6k). The outflow frequencies are overestimated by the model (4–8%) in this region and further east over Europe (Fig. 8.7k).

The UKMO model has lower WCB activity compared to the NCEP model with highest frequencies over the central and northeastern Atlantic (5–10%) (Fig. 8.6l). Consequently, the outflow frequencies are significantly lower than observed over the western part of the incipient block (Fig. 8.7d).

In summary, WCB pathways in the four S2S models are generally similar with high outflow frequencies emerging from the western and central Atlantic and largest anomalies two to zero days upstream of the incipient block. However, there are differences in the location of the maximum frequencies and the representation of outflow frequencies over the eastern Atlantic. The NCEP and ECMWF have similar pathways into EuBL with high (overestimated) WCB activity over the central Atlantic and around Greenland. On the other hand, the UKMO and ECCC model represent WCB activity generally better over the eastern Atlantic with smaller deviations from the observed frequencies. However, the UKMO has the smallest outflow frequencies just prior to the onset of the block compared to the other models. This finding is in line with the relatively large underestimation of WCB frequencies in this region in Fig. 8.7i. In the following, the temporal evolution of Z500 and the link to differences in WCB activity is evaluated for the four S2S models.

As seen in Chapter 6, the EuBL regime emerges from a zonal flow six to four days prior to the onset (Fig. 6.3). Subsequently, the wave pattern amplifies leading to the onset of EuBL. The ECMWF's IFS reforecasts can generally capture the temporal evolution of the Z500 patterns well but overestimate the flow upstream of the incipient block (Fig. 6.3b,e,h).

Compared to the ECMWF model, the ECCC model has a stronger zonal flow six to four days before the onset with negative anomalies (-100 gpm) in the region of the incipient block and positive anomalies further south around 40°N (Fig. 8.8a). Z500 is overestimated over the eastern Atlantic and western Europe and underestimated over the northeastern part of the incipient block (Fig. 8.9a).

The NCEP model has similar negative anomalies over northern Europe compared to the ECCC model (Fig. 8.8c). Additionally, positive Z500 anomalies occur over Europe. In this region, the NCEP model significantly overestimates the wave pattern compared to the observations (Fig. 8.9c).

The UKMO model has negative Z500 anomalies in the region of the incipient block and positive anomalies which emerge over the western Atlantic (Fig. 8.8d).

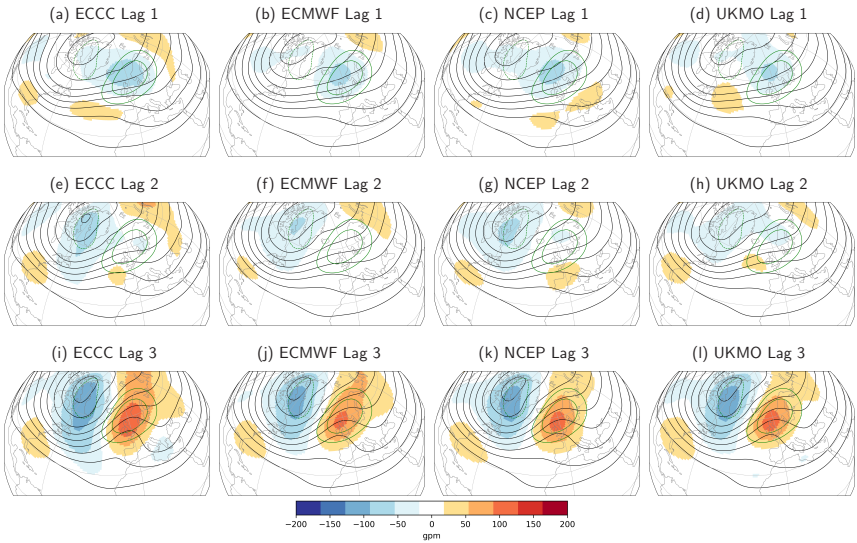


Figure 8.8: 500-hPa geopotential height anomalies (shading) 6 to 4 days (a-d), 4 to 2 days (e-h), and 0 to 2 days prior (i-l) to EuBL onset in a),e),i) ECCC reforecasts (NDJFM; 1995–2014), b),f),j) ECMWF IFS reforecasts (NDJFM; 1997–2017), c),g),k) NCEP reforecasts (NDJFM; 1999-2010), and d),h),l) UKMO reforecasts (NDJFM; 1993–2015). Contours indicate absolute fields (5100–5800 gpm every 100 gpm; NDJFM 1997–2017)

In the region upstream of the incipient block, Z500 is higher (40–60 gpm) than observed (Fig. 8.9d).

In summary, all four S2S models have a zonal flow six to four days before the EuBL with similar negative anomalies in the region of the incipient block. Differences occur upstream and over Europe where positive Z500 anomalies vary between the models.

Subsequently, the wave pattern amplifies four to two days before the onset. The negative anomalies over Europe vanish in the ECMWF model and an upper-level trough emerges over the western Atlantic (Fig. 8.8f). Z500 is significantly higher upstream of the incipient block and lower further east and over southwestern Europe (Fig. 8.9f).

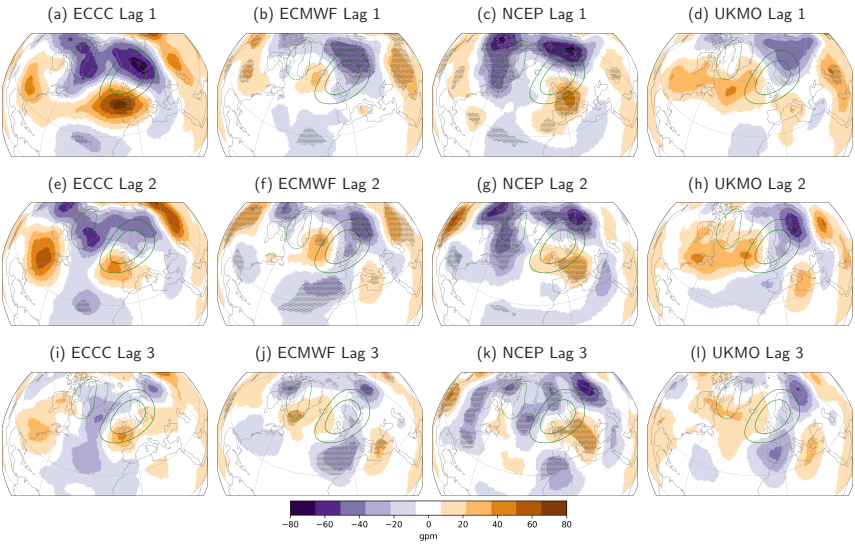


Figure 8.9: 500-hPa geopotential height differences between reforecasts and ERA-Interim 6 to 4 days (a-d), 4 to 2 days (e-h), and 0 to 2 days prior (i-l) to EuBL onset in a),e),i) ECCC reforecasts (NDJFM; 1995–2014), b),f),j) ECMWF IFS reforecasts (NDJFM; 1997–2017), c),g),k) NCEP reforecasts (NDJFM; 1999-2010), and d),h),l) UKMO reforecasts (NDJFM; 1993–2015). Significance between the two data sets (t-test; 98 th confidence interval) is indicated by the point stippling. Contours indicate absolute fields as in Fig. 8.6.

The wave amplification is stronger in the ECCC model over southwestern Europe and weaker around Iceland compared to the ECMWF model (Fig. 8.8e). This leads to an underestimated large-scale flow upstream and an overestimated flow in the southern part of the incipient block (Fig. 8.9e). Recalling the differences in WCB activity between the ECCC and ECMWF model with a southeastward shift of the highest WCB outflow frequencies, these results corroborate that the ECCC model establishes the EuBL onset via WCB activity differently than the ECMWF model.

The NCEP model has both an amplified wave pattern over Iceland and northwestern Europe, as well as positive Z500 anomalies over southwestern Europe (Fig. 8.8g). Consequently, Z500 is overestimated over Europe and the southwestern part of the incipient block (Fig. 8.9g).

The UKMO model has relatively high Z500 with positive anomalies on the western part of the incipient block (Fig. 8.8h). Upstream, the emerging trough over the western Atlantic is weaker compared to the other models. The model overestimates the Z500 field over large parts of the Atlantic upstream of the incipient block and underestimates it over eastern Europe (Fig. 8.9h).

The last days prior to EuBL onset are characterised by a strong wave amplification. In the ECMWF model positive anomalies (80–130 gpm) develop over Europe while negative anomalies occur over the western Atlantic (Fig. 8.8j). The ECMWF model captures Z500 anomalies well in the region of the block and significantly underestimates them over southwestern Europe (Fig. 8.9j).

The ECCC model has a more amplified wave pattern compared to the ECMWF model with higher positive and negative anomalies (Fig. 8.8i). Consequently, Z500 is overestimated over the southwestern part of the incipient block and underestimated upstream (Fig. 8.9i).

The NCEP and UKMO model have similar Z500 prior to the onset with positive anomalies around 80–120 gpm in the region of the block (Fig. 8.8k,l). Both models capture the emerging anomalies in the region of the block generally well (Fig. 8.9k,l) while the NCEP model underestimates Z500 upstream over the Atlantic.

In summary, all four S2S models develop the EuBL regime from a zonal flow with negative Z500 anomalies six to four days before the onset. However, differences emerge upstream and south of the developing block. The UKMO overestimates Z500 upstream of the block in line with the lower WCB activity in the last days prior to the onset (Fig. 8.7l). The WCB activity is overestimated prior to the onset in the NCEP model (Fig. 8.9k) which corresponds well with the underestimation of the Z500 patterns upstream of the block. The high WCB activity likely contributes significantly to the strong wave amplification in the model. To conclude, these findings underline the importance of WCB activity for the onset

of EuBL and show that despite similar pathways into EuBL small differences in terms of WCB activity and Z500 patterns occur between the four S2S models.

9 Conclusions and Outlook

This Chapter provides a summary of the main results of this study and answers the research questions introduced in Chapter 3. Furthermore, an outlook to further research is given in the second part of the Chapter.

The accurate weather prediction of day-to-day weather beyond the original predictability limit of around two weeks (Lorenz, 1963) has become feasible in recent years due to increase in computational power, better data assimilation and the shift from deterministic to probabilistic weather forecasts (Bauer et al., 2015). With the increase in forecast skill of the numerical weather prediction models, there has been a growing interest in accurate weather predictions on time scales between two weeks and two months. These sub-seasonal time scales depend on both, an accurate representation of the initial conditions at the forecast initialisation of the model, and an accurate representation of slower climate modes (i.e. ocean, land, and ice surfaces) which provide predictability for the atmosphere on these time scales.

The large-scale extratropical circulation on sub-seasonal time scale is governed by weather regimes which are quasi-stationary, persistent, and recurrent flow regimes. Weather regimes are modulated by slower climate modes (Cassou, 2008) but can also be influenced by synoptic-scale processes like latent heat release in warm conveyor belts (Pfahl et al., 2015). Thus, an accurate prediction of weather regimes in NWP models depends on various processes on different spatial and temporal scales. Since the weather regimes provide enhanced forecast skill for surface variables beyond medium-range time scales of around 12–14 days (Bloomfield et al., 2021, Mastrantonas et al., 2022), an accurate representation of the regimes is desirable in current NWP models.

This study, for the first time, presents a systematic investigation of the representation of warm conveyor belts (WCBs) in current NWP models and links WCB activity to the onset and life cycle of Atlantic-European weather regimes. Four research questions are introduced in Chapter 3 and addressed in Chapter 5–8. Each research question is split into more detailed sub-questions to make it more explicit. The main findings of each Chapter are now summarised in regards to the research questions. In Chapter 5, the research question "How well are warm conveyor belts represented in Numerical Weather Prediction models?" was addressed. The main findings with regard to the more detailed sub-questions are as follows:

- **Are there systematic biases for the inflow, ascent, and outflow stage of the WCB and is there a link to meteorological variables which are closely related to processes in the WCB?**

  Significant WCB frequency biases occur already at early lead times (forecast day 3) which increase to forecast day 7, and saturate afterwards. In boreal winter, there is a tendency towards a general overestimation of WCB frequency over the southern part and an underestimation over the northern part of the North Atlantic for all WCB stages. In boreal summer and autumn, WCB outflow frequencies are generally underestimated over the North Atlantic and for lead times beyond forecast week 1 also over the North Pacific. In boreal spring, the outflow frequencies are generally overestimated over the North Atlantic region and the western Pacific. The results show correlations between WCB inflow (ascent) biases and biases in meridional moisture flux at 850 hPa (500 hPa). For the WCB outflow, the correlation varies between the different predictor variables and the North Atlantic and North Pacific region. The correction of the biases in the predictor variables of a previous version of the statistical models (Wandel et al., 2021) leads to a reduction in biases for the WCB inflow and ascent, but only in some regions for the WCB outflow.

- **Until which lead time can WCBs be skillfully predicted and how reliable are the forecasts?**

The overall forecast skill horizon is around 8–10 days for instantaneous prediction of all three WCB stages in the boreal winter season. There is significantly higher skill over the North Pacific region compared to the North Atlantic region for most lead times and WCB stages. For each ocean basin, the forecast skill is generally higher over the western part compared to the eastern part. The forecasts are generally reliable at early forecast lead times while daily WCB signatures in forecast week 2 are more challenging for the NWP model to reliably predict. However, the NWP model can skillfully predict weekly mean WCB frequencies even beyond the medium range up to forecast week 3 with again more skill for the North Pacific compared to the North Atlantic.

- **Is there a systematic relationship between errors in the forecast of WCBs and errors in the large-scale flow?**

  The WCB outflow is underestimated over the eastern North Pacific and western North Atlantic which can be linked to an underestimation of the northward extent of the midlatitude flow at 300 hPa. Furthermore, there is a strong underestimation of the WCB outflow activity and northward extension of the ridge over the eastern North Pacific (western North Atlantic) two weeks after MJO phase 2 and 3 (6 and 7) which has also been shown by Vitart (2017).

Since diabatic processes associated with WCBs can be important in the onset and maintenance of blocking anticyclones (Pfahl et al., 2015, Steinfeld and Pfahl, 2019), the underestimation of WCB activity over the North Atlantic may at least partly explain negative blocking frequency biases over the Atlantic-European Region (Quinting and Vitart, 2019). This hypothesis is further evaluated in Chapter 6 in which the research question "Is there a link between the prediction of atmospheric blocking over Europe and warm conveyor belt activity?" was addressed in ECMWF's IFS sub-seasonal reforecasts and ERA-Interim reanalysis in the extended winter period from 1997–2017.

The onset of the European Blocking regime (EuBL) is generally not well captured by the reforecasts (Büeler et al., 2021, Matsueda and Palmer, 2018), which

is partly due to its low intrinsic predictability (Faranda et al., 2016, Hochman et al., 2021). The results in chapter 6 newly suggests that it is likely also the misrepresentation of WCB activity in the reforecasts that dilutes the skill for EuBL forecasts. The main findings with regard to the more detailed sub-questions are as follows:

- **How well can the reforecasts represent the characteristics of EuBL in terms of geopotential height in 500 hPa (Z500) and WCB activity?**

  The investigation of EuBL onsets in forecast week 1, 2, and 3 reveals a general underestimation of the incipient block accompanied by an underestimation of the WCB activity. The block is generally better represented in forecast week 1 together with a better representation of WCB activity compared to later lead times. The strong correlation between the underestimation of the block and the underestimation of WCB activity corroborates that there is a link between EuBL prediction and WCB activity.

- **Are there structural differences between reforecasts and reanalysis in the evolution of Z500 and WCB activity prior to EuBL onsets?**

  The analysis of the time evolution leading up to EuBL onset shows that the ECMWF's IFS reforecasts establish large-scale flow anomalies prior to EuBL onset via WCB outflow differently than observed (in ERA-Interim). The results in this study suggest that there are two observed WCB pathways into EuBL over the Atlantic: one over the central Atlantic with outflow towards Greenland and one over the eastern Atlantic with outflow centered around Iceland. The ensemble members of the reforecasts which have a EuBL onset and life cycle establish the block over Europe via the WCB pathway over the central Atlantic and strong outflow over Greenland and have difficulties in correctly representing the other pathway. Moreover, two observed pathways into EuBL also seem to emerge from upstream region over the North Pacific and western North America: one with a Rossby wave train which emerges from the central Pacific into the North Atlantic region and another one with a strong ridge over western North America. As for the North Atlantic pathway, the ensemble members with a EuBL

onsets in the reforecasts establish the block over Europe via one of the two pathways (in this case via the Rossby wave train from the Pacific) and have difficulties in correctly representing the other pathway.

- **Does the predictive skill for EuBL depend on WCB activity?** The results in this study reveal a link between the predictive skill for EuBL onsets and the representation of WCB activity. The EuBL onsets with good skill are generally associated with well represented WCB activity while the WCB activity is not represented well for onsets with bad EuBL skill. Errors in the representation of the large-scale flow patterns and WCB activity emerge predominantly over western North America and the eastern Atlantic in regions where the reforecasts have difficulties in correctly representing observed WCB pathways into EuBL. These errors might then propagate downstream and impact the prediction of EuBL onsets in the NWP model.

In Chapter 7, the research question "Do WCBs influence predictability and forecast skill of Atlantic-European weather regimes?" was addressed more broadly for the seven-year round weather regimes in the extended winter period and for blocking over Europe in the extended summer period. The main findings with regard to the more detailed sub-questions are as follows:

- **How well can the NWP model predict the onset of weather regimes?** The results show that the reforecasts can predict the onset of GL, AR, and ZO in the extended winter season generally well and has lower skill in predicting EuBL and ScBL onsets. These findings are in line with (Büeler et al., 2021) who find comparably low skill for EuBL and ScBL in winter.

- **What is the role of WCBs for the regime onsets and does it need to be resolved well in the model to capture the onset?** WCB activity likely also plays an important role for the prediction of ScBL and GL onsets in boreal winter while the impact on AR onsets seems to be smaller. For ScBL onsets, there is high WCB outflow activity over the northern part of the incipient block (Barents Sea) which is not resolved well in the reforecasts.

For GL onsets, the analysis of the temporal evolution of Z500 and WCB activity before the onset show that the block is likely established via (1) the retrogression of a ridge over Scandinavia which is strongly supported by WCB activity and (2) cyclone activity and WCB outflow which emerges just prior to the onset from North America. The ensemble members with a GL onset in the reforecasts have difficulties in capturing the WCB outflow frequencies over both the Atlantic and North America. For AR onsets, the reforecasts can establish Z500 anomaly patterns generally well with a minor role of the WCB.

- **Do WCBs play a role in the forecast of blocked regimes over Europe in boreal summer which are typically associated with heat waves?** The WCB activity around blocking over Europe in the extended summer season shows a general importance of WCB activity for EuBL and ScBL onsets in summer despite overall lower frequencies. In general, the reforecasts have more difficulties capturing the events with higher WCB activity. Recalling the correlation of EuBL and ScBL to surface heat waves in summer (Schaller et al., 2018), these findings might indicate that WCB representation is important for accurate prediction of summer heat waves.

In Chapter 8, the research question "Does WCB representation and the link to Atlantic-European weather regimes depend on the configuration of the NWP model?" is addressed for NWP models from the S2S database. The main findings with regard to the more detailed sub-questions are as follows:

- **Do similar WCB biases emerge in different NWP models and do the models have a different forecast skill horizon for WCBs?** WCB biases already emerge in forecast week 1 for all S2S models highlighting the difficulties of the NWP models in correctly representing WCB activity at early forecast lead times. The biases are generally weaker for the ECMWF and NCEP model and strongest for the CNRM and HMCR model. The bias patterns have similarities across the different S2S models which corroborates that systematic errors occur independent of the specific model set up. WCB outflow forecast skill horizon for the Northern Hemisphere varies

between the S2S models and is highest in the ECMWF and ECCC model (around 8 days). There is generally more skill for all models over the western part of the ocean basins over the North Atlantic and North Pacific compared to the eastern part.

- **Does the role of WCB activity for EuBL onsets vary between the models?** The investigation of WCB activity prior to the onset of EuBL in the S2S models with highest WCB forecast skill (ECMWF, ECCC, UKMO, NCEP) reveals that all models have strong WCB activity over the North Atlantic on the days before the EuBL onset. These findings underline the importance of WCB activity for the onset of EuBL and show that despite similar pathways into EuBL small differences in terms of WCB activity and Z500 patterns occur between the four S2S models.

Overall, the study highlights the role of synoptic-scale processes for the prediction of large-scale flow regimes on sub-seasonal time scales. The results corroborate that errors in the evolution of Atlantic-European weather regimes is strongly tied to forecast errors on the synoptic-scales. Therefore, improving the overall representation of processes like latent heat release in WCBs will likely yield better representations of weather regimes life cycles (in particular blocked regimes) which would lead to increased forecast skill for sub-seasonal prediction on time scales of 10–60 days.

In particular, the results point to the importance of improving WCB representation over the eastern Atlantic and and the eastern North Pacific, regions where WCB forecast skill is generally lower (Wandel et al., 2021). The WCB forecasts could likely be improved by an increased horizontal resolution, a better representation of microphysical processes in the WCB (Joos and Forbes, 2016), as well as a better representation of the conditions in the WCB inflow regions (Berman and Torn, 2022).

In a recent study with the Model for Prediction Across Scales (MPAS) ensemble forecasts for two events characterized by highly amplified flow over the North Atlantic associated with cyclogenesis, Berman and Torn (2022) find that a more

accurate initial conditions near the WCB inflow region likely leads to better forecasts downstream. This is in line with the results in the study at hand which identify a strong correlation between WCB inflow biases and biases in meridional moisture flux and Wandel et al. (2021) who find a reduction of the WCB bias after correcting the biases in the WCB predictor variables.

On the other hand, an improvement of WCB forecasts over the eastern North Pacific might impact the representation of teleconnection from the tropics (i.e. after active MJO phases) which would likely yield a higher forecast skill for the Atlantic-European region. In the study at hand, errors in the reforecasts are especially identified associated with ridge building over the eastern Pacific and western North America around the onsets of EuBL and ZO regimes. To further evaluate the role of the WCB in the propagation of predictive signals of the MJO to the Atlantic-European region, a systematic investigation of WCB activity over the eastern Pacific together with its representation in sub-seasonal forecast models is needed.

Despite the strong link between WCBs and the predictions of blocked weather regimes, further work is still needed to fully understand whether WCBs are the symptom of model issues or the initial cause of errors that project on the larger-scale Rossby wave pattern. One possible approach for this research problem would be relaxation experiments during which the NWP model is continuously nudged towards observations in the vicinity of the WCB (Magnusson, 2017). This approach could be applied to WCBs over the eastern Atlantic and over western North America prior to EuBL onsets to evaluate the impacts on the misrepresented WCB pathways into EuBL.

To further elaborate the link between weather regimes and WCB activity, causal effect networks (CEN) could be used to underline the impact of the WCB on the predictive skill of the regime. CENs are based on graphical models which can assess causal relationships and their time delays between different processes (Kretschmer et al., 2016). They would further show if WCBs are the cause of missed regime onsets or if they are only a symptom of model errors.

A Appendix for Chapter 5

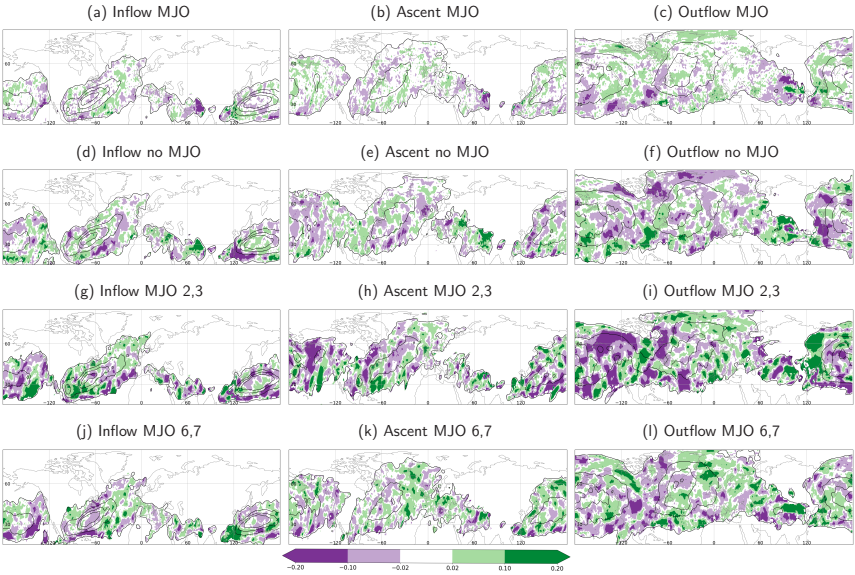


Figure A.1: Difference in Fair Brier Skill Score (*FBSS*) of WCB inflow (a,d,g,j), ascent (b,e,h,k), and outflow (c,f,i,l) and (a,b,c) forecasts initialised during an active MJO, (d,e,f) forecasts initialised during an inactive MJO, (g,h,i) forecasts initialised during an active MJO in phase 2/3, and (j,k,l) forecasts initialised during an active MJO in phase 6/7 to grid-point based *FBSS* for all forecast initial times for day 8–14 (week 2) in DJF (1997–2017). The black contours indicate a WCB frequency of 1, 5, 10, 15% in the respective layer.

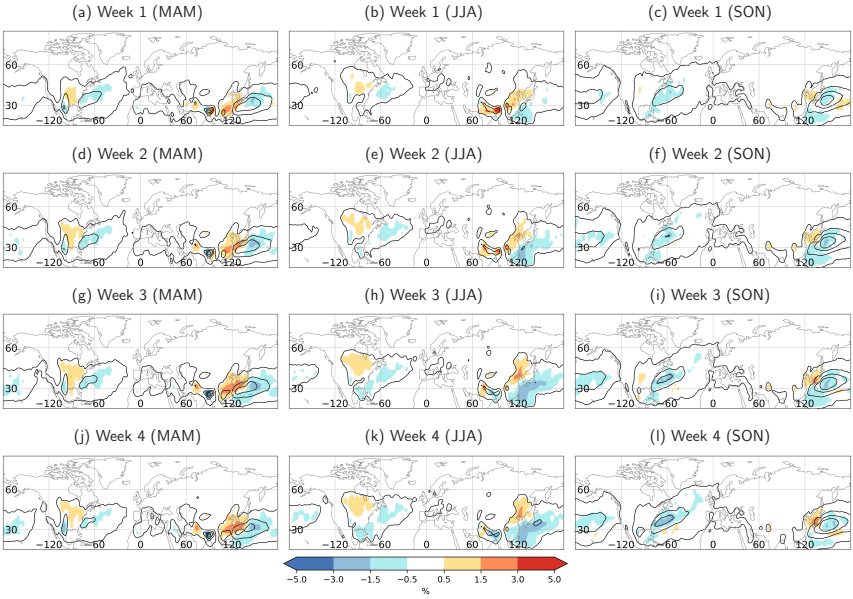


Figure A.2: Weekly frequency bias of WCB inflow in (a,d,g,j) MAM, (b,e,h,k) JJA, (c,f,i,l) SON 1997–2017 (shading) for (a-c) week 1, (d-f) week 2, (g-i) week 3, and (j-l) week 4. The black contours indicate a frequency of 1, 5, 10, 15 % in the respective layer.

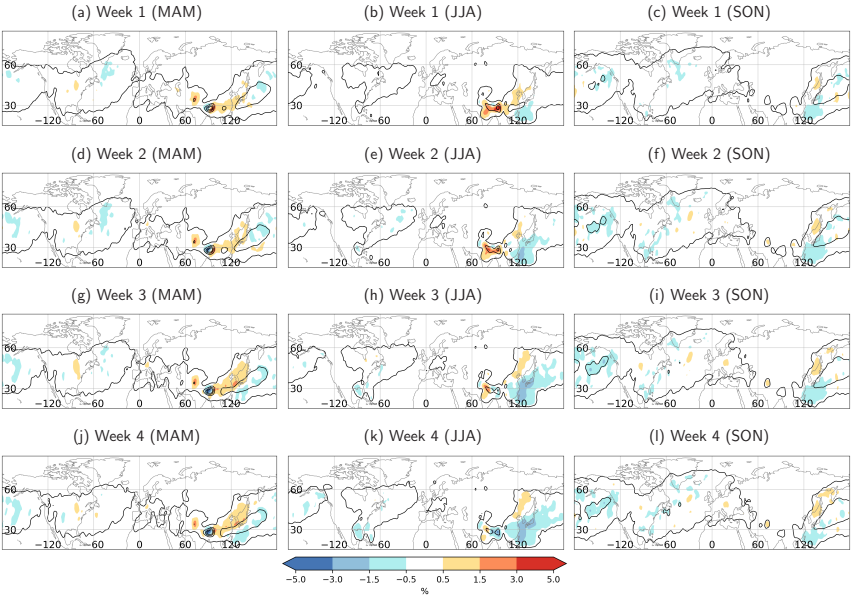


Figure A.3: Weekly frequency bias of WCB ascent in (a,d,g,j) MAM, (b,e,h,k) JJA, (c,f,i,l) SON 1997–2017 (shading) for (a-c) week 1, (d-f) week 2, (g-i) week 3, and (j-l) week 4. The black contours indicate a frequency of 1, 5, 10, 15 % in the respective layer.

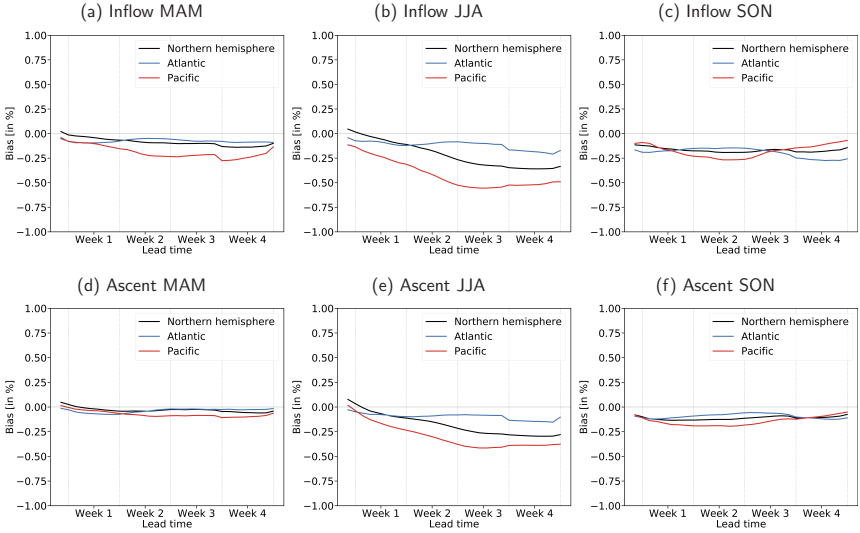


Figure A.4: Area-averaged frequency bias for WCB (a-c) inflow and (d-f) ascent at different forecast lead times for (a,d) MAM, (b,e) JJA, and (c,f) SON. The regions for the area-averaged frequency bias are indicated in Fig. 5.3a).

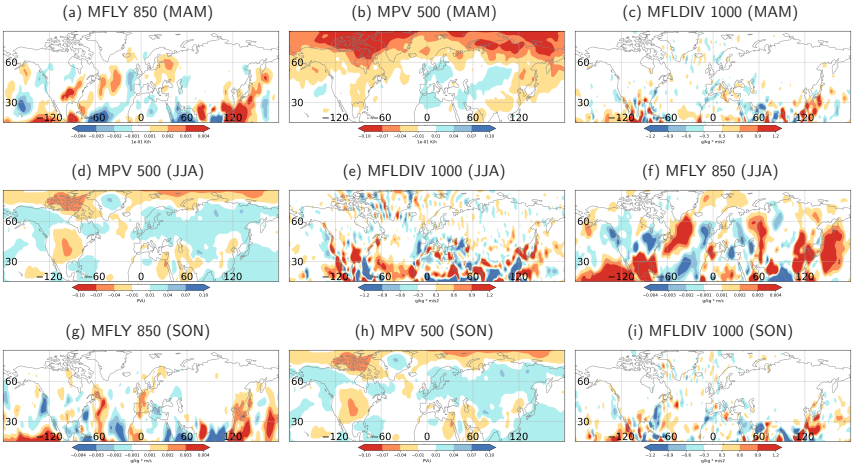


Figure A.5: Bias at forecast day 7 of predictor variables with highest correlation to WCB inflow biases in (a-c) MAM, (d-f) JJA, (g-i) SON in DJF 1997–2017

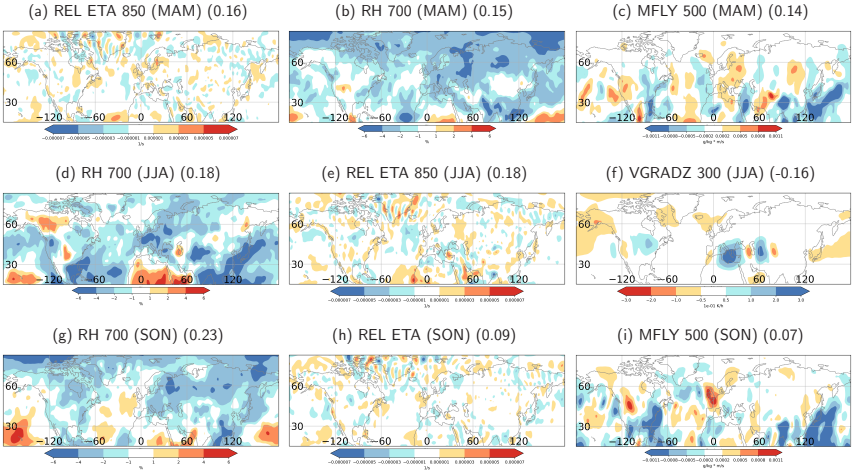


Figure A.6: Bias at forecast day 7 of predictor variables with highest correlation to WCB ascent biases in (a-c) MAM, (d-f) JJA, (g-i) SON in DJF 1997–2017

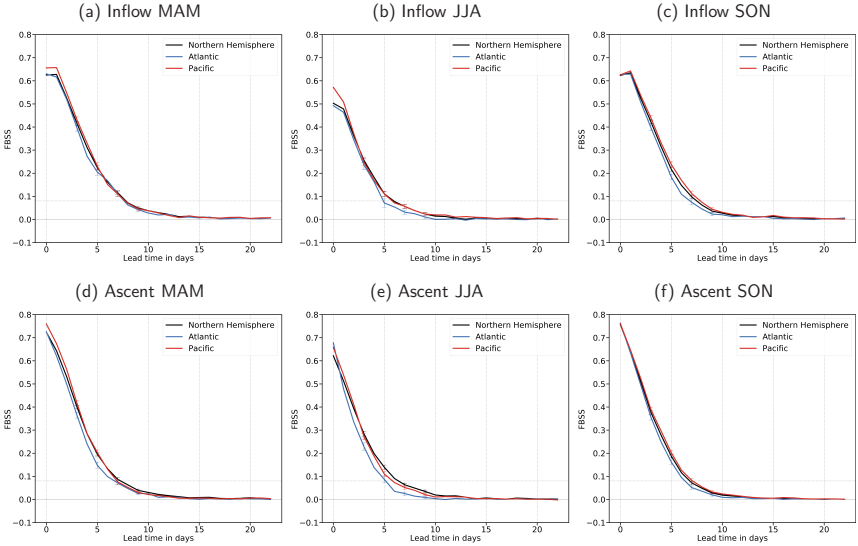


Figure A.7: Area-averaged Fair Brier Skill Score (*FBSS*) for DJF 1997–2017 at different forecast lead times for (a-c) inflow, (d-e) ascent in (a,d) MAM, (b,e) JJA, (c,f) SON. Error bars centered on forecast lead times day 3, 5, 7, and 9 show the difference between the 10 and 90 th percentile of the sampled data (variability of the *FBSS*) and are used to estimate the significant differences between the ocean basins.

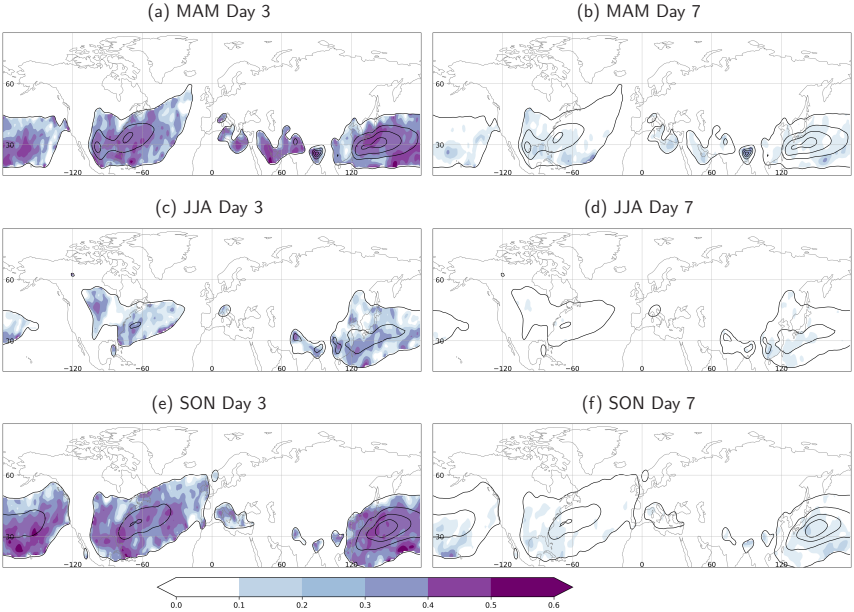


Figure A.8: Fair Brier Skill Score (*FBSS*) of WCB forecast for as in Fig. 5.4 for WCB inflow in (a,b) MAM, (c,d) JJA, (e,f) SON at (a,c,e) day 3, (b,d,f) day 7.

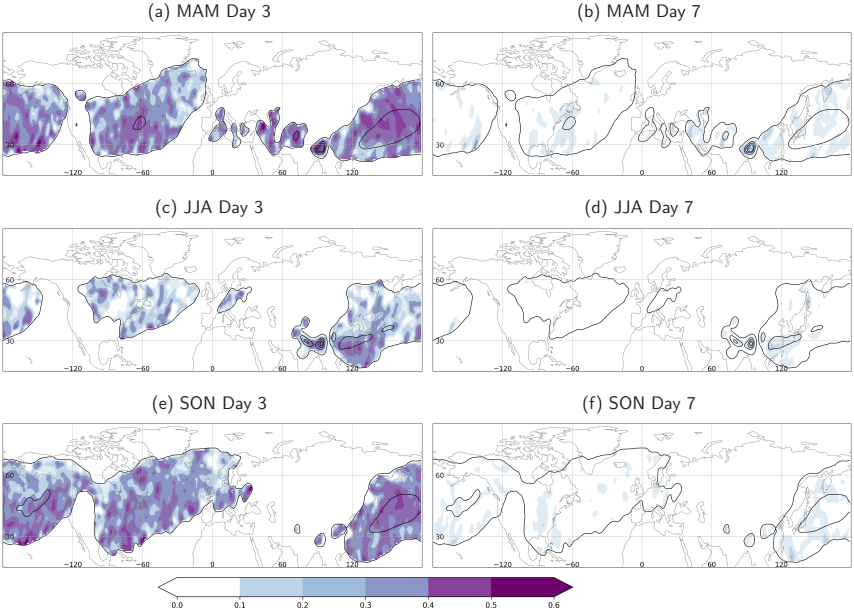


Figure A.9: Fair Brier Skill Score (*FBSS*) of WCB forecast as in Fig. 5.4 for WCB ascent in (a,b) MAM, (c,d) JJA, (e,f) SON at (a,c,e) day 3, (b,d,f) day 7.

B Appendix for Chapter 6

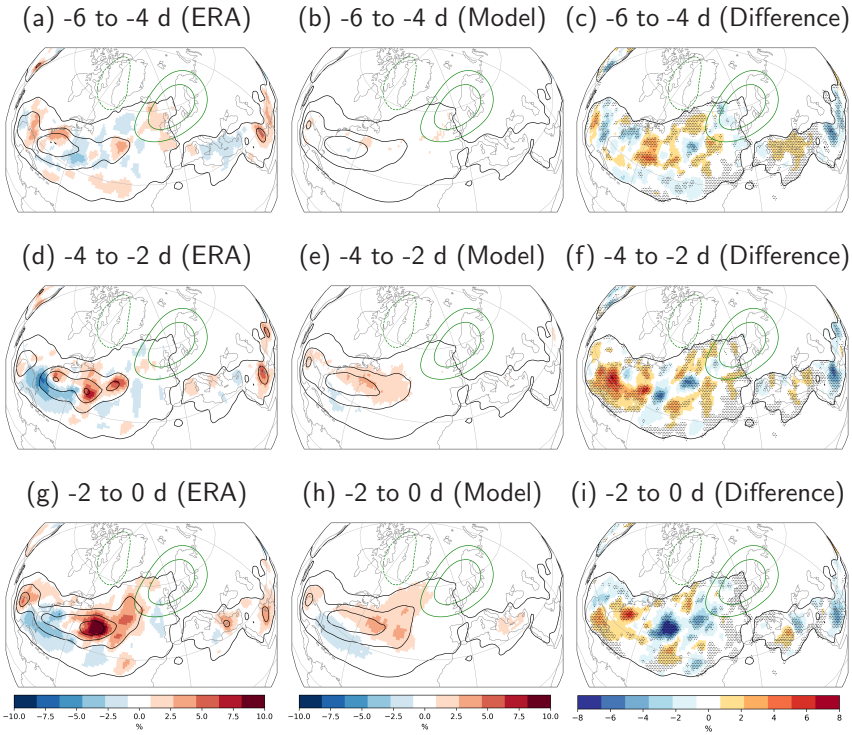


Figure B.1: WCB inflow frequency anomalies (shading) 6 to 4 days (a–c), 4 to 2 days (d–f), and 2 to 0 days (g–i) prior to EuBL onset in a),d),g) ERA-Interim and b),e),h) reforecasts (NDFJM; 1997–2017). The black contours indicate absolute WCB inflow frequencies (ERA-Interim and reforecasts) of 5, 10, 15 % and a climatological frequency of 0.5 %. (c,f,i) show differences between reforecasts and ERA-Interim (shading) with significant differences (t-test; 98 th confidence interval) indicated by the point stippling. Green contours as in Fig. 6.2

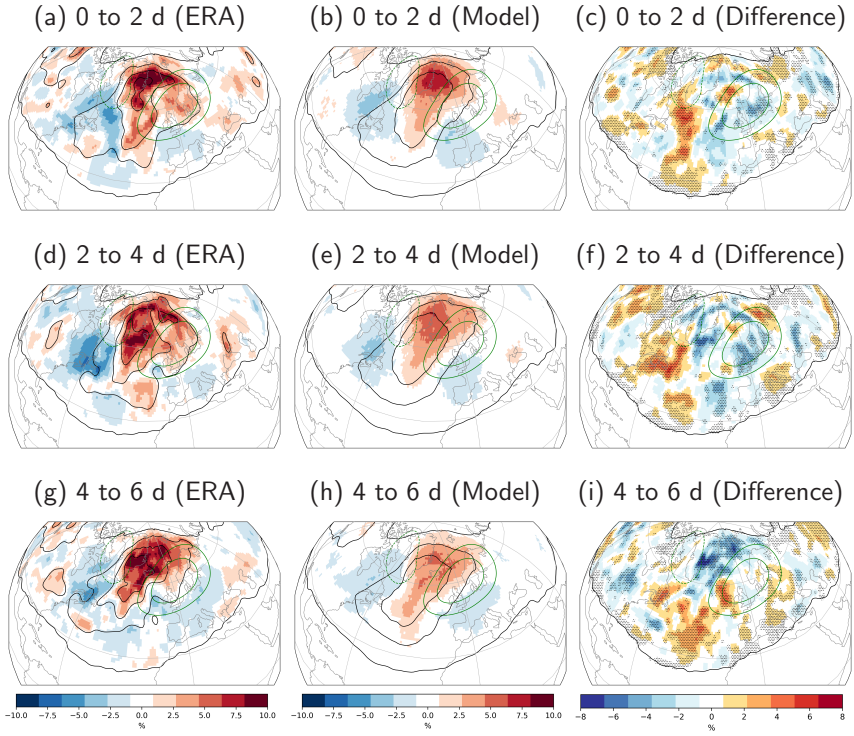


Figure B.2: WCB outflow frequency anomalies (shading) 0 to 2 days (a–c), 2 to 4 days (d–f), and 4 to 6 days (g–i) after EuBL onsets in a),d),g) ERA-Interim and b),e),h) reforecasts (NDFJM; 1997–2017). The black contours and point stippling as in Fig. B.1. Green contours as in Fig. 6.2

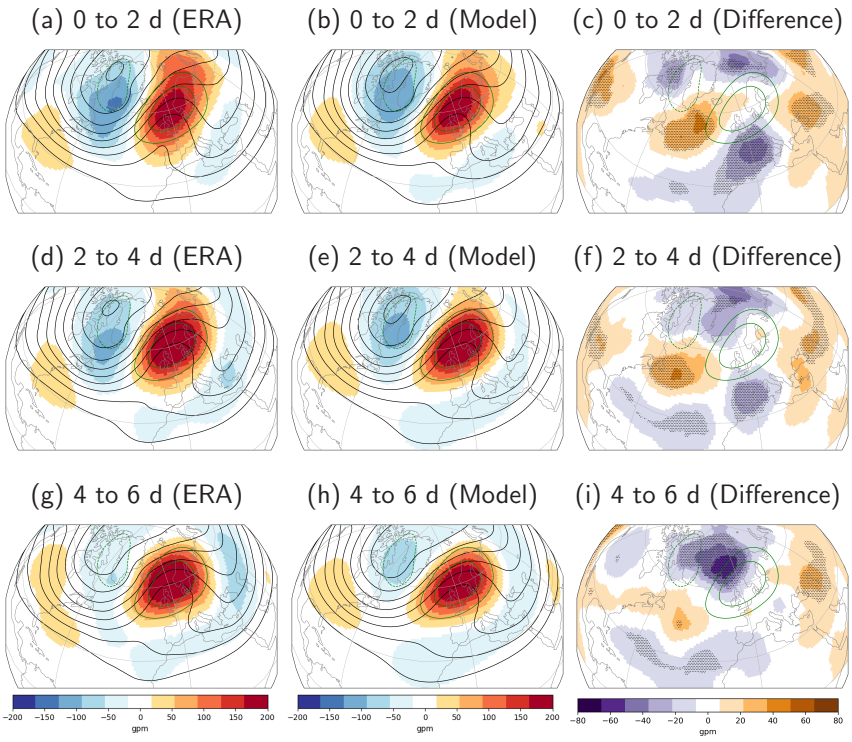


Figure B.3: As in Fig. B.2 but for Z500 anomalies. Contours indicate absolute fields (5100–5800 gpm every 100 gpm; NDJFM 1997–2017).

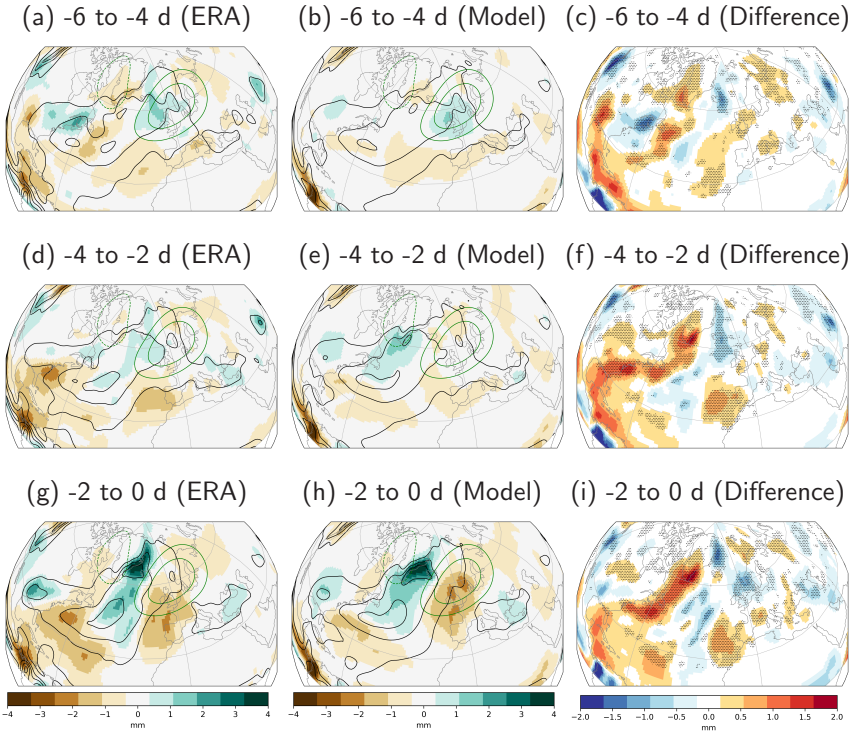


Figure B.4: Mean 24-h precipitation anomalies (shading) 6 to 4 days (a–b), 4 to 2 days (d–e), and 2 to 0 days (g–h) prior to EuBL onset in a),d),g) ERA-Interim and b),e),h) reforecasts (NDFJM; 1997–2017). The black contours indicate 24-h precipitation (ERA-Interim and reforecasts) of 2, 4, 6, 8 mm. (c,f,i) show differences between reforecasts and ERA-interim (shading). Point stippling and green contours as in Fig. 6.2.

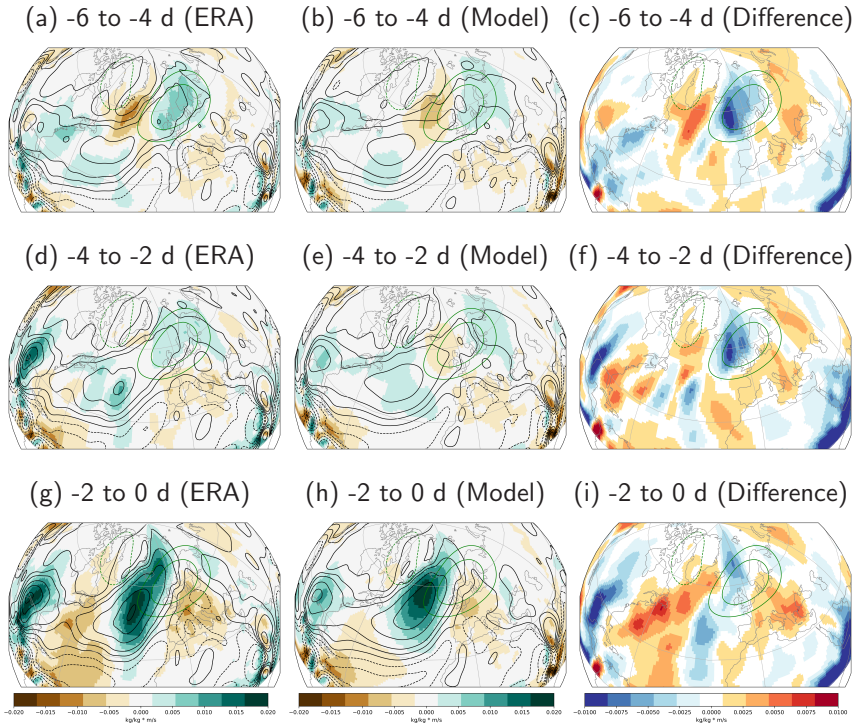


Figure B.5: 850-hPa meridional moisture flux anomalies (shading) 6 to 4 days (a–b), 4 to 2 days (d–e), and 2 to 0 days (g–h) prior to EuBL onset in a),d),g) ERA-Interim and b),e),h) reforecasts (NDFJM; 1997–2017). The black contours indicate absolute values (ERA-Interim and reforecasts) of -0.06, -0.05, -0.04, -0.03, -0.02, -0.01, -0.005, 0.005, 0.01, 0.02, 0.03, 0.04, 0.05, 0.06 kg/kg*m/s. (c,f,i) show differences between reforecasts and ERA-interim (shading). Green contours as in Fig. 6.2.

C Appendix for Chapter 7

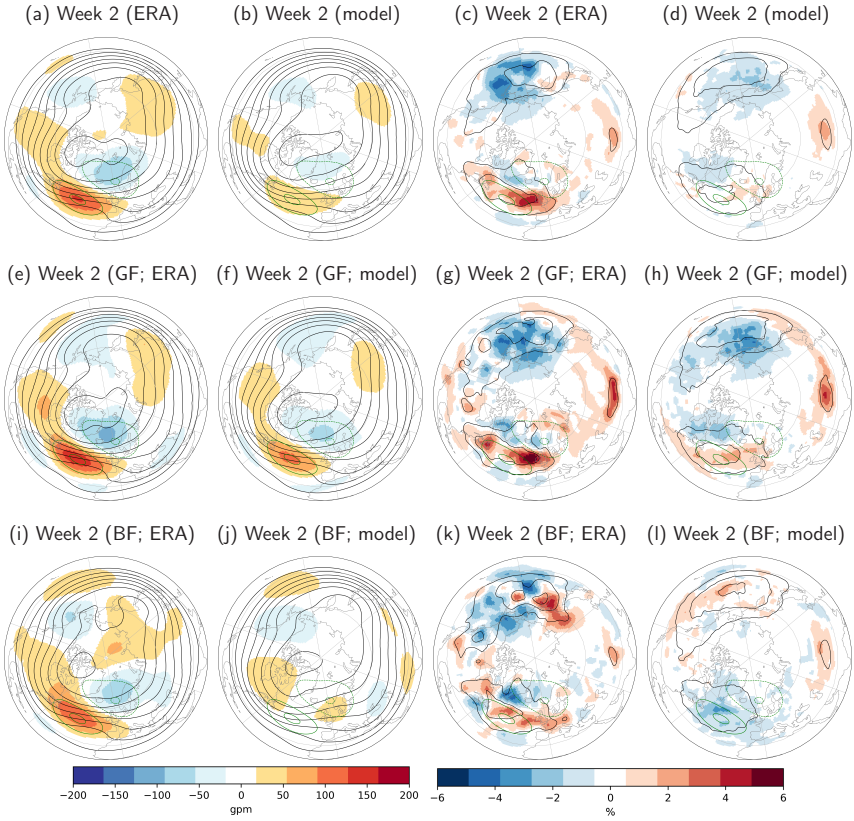


Figure C.1: As in Fig. 6.6 but for (a-d) all ScTr onsets, (e-h) good, and (i-l) bad ScTr skill.

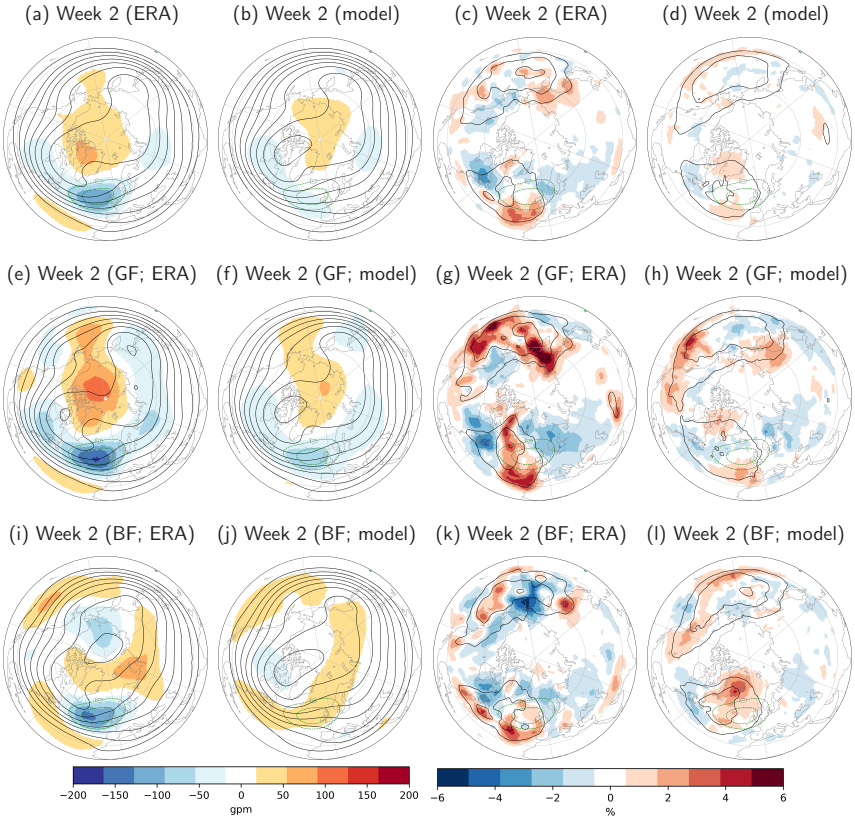


Figure C.2: As in Fig. C.1 but for (a-d) all AT onsets, (e-h) good, and (i-l) bad ScTr skill.

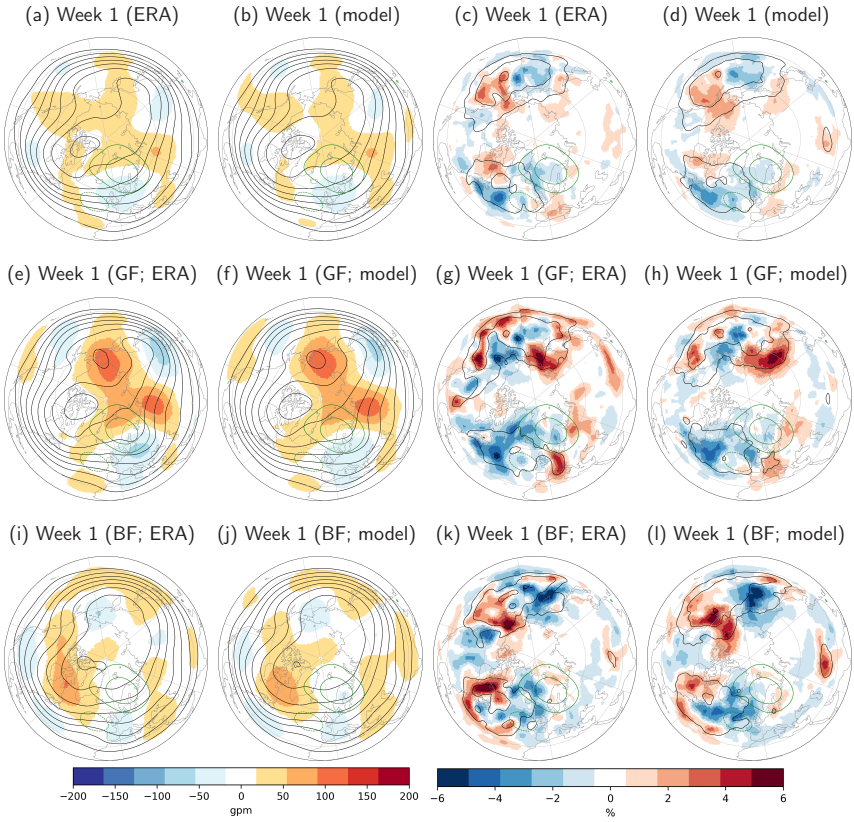


Figure C.3: As in Fig. C.1 but for forecast week 1 prior to ScBL onsets in week 2: (a-d) all ScBL onsets, (e-h) good, and (i-l) bad ScBL skill.

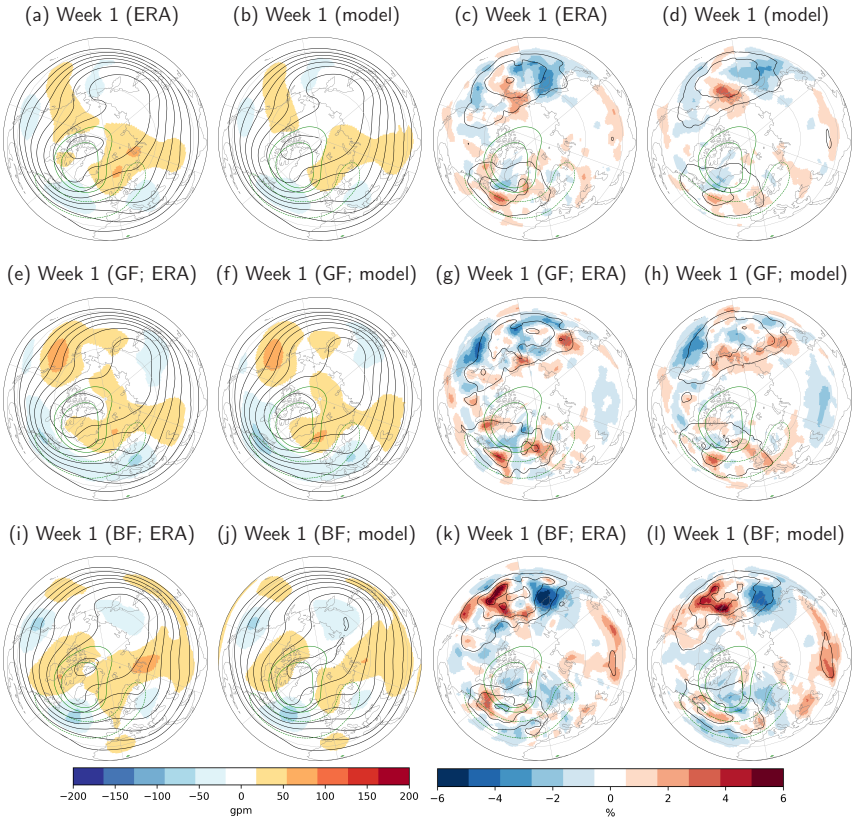


Figure C.4: As in Fig. C.1 but for forecast week 1 prior to GL onsets in week 2: (a-d) all GL onsets, (e-h) good, and (i-l) bad GL skill.

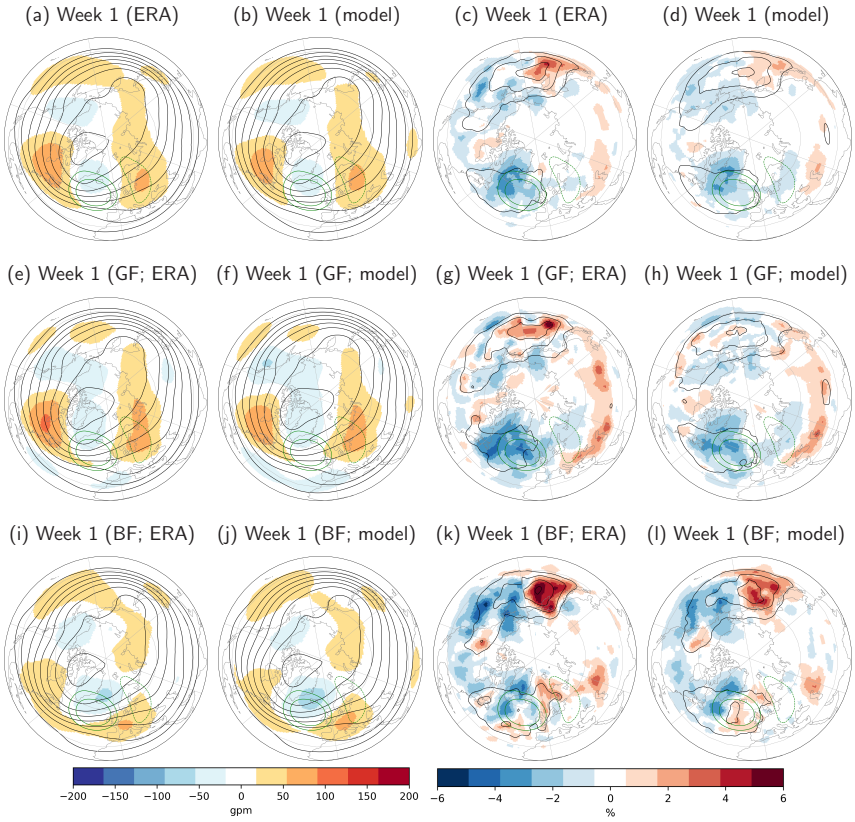


Figure C.5: As in Fig. C.1 but for forecast week 1 prior to AR onsets in week 2: (a-d) all AR onsets, (e-h) good, and (i-l) bad AR skill.

Bibliography

Abbe, C., 1901: The physical basis of long-range weather forecasts. *Monthly Weather Review*, **29 (12)**, 551–561.

Agel, L., M. Barlow, F. Colby, H. Binder, J. L. Catto, A. Hoell, and J. Cohen, 2019: Dynamical analysis of extreme precipitation in the US northeast based on large-scale meteorological patterns. *Climate Dyn.*, **52 (3-4)**, 1739–1760.

Anstey, J. A., P. Davini, L. J. Gray, T. J. Woollings, N. Butchart, C. Cagnazzo, B. Christiansen, S. C. Hardiman, S. M. Osprey, and S. Yang, 2013: Multi-model analysis of northern hemisphere winter blocking: Model biases and the role of resolution. *Journal of Geophysical Research: Atmospheres*, **118 (10)**, 3956–3971.

Baldwin, M. P. and T. J. Dunkerton, 2001: Stratospheric harbingers of anomalous weather regimes. *Science*, **294 (5542)**, 581–584.

Bauer, P., A. Thorpe, and G. Brunet, 2015: The quiet revolution of numerical weather prediction. *Nature*, **525 (7567)**, 47–55.

Baumgart, M., M. Riemer, V. Wirth, F. Teubler, and S. T. Lang, 2018: Potential vorticity dynamics of forecast errors: A quantitative case study. *Monthly Weather Review*, **146 (5)**, 1405–1425.

Beerli, R. and C. M. Grams, 2019: Stratospheric modulation of the large-scale circulation in the atlantic–european region and its implications for surface weather events. *Quarterly Journal of the Royal Meteorological Society*, **145 (725)**, 3732–3750.

Berggren, R., B. Bolin, and C.-G. Rossby, 1949: An aerological study of zonal motion, its perturbations and break-down. *Tellus*, **1 (2)**, 14–37.

Berman, J. D. and R. D. Torn, 2019: The impact of initial condition and warm conveyor belt forecast uncertainty on variability in the downstream waveguide in an ECWMF case study. *Mon. Wea. Rev.*, **147 (11)**, 4071–4089.

———, 2022: The sensitivity of downstream ridge building forecasts to upstream warm conveyor belt forecast uncertainty using mpas. *Monthly Weather Review*.

Binder, H., M. Boettcher, H. Joos, and H. Wernli, 2016: The role of warm conveyor belts for the intensification of extratropical cyclones in Northern Hemisphere winter. *J. Atmos. Sci.*, **73 (10)**, 3997–4020.

Bjerknes, V., 1904: Das problem der wettervorhersage, betrachtet vom standpunkte der mechanik und der physik. *Meteor. Z.*, **21**, 1–7.

Bloomfield, H. C., D. J. Brayshaw, P. L. Gonzalez, and A. Charlton-Perez, 2021: Pattern-based conditioning enhances sub-seasonal prediction skill of european national energy variables. *Meteorological Applications*, **28 (4)**, e2018.

Browning, K., 1997: The dry intrusion perspective of extra-tropical cyclone development. *Meteorological Applications*, **4 (4)**, 317–324.

Browning, K., M. Hardman, T. Harrold, and C. Pardoe, 1973: The structure of rainbands within a mid-latitude depression. *Quart. J. Roy. Meteor. Soc.*, **99 (420)**, 215–231.

Buehler, T., C. C. Raible, and T. F. Stocker, 2011: The relationship of winter season north atlantic blocking frequencies to extreme cold or dry spells in the era-40. *Tellus A: Dynamic Meteorology and Oceanography*, **63 (2)**, 174–187.

Büeler, D., R. Beerli, H. Wernli, and C. M. Grams, 2020: Stratospheric influence on ecmwf sub-seasonal forecast skill for energy-industry-relevant surface weather in european countries. *Quarterly Journal of the Royal Meteorological Society*, **146 (733)**, 3675–3694.

Büeler, D., L. Ferranti, L. Magnusson, J. F. Quinting, and C. M. Grams, 2021: Year-round sub-seasonal forecast skill for atlantic-european weather regimes. *Quarterly Journal of the Royal Meteorological Society*.

Buizza, R., A. Hollingsworth, F. Lalaurette, and A. Ghelli, 1999: Probabilistic predictions of precipitation using the ecmwf ensemble prediction system. *Weather and Forecasting*, **14 (2)**, 168–189.

Buizza, R. and M. Leutbecher, 2015: The forecast skill horizon. *Quarterly Journal of the Royal Meteorological Society*, **141 (693)**, 3366–3382.

Buizza, R., M. Leutbecher, and L. Isaksen, 2008: Potential use of an ensemble of analyses in the ecmwf ensemble prediction system. *Quarterly Journal of the Royal Meteorological Society: A journal of the atmospheric sciences, applied meteorology and physical oceanography*, **134 (637)**, 2051–2066.

Buizza, R. and T. N. Palmer, 1995: The singular-vector structure of the atmospheric global circulation. *Journal of the Atmospheric Sciences*, **52 (9)**, 1434–1456.

Carlson, T. N., 1980: Airflow through midlatitude cyclones and the comma cloud pattern. *Mon. Wea. Rev.*, **108 (10)**, 1498–1509.

Cassou, C., 2008: Intraseasonal interaction between the madden–julian oscillation and the north atlantic oscillation. *Nature*, **455 (7212)**, 523–527.

Catto, J. L., E. Madonna, H. Joos, I. Rudeva, and I. Simmonds, 2015: Global relationship between fronts and warm conveyor belts and the impact on extreme precipitation. *J. Climate*, **28 (21)**, 8411–8429.

Charlton-Perez, A. J., L. Ferranti, and R. W. Lee, 2018: The influence of the stratospheric state on north atlantic weather regimes. *Quarterly Journal of the Royal Meteorological Society*, **144 (713)**, 1140–1151.

Charney, J. G., 1966: The feasibility of a global observation and analysis experiment. *Bull. Amer. Meteor. Soc.*, **47**, 200–230.

Charney, J. G. and J. G. DeVore, 1979: Multiple flow equilibria in the atmosphere and blocking. *Journal of Atmospheric Sciences*, **36 (7)**, 1205–1216.

Corti, S., F. Molteni, and T. Palmer, 1999: Signature of recent climate change in frequencies of natural atmospheric circulation regimes. *Nature*, **398 (6730)**, 799–802.

Dacre, H. F., O. Martinez-Alvarado, and C. O. Mbengue, 2019: Linking atmospheric rivers and warm conveyor belt airflows. *Journal of Hydrometeorology*, **20 (6)**, 1183–1196.

Davini, P., S. Corti, F. D'Andrea, G. Rivière, and J. von Hardenberg, 2017: Improved winter european atmospheric blocking frequencies in high-resolution global climate simulations. *Journal of Advances in Modeling Earth Systems*, **9 (7)**, 2615–2634.

Davis, C. A., M. T. Stoelinga, and Y.-H. Kuo, 1993: The integrated effect of condensation in numerical simulations of extratropical cyclogenesis. *Mon. Wea. Rev.*, **121 (8)**, 2309–2330.

Dawson, A., T. Palmer, and S. Corti, 2012: Simulating regime structures in weather and climate prediction models. *Geophysical Research Letters*, **39 (21)**.

Dee, D. P., S. M. Uppala, A. Simmons, P. Berrisford, P. Poli, S. Kobayashi, U. Andrae, M. Balmaseda, G. Balsamo, d. P. Bauer, et al., 2011: The ERA-Interim reanalysis: Configuration and performance of the data assimilation system. *Quart. J. Roy. Meteor. Soc.*, **137 (656)**, 553–597.

DeFlorio, M. J., D. E. Waliser, B. Guan, D. A. Lavers, F. M. Ralph, and F. Vitart, 2018: Global assessment of atmospheric river prediction skill. *J. Hydrometeor.*, **19 (2)**, 409–426.

DeFlorio, M. J., D. E. Waliser, F. M. Ralph, B. Guan, A. Goodman, P. B. Gibson, S. Asharaf, L. D. Monache, Z. Zhang, A. C. Subramanian, et al., 2019: Experimental subseasonal-to-seasonal (S2S) forecasting of atmospheric rivers over the western United States. *J. Geophys. Res.*, **124 (21)**, 11 242–11 265.

Dirmeyer, P. A., P. Gentine, M. B. Ek, and G. Balsamo, 2019: Land surface processes relevant to sub-seasonal to seasonal (s2s) prediction. *Sub-Seasonal to Seasonal Prediction*, Elsevier, 165–181.

Dole, R. M., 1986: The life cycles of persistent anomalies and blocking over the north pacific. *Advances in Geophysics*, Elsevier, Vol. 29, 31–69.

d'Andrea, F., S. Tibaldi, M. Blackburn, G. Boer, M. Déqué, M. Dix, B. Dugas, L. Ferranti, T. Iwasaki, A. Kitoh, et al., 1998: Northern hemisphere atmospheric blocking as simulated by 15 atmospheric general circulation models in the period 1979–1988. *Climate Dynamics*, **14 (6)**, 385–407.

Faranda, D., G. Masato, N. Moloney, Y. Sato, F. Daviaud, B. Dubrulle, and P. Yiou, 2016: The switching between zonal and blocked mid-latitude atmospheric circulation: a dynamical system perspective. *Climate Dynamics*, **47 (5)**, 1587–1599.

Feng, P.-N., H. Lin, J. Derome, and T. M. Merlis, 2021: Forecast skill of the nao in the subseasonal-to-seasonal prediction models. *Journal of Climate*, **34 (12)**, 4757–4769.

Ferranti, L., S. Corti, and M. Janousek, 2015: Flow-dependent verification of the ECMWF ensemble over the Euro-Atlantic sector. *Quart. J. Roy. Meteor. Soc.*, **141 (688)**, 916–924.

Ferranti, L., L. Magnusson, F. Vitart, and D. S. Richardson, 2018: How far in advance can we predict changes in large-scale flow leading to severe cold conditions over europe? *Quarterly Journal of the Royal Meteorological Society*, **144 (715)**, 1788–1802.

Ferro, C., 2014: Fair scores for ensemble forecasts. *Quarterly Journal of the Royal Meteorological Society*, **140 (683)**, 1917–1923.

Ferro, C. A., D. S. Richardson, and A. P. Weigel, 2008: On the effect of ensemble size on the discrete and continuous ranked probability scores. *Meteorological Applications: A journal of forecasting, practical applications, training techniques and modelling*, **15 (1)**, 19–24.

Flaounas, E., K. Lagouvardos, V. Kotroni, C. Claud, J. Delanoë, C. Flamant, E. Madonna, and H. Wernli, 2016: Processes leading to heavy precipitation associated with two Mediterranean cyclones observed during the HyMeX SOP1. *Quart. J. Roy. Meteor. Soc.*, **142**, 275–286.

Fukushima, K. and S. Miyake, 1982: Neocognitron: A self-organizing neural network model for a mechanism of visual pattern recognition. *Competition and cooperation in neural nets*, Springer, 267–285.

Gibson, P. B., D. E. Waliser, A. Goodman, M. J. DeFlorio, L. Delle Monache, and A. Molod, 2020: Subseasonal-to-seasonal hindcast skill assessment of ridging events related to drought over the western united states. *Journal of Geophysical Research: Atmospheres*, **125 (22)**, e2020JD033 655.

Grams, C. M. and H. M. Archambault, 2016: The key role of diabatic outflow in amplifying the midlatitude flow: A representative case study of weather systems surrounding western north pacific extratropical transition. *Monthly Weather Review*, **144 (10)**, 3847–3869.

Grams, C. M., R. Beerli, S. Pfenninger, I. Staffell, and H. Wernli, 2017: Balancing europe's wind-power output through spatial deployment informed by weather regimes. *Nature climate change*, **7 (8)**, 557–562.

Grams, C. M., H. Binder, S. Pfahl, N. Piaget, and H. Wernli, 2014: Atmospheric processes triggering the central European floods in June 2013. *Natural Hazards and Earth System Sciences*, **14 (7)**, 1691–1702.

Grams, C. M., L. Magnusson, and E. Madonna, 2018: An atmospheric dynamics perspective on the amplification and propagation of forecast error in numerical weather prediction models: A case study. *Quarterly Journal of the Royal Meteorological Society*, **144 (717)**, 2577–2591.

Grazzini, F. and F. Vitart, 2015: Atmospheric predictability and rossby wave packets. *Quarterly Journal of the Royal Meteorological Society*, **141 (692)**, 2793–2802.

Green, J., F. Ludlam, and J. McIlveen, 1966: Isentropic relative-flow analysis and the parcel theory. *Quart. J. Roy. Meteor. Soc.*, **92**, 210–219.

Harrold, T., 1973: Mechanisms influencing the distribution of precipitation within baroclinic disturbances. *Quart. J. Roy. Meteor. Soc.*, **99 (420)**, 232–251.

Hart, R. E. and J. L. Evans, 2001: A climatology of the extratropical transition of atlantic tropical cyclones. *Journal of Climate*, **14 (4)**, 546–564.

Henderson, S. A., E. D. Maloney, and E. A. Barnes, 2016: The influence of the madden–julian oscillation on northern hemisphere winter blocking. *Journal of Climate*, **29 (12)**, 4597–4616.

Hersbach, H., B. Bell, P. Berrisford, S. Hirahara, A. Horányi, J. Muñoz-Sabater, J. Nicolas, C. Peubey, R. Radu, D. Schepers, et al., 2020: The era5 global reanalysis. *Quarterly Journal of the Royal Meteorological Society*, **146 (730)**, 1999–2049.

Hochman, A., G. Messori, J. F. Quinting, J. G. Pinto, and C. M. Grams, 2021: Do atlantic-european weather regimes physically exist? *Geophysical Research Letters*, e2021GL095574.

Hoskins, B. J. and D. J. Karoly, 1981: The steady linear response of a spherical atmosphere to thermal and orographic forcing. *Journal of Atmospheric Sciences*, **38 (6)**, 1179–1196.

Hoskins, B. J., M. E. McIntyre, and A. W. Robertson, 1985: On the use and significance of isentropic potential vorticity maps. *Quart. J. Roy. Meteor. Soc.*, **111 (470)**, 877–946.

Huffman, G. J., D. T. Bolvin, D. Braithwaite, K.-L. Hsu, R. J. Joyce, C. Kidd, E. J. Nelkin, S. Sorooshian, E. F. Stocker, J. Tan, et al., 2020: Integrated multi-satellite retrievals for the global precipitation measurement (gpm) mission (imerg). *Satellite precipitation measurement*, Springer, Cham, 343–353.

Jia, X., S. Yang, W. Song, and B. He, 2014: Prediction of wintertime northern hemisphere blocking by the ncep climate forecast system. *Journal of meteorological research*, **28 (1)**, 76–90.

Jones, S. C., P. A. Harr, J. Abraham, L. F. Bosart, P. J. Bowyer, J. L. Evans, D. E. Hanley, B. N. Hanstrum, R. E. Hart, F. Lalaurette, et al., 2003: The extratropical transition of tropical cyclones: Forecast challenges, current understanding, and future directions. *Weather and Forecasting*, **18 (6)**, 1052–1092.

Joos, H. and R. M. Forbes, 2016: Impact of different ifs microphysics on a warm conveyor belt and the downstream flow evolution. *Quarterly Journal of the Royal Meteorological Society*, **142 (700)**, 2727–2739.

Kautz*, L.-A., I. Polichtchouk*, T. Birner, H. Garny, and J. G. Pinto, 2020: Enhanced extended-range predictability of the 2018 late-winter eurasian cold spell due to the stratosphere. *Quarterly Journal of the Royal Meteorological Society*, **146 (727)**, 1040–1055.

Kolstad, E. W., C. O. Wulff, D. I. Domeisen, and T. Woollings, 2020: Tracing north atlantic oscillation forecast errors to stratospheric origins. *Journal of Climate*, **33 (21)**, 9145–9157.

Kretschmer, M., D. Coumou, J. F. Donges, and J. Runge, 2016: Using causal effect networks to analyze different arctic drivers of midlatitude winter circulation. *Journal of climate*, **29 (11)**, 4069–4081.

Lamberson, W. S., R. D. Torn, L. F. Bosart, and L. Magnusson, 2016: Diagnosis of the source and evolution of medium-range forecast errors for extratropical cyclone Joachim. *Weather and Forecasting*, **31 (4)**, 1197–1214.

Lang, A. L., K. Pegion, and E. A. Barnes, 2020: Introduction to special collection:"bridging weather and climate: Subseasonal-to-seasonal (s2s) prediction". *Journal of Geophysical Research: Atmospheres*, **125 (4)**, e2019JD031 833.

Lee, R. W., S. J. Woolnough, A. J. Charlton-Perez, and F. Vitart, 2019: Enso modulation of mjo teleconnections to the north atlantic and europe. *Geophysical Research Letters*, **46 (22)**, 13 535–13 545.

Lee, S. H., A. J. Charlton-Perez, J. C. Furtado, and S. J. Woolnough, 2020: Representation of the scandinavia–greenland pattern and its relationship with the polar vortex in s2s forecast models. *Quarterly Journal of the Royal Meteorological Society*, **146 (733)**, 4083–4098.

Legras, B. and M. Ghil, 1985: Persistent anomalies, blocking and variations in atmospheric predictability. *Journal of Atmospheric Sciences*, **42 (5)**, 433–471.

Lenggenhager, S., M. Croci-Maspoli, S. Brönnimann, and O. Martius, 2019: On the dynamical coupling between atmospheric blocks and heavy precipitation events: A discussion of the southern alpine flood in october 2000. *Quarterly Journal of the Royal Meteorological Society*, **145 (719)**, 530–545.

Lin, H., G. Brunet, and J. Derome, 2009: An observed connection between the North Atlantic Oscillation and the Madden–Julian oscillation. *J. Climate*, **22 (2)**, 364–380.

Lorenz, E. N., 1963: Deterministic nonperiodic flow. *Journal of atmospheric sciences*, **20 (2)**, 130–141.

———, 1969: The predictability of a flow which possesses many scales of motion. *Tellus*, **21 (3)**, 289–307.

———, 1982: Atmospheric predictability experiments with a large numerical model. *Tellus*, **34 (6)**, 505–513.

Madden, R. A. and P. R. Julian, 1971: Detection of a 40–50 day oscillation in the zonal wind in the tropical pacific. *Journal of Atmospheric Sciences*, **28 (5)**, 702–708.

———, 1972: Description of global-ccale circulation cells in the tropics with a 40–50 day period. *J. Atmos. Sci.*, **29 (6)**, 1109–1123.

Maddison, J., S. Gray, O. Martínez-Alvarado, and K. Williams, 2019: Upstream cyclone influence on the predictability of block onsets over the Euro-Atlantic region. *Mon. Wea. Rev.*, **147 (4)**, 1277–1296.

Madonna, E., M. Boettcher, C. M. Grams, H. Joos, O. Martius, and H. Wernli, 2015: Verification of North Atlantic warm conveyor belt outflows in ECMWF forecasts. *Quart. J. Roy. Meteor. Soc.*, **141 (689)**, 1333–1344.

Madonna, E., C. Li, C. M. Grams, and T. Woollings, 2017: The link between eddy-driven jet variability and weather regimes in the north atlantic-european sector. *Quarterly Journal of the Royal Meteorological Society*, **143 (708)**, 2960–2972.

Madonna, E., H. Wernli, H. Joos, and O. Martius, 2014: Warm conveyor belts in the ERA-Interim dataset (1979–2010). Part I: Climatology and potential vorticity evolution. *J. Climate*, **27 (1)**, 3–26.

Magnusson, L., 2017: Diagnostic methods for understanding the origin of forecast errors. *Quart. J. Roy. Meteor. Soc.*, **143 (706)**, 2129–2142.

Magnusson, L. and E. Källén, 2013: Factors influencing skill improvements in the ecmwf forecasting system. *Monthly Weather Review*, **141 (9)**, 3142–3153.

Manrique-Suñén, A., N. Gonzalez-Reviriego, V. Torralba, N. Cortesi, and F. J. Doblas-Reyes, 2020: Choices in the verification of s2s forecasts and their implications for climate services. *Monthly Weather Review*, **148 (10)**, 3995–4008.

Martínez-Alvarado, O., S. L. Gray, and J. Methven, 2016: Diabatic processes and the evolution of two contrasting summer extratropical cyclones. *Mon. Wea. Rev.*, **144 (9)**, 3251–3276.

Masato, G., T. Woollings, and B. Hoskins, 2014: Structure and impact of atmospheric blocking over the euro-atlantic region in present-day and future simulations. *Geophysical Research Letters*, **41 (3)**, 1051–1058.

Massacand, A. C., H. Wernli, and H. C. Davies, 2001: Influence of upstream diabatic heating upon an Alpine event of heavy precipitation. *Mon. Wea. Rev.*, **129 (11)**, 2822–2828.

Mastrantonas, N., L. Magnusson, F. Pappenberger, and J. Matschullat, 2022: What do large-scale patterns teach us about extreme precipitation over the mediterranean at medium-and extended-range forecasts? *Quarterly Journal of the Royal Meteorological Society*, **148 (743)**, 875–890.

Matsueda, M. and T. Palmer, 2018: Estimates of flow-dependent predictability of wintertime euro-atlantic weather regimes in medium-range forecasts. *Quarterly Journal of the Royal Meteorological Society*, **144 (713)**, 1012–1027.

Michel, C. and G. Rivière, 2011: The link between rossby wave breakings and weather regime transitions. *Journal of the Atmospheric Sciences*, **68 (8)**, 1730–1748.

Michelangeli, P.-A., R. Vautard, and B. Legras, 1995: Weather regimes: Recurrence and quasi stationarity. *Journal of the atmospheric sciences*, **52 (8)**, 1237–1256.

Mohr, S., J. Wandel, S. Lenggenhager, and O. Martius, 2019: Relationship between atmospheric blocking and warm-season thunderstorms over western and central europe. *Quarterly Journal of the Royal Meteorological Society*, **145 (724)**, 3040–3056.

Ninomiya, K. and Y. Shibagaki, 2007: Multi-scale features of the meiyu-baiu front and associated precipitation systems. *Journal of the Meteorological Society of Japan. Ser. II*, **85**, 103–122.

Nogueira, M., 2020: Inter-comparison of era-5, era-interim and gpcp rainfall over the last 40 years: Process-based analysis of systematic and random differences. *Journal of Hydrology*, **583**, 124 632.

Oertel, A., M. Boettcher, H. Joos, M. Sprenger, and H. Wernli, 2020: Potential vorticity structure of embedded convection in a warm conveyor belt and its relevance for large-scale dynamics. *Weather and Climate Dynamics*, **1 (1)**, 127–153.

Palmer, T., R. Buizza, M. Leutbecher, R. Hagedorn, T. Jung, M. Rodwell, F. Vitart, J. Berner, E. Hagel, A. Lawrence, et al., 2007: The ensemble prediction system–recent and ongoing developments. *ECMWF Technical Memoranda*, **(430)**, 53.

Palmer, T. N., 1993: Extended-range atmospheric prediction and the lorenz model. *Bulletin of the American Meteorological Society*, **74 (1)**, 49–66.

Papritz, L., 2020: Arctic lower-tropospheric warm and cold extremes: Horizontal and vertical transport, diabatic processes, and linkage to synoptic circulation features. *J. Climate*, **33 (3)**, 993–1016.

Papritz, L. and C. M. Grams, 2018: Linking low-frequency large-scale circulation patterns to cold air outbreak formation in the northeastern north atlantic. *Geophysical Research Letters*, **45 (5)**, 2542–2553.

Pfahl, S., E. Madonna, M. Boettcher, H. Joos, and H. Wernli, 2014: Warm conveyor belts in the ERA-Interim dataset (1979–2010). Part II: Moisture origin and relevance for precipitation. *J. Climate*, **27 (1)**, 27–40.

Pfahl, S., C. Schwierz, M. Croci-Maspoli, C. M. Grams, and H. Wernli, 2015: Importance of latent heat release in ascending air streams for atmospheric blocking. *Nature Geoscience*, **8 (8)**, 610–614.

Pfahl, S. and H. Wernli, 2012: Quantifying the relevance of atmospheric blocking for co-located temperature extremes in the northern hemisphere on (sub-) daily time scales. *Geophysical Research Letters*, **39 (12)**.

Piaget, N., P. Froidevaux, P. Giannakaki, F. Gierth, O. Martius, M. Riemer, G. Wolf, and C. M. Grams, 2015: Dynamics of a local alpine flooding event in october 2011: moisture source and large-scale circulation. *Quarterly Journal of the Royal Meteorological Society*, **141 (690)**, 1922–1937.

Pickl, M., S. T. Lang, M. Leutbecher, and C. M. Grams, 2022: The effect of stochastically perturbed parametrisation tendencies (SPPT) on rapidly ascending air streams. *Quarterly Journal of the Royal Meteorological Society*, **148 (744)**, 1242–1261.

Priestley, M. D., H. F. Dacre, L. C. Shaffrey, S. Schemm, and J. G. Pinto, 2020: The role of secondary cyclones and cyclone families for the north atlantic storm track and clustering over western europe. *Quart. J. Roy. Meteor. Soc.*, **146 (728)**, 1184–1205.

Quinting, J. and C. Grams, 2021a: Eulerian identification of ascending air streams (elias 2.0) in numerical weather prediction and climate models. part i: Development of deep learning model. *Geoscientific Model Development Discussions*, 1–29.

———, 2021b: Toward a systematic evaluation of warm conveyor belts in numerical weather prediction and climate models. part i: Predictor selection and logistic regression model. *Journal of the Atmospheric Sciences*, **78 (5)**, 1465–1485.

Quinting, J. and F. Vitart, 2019: Representation of synoptic-scale Rossby wave packets and blocking in the S2S prediction project database. *Geophys. Res. Lett.*, **46 (2)**, 1070–1078.

Rex, D. F., 1950: Blocking action in the middle troposphere and its effect upon regional climate. *Tellus*, **2 (4)**, 275–301.

———, 1951: The effect of atlantic blocking action upon european climate. *Tellus*, **3 (2)**, 100–112.

Rodwell, M. J., L. Magnusson, P. Bauer, P. Bechtold, M. Bonavita, C. Cardinali, M. Diamantakis, P. Earnshaw, A. Garcia-Mendez, L. Isaksen, et al., 2013: Characteristics of occasional poor medium-range weather forecasts for europe. *Bulletin of the American Meteorological Society*, **94 (9)**, 1393–1405.

Rodwell, M. J., D. S. Richardson, D. B. Parsons, and H. Wernli, 2018: Flow-dependent reliability: A path to more skillful ensemble forecasts. *Bulletin of the American Meteorological Society*, **99 (5)**, 1015–1026.

Rossa, A., H. Wernli, and H. Davies, 2000: Growth and decay of an extra-tropical cyclone's PV-tower. *Meteorology and Atmospheric Physics*, **73 (3-4)**, 139–156.

Schäfler, A. and F. Harnisch, 2015: Impact of the inflow moisture on the evolution of a warm conveyor belt. *Quart. J. Roy. Meteor. Soc.*, **141 (686)**, 299–310.

Schaller, N., J. Sillmann, J. Anstey, E. M. Fischer, C. M. Grams, and S. Russo, 2018: Influence of blocking on northern european and western russian heatwaves in large climate model ensembles. *Environmental Research Letters*, **13 (5)**, 054 015.

Schemm, S., M. Sprenger, and H. Wernli, 2018: When during their life cycle are extratropical cyclones attended by fronts? *Bull. Amer. Meteor. Soc.*, **99 (1)**, 149–165.

Schiraldi, N. J. and P. E. Roundy, 2017: Seasonal-to-subseasonal model forecast performance during agricultural drought transition periods in the US Corn Belt. *Mon. Wea. Rev.*, **145 (9)**, 3687–3708.

Shapiro, M. A. and A. J. Thorpe, 2004: Thorpex international science plan. *WMO/TD*, **1246**.

Shutts, G., 1983: The propagation of eddies in diffluent jetstreams: Eddy vorticity forcing of 'blocking'flow fields. *Quarterly Journal of the Royal Meteorological Society*, **109 (462)**, 737–761.

Simmons, A. J. and A. Hollingsworth, 2002: Some aspects of the improvement in skill of numerical weather prediction. *Quarterly Journal of the Royal Meteorological Society: A journal of the atmospheric sciences, applied meteorology and physical oceanography*, **128 (580)**, 647–677.

Smagorinsky, J., 1969: Problems and promises of deterministic extended range forecasting. *Bulletin of the American Meteorological Society*, **50 (5)**, 286–312.

Son, S.-W., H. Kim, K. Song, S.-W. Kim, P. Martineau, Y.-K. Hyun, and Y. Kim, 2020: Extratropical prediction skill of the subseasonal-to-seasonal (s2s) prediction models. *Journal of Geophysical Research: Atmospheres*, **125 (4)**, e2019JD031 273.

Spensberger, C., M. J. Reeder, T. Spengler, and M. Patterson, 2020: The connection between the southern annular mode and a feature-based perspective on southern hemisphere midlatitude winter variability. *Journal of Climate*, **33 (1)**, 115–129.

Steinfeld, D. and S. Pfahl, 2019: The role of latent heating in atmospheric blocking dynamics: a global climatology. *Climate Dyn.*, **53 (9-10)**, 6159–6180.

Subramanian, A. C., M. A. Balmaseda, L. Centurioni, R. Chattopadhyay, B. D. Cornuelle, C. DeMott, M. Flatau, Y. Fujii, D. Giglio, S. T. Gille, et al., 2019: Ocean observations to improve our understanding, modeling, and forecasting of subseasonal-to-seasonal variability. *Frontiers in Marine Science*, **6**, 427.

Toth, Z. and E. Kalnay, 1993: Ensemble forecasting at nmc: The generation of perturbations. *Bulletin of the american meteorological society*, **74 (12)**, 2317–2330.

Vautard, R., 1990: Multiple weather regimes over the North Atlantic: Analysis of precursors and successors. *Mon. Wea. Rev.*, **118 (10)**, 2056–2081.

Vautard, R. and B. Legras, 1988: On the source of midlatitude low-frequency variability. part ii: Nonlinear equilibration of weather regimes. *Journal of the atmospheric sciences*, **45 (20)**, 2845–2867.

Vitart, F., 2004: Monthly forecasting at ecmwf. *Monthly Weather Review*, **132 (12)**, 2761–2779.

———, 2014: Evolution of ECMWF sub-seasonal forecast skill scores. *Quart. J. Roy. Meteor. Soc.*, **140 (683)**, 1889–1899.

———, 2017: Madden—Julian Oscillation prediction and teleconnections in the S2S database. *Quart. J. Roy. Meteor. Soc.*, **143 (706)**, 2210–2220.

Vitart, F., C. Ardilouze, A. Bonet, A. Brookshaw, M. Chen, C. Codorean, M. Déqué, L. Ferranti, E. Fucile, M. Fuentes, et al., 2017: The subseasonal to seasonal (s2s) prediction project database. *Bulletin of the American Meteorological Society*, **98 (1)**, 163–173.

Wandel, J., J. F. Quinting, and C. M. Grams, 2021: Toward a systematic evaluation of warm conveyor belts in numerical weather prediction and climate models. part ii: Verification of operational reforecasts. *Journal of the Atmospheric Sciences*, **78 (12)**, 3965–3982.

Wernli, B. H. and H. C. Davies, 1997: A Lagrangian-based analysis of extratropical cyclones. I: The method and some applications. *Quart. J. Roy. Meteor. Soc.*, **123 (538)**, 467–489.

Wernli, H., 1997: A lagrangian-based analysis of extratropical cyclones. ii: A detailed case-study. *Quarterly Journal of the Royal Meteorological Society*, **123 (542)**, 1677–1706.

Wernli, H., M. Paulat, M. Hagen, and C. Frei, 2008: SAL—A novel quality measure for the verification of quantitative precipitation forecasts. *Mon. Wea. Rev.*, **136 (11)**, 4470–4487.

Wheeler, M. C. and H. H. Hendon, 2004: An all-season real-time multivariate MJO index: Development of an index for monitoring and prediction. *Mon. Wea. Rev.*, **132 (8)**, 1917–1932.

White, C. J., H. Carlsen, A. W. Robertson, R. J. Klein, J. K. Lazo, A. Kumar, F. Vitart, E. Coughlan de Perez, A. J. Ray, V. Murray, et al., 2017: Potential applications of subseasonal-to-seasonal (S2S) predictions. *Meteor. Appl.*, **24 (3)**, 315–325.

Wilks, D. S., 2011: *Statistical methods in the atmospheric sciences*, Vol. 100. Academic press.

Yihui, D. and J. C. Chan, 2005: The east asian summer monsoon: an overview. *Meteorology and Atmospheric Physics*, **89 (1)**, 117–142.

Yiou, P. and M. Nogaj, 2004: Extreme climatic events and weather regimes over the north atlantic: when and where? *Geophysical Research Letters*, **31 (7)**.

Zamora, R. A., B. F. Zaitchik, M. Rodell, A. Getirana, S. Kumar, K. Arsenault, and E. Gutmann, 2021: Contribution of meteorological downscaling to skill and precision of seasonal drought forecasts. *Journal of Hydrometeorology*, **22 (8)**, 2009–2031.

Zhang, C., 2005: Madden-julian oscillation. *Reviews of Geophysics*, **43 (2)**.

Zheng, C., E. K.-M. Chang, H. Kim, M. Zhang, and W. Wang, 2019: Subseasonal to seasonal prediction of wintertime northern hemisphere extratropical cyclone activity by S2S and NMME models. *J. Geophys. Res.*, **124 (22)**, 12 057–12 077.

Zschenderlein, P., S. Pfahl, H. Wernli, and A. H. Fink, 2020: A lagrangian analysis of upper-tropospheric anticyclones associated with heat waves in europe. *Weather and Climate Dynamics*, **1 (1)**, 191–206.

Acknowledgments

First of all I would like to thank my supervisors Christian Grams and Peter Knippertz for their support and advice throughout the times of my PhD project. Christian, thank you for the idea of the project, for giving me the opportunity to come to your work group and your amazing support and advice over the course of the last years. It has been a special time and I am very grateful to have been part of your research group at IMK-TRO. Thank you Peter for the helpful discussions feedback that always brought new ideas and different perspectives for my work.

I would like to thank everyone in the large-scale dynamics and predictability group for an amazing time in the course of the past years. Moritz and Seraphine, it was a lot of fun to go through this PhD time together and I will miss our time together in 316a. Thank you for your valuable support for my PhD work, skiing holidays and all the times watching and discussing German TV shows. Moritz, I really enjoyed the research visit in Japan with you and the rest of the team. Thank you for the ping-pong games and Miso soup experiences.

Julian and Dominik, it has been extremely valuable to me to have your support for my work, especially during the beginning of my PhD. I really enjoyed going to conferences and on vacation together and I will always remember our time together in Japan. Thank you also to Annika Oertel, Marisol Osman, Marta Wenta, Joshua Dorrington, Fabian Mockert, and Maria Madsen for all the support and the ideas for my PhD work and thank you for the fun group activities outside of work. Further, I would like to thank everybody at IMK-TRO for the great atmosphere and different lunch groups before a global pandemic made everything a bit more challenging.

The research in this study was funded by the Helmholtz Association as part of the Young Investigator Group "Sub-seasonal Predictability: Understanding the Role of Diabatic Outflow" (SPREADOUT, grant VH-NG-1243). I acknowledge the subseasonal-to-seasonal (S2S) community since the results in this work are mainly based on S2S data. S2S is a joint initiative of the World Weather Research Programme (WWRP) and the World Climate Research Programme (WCRP). The original S2S database is hosted at ECMWF as an extension of the TIGGE database. Furthermore, I acknowledge the ECMWF and Deutscher Wetterdienst for granting access to the ERA-Interim dataset and Marlon Maranan for help with the GPM-IMERG data set.

Thank you to Judith Berner (NCAR) and Aneesh Subramanian (CU Boulder) for organizing the Advanced Study Program "The Science of Subseasonal to Seasonal (S2S) Predictions" and giving me the opportunity to be part of this exciting summer school. Furthermore, I would like to thank Mio Matsueda, Akio Yamagani, and Takumi Matsunobu (University of Tsukuba) for organizing and hosting our trip to Japan. Thank you for being so kind to us and thank you for the many scientific discussion. I would also like to thank colleagues from ECMWF (Laura Ferranti, Linus Magnusson, Magdalena Alonso Balmaseda, Frédéric Vitart, and Chris Roberts) and Hai Lin (ECCC) for their feedback and comments to the results during the course of the PhD.

A big thank you to my parents, grand-parents, brother and aunt for supporting me through all the years of school and university. Thank you to help me follow my dreams and letting me do the things I love to do. Thank you also to all of my friends who always gave me a good and healthy perspective on my work and helped me focus on things outside of science. Lastly, I would like to thank my wonderful wife Emilie and our daughter Eloise for their love and support throughout these last years. It really has been a journey with lots of ups and downs and I am grateful to be able to go through life with you. I love you and thank you for everything you have done for me!

Wissenschaftliche Berichte des Instituts für Meteorologie und Klimaforschung des Karlsruher Instituts für Technologie (0179-5619)

Bisher erschienen:

Nr. 1: *Fiedler, F. / Prenosil, T.*
Das MESOKLIP-Experiment. (Mesoskaliges Klimaprogramm im Oberrheintal)

Nr. 2: *Tangermann-Dlugi, G.*
Numerische Simulationen atmosphärischer Grenzschichtströmungen über langgestreckten mesoskaligen Hügelketten bei neutraler thermischer Schichtung

Nr. 3: *Witte, N.*
Ein numerisches Modell des Wärmehaushalts fließender Gewässer unter Berücksichtigung thermischer Eingriffe

Nr. 4: *Fiedler, F. / Höschele, K. (Hrsg.)*
Prof. Dr. Max Diem zum 70. Geburtstag

Nr. 5: *Adrian, G.*
Ein Initialisierungsverfahren für numerische mesoskalige Strömungs modelle

Nr. 6: *Dorwarth, G.*
Numerische Berechnung des Druckiderstandes typischer Geländeformen

Nr. 7: *Vogel, B.; Adrian, G. / Fiedler, F.*
MESOKLIP-Analysen der meteorologischen Beobachtungen von mesoskaligen Phänomenen im Oberrheingraben

Nr. 8: *Hugelmann, C.-P.*
Differenzenverfahren zur Behandlung der Advektion

Die Bände sind unter www.ksp.kit.edu als PDF frei verfügbar oder als Druckausgabe bestellbar.

Nr. 9: *Hafner, T.*
Experimentelle Untersuchung zum Druckwiderstand der Alpen

Nr. 10: *Corsmeier, U.*
Analyse turbulenter Bewegungsvorgänge in der maritimen atmosphärischen Grenzschicht

Nr. 11: *Walk, O. / Wieringa, J.(eds)*
Tsumeb Studies of the Tropical Boundary-Layer Climate

Nr. 12: *Degrazia, G. A.*
Anwendung von Ähnlichkeitsverfahren auf die turbulente Diffusion in der konvektiven und stabilen Grenzschicht

Nr. 13: *Schädler, G.*
Numerische Simulationen zur Wechselwirkung zwischen Landoberflächen und atmophärischer Grenzschicht

Nr. 14: *Heldt, K.*
Untersuchungen zur Überströmung eines mikroskaligen Hindernisses in der Atmosphäre

Nr. 15: *Vogel, H.*
Verteilungen reaktiver Luftbeimengungen im Lee einer Stadt – Numerische Untersuchungen der relevanten Prozesse

Nr. 16: *Höschele, K.(ed.)*
Planning Applications of Urban and Building Climatology – Proceedings of the IFHP / CIB-Symposium Berlin, October 14-15, 1991

Nr. 17: *Frank, H. P.*
Grenzschichtstruktur in Fronten

Nr. 18: *Müller, A.*
Parallelisierung numerischer Verfahren zur Beschreibung von Ausbreitungs- und chemischen Umwandlungsprozessen in der atmosphärischen Grenzschicht

Nr. 19: *Lenz, C.-J.*
Energieumsetzungen an der Erdoberfläche in gegliedertem Gelände

Die Bände sind unter www.ksp.kit.edu als PDF frei verfügbar oder als Druckausgabe bestellbar.

Nr. 20: *Schwartz, A.*
Numerische Simulationen zur Massenbilanz chemisch reaktiver Substanzen im mesoskaligen Bereich

Nr. 21: *Beheng, K. D.*
Professor Dr. Franz Fiedler zum 60. Geburtstag

Nr. 22: *Niemann, V.*
Numerische Simulation turbulenter Scherströmungen mit einem Kaskadenmodell

Nr. 23: *Koßmann, M.*
Einfluß orographisch induzierter Transportprozesse auf die Struktur der atmosphärischen Grenzschicht und die Verteilung von Spurengasen

Nr. 24: *Baldauf, M.*
Die effektive Rauhigkeit über komplexem Gelände – Ein Störungstheoretischer Ansatz

Nr. 25: *Noppel, H.*
Untersuchung des vertikalen Wärmetransports durch die Hangwindzirkulation auf regionaler Skala

Nr. 26: *Kuntze, K.*
Vertikaler Austausch und chemische Umwandlung von Spurenstoffen über topographisch gegliedertem Gelände

Nr. 27: *Wilms-Grabe, W.*
Vierdimensionale Datenassimilation als Methode zur Kopplung zweier verschiedenskaliger meteorologischer Modellsysteme

Nr. 28: *Grabe, F.*
Simulation der Wechselwirkung zwischen Atmosphäre, Vegetation und Erdoberfläche bei Verwendung unterschiedlicher Parametrisierungsansätze

Nr. 29: *Riemer, N.*
Numerische Simulationen zur Wirkung des Aerosols auf die troposphärische Chemie und die Sichtweite

Die Bände sind unter www.ksp.kit.edu als PDF frei verfügbar oder als Druckausgabe bestellbar.

Nr. 30: *Braun, F. J.*
Mesoskalige Modellierung der Bodenhydrologie

Nr. 31: *Kunz, M.*
Simulation von Starkniederschlägen mit langer Andauer über Mittelgebirgen

Nr. 32: *Bäumer, D.*
Transport und chemische Umwandlung von Luftschadstoffen im Nahbereich von Autobahnen – numerische Simulationen

Nr. 33: *Barthlott, C.*
Kohärente Wirbelstrukturen in der atmosphärischen Grenzschicht

Nr. 34: *Wieser, A.*
Messung turbulenter Spurengasflüsse vom Flugzeug aus

Nr. 35: *Blahak, U.*
Analyse des Extinktionseffektes bei Niederschlagsmessungen mit einem C-Band Radar anhand von Simulation und Messung

Nr. 36: *Bertram, I.*
Bestimmung der Wasser- und Eismasse hochreichender konvektiver Wolken anhand von Radardaten, Modell-ergebnissen und konzeptioneller Betrachtungen

Nr. 37: *Schmoeckel, J.*
Orographischer Einfluss auf die Strömung abgeleitet aus Sturmschäden im Schwarzwald während des Orkans „Lothar"

Nr. 38: *Schmitt, C.*
Interannual Variability in Antarctic Sea Ice Motion: Interannuelle Variabilität antarktischer Meereis-Drift

Nr. 39: *Hasel, M.*
Strukturmerkmale und Modelldarstellung der Konvektion über Mittelgebirgen

Die Bände sind unter www.ksp.kit.edu als PDF frei verfügbar oder als Druckausgabe bestellbar.

Ab Band 40 erscheinen die Wissenschaftlichen Berichte des Instituts für Meteorologie und Klimaforschung bei KIT Scientific Publishing (ISSN 0179-5619). Die Bände sind unter www.ksp.kit.edu als PDF frei verfügbar oder als Druckausgabe bestellbar.

Nr. 40: *Lux, R.*
Modellsimulationen zur Strömungsverstärkung von orographischen Grundstrukturen bei Sturmsituationen
ISBN 978-3-86644-140-8

Nr. 41: *Straub, W.*
Der Einfluss von Gebirgswellen auf die Initiierung und Entwicklung konvektiver Wolken
ISBN 978-3-86644-226-9

Nr. 42: *Meißner, C.*
High-resolution sensitivity studies with the regional climate model COSMO-CLM
ISBN 978-3-86644-228-3

Nr. 43: *Höpfner, M.*
Charakterisierung polarer stratosphärischer Wolken mittels hochauflösender Infrarotspektroskopie
ISBN 978-3-86644-294-8

Nr. 44: *Rings, J.*
Monitoring the water content evolution of dikes
ISBN 978-3-86644-321-1

Nr. 45: *Riemer, M.*
Außertropische Umwandlung tropischer Wirbelstürme: Einfluss auf das Strömungsmuster in den mittleren Breiten
ISBN 978-3-86644-766-0

Nr. 46: Nicht erschienen

Nr. 47: Nicht erschienen

Nr. 48: Nicht erschienen

Nr. 49: *Peters, T.*
Ableitung einer Beziehung zwischen der Radarreflektivität, der Niederschlagsrate und weiteren aus Radardaten abgeleiteten Parametern unter Verwendung von Methoden der multivariaten Statistik
ISBN 978-3-86644-323-5

Nr. 50: *Khodayar Pardo, S.*
High-resolution analysis of the initiation of deep convection forced by boundary-layer processes
ISBN 978-3-86644-770-7

Nr. 51: *Träumner, K.*
Einmischprozesse am Oberrand der konvektiven atmosphärischen Grenzschicht
ISBN 978-3-86644-771-4

Nr. 52: Nicht erschienen

Nr. 53: *Lundgren, K.*
Direct Radiative Effects of Sea Salt on the Regional Scale
ISBN 978-3-86644-773-8

Nr. 54: *Sasse, R.*
Analyse des regionalen atmosphärischen Wasserhaushalts unter Verwendung von COSMO-Simulationen und GPS-Beobachtungen
ISBN 978-3-86644-774-5

Nr. 55: *Grenzhäuser, J.*
Entwicklung neuartiger Mess- und Auswertungs-strategien für ein scannendes Wolkenradar und deren Anwendungsbereiche
ISBN 978-3-86644-775-2

Nr. 56: *Grams, C.*
Quantification of the downstream impact of extratropical transition for Typhoon Jangmi and other case studies
ISBN 978-3-86644-776-9

Nr. 57: *Keller, J.*
Diagnosing the Downstream Impact of Extratropical Transition Using Multimodel Operational Ensemble Prediction Systems
ISBN 978-3-86644-984-8

Nr. 58: *Mohr, S.*
Änderung des Gewitter- und Hagelpotentials im Klimawandel
ISBN 978-3-86644-994-7

Nr. 59: *Puskeiler, M.*
Radarbasierte Analyse der Hagelgefährdung in Deutschland
ISBN 978-3-7315-0028-5

Nr. 60: *Zeng, Y.*
Efficient Radar Forward Operator for Operational Data Assimilation within the COSMO-model
ISBN 978-3-7315-0128-2

Nr. 61: Nicht erschienen

Nr. 62: *Jerger, D.*
Radar Forward Operator for Verification of Cloud Resolving Simulations within the COSMO Model
ISBN 978-3-7315-0172-5

Nr. 63: *Maurer, V.*
Vorhersagbarkeit konvektiver Niederschläge: Hochauflösende Ensemblesimulationen für Westafrika
ISBN 978-3-7315-0189-3

Nr. 64: *Stawiarski, C.*
Optimizing Dual-Doppler Lidar Measurements of Surface Layer Coherent Structures with Large-Eddy Simulations
ISBN 978-3-7315-0197-8

Nr. 65: *Mahlke, H.*
Mechanismen der Auslösung hochreichender Konvektion im südwestdeutschen Mittelgebirgsraum
ISBN 978-3-7315-0203-6

Nr. 66: *Fosser, G.*
Precipitation statistics from regional climate model at resolutions relevant for soil erosion
ISBN 978-3-7315-0227-2

Nr. 67: *Adler, B.*
Boundary-Layer Processes Producing Mesoscale Water-Vapour Variability over a Mountainous Island
ISBN 978-3-7315-0247-0

Nr. 68: *Kraut, I.*
Separating the Aerosol Effect in Case of a „Medicane“
ISBN 978-3-7315-0405-4

Nr. 69: *Breil, M.*
Einfluss der Boden-Vegetation-Atmosphären Wechselwirkungen auf die dekadische Vorhersagbarkeit des Westafrikanischen Monsuns
ISBN 978-3-7315-0420-7

Nr. 70: *Lott, F. F.*
Wind Systems in the Dead Sea and Footprints in Seismic Records
ISBN 978-3-7315-0596-9

Nr. 71: *Rieger, D.*
Der Einfluss von natürlichem Aerosol auf Wolken über Mitteleuropa
ISBN 978-3-7315-0672-0

Nr. 72: *Loewe, K.*
Arctic mixed-phase clouds. Macro- and microphysical insights with a numerical model
ISBN 978-3-7315-0686-7

Nr. 73: *Piper, D. A.*
Untersuchung der Gewitteraktivität und der relevanten großräumigen Steuerungsmechanismen über Mittel- und Westeuropa
ISBN 978-3-7315-0701-7

Nr. 74: *Metzger, J.*
Wind Systems and Energy Balance in the Dead Sea Valley
ISBN 978-3-7315-0699-7

Nr. 75: *Deetz, K.*
Assessing the Aerosol Impact on Southern West African Clouds and Atmospheric Dynamics
ISBN 978-3-7315-0744-4

Nr. 76: *Ehmele, F. T.*
Stochastische Simulation großflächiger, hochwasserrelevanter Niederschlagsereignisse
ISBN 978-3-7315-0761-1

Nr. 77: *Hackenbruch, J.*
Anpassungsrelevante Klimaänderungen für städtische Baustrukturen und Wohnquartiere
ISBN 978-3-7315-0771-0

Nr. 78: *Schmidberger, M.*
Hagelgefährdung und Hagelrisiko in Deutschland basierend auf einer Kombination von Radardaten und Versicherungsdaten
ISBN 978-3-7315-0846-5

Nr. 79: *Gruber, S.*
Contrails and Climate Engineering - Process Studies on Natural and Artificial High-Level Clouds and Their Impact on the Radiative Fluxes
ISBN 978-3-7315-0896-0

Nr. 80: *Walter, C.*
Simulationen der Ausbreitung von Vulkanasche unter expliziter Berücksichtigung der optischen Eigenschaften der Aschepartikel
ISBN 978-3-7315-0939-4

Nr. 81: *Caldas-Alvarez, A.*
Atmospheric Moisture Effects on Deep Convection in the Western Mediterranean
ISBN 978-3-7315-0947-9

Nr. 82: *Sedlmeier, K.*
Near future changes of compound extreme events from an ensemble of regional climate simulations
ISBN 978-3-7315-0476-4

Nr. 83: *Brecht, B. M.*
Die urbane Wärmebelastung unter Einfluss lokaler Faktoren und zukünftiger Klimaänderungen
ISBN 978-3-7315-0990-5

Nr. 84: *Singh, S.*
Convective precipitation simulated with ICON over heterogeneous surfaces in dependence on model and land-surface resolution
ISBN 978-3-7315-1068-0

Nr. 85: *Wilhelm, J.*
Einfluss atmosphärischer Umgebungsbedingungen auf den Lebenszyklus konvektiver Zellen in der Echtzeit-Vorhersage
ISBN 978-3-7315-1182-3

Nr. 86: *Pickl, M.*
Perspectives on warm conveyor belts – sensitivities to ensemble configuration and the role for forecast error
ISBN 978-3-7315-1236-3

Nr. 87: *Wandel, J.*
Representation of warm conveyor belts in sub-seasonal forecast models and the link to Atlantic-European weather regimes
ISBN 978-3-7315-1249-3

87

JAN LUCAS WANDEL

Representation of warm conveyor belts in sub-seasonal forecast models and the link to Atlantic-European weather regimes

Warm conveyor belts (WCBs) are important components of the large-scale circulation in the midlatitudes since they transport air from the lower troposphere into the tropopause region and contribute to upper-level ridge building and the formation of blocking anticyclones. This work systematically investigates the representation of WCBs in large reforecast data sets of different numerical weather forecast models from the Subseasonal-to-Seasonal (S2S) database and evaluates the role of WCBs for the onset and life cycle of Atlantic-European weather regimes in the reforecasts.

ISSN 0179-5619
ISBN 978-3-7315-1249-3

Gedruckt auf FSC-zertifiziertem Papier